Understanding the history of a volcanic arc: linking geochemistry of Cenozoic volcanic cobbles from the Wrangell arc, Alaska, to upper plate and subducting slab tectonic processes

by

Bethany Kathleen Morter

B.S., University of Oregon, 2015

A THESIS

submitted in partial fulfillment of the requirements for the degree

MASTER OF SCIENCE

Department of Geology
College of Arts and Sciences

KANSAS STATE UNIVERSITY
Manhattan, Kansas

2017

Approved by:

Major Professor
Dr. Matthew Brueseke

Abstract

The Wrangell arc (WA) is a ~29 Ma magmatic belt, extending from south-central Alaska into the Yukon Territory, that lies above the edges and leading front of the Yakutat microplate, a buoyant oceanic plateau that is causing shallow subduction (11-16º) in the region. The WA occurs in a transition zone between "normal" Aleutian subduction to the west and dextral strike-slip tectonics to the east, accomplished by the Totschunda, Denali, and Duke River faults. This geologic setting offers a chance to study the interrelations between subduction, strike-slip motion, and slab-edge magmatic processes in a relatively well-exposed arc. We implemented a novel technique of applying geochemical and geochronologic analyses on volcanic cobbles collected from glacio-fluvial systems (rivers, streams, and glaciers) encircling/draining the WA. Our primary objective is to integrate our cobble datasets with the existing bedrock and detrital sand records to develop a comprehensive understanding of WA magmatism through time and space. Our secondary objective is to test the validity of this novel technique for reproducing what is documented from bedrock samples and its potential for utilization in other locations. This study provides new major element data from 215 samples and trace element data from 236 samples collected from 17 major rivers that drain from the modern western and central WA (this study excludes the eastern WA). This study also provides new age data from a total of 119 samples from 10 major rivers. New geochronology of modern detrital volcanic cobbles and sand/zircons reveal that the WA initiated at ~29 Ma and that magmatism migrated northwestward through time. Cobble ages and locations across the arc agree with the northwestward progression of magmatism previously identified by Richter et al. (1990). Forty-seven cobbles are dated <~1 Ma and only nine cobbles are dated 29 – ~20 Ma, whereas there are no cobbles from 17 – ~13 Ma. Geochemical data reveal similarities between our data and that of the <~5 Ma WA defined by Preece and Hart (2004): Trend 1 (transitional-tholeiitic), Trend 2a (calc-alkaline), Trend 2b (calc-alkaline, adakite-like). Therefore, we use the geochemical framework defined in Preece and Hart (2004) to contextualize spatio-temporal trends of magmatism and tectonic implications in the WA during its ~29 m.y. history. Trend 2a and 2b cobbles are spatially and temporally ubiquitous in the WA, indicating that subduction and partial slab melting have been the dominant tectonic processes throughout WA history. Trend 1 cobbles are not found in southwestern WA rivers and are temporally restricted to ~11 – ~6 Ma and <1

Ma, suggesting intra-arc extension has occurred in discrete periods during WA history. These conclusions are confirmed by the existing (Richter et al., 1990; Skulski et al., 1991; 1992; Preece and Hart, 2004; Trop et al., 2012) and new (Berkelhammer, 2017; Weber et al., 2017) bedrock records. Finally, this study shows that the sampled cobble lithologies largely reproduce the known bedrock record in geochemical, temporal, and spatial contexts, which suggests the novel methodology applied here can be used in other locations where field conditions limit access to bedrock.

Table of Contents

List of Figures

List of Tables

Acknowledgements

I'd like to start by going back to the beginning and thanking Madison Myers, my TA and peer-advisor at the University of Oregon. You sparked my interest, you gave me a chance, and you gave me confidence to use expensive lab equipment (eventually without supervision!), to conduct research, and to eventually apply for grad school. I'll never forget my days of sieving and blasting music with you in the lab. Without you—and I am not exaggerating—none of this would've been possible. Thank you.

I want to thank Matt Brueseke, for everything. But first and foremost, for responding to my initial email and for taking me seriously. Thank you for giving me the opportunity to work with you, for guiding me through the tedious process of crafting a thesis, for taking me to Alaska (and Big Bend), and everything else that I can't put into words.

I'd like to thank my roommate throughout my time at Kansas State, Michelle Berube. We started this Midwestern adventure as roommates that didn't know each other (good thing we got along!) and ended as close friends… that were still roommates! I hope we remain close and I can't wait to see what you end up doing with your life. I also hope you move somewhere cool so I can come visit!

Sam Berkelhammer, I never would've been able to keep going without your constant help and willingness to grab a beer after a particularly long class of advanced igneous petrology or an entire day spent with the rock crusher. I know we'll be friends for a long time and I look forward to seeing what kind of crazy successful things you do. Also, that was pretty neat of you to expand to the biology department because you brought CC into all our lives.

CC—you're such a super lady! Seriously, I mean that from the bottom of my heart. You are always so fun to be around, have a great sense of humor, and are up for just about any adventure. You are also an all-around amazing advice-giver. I am so grateful that I could meet you and best of luck in Missoula!

Grant Zwiefelhofer and Jacob Huges (sorry… I mean Huge): thanks for being there to listen to me rant and rave whenever I needed to. I'm sure I annoyed you most of the time, but thanks for listening and sometimes participating. I look forward to battling you guys in fantasy football for many years to come!

Colleen, you have always, always, always been there whenever any of us needed help. Whether that be help with using the XRF, how to phrase a particular paragraph, help with our deadlift technique, or just a sounding board, you have always been there. I cannot thank you enough.

Pamela Kempton, thank you for setting an example of what a strong female scientist is. Thank you for teaching us what kind of questions to ask, for forcing us to brush up on our microscope skills, and for giving us all multiple attempts on just about *every* advanced igneous petrology assignment. That was a lot more work for you than it was for us, but I appreciate it immensely. I also want to thank you for the quality of edits and feedback you provide, which were an indispensable help when writing this thesis (and just about everything else I wrote during my time at K-State).

For everyone else I did not mention here—Claire, Katie, Bayley, Victoria, Brent, Kyle, Trenton, Austin, Ian, Anna, Jacob Clayton, Julia—thanks for being great and supportive friends. Best of luck in what you do next. I'm sure whatever it is will be great!

And of course I couldn't finish this without thanking everyone that made it possible for the Wrangell arc project to be a reality. That begins with the four PIs of the NSF grant, Jeff Benowitz, Jeff Trop, Matt Brueseke, and Paul Layer. I can't express how lucky I was to be able to stumble into a fully-funded project with such great people that led to some amazing opportunities. Thank you all for allowing me to go to Alaska and see the Wrangell Mountains with my own eyes. That experience was truly once in a lifetime, and I won't soon forget it.

Jeff, Kailyn, and Paul—thanks for letting me join in your dinners in the field, eat your food, and drink your nice liquor. Collectively you made nights at camp so enjoyable and showed me that if you really put your mind to it, you can drunk dial someone on a satellite phone from deep in the Alaskan wilderness.

Jeff, thanks for giving me an arsenal of "good" jokes, for teaching me about the phrase "no idear" (which I've used countless times since), for dating *so many* rocks, and for helping with my thesis edits.

Kailyn, thanks for being such a fun person in the field and a nice distraction from the fact that we were trudging through muskeg day after day (and also for dating *so many* rocks). Some of my favorite field days were the ones when it was just you and I trying to figure things out on

our own, including where the fish were in Little Beaver Lake. Oh, and thanks for not losing your cool when we saw that mama griz or got lost in Tucson (like I did).

Paul, thank you so much for letting me stay in your home with you and your family for multiple days. It was really nice to come out of the field to a hot shower, a real bed, and a new episode of the Great British Baking Show.

Trop, thanks for teaching me how to *actually* measure section, for all the prompt replies via email, and for letting me go to Arizona to work in the LaserChron Center (and of course thank you for the cookies and coffee every morning after our night shift!).

So, I guess from the extent of this acknowledgements section (and all the references at the end), it is abundantly clear I had a ton of help getting to the finish line, not only from people in my daily life but also from previous researchers that have devoted their careers to these topics. It sounds cliché, but as I was writing this thesis, the phrase "you don't accomplish anything great alone" kept coming into my mind. And while I wouldn't consider this thesis "great", I think I really get the meaning of that phrase now.

Chapter 1 - Introduction

Studies of detrital material have typically been restricted to applications in sedimentary systems (e.g., geochronology of detrital zircons and provenance analyses). Recently the scope of detrital studies has been expanded to utilize sand, pebbles, and cobbles to understand processes such as cooling and exhumation rates in glaciated areas by using thermochronology and geochronology (Grabowski et al., 2013; Ehlers et al., 2015; Enkelmann and Ehlers, 2015; Falkowski et al., 2016; Lease et al., 2016). Studying detritus in heavily glaciated areas is a useful technique because it acts as a proxy to study bedrock that is inaccessible due to permanent ice cover, challenging terrain, or both. However, applying geochronology and geochemistry analyses of cobble-sized igneous detritus in complement to *in situ* bedrock for petrological studies is not found in current literature. The detrital petrological technique that is the focus of this study allows large areas of land to be targeted by relatively few sampling locales, thus providing a "high-return investment." This study is the first of its kind to utilize a sedimentary system technique for a purely petrological outcome: igneous river cobbles are used to indirectly sample *in situ* bedrock in the understudied and remote Wrangell arc (WA) of south-central Alaska. This project combines applied geochronology and geochemistry of igneous river cobbles from the WA to achieve the overall general objective of better understanding how the WA progressed, both geochemically and tectonically, through time.

The WA is a relatively well-exposed continental volcanic arc in south-central Alaska that is characterized by large shield volcanoes, stratovolcanoes, and cinder cones (Preece and Hart, 2004), as well as ice fields, glaciers, and huge river systems (Fig. 1.1). The WA covers 15,000 to 20,000 km^2 with peak heights ranging from about 700m to 5000m (Richter et al., 1990). Of this huge area spanned by the WA, nearly one-third is covered by ice fields or glaciers, which effectively restricts access to the rocks beneath this ice. However, major river systems drain watersheds within the WA, thereby providing a weathering and transportation mechanism for many of these inaccessible rock units. Some river cobbles come from areas that have accessible bedrock exposures while others are derived from ice-covered areas and have therefore never been sampled. The sizable spatial extent of WA, as well as expansive ice cover, large river drainage networks, and the potential to sample previously unavailable rocks, make this site an

excellent location to implement the use of fluvial igneous cobbles as an indirect method for bedrock sampling.

To understand how the WA geochemically and tectonically progressed through time, we must answer specific questions regarding the history of the WA. The questions we will be addressing about the history of the WA are as follows:

- Did WA magmatism begin earlier than 26 Ma (Richter et al., 1990)? Additionally, what do new cobble, detrital sand, and bedrock ages reveal about the progression of WA magmatism through time?
- Are specific time intervals during WA history linked to eruptions of different magma types? If so, what—if any—tectonic implications do these temporal trends reveal throughout the arc?
- Are the controls on the occurrence of various magma types local or arc-wide?
- What does the temporal migration of magmatism reveal about the tectonic controls on where WA magmatism was focused with time?
- Are the compositions of the igneous cobbles in this study reflected in the existing bedrock record? Can using igneous cobbles as a way of indirectly sampling bedrock be implemented in other locations?

To address these questions, we present and interpret geochemical data on 236 cobble samples collected from 17 major rivers that drain and in their entirety circumvent the WA (Fig. 1.2). New geochronological data on 119 of these samples allow us to place cobble geochemistry within a temporal context, thereby creating a geochemical timeline for the WA. Ages for the remaining samples are currently being obtained. To create a robust dataset, we will integrate our geochemistry and ages with all other WA bedrock and detrital data to understand where the cobbles fit in with existing data as well as where the cobbles present new results.

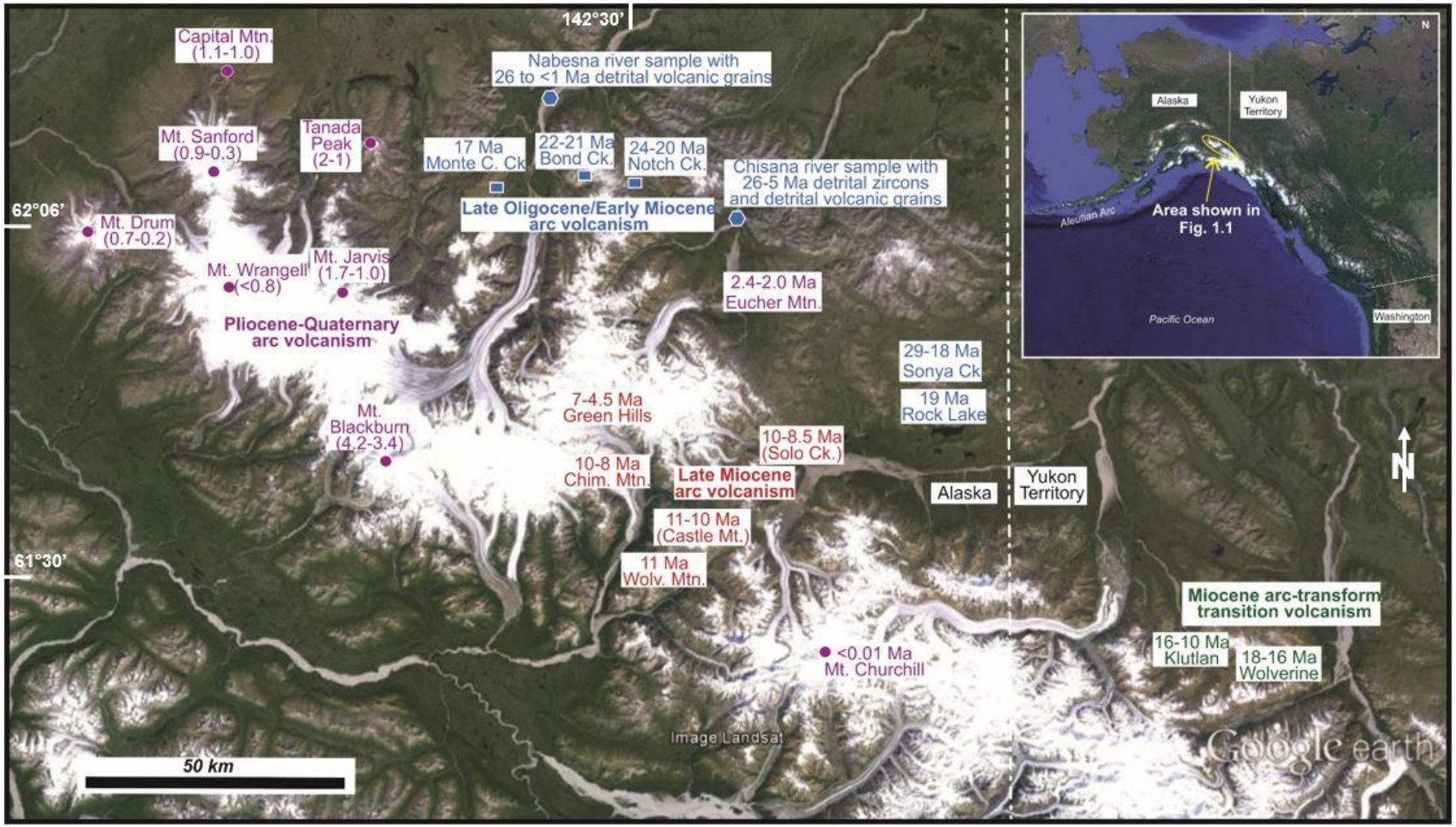

Figure 1.1 Satellite image of the WA. Note the large amount of ice cover present, making this an ideal location to test the use of igneous cobble sampling to indirectly study bedrock. Map is annotated with published bedrock and detrital ages. Purple circles and blue rectangles are locations of bedrock ages; blue hexagons are locations of detrital sand ages. Note the general northwestward younging trend, apart from Mt. Churchill and Eucher Mountain. Purple text = Pliocene-Quaternary in age; red text = Late Miocene; Green = Miocene (Yukon); Blue = Late Oligocene/Early Miocene.

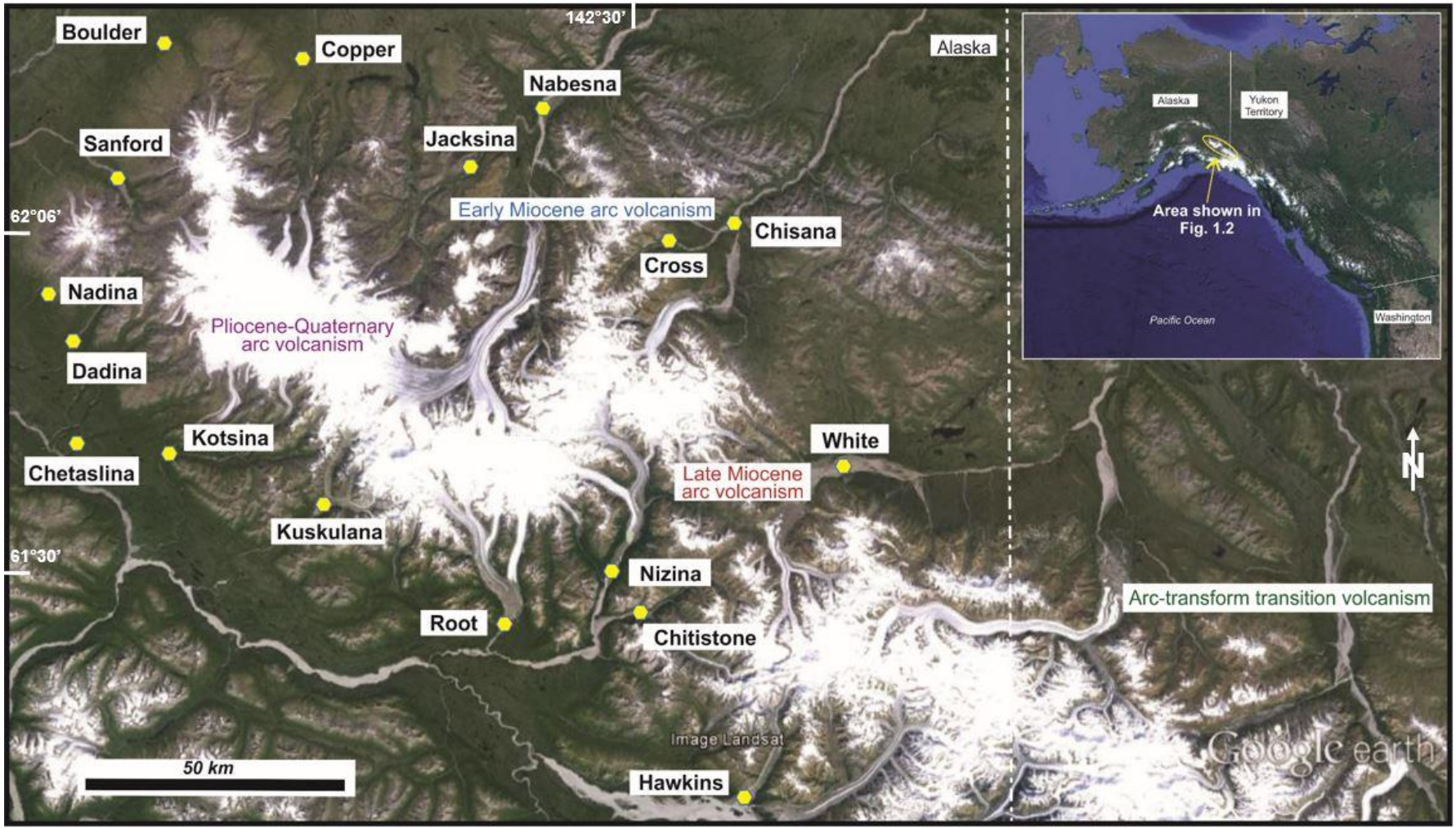

Figure 1.2 Map locations of sample collections. Yellow hexagons represent cobble collection sites and boxes note the river name from which the samples were collected.

Chapter 2 - Geologic Framework

The WA is a NW-SE trending continental volcanic arc that is ~29.0 m.y. old (Trop et al., 2017; Davis et al., 2017) and covers 15,000 – 20,000 km^2, extending from south-central Alaska into the neighboring Yukon Territory of Canada (Fig. 1.1). The WA occurs where the northernmost portion of the Pacific plate plunges beneath the North American plate. The Pacific plate in this locality includes the Yakutat microplate, which is interpreted as a wedge-shaped oceanic plateau made of thick, buoyant oceanic crust (Worthington et al., 2012) that originated at lower latitudes and has been translated northward to its current location along the Fairweather-Queen Charlotte fault system (Plafker and Berg, 1994; Perry et al., 2009). The presence of the Yakutat microplate causes subduction here to occur at a shallow angle that ranges from 6° to 16° in its imaged entirety (Bauer et al., 2014; Eberhart-Phillips et al., 2006). The subducted Yakutat has been imaged as continuous to a point beneath the WA and is therefore associated with Wrangell magmatism. However, the full geometry of the microplate north of the WA is unknown due to a lack of seismic stations in the region or the possibility of the lack of the Yakutat microplate north of the WA (Bauer et al., 2014). Major strike-slip faults (Denali fault, Totschunda fault, and Duke River fault) also interact with the WA subduction zone, creating an intersection between a convergent margin and strike-slip faults: an arc-transform junction (Fig 2.1).

In a regional context, this subduction zone is bracketed by "normal" Aleutian subduction to the west and by strike-slip motion to the east and north, creating an area where normal subduction transitions to shallow subduction and finally to a strike-slip regime (Haeussler, 2008; Gulick et al., 2013; Fig 2.2). The western portion of this transitional area is characterized by arc magmatism associated with "normal" subduction of the Pacific plate marked by the Aleutian arc. The central portion is characterized by the Yakutat microplate subducting at a near-horizontal angle of ~6° (Eberhart-Phillips et al., 2006) and a subsequent lack of active magmatism (Fig. 2.2). The eastern region of this transitional area—the focus of this study— is characterized by active, dormant, and extinct WA magmatism associated with subduction of the Yakutat microplate (Bauer et al., 2014) as well as strike-slip motion along the Denali fault system (Skulski et al., 1991, 1992; Richter et al., 1994; Trop et al., 2012). The dip angle of the Yakutat steepens slightly beneath the WA, ranging from 11º to 16º from west to east, thereby placing it at

a Benioff depth of ~80 km and therefore deep enough to be associated with magmatism observed in the WA (Bauer et al., 2014).

The WA itself can be divided into western, central, and eastern regions for ease of study and discussion (Fig. 2.3). The western and central regions are in Alaska and the eastern region lies across an international border in the Yukon Territory of Canada. Data from this study focus on only the western and central WA, but previous work from the eastern WA is used here for interpretations and context. The western WA is dominated by a subduction tectonic regime and the central and eastern WA have both subduction and strike-slip tectonic components (e.g., Eberhart-Philips et al., 2006; Haussler, 2008, Gulick et al., 2013; Totschunda fault in central and Denali and Duke River faults in eastern; Fig. 2.3). Previous geological investigations in the WA have individually focused on the western, central, and eastern regions and reveal that WA magmatism consists of four distinct geochemical groups that vary in space and time. The four groups are:

- ubiquitous and voluminous calc-alkaline magmatism (Skulski et al., 1991, 1992; Preece and Hart 2004; Trop et al., 2012; Berkelhammer, 2017; Davis et al., 2017; Trop et al., 2017; this study).
- low-volume alkaline magmatism restricted to the eastern WA adjacent to the Denali and Duke River faults (Skulski et al., 1991, 1992).
- voluminous transitional tholeiitic magmatism in the western and central WA associated with intra-arc extension (Preece and Hart 2004; Trop et al., 2012; Berkelhammer, 2017; this study).
- adakitic magmatism restricted to two young volcanoes; Mount Drum in the western WA and Mt. Churchill in the central WA (Preece and Hart, 2004; Preece et al., 2014; this study), as well as adakite-like magmatism in the ~29 – 20 Ma WA Sonya Creek volcanic field and areas to the west (Berkelhammer, 2017; Weber et al., 2017).

These geochemical groups reflect the tectonic regime(s) that formed them and, when these groups are coupled with their respective ages, have important implications for the magmatic history of the WA.

Calc-alkaline magmas are a signature of "typical" subduction. They are generated by melting in the mantle wedge in response to fluid influx via dehydration of the subducting slab; fluid-fluxing of the mantle wedge lowers the solidus and facilitates larger degrees of partial

melting than would otherwise be obtained. Because the WA occurs above a subduction zone where mantle wedge melting is occurring, calc-alkaline magmas are the dominant series throughout the entire WA (western, central, and eastern regions) and are temporally ubiquitous, beginning at ~29.0 Ma and continuing to essentially the present (Richter et al., 1990; Preece and Hart, 2004; Trop et al., 2012; Berkelhammer, 2017; Trop et al., 2017; Davis et al., 2017; this study). Northwestward migration of magmatism was initially identified based on ages and locations of calc-alkaline magmas throughout the WA (Fig. 2.4; Richter et al., 1990), but new data require modification of this interpretation (Berkelhammer, 2017; Trop et al., 2017; Davis et al., 2017; this study). Preliminary geochemical and geochronologic analyses of samples were performed for a National Science Foundation sponsored collaborative investigation of the WA between University of Alaska-Fairbanks, Bucknell University, and Kansas State University (this study is a sub-project). These preliminary data reveal calc-alkaline magmas with ages that range from ~30.0 to ~17.0 Ma that plot north of previously documented younger ages. These preliminary analyses suggest an additional migration component prior to the northwestward migration proposed by Richter et al. (1990), but require further study (Fig. 2.4). Prior to our investigation of the WA and other new studies (Berkelhammer, 2017; Davis et al., 2017; Trop et al., 2017), bedrock geochronology and geochemistry data were sparse in the WA and large sampling gaps existed, limiting the ability of researchers to discern spatial and temporal variations in magma type. These new data (Berkelhammer, 2017; Trop et al., 2017; Davis et al., 2017; this study) indicate that a southward migration preceded the well-documented northwestward migration of magmatism in the WA (Fig. 2.4). This previously undocumented southward migration has implications for upper plate and/or subducting slab processes through time in the WA and will be further explored in the Discussion section.

Alkaline magmas are only found in the eastern WA (Yukon) where major strike-slip faults are present (Denali and Duke River faults). Alkaline magmas have only been documented in spatially isolated volcanic fields in the Yukon (St. Clare, Alsek, and Stanley Creek), where they erupted in small volumes via fissure eruptions and subparallel to the Duke River fault (Skulski et al., 1991, 1992; Figs. 2.1 and 2.3), which hints at a genetic link between motion along the fault and magmatism (Skulski et al., 1991). Eruptive centers in these fields were active from 18.0 to ~10.0 Ma: St. Clare Creek from 18.0 – 10.0 Ma, Nines Creek from 15.5 – ~13.0 Ma, and Alsek from 13.5 – ~10.8 Ma (Skulski et al., 1992). While there was coeval magmatic activity in

these fields, they display a general southeastward younging trend (Skulski et al., 1992). Magmas from these fields are dominantly transitional, but stratigraphy reveal there are minor alkaline eruptions *before* the transitional magmas and minor calc-alkaline eruptions *after* the transitional magmas (Skulski et al., 1991). The occurrence of all three of these magma types in the same locality, and the sequence of their eruptions, has been interpreted as adiabatic melting of heterogeneous mantle (e.g., continental lithosphere and asthenosphere) triggered by extension and strike-slip motion (i.e., transtention) across the Duke River fault to generate alkaline then transitional magmas. This was followed by interaction with the edge of the active WA to generate calc-alkaline magmas that are chemically transitional between arc and intraplate tectonic settings (Skulski et al., 1991; Thorkelson et al., 2011).

Transitional-tholeiitic magmas in the WA were generated by localized intra-arc extension that formed basins in the western and central WA (Preece and Hart, 2004; Trop et al., 2012). Most transitional tholeiitic magmas are found in the younger western WA (Preece and Hart, 2004) and central WA (Trop et al., 2012; Berkelhammer, 2017). Basin development and accompanying magmatism—some of which was transitional tholeiitic in nature—has occurred in phases throughout the history of the WA. The earliest known transitional tholeiitic magmas associated with basin development are found in the Sonya Creek volcanic field, located on the northern flanks of the central WA (Fig. 2.1). The formation of these magmas began by ~23.0 Ma and continued to ~18.0 Ma (Berkelhammer, 2017). Additional tholeiitic magmas have been identified in the central WA, but they are south of the Sonya Creek center (Fig. 2.3) and younger: they began by ~12.5 – ~11.0 Ma and continued until ~5.3 Ma in some parts of the central WA (Trop et al., 2012) and to ~2.5 Ma in other central WA locations (Eucher Mountain, Fig. 1.1; Keast et al., 2016). The same processes acted over at least the last ~1.0 Ma in the western WA (Preece and Hart, 2004). The presence of transitional tholeiitic magmas is indicative of intra-arc basin development in areas of both the central and western WA.

Adakitic magmas have been identified in a variety of localities around the world and, in some occurrences, are indicative of basaltic slab melts (orogenic adakites; Martin et al., 2005). In other instances, more complex processes are thought to be responsible for the formation of so-called anorogenic adakites (Martin et al., 2005). Adakitic magmas have been documented in the central and western WA and have been interpreted as the products of partial melting of the subducting slab (Preece and Hart, 2004), thereby qualifying them as orogenic adakites. A

variety of tectonic settings can generate partial slab melts and adakites, including, but not limited to, subduction initiation (Sajona et al., 1993) or termination (Sajona et al., 1996), highly oblique subduction (Yogodzinski et al., 1995), shallow or stalled subduction (Beate et al., 2001; Bourdon et al., 2002; Gutscher at al., 2000), and breaking or tearing of the subducting slab (Calmus et al., 2003; Thorkelson and Breitsprecher, 2005; Yogodzinski et al., 2001). Adakitic magmas are geochemically recognized based on specific trace element criteria initially set forth by Kay (1978) and later modified by Defant and Drummond (1990). These criteria include intermediate to high-silica (≥ 56 wt. %), high Sr (>~300 ppm), low Y (<~10 ppm), high Sr/Y (>~20 ppm), and high La/Yb (>~20 ppm).

Adakitic magmas have been documented in the central WA at Mt. Churchill (<~10 ka) and in the western WA at Mt. Drum (0.7 – 0.2 Ma; Fig. 1.1) and were derived from partial melting of the subducting Yakutat microplate (Preece and Hart, 2004; Preece et al., 2014). The locations of these adakitic magmas are of particular interest because they appear above edges of the Yakutat microplate (Preece and Hart, 2004; Bauer et al., 2014), which suggests these magmas were generated by partial melting of the Yakutat microplate edge (Preece and Hart, 2004).

Although the geochemical data collected for this study include most of the necessary parameters to identify adakites, we lack Yb concentrations and, will, therefore, refer to our samples as "adakite-like", where appropriate. Additionally, given what is known about tectonic settings that can form adakites (see references above) and the tectonics of the WA, tectonic constraints can also be considered in conjunction with geochemical data to aid in the designation of an adakite-like magma when geochemical data are lacking.

In summary, Wrangell magmatism has been continuously active since ~29.0 Ma and continues to essentially present-day (Trop et al., 2017; Davis et al., 2017; this study; Fig. 2.5). Magmatism in the central and western WA first migrated southward and then northwestward through time (Richter et al., 1990; Brueseke et al., 2015; Trop et al., 2017) and magmatism in the eastern WA has migrated generally southeastward but with much coeval magmatic activity among volcanic fields there (Skulski et al., 1991, 1992; Figs. 2.1 and 2.3). Eruption of calc-alkaline magmas marked the inception of the arc at ~29.0 Ma and magmas with these compositions have spanned the arc's lifetime (Richter et al., 1990; Trop et al., 2017; this study). Calc-alkaline magmas erupted contemporaneously with all other magma types in the WA.

Minor alkaline magmas erupted in the eastern WA from brief and discrete fissural eruptions sometime during the span from 18.0 – 10.0 Ma (Skulski et al., 1991, 1992). Tholeiitic magmas mark a period of extension and basin development from ~23.0 Ma to ~18.0 Ma and ~12.5 Ma to ~1.0 Ma in the central and western WA (Trop et al., 2012; Preece and Hart, 2004; Berkelhammer, 2017). Adakitic-like rocks are found in the western and central WA and are temporally restricted to early arc magmatism, ~29.0 – ~20.0 Ma (Berkelhammer, 2017; Weber et al., 2017; this study) or late arc magmatism (<5.0 Ma; Preece and Hart, 2004; this study; Fig. 2.5).

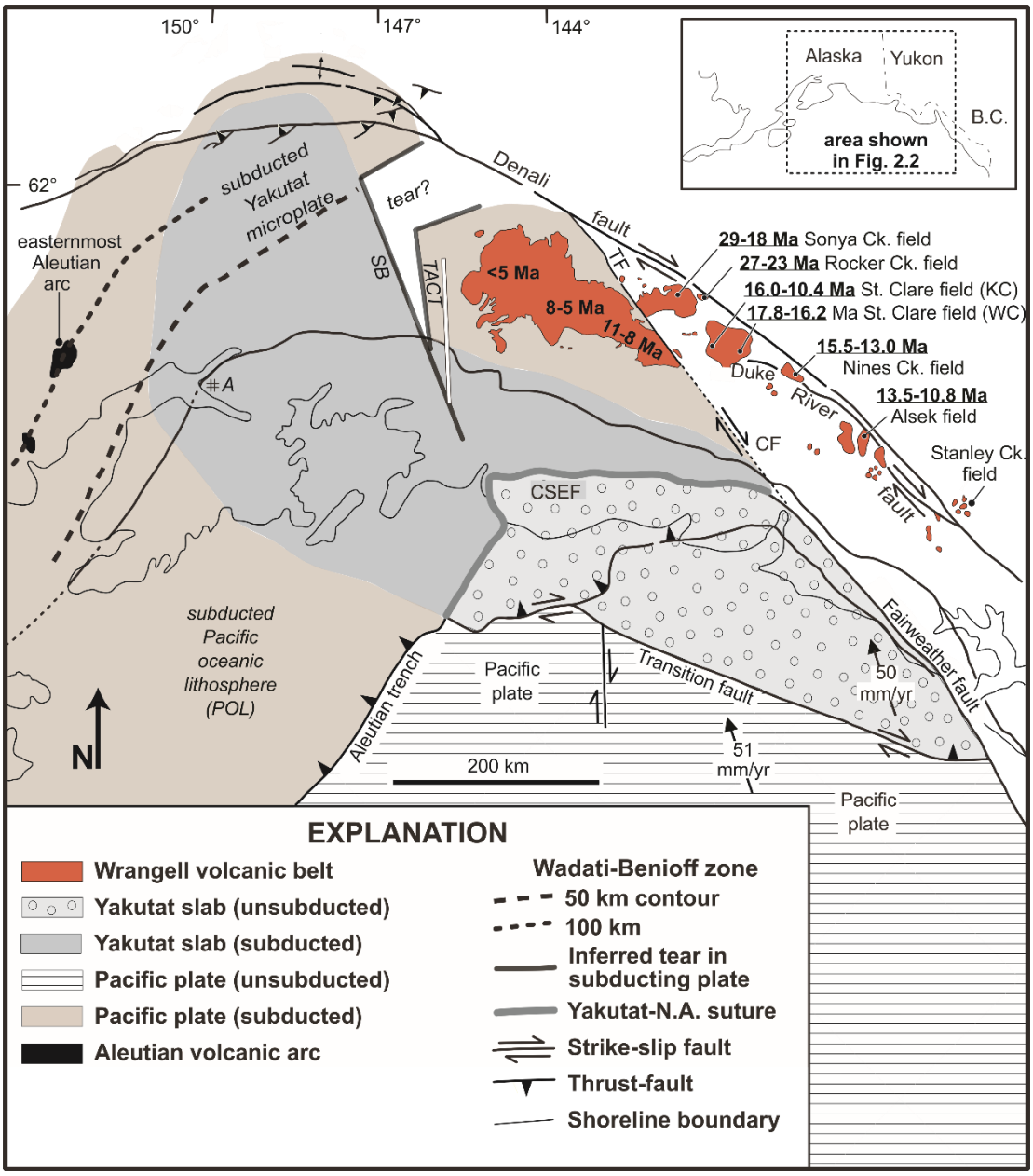

Figure 2.1 Map showing the regional tectonics of south-central Alaska and western Canada. Tectonic regimes transition from west to east: "normal" Aleutian subduction transitions to strike-slip faulting (Denali and Totschunda faults) to create an arc-transform junction. Note the ages of magmatism along strike-slip faults (Duke River). TF = Totschunda fault; CF = inferred Fairweather-Totschunda connecting fault; CSEF = Chugach-Saint Elias fault; SB = seismic anomaly that defines the eastern boundary of the subducted Yakutat slab; TACT = Trans-Alaska Crustal Transect (geophysical survey that aids in defining crustal structure along western edge of WA). Adapted from Trop et al., 2012.

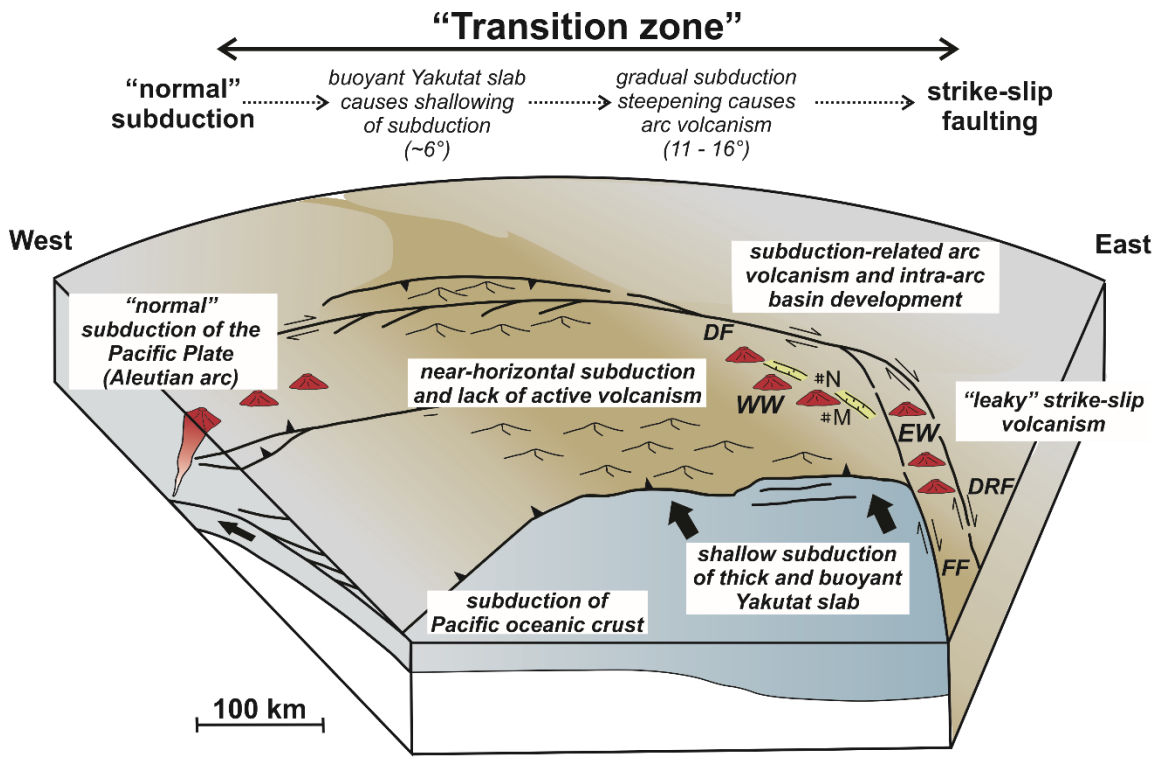

Figure 2.2 Schematic diagram reiterating the transition zone concept. In the western portion of this transition zone, the Pacific Plate is subducting "normally" and is reflected by the presence of the Aleutian arc. In the central portion, the Yakutat slab is causing near-horizontal subduction which is reflected by the lack of active magmatism in the region. The western portion of this transition zone is associated with Wrangell arc and leaky strike-slip magmatism caused by a gradual subduction steeping and the interaction between the subducting Yakutat and major strike-slip faults. WW = Western Wrangell arc; DF = Denali fault; EW = Eastern Wrangell arc; DRF= Duke River fault; FF = Fairweather fault; N = Nabesna, AK; M = McCarthy, AK. Figure adapted from Kortyna et al., 2014).

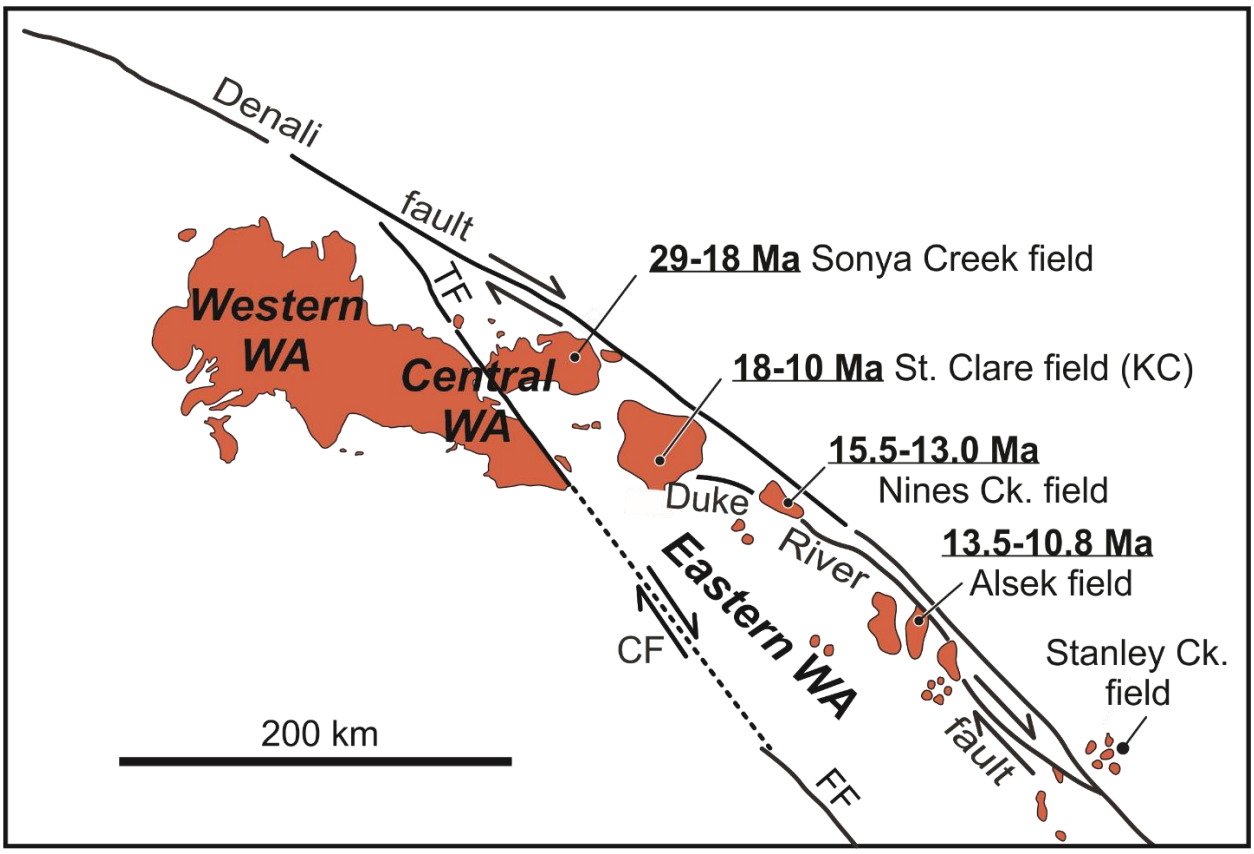

Figure 2.3 Map showing the loosely defined western, central, and eastern regions of the Wrangell arc. These regions are generally informal and there is in fact overlap between the western and central regions. However, the eastern region is distinct from the other two and there is no ambiguity as to its boundaries. These differences are reinforced by the chemistries observed from each region. Chemistries in the western and central WA are similar and reveal a dominant subduction signature (calc-alkaline) while chemistries from the eastern WA display characteristics of both subduction and "leaky" strike-slip (alkaline) processes (Skulski et al., 1991; 1992). TF = Totschunda fault; CF = inferred Fairweather-Totschunda connecting fault; FF = Fairweather fault. Figure adapted from Trop et al., 2012.

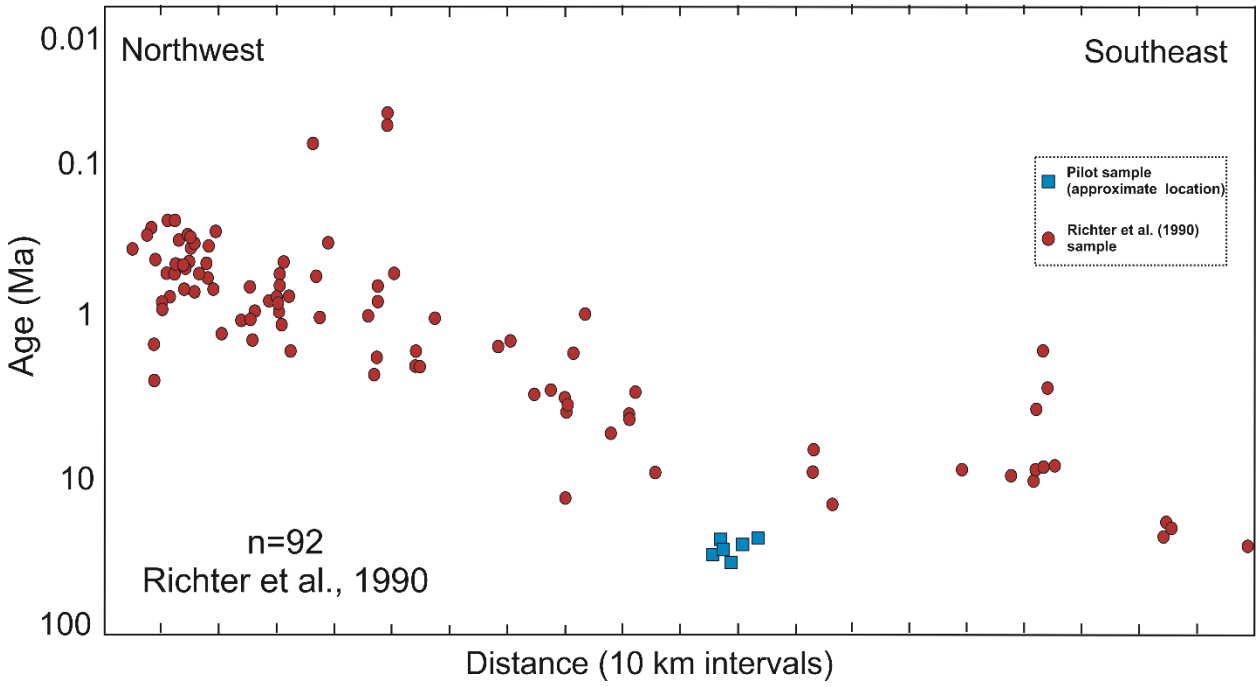

Figure 2.4 Distance versus age plot using data from Richter et al., (1990) that reveal a northwestward migration of magmatism through time. Ages are projected to line A-A' (which trends N70°W through the WA) in Figure 2 from Richter et al. (1990), which is interpreted as the main axis of the arc.

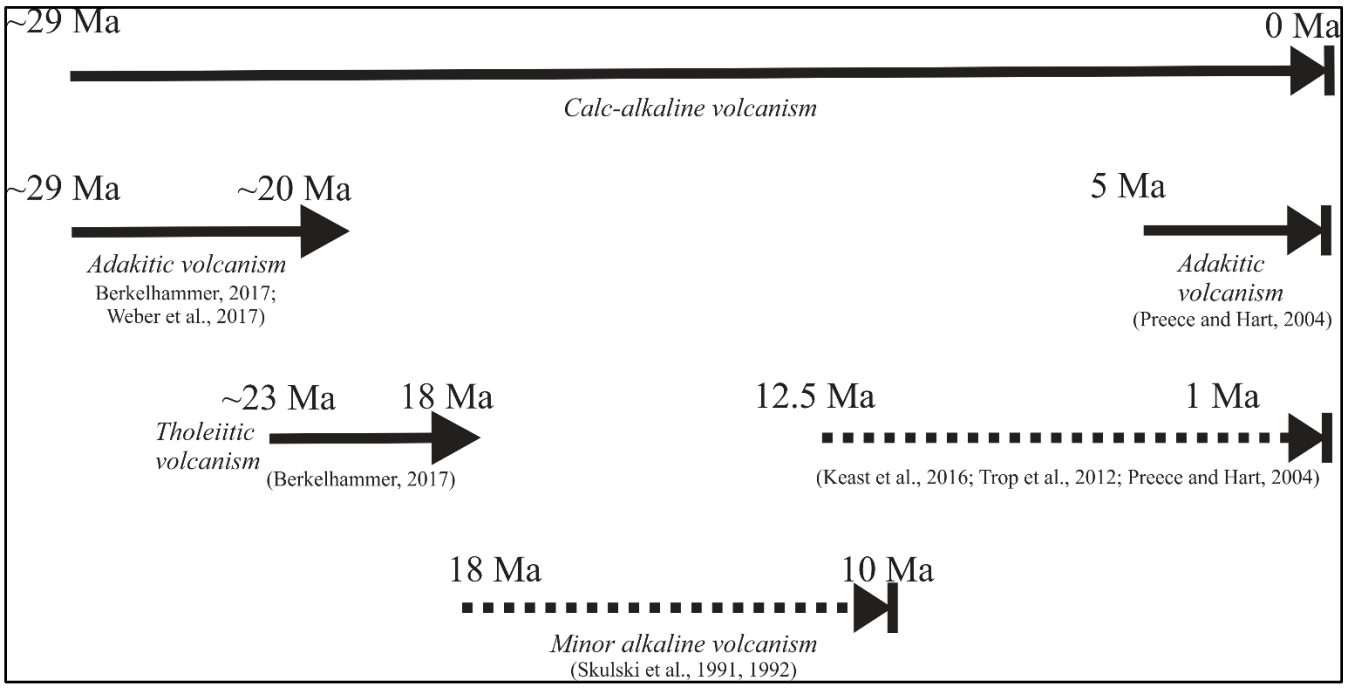

Figure 2.5 Generalized geochemical timeline of the entire Wrangell arc showing when geochemistries have been documented in the bedrock. Calc-alkaline chemistries span the entire life of the arc, beginning of ~29.0 Ma. Adakitic chemistries are documented during

early (~29.0 – ~20.0 Ma) and late (<5 Ma) arc phases. Dashed lines indicate discontinuous or small volume magmatic events. Transitional-tholeiitic occurrences have been documented from ~23.0 – 18.0 Ma and during discrete periods between ~12.5 to present. Small volume alkaline magmatism has only been documented during 18.0 – 10.0 Ma in the eastern WA (Skulski et al., 1991, 1992).

Chapter 3 - Methods

For this study, igneous cobbles were collected from rivers draining the WA, analyzed for major and trace elements using X-ray fluorescence spectroscopy (XRF), and dated using $^{40}Ar/^{39}Ar$ single-grain fusion analyses on all samples, and $^{40}Ar/^{39}Ar$ step-heat analyses on a subset of six samples. Sample preparation and hand sample petrography were done at Kansas State University (KSU), XRF analyses occurred at Franklin and Marshall College, and $^{40}Ar/^{39}Ar$ analyses were performed by Drs. Jeffrey Benowitz and Paul Layer at the Geochronology Facility at the University of Alaska-Fairbanks (UAF).

Field Methods

Cobble-sized samples were collected by Drs. Matt Brueseke, Jeff Trop, and Jeff Benowitz from 17 modern rivers that surround and drain the WA over the course of two field seasons, summer 2015 and summer 2016. These rivers are: Boulder, Chetaslina, Chisana, Chitistone, Copper, Cross Creek, Dadina, Hawkins, Kotsina, Kuskulana, Nabesna, Nizina, Root, Sanford, and White (Fig. 3.1). A brief petrological survey was done upon arrival at each collection site to determine the variety of lithologies present at the site (Fig. 3.2) and only the freshest of those lithologies were collected. In some cases, collection sites were strategically chosen downstream of major river confluences to capture tributary input. Access to field sites was by plane and/or helicopter, so limitations to the collection procedure included locating a suitable landing site and limiting total sample weight. Individual samples were split into multiple fragments by hammer at UAF and roughly half of those fragments were kept at UAF for geochronology analyses. The remaining fragments of each sample were shipped to Kansas State University (KSU) to be prepared for XRF analyses.

Sample Preparation

Upon arrival at KSU, samples were initially split into roughly golf ball-sized pieces using a RockLabs Hydraulic Press with tungsten jaws. Once split, samples were inspected for extent of secondary alteration. Those with any primary mineral replacement, pervasive groundmass alteration, or vesicle/cavity-fill were discarded (Fig. 3.3, 3.4, 3.5). The remaining samples had

weathering surfaces that were removed by either grinding the surface off using a sandpaper wheel, utilizing a tile saw with a diamond-tipped blade, or by a combination of the two. Most weathering surfaces were removed by grinding the rock against a 60 grit, 8" silicon carbide (sandpaper) disk on a grinding wheel. However, if the weathering surface was found to be particularly thick and wouldn't easily grind, the tile saw was used to cut off the altered portion from the sample. The areas that were cut were also ground to remove any possibility of contamination from the saw blade. All samples were then washed with deionized water, scrubbed using a standard toothbrush, and allowed to dry completely. Once dry, the samples were coarsely crushed into pea-sized pieces using the crushing plates attachment of the RockLabs Hydraulic Press. Coarsely crushed samples were randomized using the cone-and-quarter method, taking care to keep all surfaces clean and free of sample cross-contamination. Each sample was eventually powdered by placing roughly 20 mL of each coarsely crushed sample in a Spec Industries Shatterbox machine with aluminum oxide ring and puck pulverizer. The samples were set to run for exactly eight minutes in the Shatterbox, which turned them into homogenous powders. The powders were stored in glass vials that were double-labeled and shipped to Franklin and Marshall College for XRF analyses.

Analytical Methods

Geochemistry

XRF analyses of major and trace elements, as well as loss on ignition (LOI) values, were completed at Franklin and Marshall College following the method outlined in Mertzman (2000, 2015) and online at https://www.fandm.edu/earth-environment/laboratory-facilities/instrument-use-and-instructions. LOI values were measured for each sample by weighing out one-gram of powder then heating it at 950°C in a muffle furnace for 1.5 hours. The samples were then allowed to cool to room temperature and reweighed. The percent change in weight was reported as the LOI and generally represents how altered a sample has been by volatile constituents. Any analysis with LOI > 3.5 wt% was discarded from the major element dataset, but retained in both the trace element and age datasets (Trop et al., 2012). Twenty-one samples out of the original dataset of 236 had LOI > 3.5 wt%. Negative LOI values were also measured for some samples. Negative LOI values mean the sample gained more weight during the heating process due to the

oxidation of Fe^{2+} to Fe^{3+} than it lost from the release of volatile components (S. Mertzman, pers. comm.).

After LOI determinations, 0.4 grams of each rock powder was mixed with 3.6 grams of lithiumtetraborate and melted in a platinum crucible. This molten material was placed in a platinum disk-shaped casting dish and quenched to produce a glass disk that was used for major element XRF analyses using a PANalytical 2404 ZRF vacuum spectrometer equipped with a 4kW Rh X-ray tube. Major elements are reported as weight percent oxide (SiO_2, TiO_2, Al_2O_3, Fe_2O_3, MnO, MgO, CaO, Na_2O, K_2O, and P_2O_5). Nineteen trace elements (Rb, Sr, Y, Zr, V, Ni, Cr, Nb, Ga, Cu Zn, Co, Ba, La, Ce, U, Th, Sc, Pb) were analyzed by using pressed powder briquettes that are made by mixing 7.0 grams of whole-rock powder and 1.4 grams of high purity Copolywax powder. Trace element concentrations are reported as parts per million (ppm). Iron analyzed for all the samples was initially reported as Fe_2O_{3total} and was split into FeO and Fe_2O_3 following LeMaitre (1976). All data presented here in diagrams and discussion have been normalized anhydrous.

$^{40}Ar/^{39}Ar$ Geochronology

All cobble samples were analyzed for $^{40}Ar/^{39}Ar$ ages at the University of Alaska Fairbanks Geochronology lab. Rock samples were crushed using a stainless-steel mortar and pestle, then sieved using 500-1000 micron sieves. Samples were then washed and sonically bathed in deionized water to remove and decant clay particles. Samples were then dried in an oven overnight at ~60 °C and then grains were hand-picked under an optical microscope to select phenocryst-free homogenous groundmass chips, hornblende, and biotite mineral separates. The monitor mineral TCR-2 with an age of 28.619 Ma (Renne et al, 2010) was used to monitor neutron flux and calculate the irradiation parameter (J) for all samples. The samples and standards were wrapped in aluminum foil and loaded into aluminum cans of 2.5 cm diameter and 6 cm height. Mineral separates were sent to the uranium enriched research reactor of McMaster University in Hamilton, Ontario, Canada and irradiated for 20 megawatt-hours. After irradiation, samples were loaded into 2mm diameter holes in a copper tray and loaded in an ultra-high vacuum extraction line. The monitors were fused, and samples heated, using a 6-watt argon-ion laser following the technique described in York et al. (1981), Layer et al. (1987), and Benowitz et al. (2014). Argon purification was achieved using a liquid nitrogen cold trap and a SAES Zr-

Al getter at 400° C. The samples were analyzed in a VG-3600 mass spectrometer. The argon isotopes measured were corrected for system blank and mass discrimination, as well as calcium, potassium, and chlorine interference reactions following procedures outlined in McDougall and Harrison (1999). Typical full-system 8 min laser blank values (in moles) were generally 2 x 10^{-18} mol ^{40}Ar, 3×10^{-18} mol ^{39}Ar, 9×10^{-18} mol ^{38}Ar, and 2×10^{-18} mol ^{36}Ar, which are 10 – 50 times smaller than the sample/standard volume fractions. Correction factors for nucleogenic interferences during irradiation were determined from irradiated CaF_2 and K_2SO_4 as follows: $(^{39}Ar/^{37}Ar)Ca = 7.06 \times 10^{-4}$, $(^{36}Ar/^{37}Ar)Ca = 2.79 \times 10^{-4}$ and $(^{40}Ar/^{39}Ar)K = 0.0297$. Mass discrimination was monitored by running calibrated air shots. The mass discrimination during these experiments was 0.8% per mass unit.

The majority of samples were analyzed as single-grain or multi-grain fusion analysis approach. We developed a procedure to limit the effects of alteration by degassing each sample at 0.5 watts for 60 seconds, and the released gas was not measured and pumped off for time efficiency and increased throughput. The results have a single-grain and/or multi-grain precision of 1%. Samples selected for further geochronology analysis were step-heated from relatively low temperatures until reaching fusion temperatures using the 6-watt argon-ion laser (Sliwinski et al, 2012).

Petrography

Each sample was assessed and given a hand sample description. The descriptions include a general compositional classification based on color (e.g., mafic/felsic); Figs. 3.6 and 3.7), textural descriptions (i.e., porphyritic-volcanic, porphyritic-plutonic, aphanitic, phaneritic, pyroclastic), and assessment of any identifiable mineral phases present. These descriptions are used to determine the relative proportions of volcanic (lavas) and plutonic (intrusions) cobbles in the dataset and to assess any relations between volcanic/plutonic rocks, geochemistry, and age. These descriptions are compiled in Appendix A and results with relation to geochemistry and geochronology are included in the Results section.

Watershed Map Creation

Geographic Information System (GIS) was used to delineate the watersheds and determine the percentage of ice and geologic units within the watersheds by Brian Moretti at Bucknell University. ArcMap by Esri is a computer program of Geographic Information System that was used to combine, analyze, and present spatial data. The data were projected with the NAD_1983_Alaska_Albers projection in Esri ArcMap Version 10.4.0.5524. Digital geologic maps and elevation maps utilized were publicly available through the U.S. Geological Survey (Richter et al., 2006; Wilson et al. 2015). Sample sites were plotted based on coordinates collected in the field using a handheld Global Positing System (GPS).

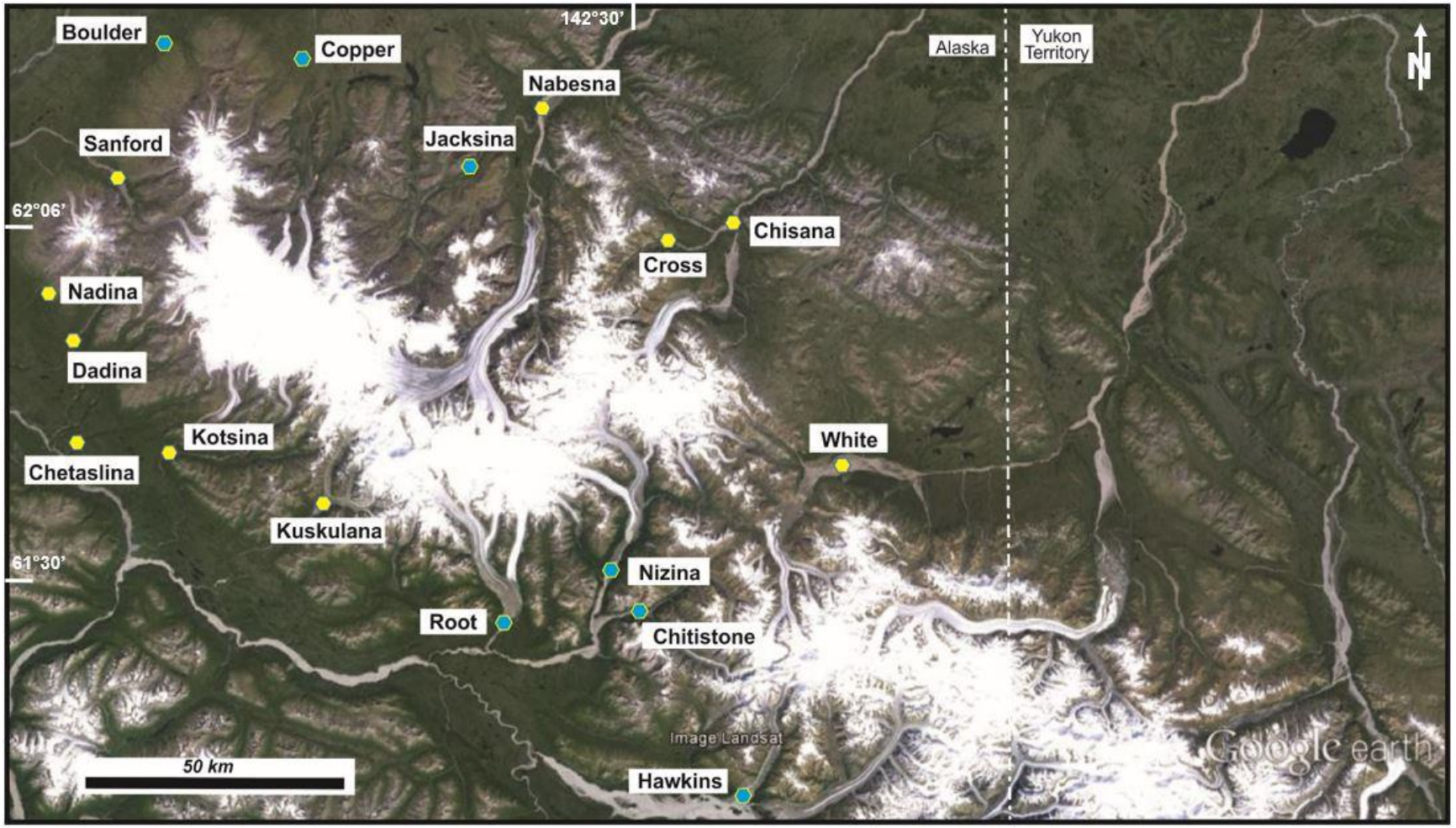

Figure 3.1 Satellite image showing the various collection sites. River names are labeled. Yellow hexagons are locations with geochemical data and ages; blue hexagons are locations with geochemical data but have not yet been dated.

Figure 3.2 An example of cobble diversity collected from one river (White River).

Figure 3.3 Discarded sample Che 1C-1 displays pervasive groundmass alteration and secondary vesicle fill (amygdules).

Figure 3.4 Discarded sample Cross 8 displays pervasive groundmass and primary mineral alteration/replacement.

Figure 3.5 Discarded sample Nabesna 9 displays bright yellow material lining the vesicles, suggesting heavy secondary alteration.

Figure 3.6 Sanford 6, an example of a mafic rock with porphyritic-volcanic texture from the dataset.

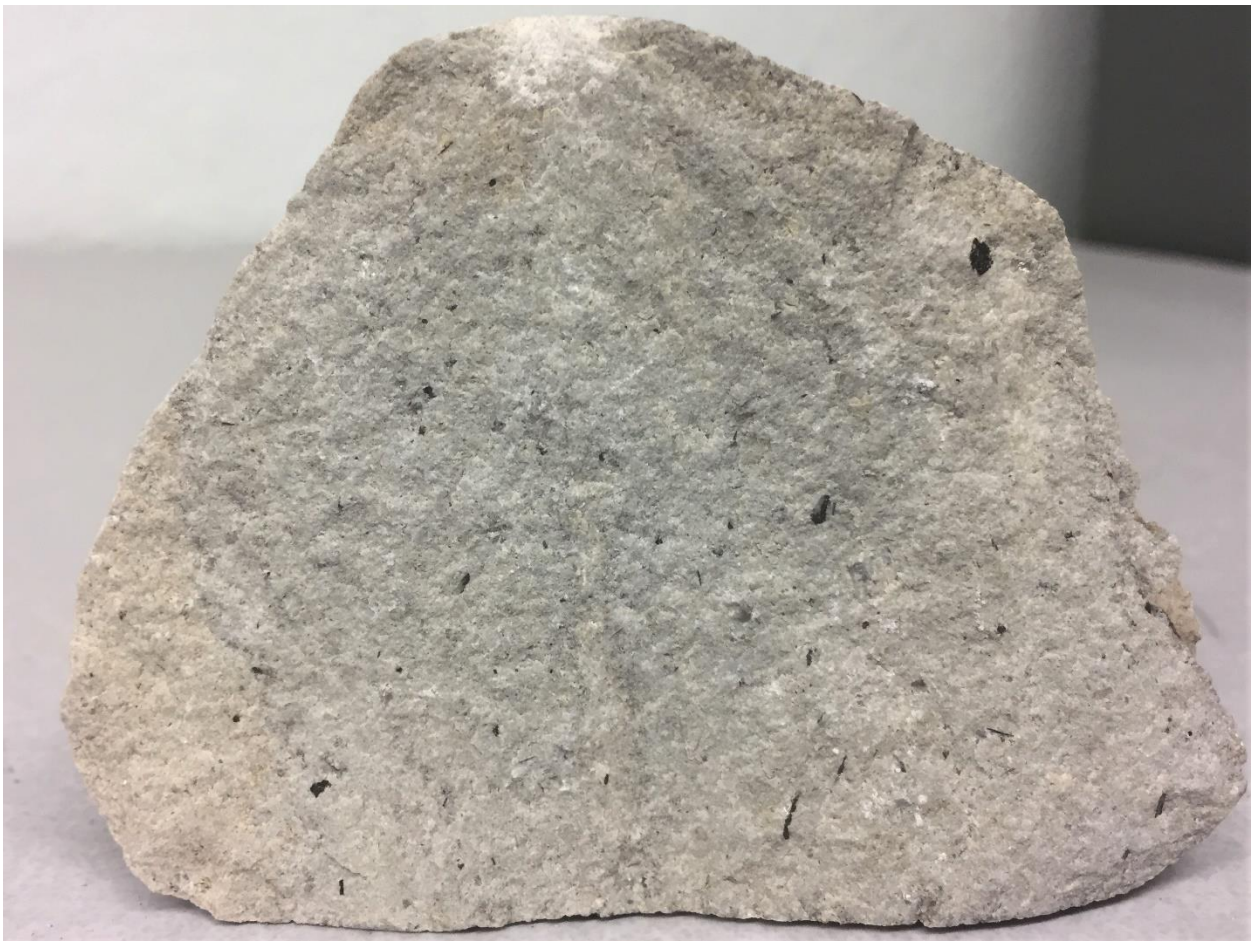

Figure 3.7 Dadina 1C-4, an example of a felsic rock with porphyritic-volcanic texture from the dataset.

Figure 3.8 White 14, an example of a rock with porphyritic-plutonic texture from this dataset.

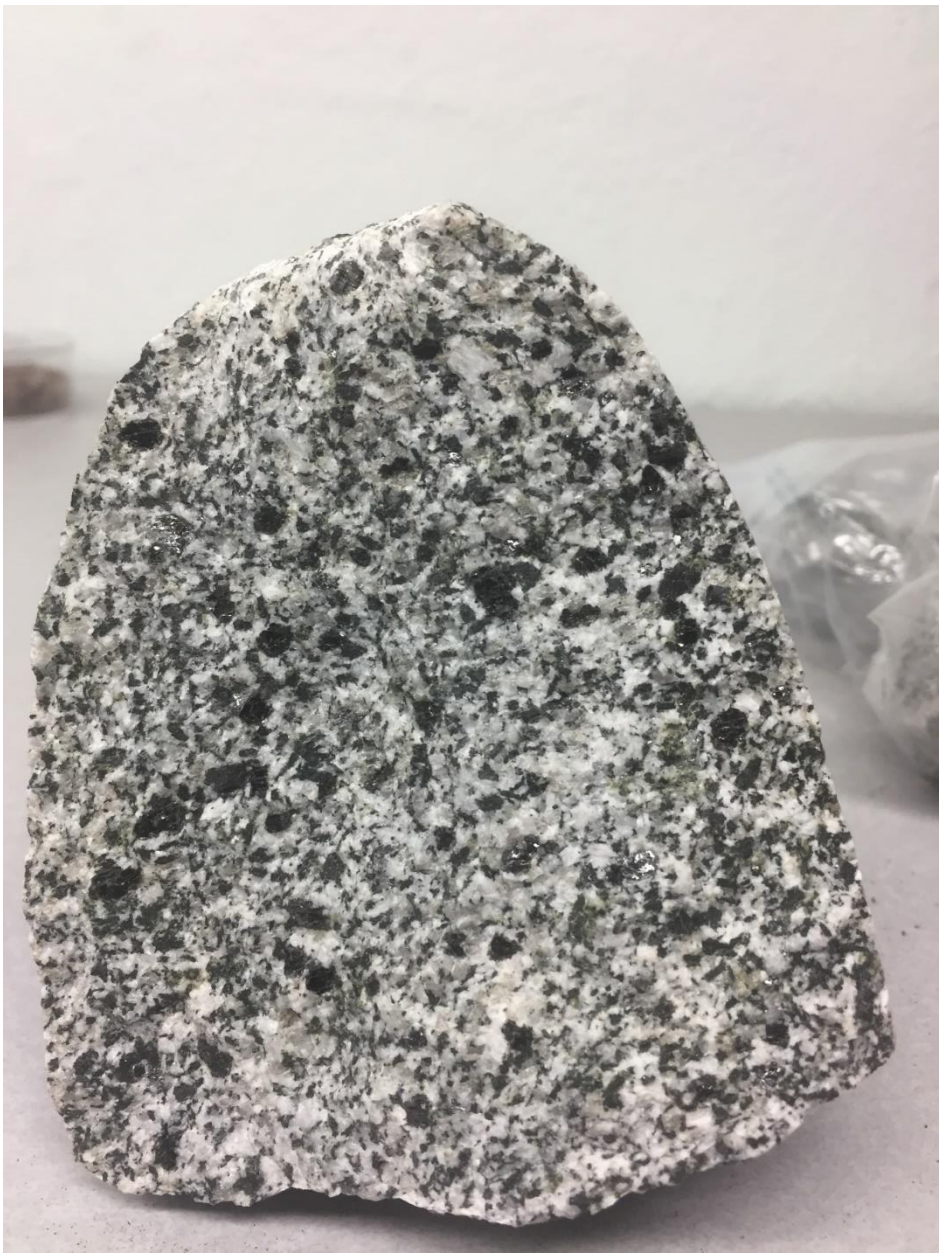

Figure 3.9 Chetaslina 1B-1, an example of a rock with phaneritic texture from our dataset.

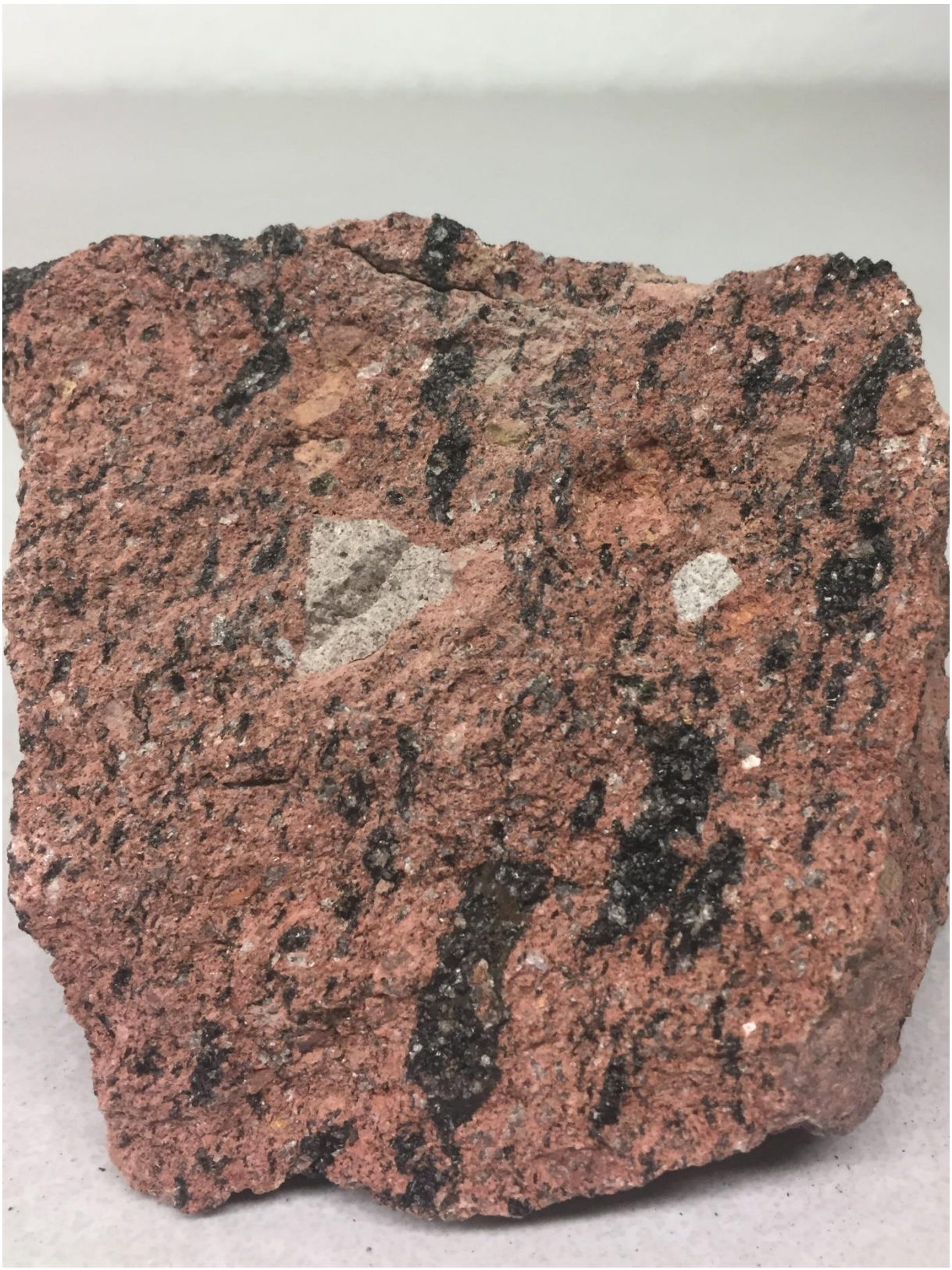

Figure 3.10 Chetaslina 1A-3, an example of a rock with pyroclastic texture from our dataset.

Figure 3.11 Chisana 6, another example of a rock with pyroclastic texture from our dataset.

Chapter 4 - Results

This study provides new major element data from 215 samples and trace element data from 236 samples collected from 17 major rivers that drain from the modern western and WA. This study also provides new age data from a total of 119 samples from 10 major rivers (Fig. 3.1). Geochemical analyses and ages of early arc samples (~28.0 Ma – ~19.0 Ma) are presented in Table 4.1. A complete list of samples and geochemical/age data is provided in Appendix B.

Geochronology

Sample ages in this dataset range from ~300 Ma to less than 1 Ma. Samples with ages greater than ~30.0 Ma are from older volcanic arcs (e.g., Talkeetna, Chitina, and Chisana arcs) and are reported in the dataset but are not considered to have implications for WA volcanism. Sixteen samples are too old to be associated with WA volcanism and one sample has a negative age, reducing the total number of WA ages to 102. WA-related samples range from ~28.0 Ma to less than 1.0 Ma, but a histogram of the results indicates that not all ages are equally represented (Fig. 4.1). There is one sample from the White River, White 14, which has an age of ~35.0 Ma. This age is questionable for analytical reasons (explained in "$^{40}Ar/^{39}Ar$ step-heating geochronology" section) and because no bedrock older than ~30.0 Ma has been documented in the WA. This ~35.0 Ma sample will be investigated further but, given doubts of its accuracy, cannot currently be considered the oldest cobble. Forty-seven of the samples in the dataset are younger than 1.0 Ma (Figs. 4.1 and 4.2) and come from rivers that drain the western WA, which is the youngest portion of the arc (Figs. 1.1, 2.1 and 2.4; Richter et al., 1990; Preece and Hart, 2004). There are no samples from ~17.0 – ~13.0 Ma in this entire dataset, however there are still 117 samples that are not dated. There are twelve samples in this dataset that range from ~28.0 – ~17.0 Ma, from the older central portion of the arc. The ~35.0 Ma sample, White 14, is questionable, but will be acknowledged as an early arc (~28.0 – ~17.0 Ma) sample without a definitive age for the time being. These early arc (~28.0 – ~17.0 Ma) samples are significant because they could indicate the onset of WA magmatism and the initiation of the arc. Table 4.2 summarizes all the relevant age data and possible bedrock sources drained by each river.

$^{40}Ar/^{39}Ar$ step-heating geochronology

A subset of six samples was dated using $^{40}Ar/^{39}Ar$ step-heating methodology. $^{40}Ar/^{39}Ar$ step-heat methodology can provide a more accurate age of initial cooling, because it can get around issues created by argon diffusion near grain boundaries and later heating events. The six samples dated using this methodology are: Nabesna 2, Nabesna 13, White 5, White 15, Chisana 2, and Chisana 11 (Table 4.1). The step-heated samples were selected based on the fact that A) The single-grain fusion $^{40}Ar/^{39}Ar$ ages of these samples ranged from ~30.0 – ~27.0 Ma and their geochemical characteristics suggested a slab melt component, and B) Theses samples had high atmospheric ^{40}Ar content (>50%), suggesting alteration. One the objectives of this work is to date the initiation of the WA and step-heating these samples, which have some of the oldest ages in the dataset at ~30.0 – ~27.0 Ma, could more accurately constrain the age of arc initiation. Furthermore, all six samples that were step-heated have geochemical characteristics consistent with slab melt, which suggests a possible link between arc initiation and the melting of the subducting Yakutat microplate. This link could have important tectonic implications for the initiation of WA magmatism. These reasons are why initial single-grain fusion ages with slab melt geochemistry were the first criterion used to choose samples for step-heats. Additionally, these six samples also had relatively high atmospheric ^{40}Ar content (>50%), suggesting they are some of the most altered samples in the dataset and their single-grain fusion ages are therefore questionable. This is why high atmospheric ^{40}Ar was the second criterion used to choose samples for step-heats.

Figure 4.3 shows the step-heat plateau ages provided by this method. Table 4.3 provides a summary of $^{40}Ar/^{39}Ar$ step-heat ages, with all ages quoted to the ±1 sigma level and calculated using the constants of Renne et al. (2010). The integrated age is the age given by the total gas measured and is equivalent to a potassium – argon (K-Ar) age. The age spectrum provides a plateau age if three or more consecutive gas fractions represent at least 50% of the total gas release and are within two standard deviations of each other (MSWD <2.5). For select samples, inverse isochron ages were calculated from an inverse isochron diagram of $^{36}Ar/^{40}Ar$ vs. $^{39}Ar/^{40}Ar$ ratios measured during each heating step (Roddick, 1978; Roddick, 1980; Benowitz et al, 2011). Table 4.4 presents the single-grain fusion ages and the step-heat ages of this subset for comparison between the two dating methods. Apart from sample White 15, the plateau ages are generally younger than the initial single-grain fusion ages. However, this does not mean that all

single-grain fusion ages in the dataset are unreliable given the criteria for choosing samples to step-heat that is outlined above. White 15 was step-heated in error (White 14, with the oldest age in the cobble dataset at 34.58 ± 0.47 Ma, was supposed to be dated with step-heat methodology but was not) and is a relatively young sample at 10.4 ± 0.3 Ma compared to the rest of the step-heated samples (Fig. 4.3; Tables 4.3 and 4.4). The age of White 15 remains essentially constant between the two dating methods (Table 4.4). It is also the only step-heated sample that released 100% of its Ar and exhibits the flattest plateau of the six step-heated samples (Fig. 4.3). Given that White 15 is at least 10 m.y. younger than the rest of the step-heated samples and the quality of its plateau, it is possible that the other samples were affected by alteration processes because they have been on the earth's surface for at least 10 m.y. longer. The single grain fusion age determination for White 14 produced the oldest age in the cobble dataset at 34.58 ± 0.47 Ma. This age is discounted based on the high atmospheric ^{40}Ar content of the gas release (>50%) for this sample, indicating possible alteration, and the fact that there is no WA bedrock dated older than ~30.0 Ma. We assign White 14 to the oldest group of samples (~28.0 Ma to ~17.0 Ma) given A) The step-heat results confirm no to limited excess ^{40}Ar in the cobbles, and B) The step-heat results also demonstrate that a similar aged cobble with similar ^{40}Ar atmospheric content (White 5) falls in this age category.

Petrographic Classification

Hand sample descriptions offer five distinct textural groups: aphanitic, phaneritic, porphyritic-volcanic, porphyritic-plutonic, and pyroclastic. A majority of samples have porphyritic-volcanic texture (123), followed by porphyritic-plutonic (54), phaneritic (36), aphanitic (16), and pyroclastic (7). These petrographic descriptions show that extrusive (porphyritic-volcanic and aphanitic) cobbles are the majority, whereas intrusive (phaneritic and porphyritic-plutonic) and pyroclastic cobbles are minority. Extrusive and intrusive rocks occur across the entire arc, but pyroclastic rocks, indicative of explosive eruptions, are seen in only limited locations in both the western and central WA (Sanford, Chetaslina, Nizina, and Chisana Rivers; Fig. 4.4). Notably, all early arc (~28.0 – ~17.0 Ma) cobbles are intrusive but younger cobbles (<5.0 Ma) are generally extrusive. Pyroclastic rocks are only associated with distinct ages or age groups: ~7.0 – 6.0 Ma, ~1.7 Ma, and ~1.0 Ma.

Geochemistry

Approach to sample classification

Data here are presented in spatial and temporal contexts to parse both spatial and temporal variations throughout the WA. The age divisions are based on age groupings observed from this new dataset but not necessarily on significant intervals of time throughout the history of the WA. Each dated sample has been assigned to one of the following age groups: ~28.0 – 17.0 Ma, 17.0 – 13.0 Ma, 13.0 – 8.0 Ma, 8.0 – 5.0 Ma, 5.0 – 3.0 Ma, 3.0 – 1.0 Ma, and <1.0 Ma. Samples over ~28.0 Ma are excluded on the basis that they precede WA magmatism. Additionally, over half of the dataset has not yet been dated but has geochemical data; these samples are included in these plots and coded as "No age." The spatial divisions are determined primarily based on the location and spatial extent of each river's drainage on a watershed map (Fig. 4.5). As a secondary qualification, the age range of cobbles in this dataset drained from each river is considered since the western WA is known to be the youngest region in the WA at <5.0 Ma (Figs. 1.1, 2.1, and 2.4; Preece and Hart, 2004). The spatial divisions assigned are western WA, central WA, and both. Rivers assigned to the western WA category drain bedrock from the western WA, rivers assigned to the central WA category drain bedrock from the central WA, and rivers assigned both drain bedrock in both the western and central WA. All western WA rivers drain bedrock that is <5.0 Ma, all central WA rivers drain bedrock that is >5.0 Ma, and rivers that drain both have no age cutoff. Table 4.5 shows which spatial category each river drainage belongs to. Note the only rivers assigned to the both category are the Nabesna and Jacksina Rivers. The watershed of the Nabesna River is so large that it captures both western and central WA bedrock and the Jacksina River is a tributary. The plots coded by age directly show geochemical variations through time, but the spatially coded plots inherently contain a rough aspect of time as well, given that the central WA is older than the western WA. Therefore, spatially coded plots show some broad temporal variations in addition to spatial variations.

Geochemical classification

On the total alkalis versus silica (TAS) diagram of LeBas et al. (1989), dated WA eruptive products plot as subalkaline to transitional and range from basaltic (trachy) andesite to rhyolite (Figs. 4.6 and 4.7). There is a larger compositional range of eruptive products from the central WA than from the western WA (Fig. 4.7). Note that some samples plot outside this

geochemical range (i.e., basaltic (trachy) andesite to rhyolite) on the TAS diagram, but their ages are unknown and therefore cannot be attributed to WA magmatism yet. A large proportion of the samples are andesite or dacite in composition. Of the andesites, most are classified as medium-K; they tend to be <1 Ma (Fig 4.8) and come from rivers that drain the western WA (Fig. 4.9). There are two high-K andesites from the central WA, one from the Chisana 18 and White 17, which are 8.02 ± 0.18 Ma and 10.84 ± 0.08 Ma, respectively (Figs. 4.8 and 4.9). There is one high-K andesite from the western WA, Sanford 14, which is 0.4 ± 0.05 Ma (Figs. 4.8 and 4.9). There are seven high-K andesites which are not yet dated (Fig. 4.8) and have drained from the western and central WA (Fig. 4.9).

In an AFM diagram, most WA rocks follow a calc-alkaline trend (Figs. 4.10 and 4.11). A few samples that have not yet been dated and come from rivers that drain the central WA (Fig. 4.11), plus one sample from the 13.0 – 8.0 Ma group (Fig. 4.10), may have tholeiitic characteristics. Upon petrographic inspection, this sample (White 6) has sparse amygdules filled with red alteration material that may be the cause for the higher FeO content and is likely petrogenetically insignificant.

These new data fit well with most existing WA geochemical data, apart from the alkaline samples observed in the Yukon (Skulski et al., 1991, 1992) from the eastern WA (Fig. 4.12). This is expected since our samples drained from only the western and central WA. Our new data overlap the compositions of WA rocks previously reported by Preece and Hart (2004) and Trop et al. (2012) (Fig. 4.13). Because of this overlap, the previous work of Preece and Hart (2004) will provide a framework for interpreting our new geochemical data (we chose Preece and Hart (2004) and not Trop et al. (2012) as our framework because Preece and Hart delve heavily into WA geochemical variations whereas Trop et al. (2012) focus more on tectonics). To utilize this framework, we divided our dataset into the three rock suites recognized by Preece and Hart (2004) using their criteria

- Trend 1: high TiO_2, transitional-tholeiitic
- Trend 2a: low TiO_2, calc-alkaline
- Trend 2b: low TiO_2, calc-alkaline, adakitic/adakite-like

According to the criteria set forth by Preece and Hart (2004), at SiO_2 contents less than 60 wt.%, all samples with TiO_2 > 1.15 wt. % are classified as Trend 1 whereas all samples with TiO_2 < 1.15 wt. % are classified as Trend 2 (Fig. 4.14a). The next step considers Y concentrations

throughout the dataset, not just at less than 60 wt. % SiO_2. Preece and Hart's (2004) data show a distinct branch in Y concentrations at SiO_2 > 60 wt. %: Trend 1 classification is extended to all samples with elevated Y concentrations (> ~30 ppm); samples with lower Y concentrations (< ~30 ppm) are classified as Trend 2 (Fig. 4.14b). Trend 2 is further subdivided based on two arrays of Y concentrations at SiO_2 > ~61 wt.%: the Trend 2a array is defined by relatively higher Y concentrations and Trend 2b by the relatively lower Y array (Fig. 4.14b). Trend 2b also has adakitic characteristics (Fig. 4.15). Although the geochemical data collected for this study include most of the necessary parameters to identify adakites (Sr, Y, La), we lack Yb concentrations and, will, therefore, refer to our samples as "adakite-like", where appropriate. Our new dataset includes samples that do not fit perfectly within the Preece and Hart (2004) classification scheme, but they do show similar trends: Trend 1 has elevated Y values relative to Trend 2 and Trend 2a has elevated Y values relative to 2b (Fig. 4.14b). Trend 1 and Trend 2a are generally contained in the andesite-dacite-rhyolite (ADR) field on a Sr/Y vs. Y plot whereas Trend 2b fall into the "adakite-like" field (Fig. 4.15).

Our data reveal an age-dependent bimodal clustering of adakite-like (Trend 2b) magmas: one group from ~28.0 – ~20.0 Ma and another group with ages <1.0 Ma. Adakites identified by Preece and Hart (2004) are all less than 1.0 Ma and spatially restricted to the edges of the subducting Yakutat. Our young adakite-like magmas align temporally with definitive adakites identified by Preece and Hart (2004), but our older adakite-like magmas are more ambiguous. They could indicate older slab melting during the arc's initiation that was previously unrecognized or they could be calc-alkaline rocks with high Sr and low Y for reasons other than slab melt input. The geochemical classification of our data according to the criteria of Preece and Hart (2004) will be explored further in the discussion about geochemical trends through time and space.

Major element geochemical characteristics

Major elements in the dataset show distinct temporal and spatial trends with increasing SiO_2 content. In general, as SiO_2 content increases, TiO_2, FeO*, MgO, and CaO decrease. Al_2O_3 and P_2O_5 first increase and then follow the same decreasing trend with higher SiO_2 content; Na_2O and K_2O both increase as SiO_2 increases (Figs. 4.16 and 4.17). Older WA rocks (~28.0 – ~17.0 Ma) cluster together and show little variability when compared to all other rocks younger than

~17.0 Ma (Fig. 4.16). It should be noted that the ~28.0 – ~17.0 Ma range spans the longest amount of time and has the fewest samples when compared to the number of samples in all other age divisions. This is not surprising given a volcanic arc often builds upon itself, leading to less exposure of older volcanic products with time.

In a spatial context, rocks from the central WA exhibit a larger range of all major element concentrations and are more geochemically diverse than rocks from the western WA (Fig. 4.17 and Table 4.6). Recall that rocks form the central WA are older than rocks from the western WA: the age range for central WA rocks is ~28.0 Ma – ~6.0 Ma whereas rocks from the western WA span ~5.0 – 0.0 Ma. However, given the clustering of the oldest WA samples (28.0 – 17.0 Ma) mentioned previously, it should be noted that rocks in this oldest group don't necessarily contribute to the observed geochemical diversity. Therefore, it can be inferred that, in general, rocks older than 5.0 Ma but less than 17.0 Ma show more geochemical diversity than rocks outside of this age range.

TiO_2 content in the central WA reaches a maximum of ~3 wt. % but only reaches a maximum of ~2 wt. % in the western WA (Fig. 4.16 and Table 4.6). Al_2O_3 in the central WA first increases then decreases with increasing SiO_2 content whereas Al_2O_3 content in the western WA shows only a decreasing array (Fig. 4.17). There is also a larger range of Al_2O_3 values in the central WA as opposed to the western WA (Table 4.6). The maximum FeO* (total iron as Fe^{2+}) content in the central WA is nearly 14 wt. % but only reaches ~9 wt. % in the western WA (Table 4.6). Similarly, the maximum MgO content in the central WA is ~13 wt. % as opposed to the maximum of ~7 wt. % in the western WA (Table 4.6). Na_2O values in the central WA show a rapid increase over a small range in SiO_2 (49 to 53 wt. %), then more gradually increase until there is a branching of this trend at about 70 wt. % SiO_2 (Fig. 4.17). In the western WA, Na_2O values gradually increase with increasing SiO_2 but there is a less distinct branch observed at ~70 wt. % SiO_2 (Fig. 4.17). K_2O values in the central and western WA show essentially the same trend, but the entire data range is constricted in the western WA compared to the central WA (Table 4.6).

Trace element geochemical characteristics

Trace elements also show distinct temporal and spatial trends with increasing SiO_2 content. In general, as SiO_2 content increases, Ni and Sc concentrations decrease whereas Ba

and La concentrations increase (Figs. 4.18 and 4.19). Other trace elements, e.g. Y, Zr, and Nb, are more scattered (Figs. 4.18 and 4.19). Sr shows first an increase and then a decrease with SiO_2 concentration (Figs. 4.18 and 4.19). Like major element trends, the oldest of the WA rocks (28 – 17 Ma) are generally clustered and show little variability when compared to rocks younger than 17 Ma, apart from a large spread of Ba concentrations (Fig. 4.18 and Table 4.7). Rocks younger than 5.0 Ma in this dataset generally show more distinct trends, with the exception of Sr, Zr, and La, which are more scattered (Fig. 4.18). Rocks ~13.0 – ~8.0 Ma show more scattering or completely different trends when compared to rocks that are less than 5 Ma (Fig. 4.18). Rocks greater than 5.0 Ma show generally higher Ba, La, Y, Zr, and Nb values at a given SiO_2 content than rocks younger than 5.0 Ma display. Note the grouping of young (<5.0 Ma) and old (28.0 – 17.0 Ma) at low Y concentrations for a given SiO_2 value and the reverse of this in Sr concentrations (Fig. 4.18). In a spatial context, rocks from the central WA generally span a larger range of all trace element concentrations than rocks from the western WA do (Fig. 4.19 and Table 4.7). Rocks from the western WA generally show tighter clustering (Fig. 4.19) and smaller ranges of trace element values than rocks from the central WA do (Table 4.7). Like the major elements, there appears to be more trace element diversity in rocks from the central WA as opposed to rocks from the western WA.

Trace element ratio plots

Trace element ratio plots (Figs. 4.20 – 4.25) are used to highlight variations through time and space that have tectonic implications because certain ratios can reveal the role of a subduction component (or lack of one) in the petrogenesis of WA magmas beyond whether a rock is calc-alkaline or tholeiitic (Borg et al., 1997). The x-axis variable on all of these plots is a Sr/P ratio normalized to primitive mantle, $(Sr/P)_n$. High $(Sr/P)_n$ ratios ($(Sr/P)_n > 5.5$) in primitive (i.e., MgO > 6.0 wt.%, Ni >100 ppm, and Cr >200 ppm) calc-alkaline rocks are indicators of considerable slab components because these ratios are generated by the melting of a MORB-source-like peridotite that is fluxed with slab-derived fluid (Borg et al., 1997). A high $(Sr/P)_n$ ratio in more evolved rocks (i.e., MgO < 6.0 wt.%) may reflect magma evolution processes and are not always indicative of fluid addition/subduction (Borg et al., 1997). There are four primitive (MgO > 6.0 wt.%, Ni >100 ppm, and Cr >200 ppm) samples out of the total dataset of 215 samples (samples with LOI > 3.5 wt.% are not included here because major elements are considered when qualifying a sample as primitive and P_2O_5 values are used in the calculation of

$(Sr/P)_n$ ratios). The four primitive samples drain from the Chetaslina (western WA), Jacksina (both), Hawkins (central WA), and Chitistone (central WA) rivers and have $(Sr/P)_n$ ratios that range from 0.5 – 3.2. Only the Chetaslina sample has an age, which is 0.35 ± 0.11 Ma. Nevertheless, both primitive and evolved samples are presented in these plots to show the geochemical variation between primitive and evolved rocks, but the primitive rocks are coded differently for reference (Figs. 4.20 – 4.25).

The ratios used on the y-axis of these plots are Ba/Nb, Nb/Zr, and Sr/Y, which are all good indicators of different tectonic processes. A high Ba/Nb ratio (> ~100; Pearce et al., 2005) highlights total subduction input because, while both Ba and Nb are incompatible, Ba is fluid mobile and released over a wide range of subduction temperatures, making it subduction mobile, (Pearce et al., 2005), but Nb is only mobilized in the hottest of melts, making it subduction immobile (Ryerson and Watson, 1987; Ayers and Watson, 1993; Brenan et al., 1994). High Nb/Zr ratios (> 0.135; Sun and McDonough, 1989) are associated with decompression melting of lithosphere and asthenosphere in intraplate environments (Thorkelson et al., 2011), because Nb and Zr are both incompatible elements, but Nb is slightly more incompatible meaning that it will increase more relative to Zr with small degrees of melting. A high Sr/Y (> ~20 ppm) ratio is indicative of garnet, hornblende, and clinopyroxene in the source of the melt, suggesting partial melting of the subducting slab is contributing to the magma (Kay, 1978; Defant and Drummond, 1990; Peacock et al., 1994; Rollinson and Martin, 2005; Martin et al., 2005; Castillo, 2012).

A Ba/Nb versus $(Sr/P)_n$ plot (Fig. 4.20) shows that the oldest WA rocks (28.0 – 17.0 Ma) and rocks <5.0 Ma generally have higher Ba/Nb and $(Sr/P)_n$ ratios than rocks in the 13.0 – 5.0 Ma age range and primitive samples, which are clustered at lower Ba/Nb and $(Sr/P)_n$ values (Fig. 4.20). The oldest (28.0 – 17.0 Ma) and youngest (<5.0 Ma) have Ba/Nb > 100 and $3 < (Sr/P)_n < 6$, whereas the 13.0 – 5.0 Ma range and primitive samples have Ba/Nb < 100 and $(Sr/P)_n$ < ~3. In a spatial context, western WA rocks generally have higher Ba/Nb (> 100) and $(Sr/P)_n$ (> ~3) ratios than central WA rocks, which are more clustered at Ba/Nb < 100 and $(Sr/P)_n$ < ~3 (Fig. 4.21).

A Nb/Zr versus $(Sr/P)_n$ shows that the oldest WA rocks (28.0 – 17.0 Ma) and rocks <5.0 Ma generally have higher $(Sr/P)_n$ (> 2.5) for a given Nb/Zr ratio than rocks in the 13.0 – 5.0 Ma age range and primitive samples (Fig. 4.22). The primitive samples (and some undated samples) have some of the highest Nb/Zr ratios in the dataset, but only reach a maximum of ~0.06 (Figs.

4.22 and 4.23, inset) and are not high enough (> 0.135; Sun and McDonough, 1989) to be considered indicative of an intraplate tectonic setting. In a spatial context, western WA rocks generally have lower Nb/Zr ratios and higher $(Sr/P)_n$ ratios than central WA rocks (Fig. 4.22). Central WA rocks are generally clustered at (Sr/P)n < 2.5 and Nb/Zr < 0.08 whereas western WA rocks show a greater spread of $(Sr/P)_n$ values (1 – ~4.8) over a relatively restricted range of Nb/Zr values (0.02 – 0.04). Primitive samples and rocks from the central WA show some of the highest Nb/Zr ratios in the dataset (Nb/Zr = ~0.05 – ~0.07), which occur at some of the lowest $(Sr/P)_n$ ratios, $(Sr/P)_n$ < 1.5 (Fig. 4.22). The one primitive sample draining from the western WA has the lowest Nb/Zr (0.05) out of all primitive samples (Fig. 4.22).

A Sr/Y versus $(Sr/P)_n$ plot shows that the oldest WA rocks (28.0 – 17.0 Ma) and rocks <5.0 Ma generally have higher $(Sr/P)_n$ and higher Sr/Y ratios than rocks in the 13.0 – 5.0 Ma age range and primitive samples (Fig. 4.24). Most primitive samples and rocks aged 13.0 – 5.0 Ma are clustered at the lowest Sr/Y and $(Sr/P)_n$ ratios in the dataset: $(Sr/P)_n$ < 3 and Sr/Y < ~25 (Fig. 4.24). The oldest (28.0 – 17.0 Ma) and youngest (<5.0 Ma) samples show a larger spread of $(Sr/P)_n$ values (3 – 7) and Sr/Y values (25 – 150) across the dataset (Fig. 4.24). Rocks collected from rivers draining the central WA show a distinct cluster at low Sr/Y (< 25) and $(Sr/P)_n$ (< 3) ratios whereas rocks from the western WA display a larger spread of values: $(Sr/P)_n$ values = 3 – 7 and Sr/Y values = 25 – 150 (Fig. 4.25 and inset.)

In summary, these plots show similar characteristics for the oldest (28.0 – 17.0 Ma) and youngest (<5.0 Ma) rocks in the dataset and these arrays contrast with primitive and intermediately-aged (13.0 – 5.0 Ma) rocks (Figs. 4.20 – 4.25). These oldest (28.0 – 17.0 Ma) and youngest (< 5.0 Ma) samples have a subduction signature (Ba/Nb > 100) while intermediately-aged (13.0 – 5.0 Ma) samples typically have less of a subduction signature (Ba/Nb < 100), although not necessarily an intraplate signature (Nb/Zr values are well below 0.135; Figs. 4.22 and 4.23, and inset). Notably, these intermediately-aged (13.0 – 5.0 Ma) samples drain from the central WA, which may explain the spatial observations: rocks from the western WA tend to follow similar arrays between plots—and similar to the oldest and youngest WA rocks—and generally contrast with rocks from the central WA—and intermediately-aged rocks (Figs. 4.21, 4.23, and 4.25). It should be noted that rocks from the western WA tend to be younger than rocks from the central WA, which could be responsible for the continuation of

arrays between age and space. The tectonic implications of these trace element ratios through time and space will be further explored in the discussion.

Table 4.1 Raw geochemical data of early WA rocks, aged ~28.0 - ~19.0 Ma

Sample	Nabesna 4	**Chisana 11**	**Chisana 2**	Nabesna 14	**White 5**	**Nabesna 2**	Chisana 3	Cross 7	**Nabesna 13**	White 14
Age (Ma)	19.21±0.22	**20.6±0.5**	**22.9±0.4**	22.63±0.28	**23.5±0.7**	**23.9±0.4**	25.12±0.26	26.6±0.31	**27.7±0.2**	~~34.58±0.7~~
SiO_2	66.63	67.82	67.83	63.73	65.94	55.46	65.07	67.42	66.59	66.39
TiO_2	0.36	0.33	0.31	0.44	0.34	0.51	0.46	0.39	0.37	0.33
Al_2O_3	16.82	16.3	16.44	17.65	16.56	15.79	17.15	16.41	16.84	16.62
Fe_2O_3	3.74	3.05	2.98	4.49	3.51	8.04	3.97	3.09	3.15	3.37
MnO	0.09	0.06	0.06	0.11	0.08	0.13	0.10	0.07	0.08	0.07
MgO	1.73	1.8	1.80	2.64	2.54	6.27	1.76	2.29	1.78	2.27
CaO	4.47	2.75	3.48	4.34	4.43	8.74	4.22	4.37	4.27	4.36
Na_2O	4.63	6.08	5.61	5.2	5.24	3.68	5.07	4.62	4.91	5.20
K_2O	1.27	1.42	1.03	1.01	0.90	0.55	1.73	1.18	1.64	0.97
P_2O_5	0.15	0.13	0.13	0.22	0.13	0.28	0.24	0.15	0.18	0.13
LOI	2.05	1.33	1.22	2.18	1.29	0.97	1.52	3.49	1.24	2.44
Total	99.89	99.74	99.67	99.83	99.67	99.45	99.77	99.99	99.81	99.71
Rb	25.0	31.1	18.3	16.1	24.0	12.1	37.6	26.9	39.0	26.2
Sr	649	733	752	878	648	872	905	665	750	710
Y	11.4	8.6	8.4	14.6	11.2	15.2	12.9	10.5	9.8	9.5
Zr	94	109	137	99	93	70	147	115	124	103
V	72	67	71	96	82	195	73	64	64	74
Ni	13	26	29	29	47	82	12	46	15	35
Cr	16	47	51	24	88	70	18	54	26	51
Nb	2.1	2.3	1.0	1.5	2.5	0.7	10.6	5.6	5.7	2.4
Ga	20.2	19.4	19.6	21.4	20.3	17.0	20.8	19.6	20.2	20.1
Cu	31	49	18	37	13	89	17	28	18	12
Zn	65	34	27	75	46	91	57	48	55	44
Co	4	5	4	9	8	29	6	5	2	7
Ba	578	1845	994	404	522	308	1014	719	909	545
La	21	18	19	16	13	19	29	18	25	12
Ce	27	27	28	29	20	32	48	23	42	18
U	<0.5	<0.5	0.5	<0.5	<0.5	<0.5	1.2	<0.5	0.7	<0.5
Th	<0.5	0.5	0.5	<0.5	1.3	<0.5	1.6	0.6	0.5	1.6
Sc	5	4	4	9	9	23	3	4	4	7
Pb	8	3	3	6	2	<1	5	16	7	1

Note: All major element data expressed as raw weight % oxides; all other concentrations in ppm. Sample names in bold had additional step-heats performed on them to more accurately constrain their age. The strikethrough the age of White 14 indicates the age is questionable.

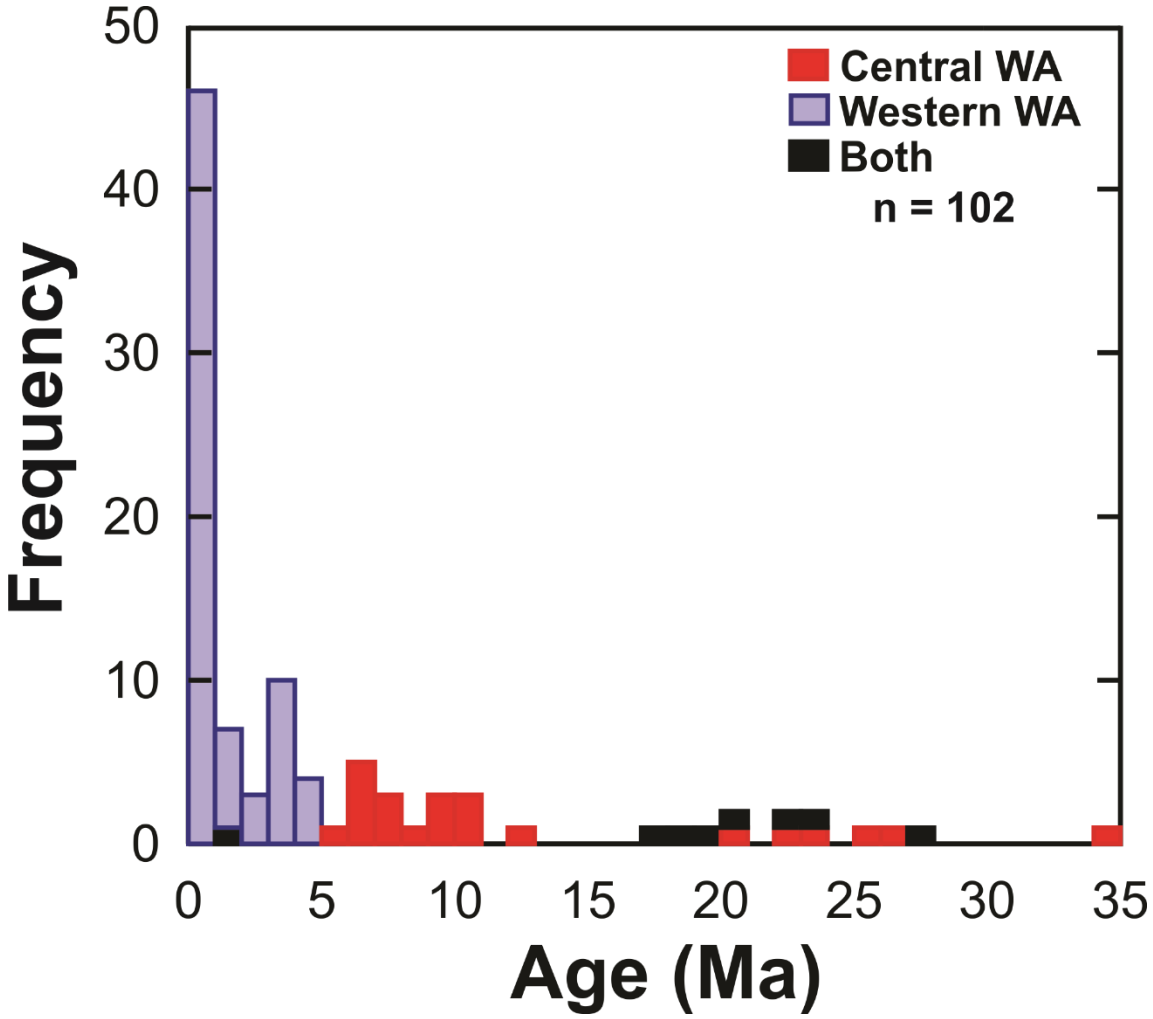

Figure 4.1 Histogram of WA-related cobble ages showing the distribution of sample ages. Colors are indicative of the approximate location of rocks and show that, in general, rocks draining from the western WA are younger than rocks draining from the central WA. The "Both" category refers to the Nabesna drainage and its tributary the Jacksina, which drain areas of both the central and western WA. Note that more than half of the samples are younger than 5 Ma, with a clear majority 5 Ma or younger. The ~35 Ma cobble is sample White 14 and we note in the text this age is questionable.

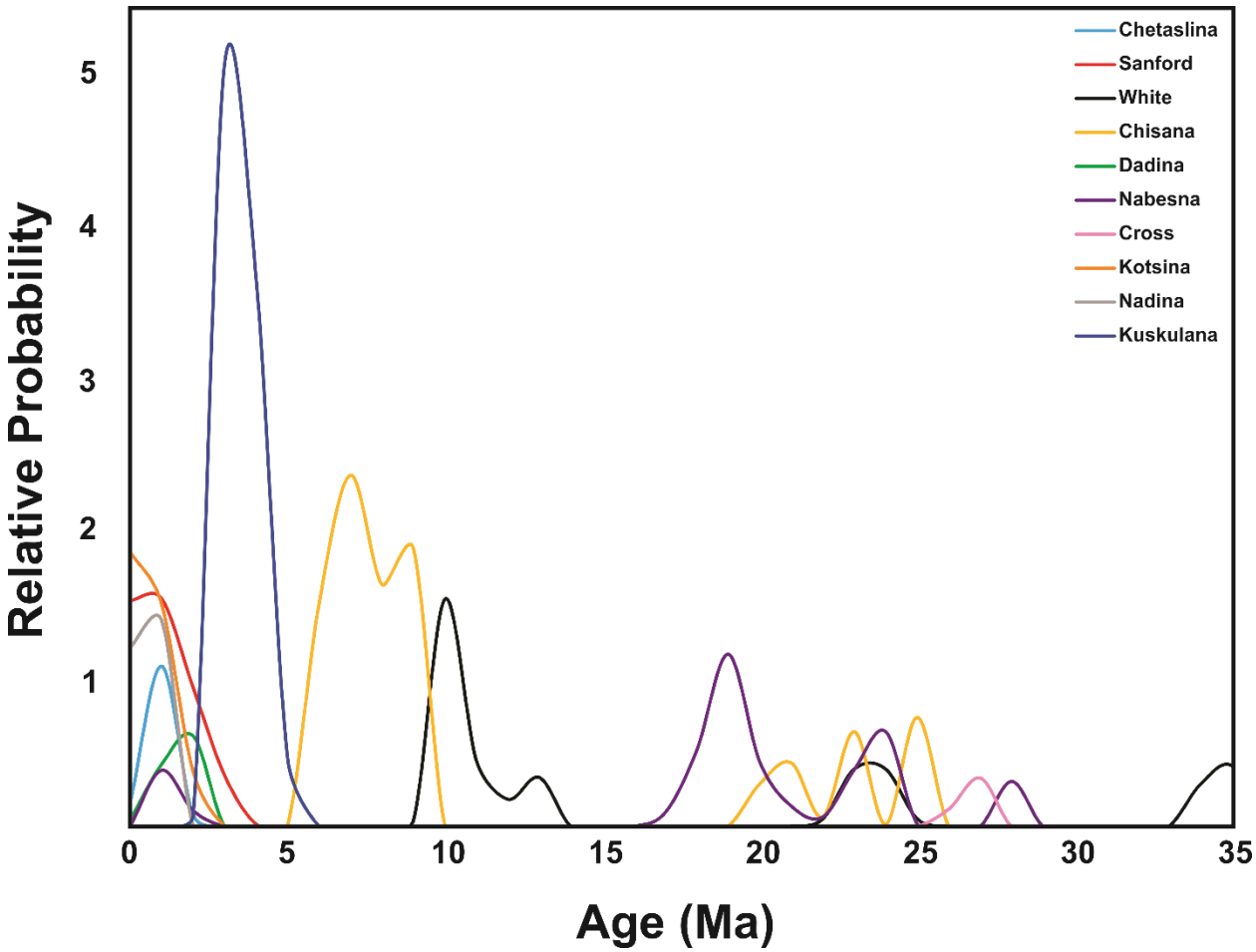

Figure 4.2 Relative probability distribution plot (i.e., ideogram) of all WA-aged (<30 Ma) cobbles showing distribution and relative probability of WA magmatism through time. Different colored curves correspond to the rivers from which the samples were collected. The ~35 Ma cobble is sample White 14 and we note this age is questionable.

Table 4.2 Summary of age ranges from each river drainage along with possible bedrock sources drained.

River	Number of samples	Spatial division	Possible bedrock sources*	Entire age range	WA-only age range
Nabesna	10	Central/western	Mt. Gordon, Ice Fields Plateau, Skookum Creek Center	1.37-153.31 Ma	1.37-27.7 Ma
Cross	4	Central	Frederika Mountain	26.6 – 147.97 Ma	26.6 Ma
Chisana	17	Central	Frederika Mountain, Eucher Mountain	5.88 – 162.45 Ma	5.88 – 25.12 Ma
White	13	Central	Mt. Churchill, Mt. Bona, Castle Mountain, Frederika Mountain	9.31 – 300.97 Ma	9.31 – 23.50 Ma
Kuskulana	16	Western	Mt. Blackburn, Mt. Wrangell(?)	2.79 – 4.55 Ma	2.79 – 4.55 Ma
Kotsina	13	Western	Mt. Wrangell, Mt. Blackburn	0.02 – 215.07 Ma	0.02 – 1.54 Ma
Chetaslina	9	Western	Mt. Wrangell	0.23 – 152.42 Ma	0.23 – 0.92 Ma
Dadina	11	Western	Mt. Drum, Mt. Wrangell	0.31 – 1.86 Ma	0.31 – 1.86 Ma
Nadina	8	Western	Mt. Drum	0.17 – 0.88 Ma	0.17 – 0.88 Ma
Sanford	18	Western	Mt. Drum, Mt. Wrangell, Mt. Sanford	0 – 2.3 Ma	0.07 – 2.3 Ma

* Possible bedrock sources are inferred from Richter et al., 2006.

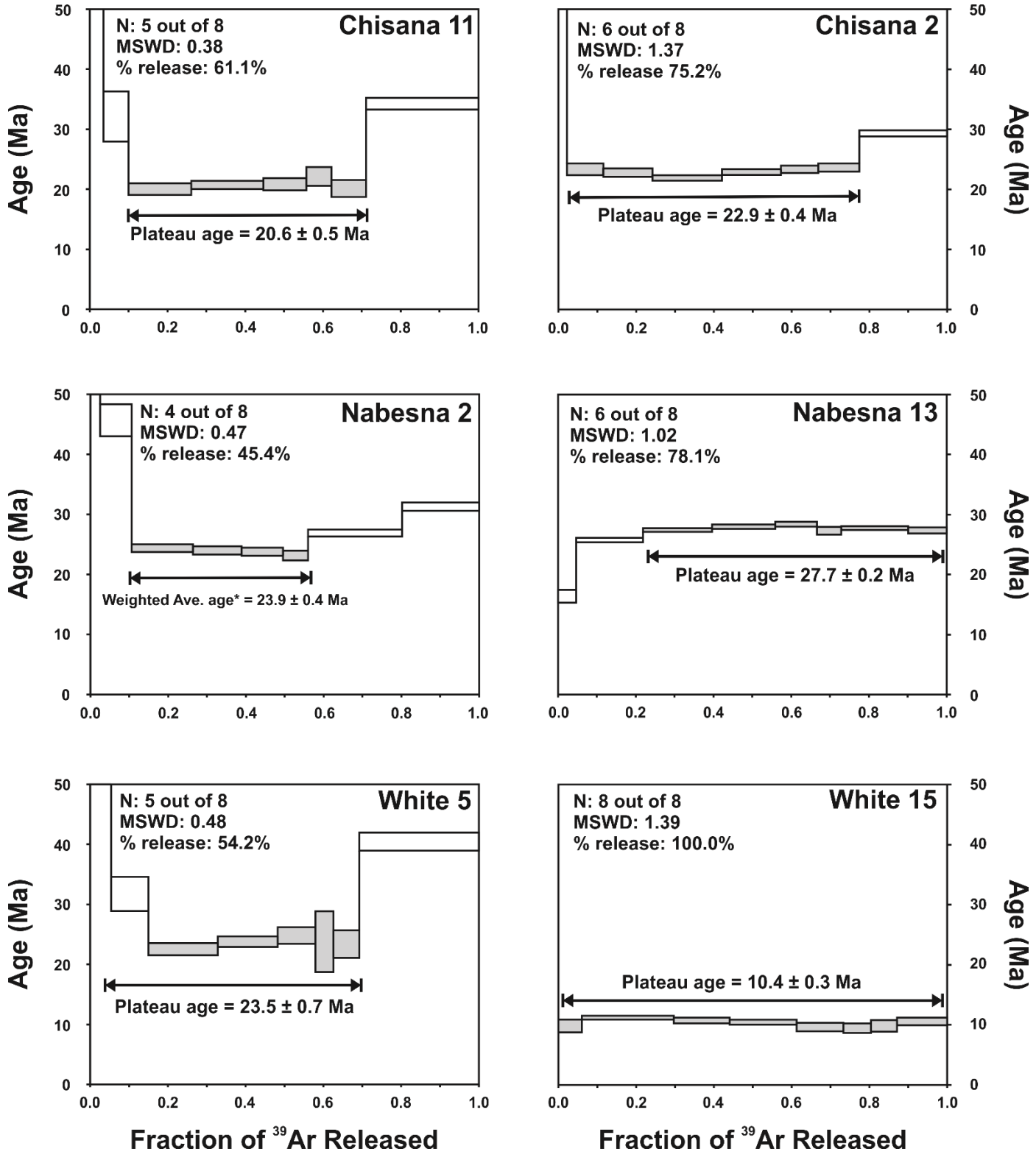

Figure 4.3 $^{40}Ar/^{39}Ar$ spectra showing plateau ages that were produced using step-heat methodology for six select samples out of the entire dataset.

Table 4.3 $^{40}Ar/^{39}Ar$ step-heat data for subset of six cobbles with early arc ages.

Sample	Mineral or Whole rock	Integrated Age (Ma)	Plateau Age (Ma)	Plateau Information	Isochron Age (Ma)	Isochron or other Information
White 5	Whole Rock	33.2 ± 1.0	**23.5 ± 0.7**	5 out of 8 fractions 100% ^{39}Ar release MSWD = 0.48	25.9 ± 1.9	$^{40}Ar/^{36}Ar_i$ = 263.8 ± 24.0 MSWD = 0.10
White 15	Whole Rock	10.4 ± 0.2	**10.4 ± 0.3**	8 out of 8 fractions 100% ^{39}Ar release MSWD = 1.39	10.9 ± 0.4	$^{40}Ar/^{36}Ar_i$ = 287.8 ± 17.1 MSWD = 1.44
Chisana 2	Whole Rock	25.4 ± 0.4	**22.9 ± 0.4**	6 out of 8 fractions 75.2% ^{39}Ar release MSWD = 1.37	22.8 ± 0.5	$^{40}Ar/^{36}Ar_i$ = 296.2 ± 5.3 MSWD = 1.69
Chisana 11	Whole Rock	27.7 ± 0.6	**20.6 ± 0.5**	5 out of 8 fractions 61.1% ^{39}Ar release MSWD = 0.38	21.0 ± 0.6	$^{40}Ar/^{36}Ar_i$ = 291.1 ± 5.4 MSWD = 0.30
Nabesna 2	Whole Rock	30.3 ± 0.4	**23.9 ± 0.4***	4 out of 8 fractions 45.4% ^{39}Ar release MSWD = 0.47	20.5 ± 4.2	$^{40}Ar/^{36}Ar_i$ = 317.9 ± 27.7 MSWD = 0.32
Nabesna 13	Whole Rock	26.8 ± 0.2	**27.7 ± 0.2**	6 out of 8 fractions 78.1% ^{39}Ar release MSWD = 1.02	N/A	N/A

Note: Preferred age (between integrated, plateau, and isochrone age) in bold

*Weighted average presented when all the criteria for a plateau age were not met.

Table 4.4 Comparison between single fusion and plateau ages (step-heat).

Sample	Single-fusion age (Ma)	Plateau age (Ma)
Nabesna 2	29.66 ± 0.98	23.9 ± 0.4
Nabesna 13	26.82 ± 0.19	27.7 ± 0.2
Chisana 11	27.31 ± 0.82	20.6 ± 0.5
Chisana 2	28.04 ± 0.58	22.9 ± 0.4
White 5	30.09 ± 0.56	23.5 ± 0.7
White 15	10.07 ± 0.15	10.4 ± 0.3

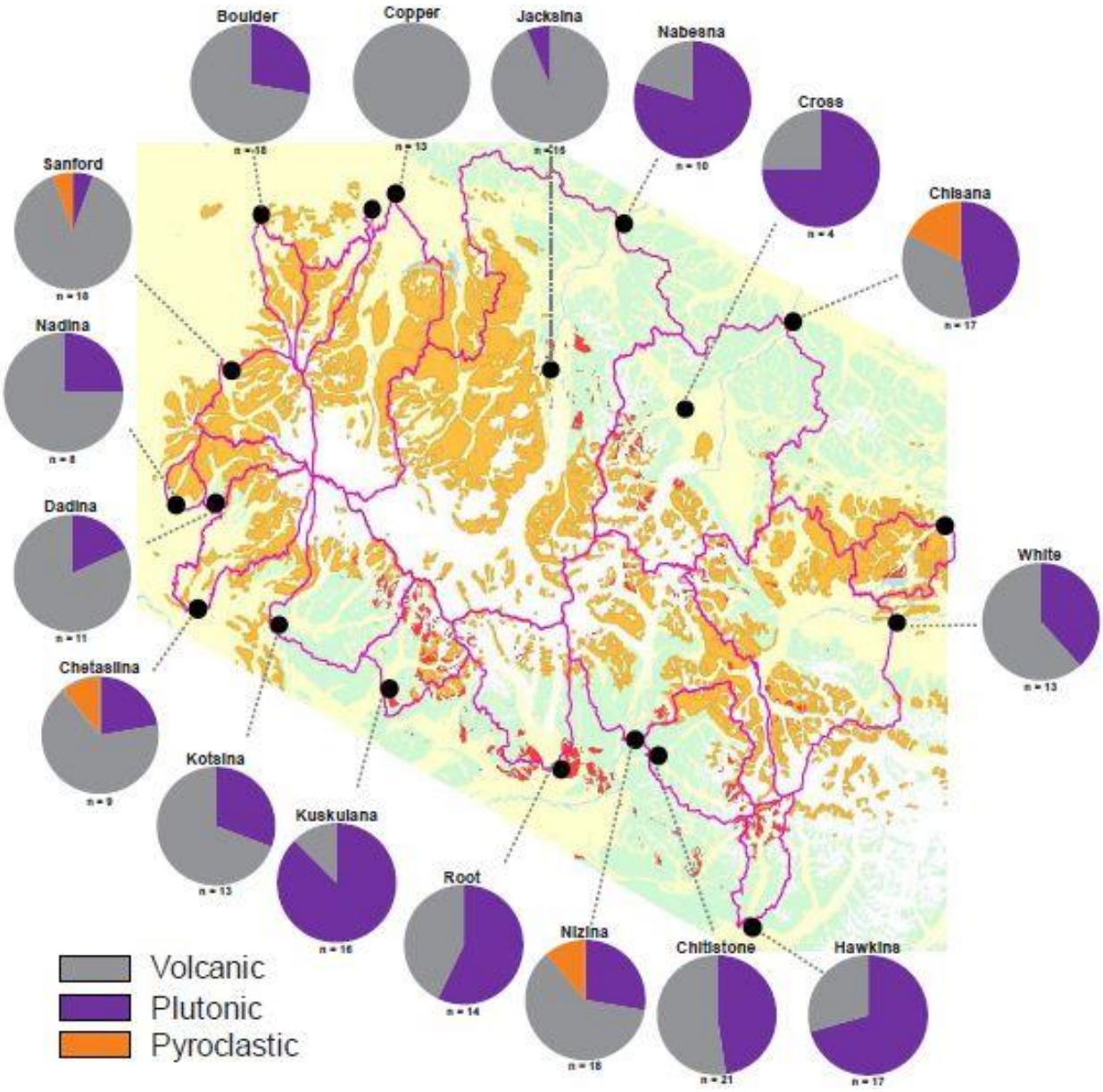

Figure 4.4 Map showing the variety of textures from this dataset. The term "volcanic" includes both porphyritic-volcanic and aphanitic textures. The term "plutonic" includes both porphyritic-plutonic and phaneritic textures. Note that pyroclastic textures, while rare, are found in the western and central WA.

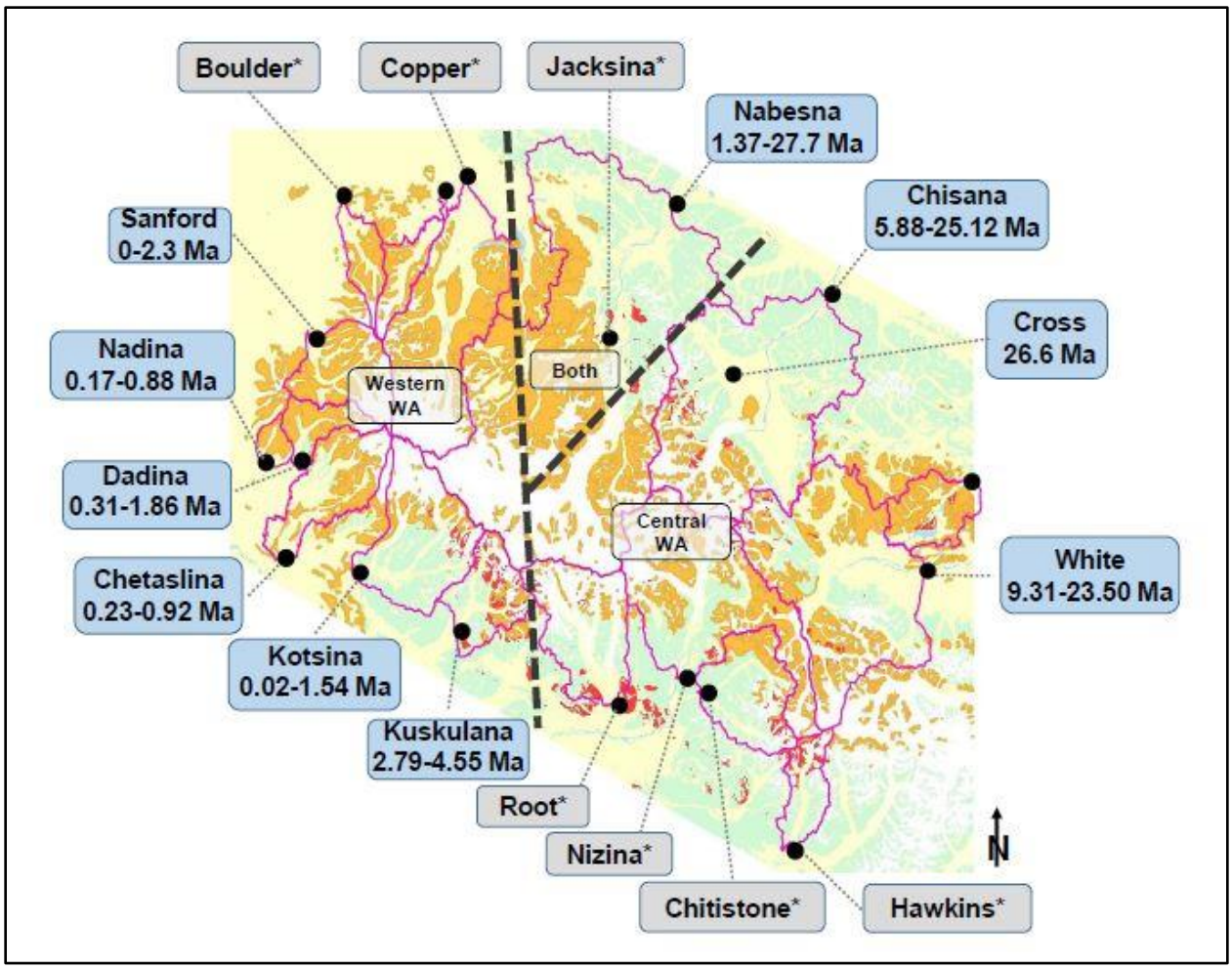

Figure 4.5 Map of study area with watersheds delineated (pink lines), river drainages labeled (including ages), and spatial divisions assigned (western, central, both). Black dashed line is the approximate boundary used for spatial divisions. The Nabesna drainage—and its tributary the Jacksina—classify as "Both" because their watershed area is so enormous that it drains rocks from the western *and* central WA. This is reinforced by the wide age range observed from the Nabesna River. The unlabeled watershed north of the White River is Ptarmagin Creek, which drains the SCVF. *Names in gray boxes do not yet have age data but have geochemical data and are therefore included in spatial divisions.

Table 4.5 Summary of the rivers included in each spatial division category used for all plots and discussion herein. Note that rivers from the western WA generally drain younger rocks whereas rivers from the central WA generally drain older rocks. The Nabesna and Jacksina rivers capture bedrock input associated with both the western and the central WA, so they are considered "Both".

Spatial division	Rivers included	Age range (Ma)
Central WA	Chisana, White, Hawkins, Cross, Chitistone, Nizina, Root	5.88 – 23.50
Western WA	Kuskulana, Kotsina, Dadina, Nadina, Sanford, Boulder, Copper	0 – 4.55
Both	Nabesna, Jacksina	1.37 – 27.70

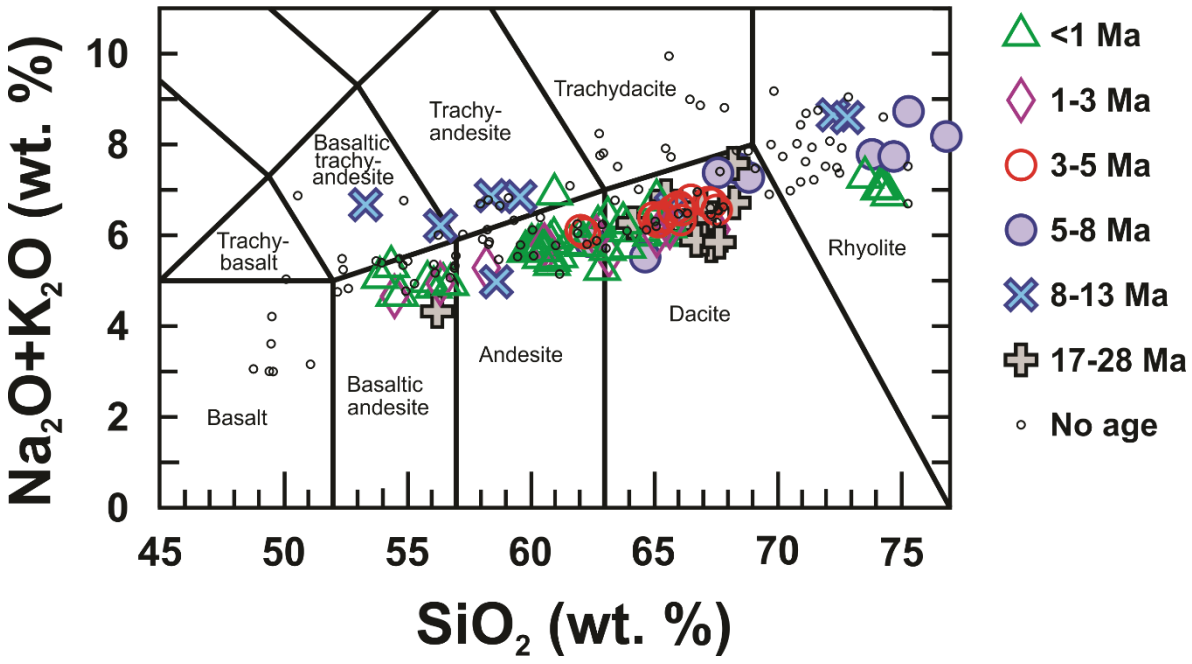

Figure 4.6 Total alkalis versus silica diagram with cobble samples coded based on their age.

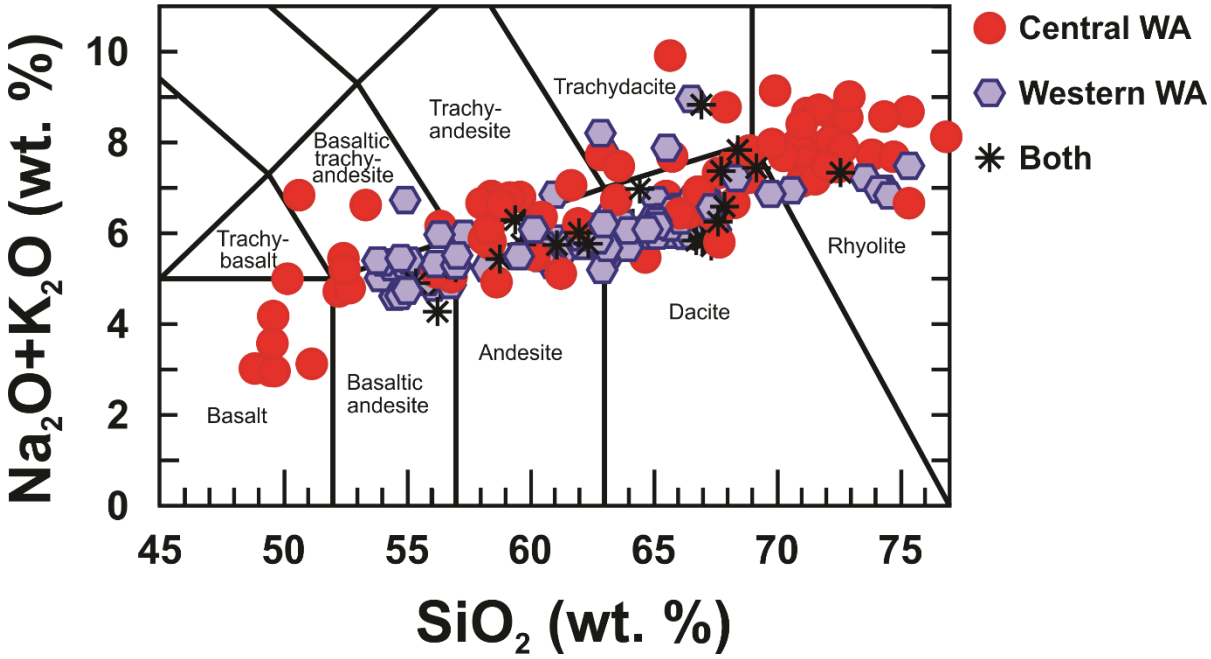

Figure 4.7 Total alkalis versus silica diagram with cobble samples coded based on their spatial location.

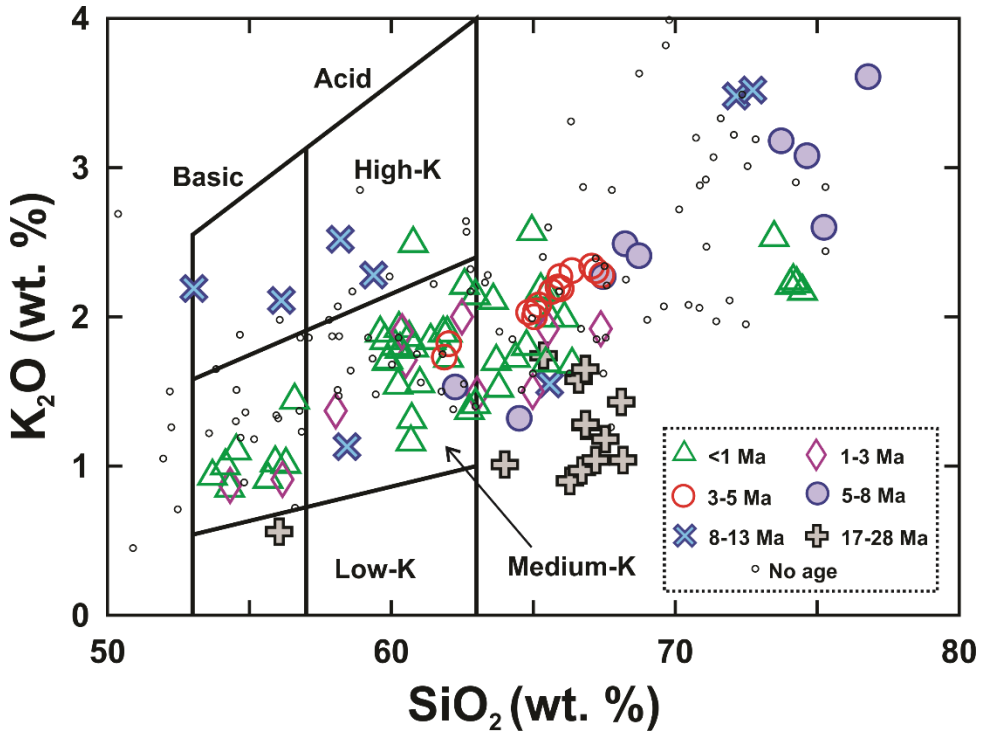

Figure 4.8 Andesite type diagram (Gill, 1981) with cobble samples coded based on their age. Most medium-K andesites are <1 Ma.

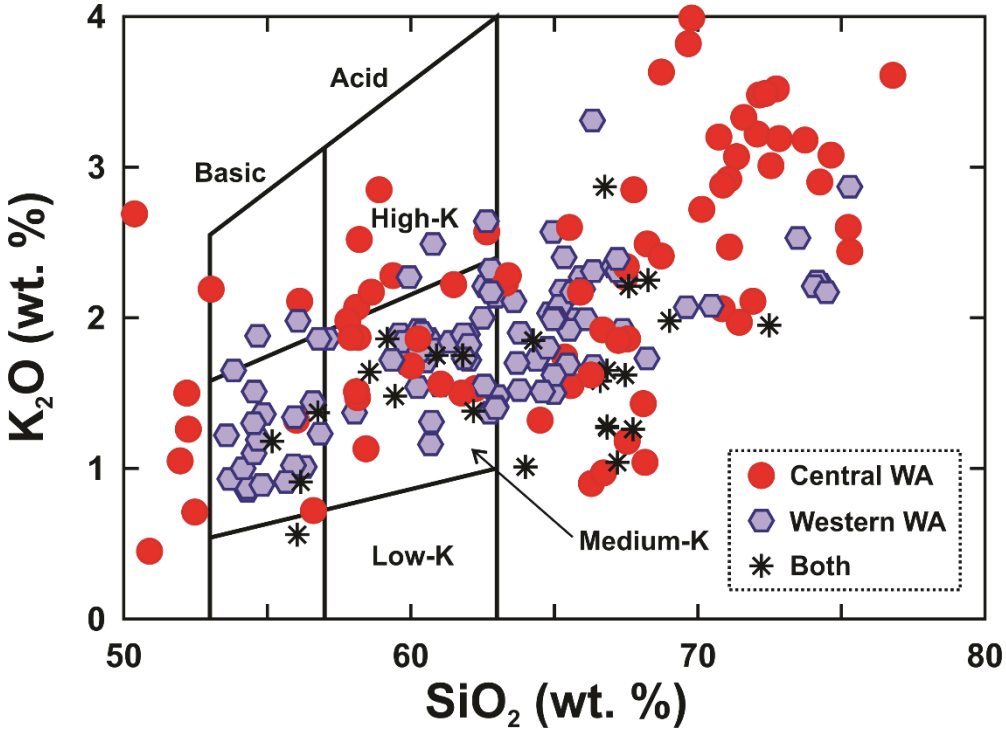

Figure 4.9 Andesite type diagram (Gill, 1981) with cobble samples coded based on their spatial location. Most medium-K andesites drain from the western WA.

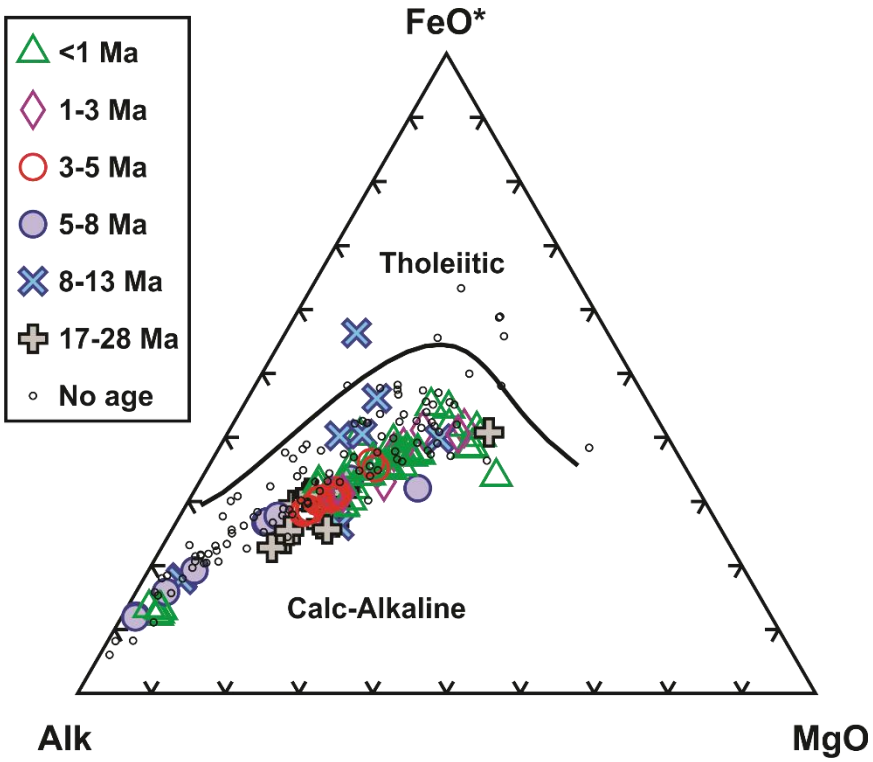

Figure 4.10 AFM diagram with cobble samples coded based on their age.

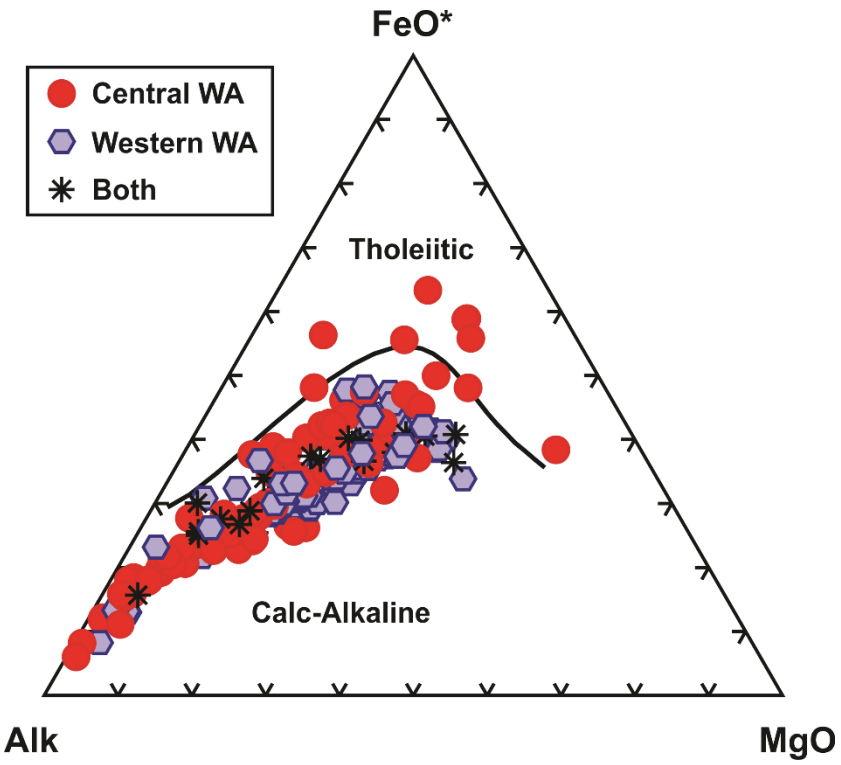

Figure 4.11 AFM diagram with cobble samples coded based on their spatial location.

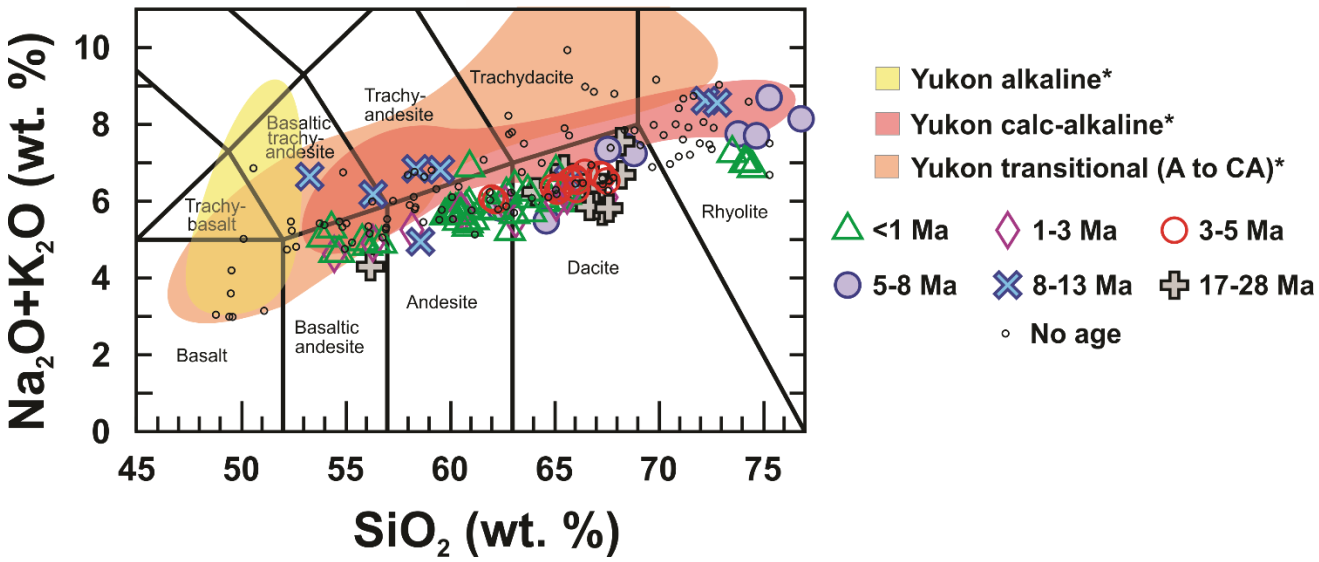

Figure 4.12 Total alkalis versus silica diagram showing the general dissimilarity between this cobble dataset and alkaline compositions (yellow field) documented by Skulski et al. (1991; 92). The colored fields labeled "Yukon" represent data from Skulski et al. (1991; 92).

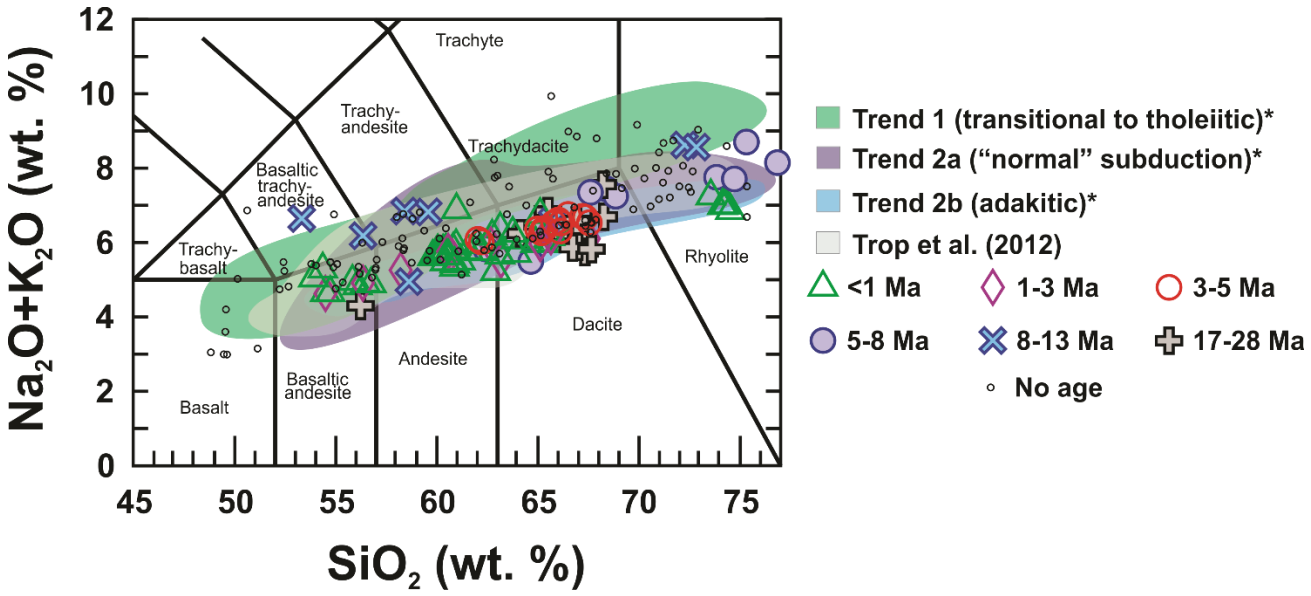

Figure 4.13 Total alkalis versus silica diagram showing the general similarity between this cobble dataset and that of Preece and Hart (2004) and Trop et al. (2012). Because Preece and Hart (2004) focused on geochemical variations within WA rocks, we use their criteria to group these new data into their trends for further comparison.

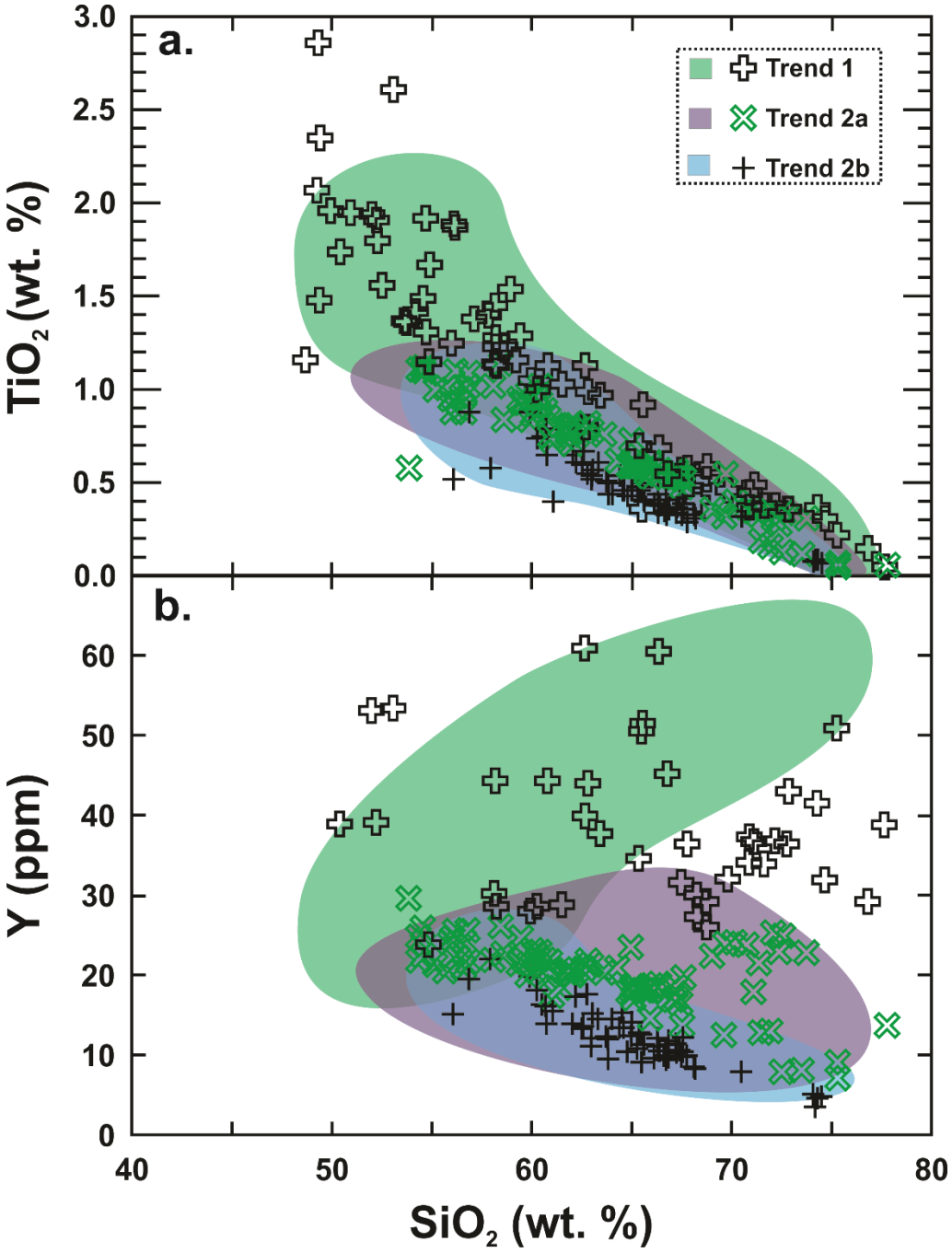

Figure 4.14 Classification of cobble data according to Preece and Hart (2004) criteria. The colored fields represent data from Preece and Hart (2004); symbols are cobble data classified according to Preece and Hart (2004) criteria. (a) TiO_2 versus SiO_2 diagram. Note the much larger range of TiO_2 values at SiO_2 < 60 wt. % than at SiO_2 > 60 wt. %. (b) Yttrium versus SiO_2 diagram. Note samples from this dataset don't perfectly fit within the confines of the Preece and Hart (2004) data, but they do show similar trends, i.e., Trend 1 has elevated Y values relative to Trend 2 and Trend 2a has elevated Y values relative to 2b.

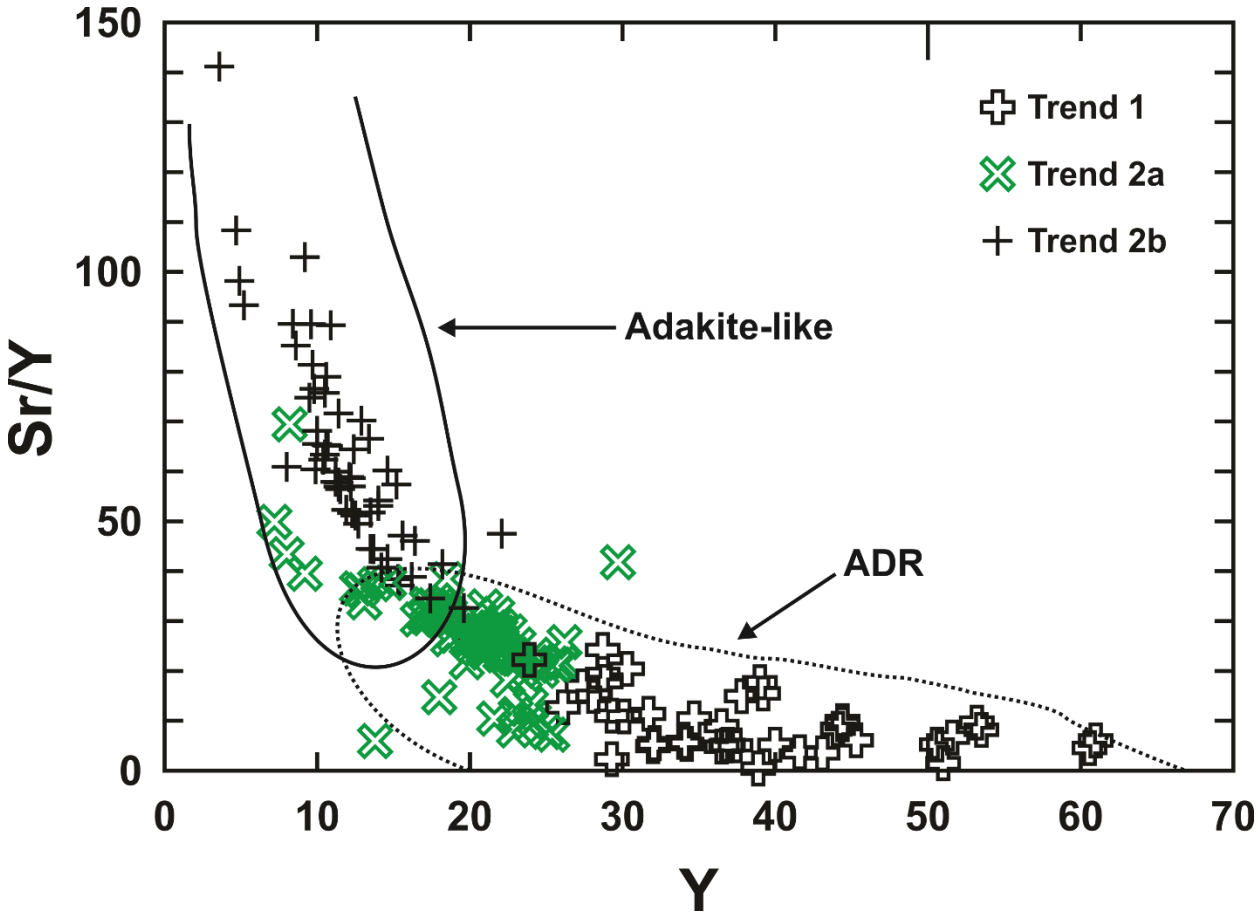

Figure 4.15 Classification of cobble data according to Preece and Hart (2004) criteria. Note that most Trend 2b samples from the cobble dataset are within the "adakite-like" field (Defant and Drummond, 1990). ADR = andesite-dacite-rhyolite and is characteristic of volcanic arc compositions (Defeant and Drummond, 1990).

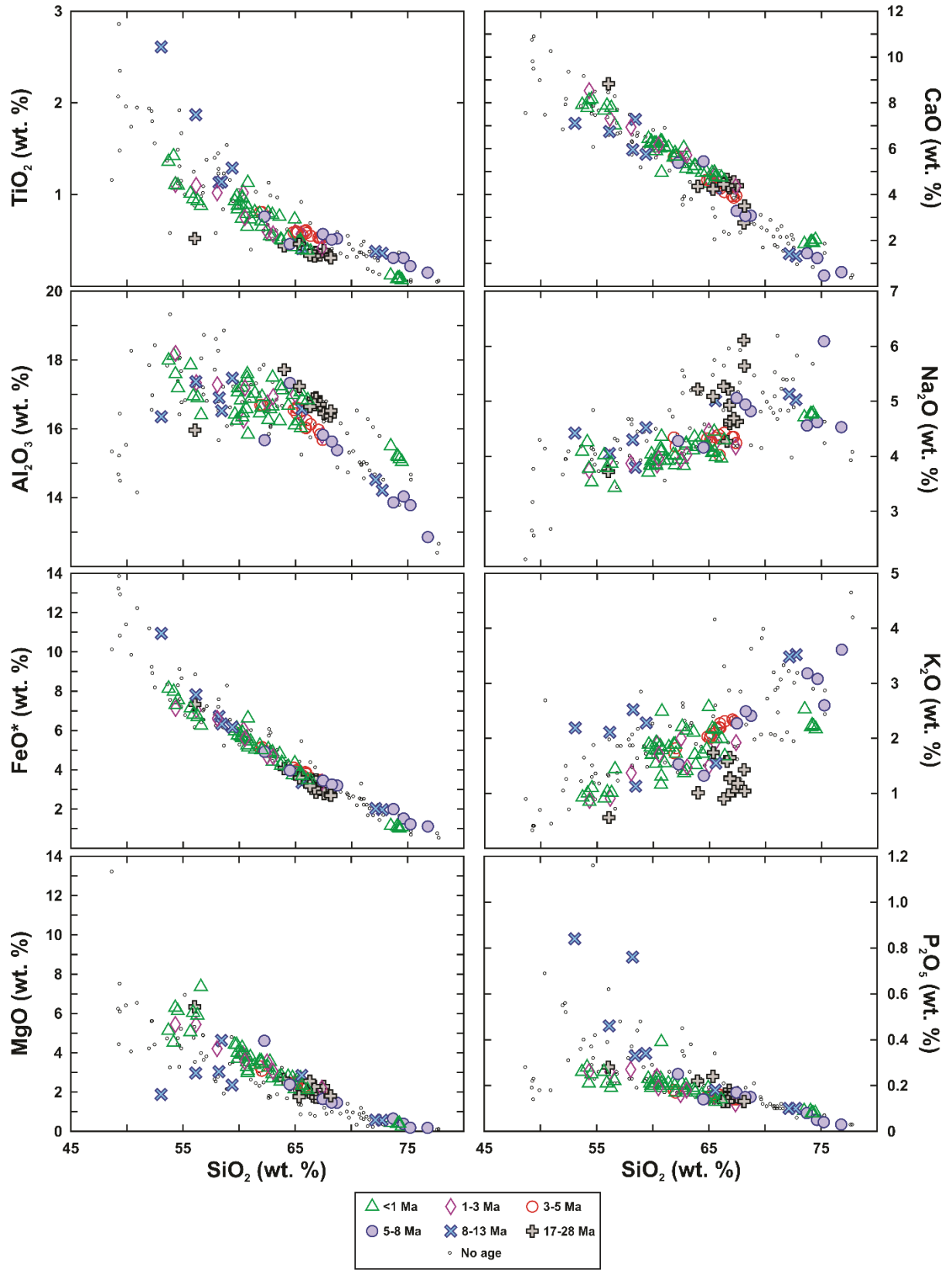

Figure 4.16 Harker diagrams showing major element variations through time. Samples are coded based on their age. FeO* indicates total iron as Fe^{2+}.

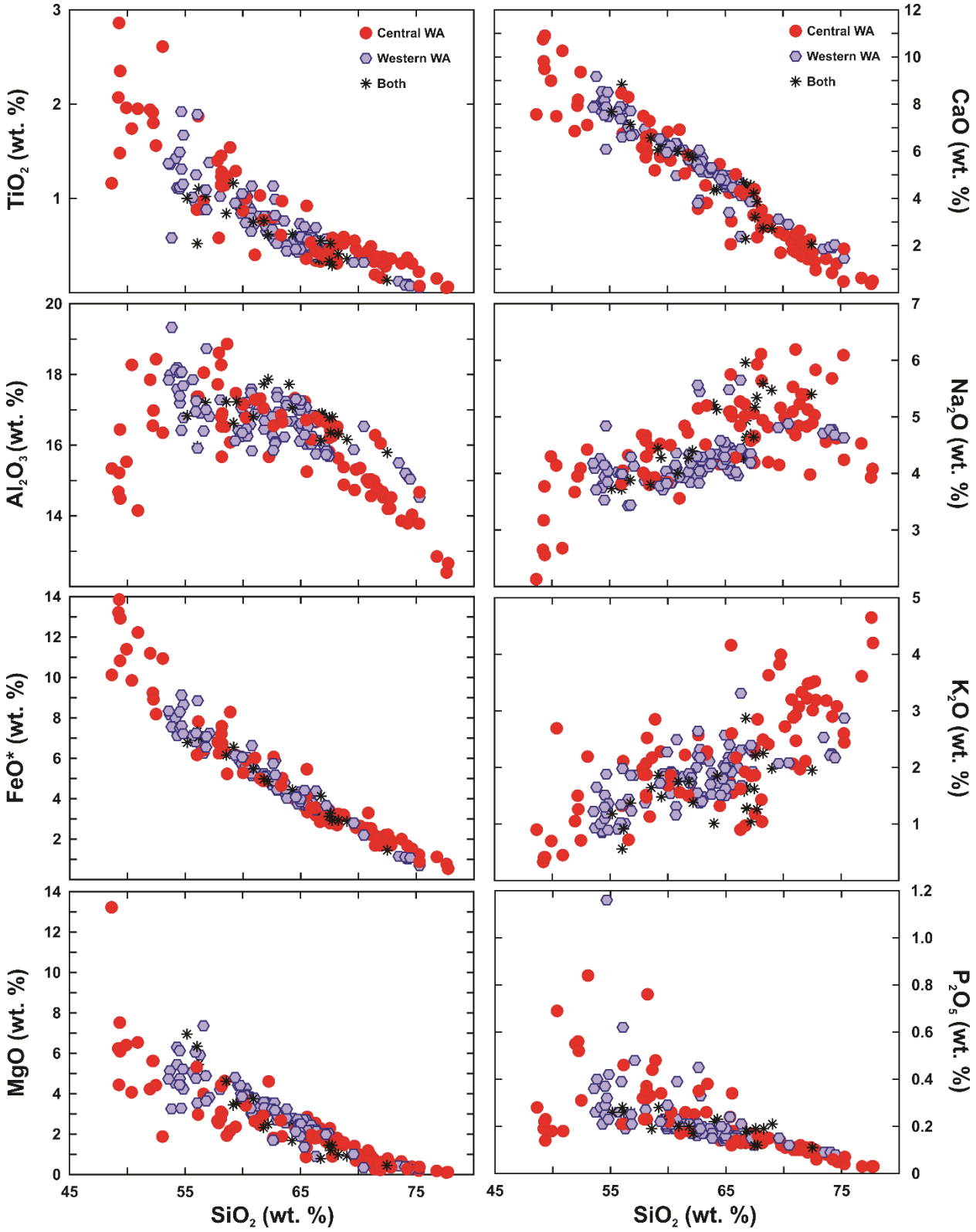

Figure 4.17 Harker diagrams showing major element variations through space. Samples are coded based on their spatial location. FeO* indicates total iron as Fe^{2+}.

Table 4.6 Major element and magnesium number ranges for the total dataset, each spatial division, and each age division.

		Spatial Divisions			*Age Divisions*					
	Total range (wt. %)	**Central WA**	**Western WA**	**Both**	**<1Ma**	**1-3 Ma**	**3-5 Ma**	**5-8 Ma**	**8-13 Ma**	**17-28 Ma**
	n = 207	n = 83	n - 100	n = 24	n = 47	n = 10	n = 14	n = 9	n = 8	n = 13
SiO_2	48.64 - 77.76	48.64 - 77.76	53.58 - 75.29	55.17 - 72.49	53.70 - 74.48	54.32 - 67.38	61.87 - 67.42	62.25 - 76.79	53.05 - 72.24	56.05 - 68.16
TiO_2	0.05 - 2.86	0.05 - 2.86	0.05 - 1.92	0.13 - 1.16	0.07 - 1.42	0.42 - 1.11	0.53 - 0.81	0.15 - 0.76	0.36 - 2.61	0.31 - 0.52
Al_2O_3	12.4 - 19.33	12.4 - 18.86	14.52 - 19.33	15.79 - 17.86	15.04 - 18.13	15.80 - 18.19	15.68 - 16.69	12.85 - 17.33	14.21 - 17.47	15.96 - 17.72
FeO*	0.54 - 13.86	0.54 - 13.86	0.7 - 9.13	1.45 - 7.32	1.02 - 8.14	3.38 - 7.12	3.41 - 5.15	1.12 - 4.92	1.97 - 10.94	2.70 - 7.32
MnO	0.03 - 0.3	0.03 - 0.3	0.05 - 0.2	0.07 - 0.15	0.06 - 0.15	0.08 - 0.15	0.08 - 0.10	0.04 - 0.11	0.07 - 0.15	0.06 - 0.13
MgO	0.1 - 13.22	0.1 - 13.22	0.25 - 7.36	0.45 - 6.95	0.25 - 7.36	2.19 - 5.44	1.99 - 3.30	0.18 - 4.61	0.57 - 4.63	1.72 - 6.34
CaO	0.37 - 10.9	0.37 - 10.9	1.45 - 9.17	2.05 - 8.83	1.85 - 8.16	4.36 - 8.53	3.87 - 5.72	0.47 - 5.45	1.31 - 7.28	2.76 - 8.83
Na_2O	2.13 - 6.19	2.13 - 6.19	3.43 - 5.65	3.72 - 5.96	3.43 - 4.78	3.74 - 4.46	4.02 - 4.43	4.16 - 6.09	3.80 - 5.13	3.72 - 6.11
K_2O	0.33 - 4.65	0.33 - 4.65	0.85 - 3.31	0.56 - 2.87	0.85 - 2.57	0.87 - 2.00	1.73 - 2.34	1.32 - 3.61	1.13 - 3.52	0.56 - 1.74
P_2O_5	0.03 - 1.16	0.03 - 0.84	0.07 - 1.16	0.11 - 0.28	0.08 - 0.39	0.12 - 0.27	0.14 - 0.18	0.03 - 0.25	0.10 - 0.84	0.13 - 0.28
Mg#	18.9 - 69.9	18.9 - 69.9	21.6 - 67.7	25.4 - 64.6	29.2 - 67.7	52.1 - 57.9	50.80 - 53.57	21.7 - 62.5	23.4 - 60.3	46.7 - 60.7

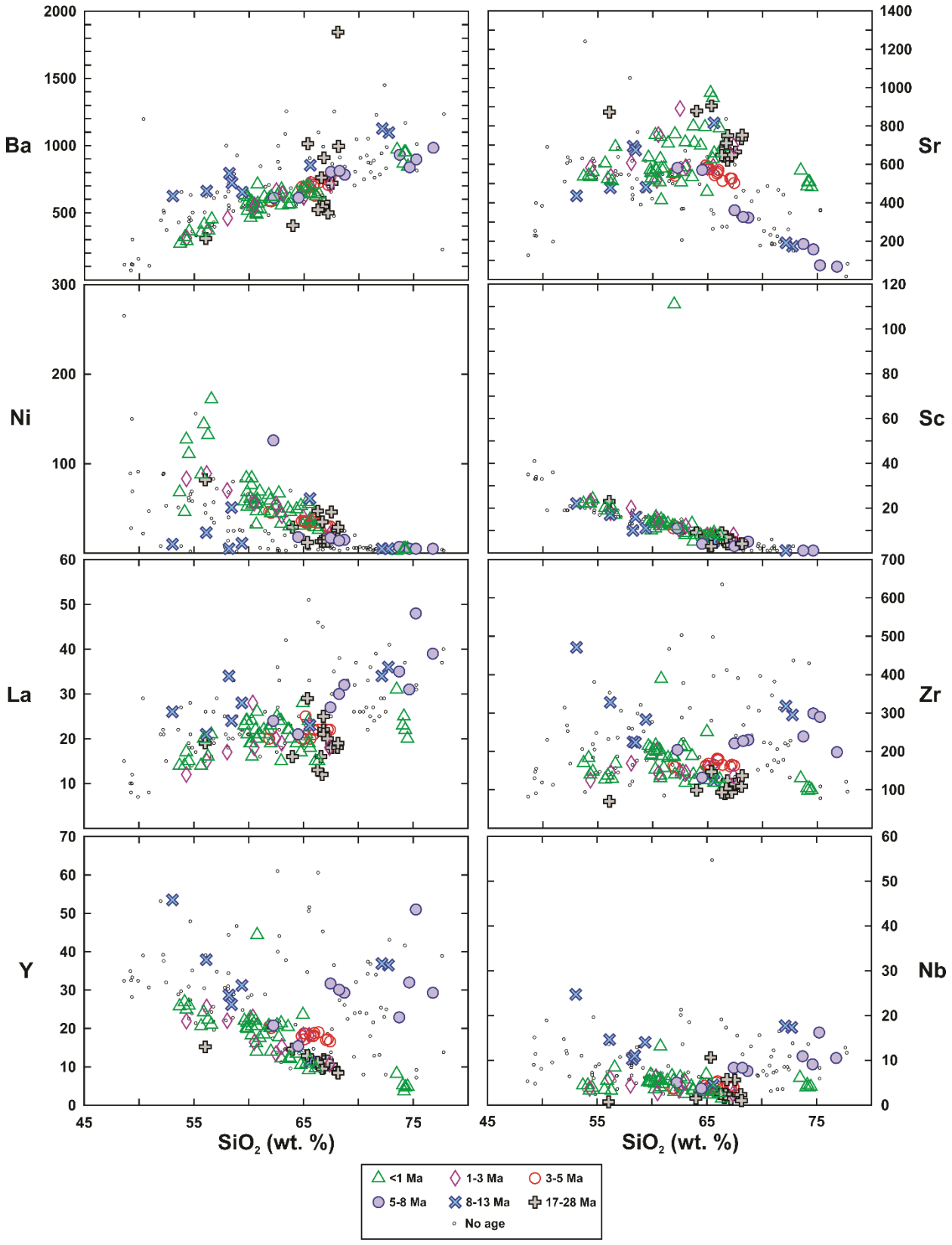

Figure 4.18 Harker diagrams showing trace element variations through time. Samples are coded based on their age.

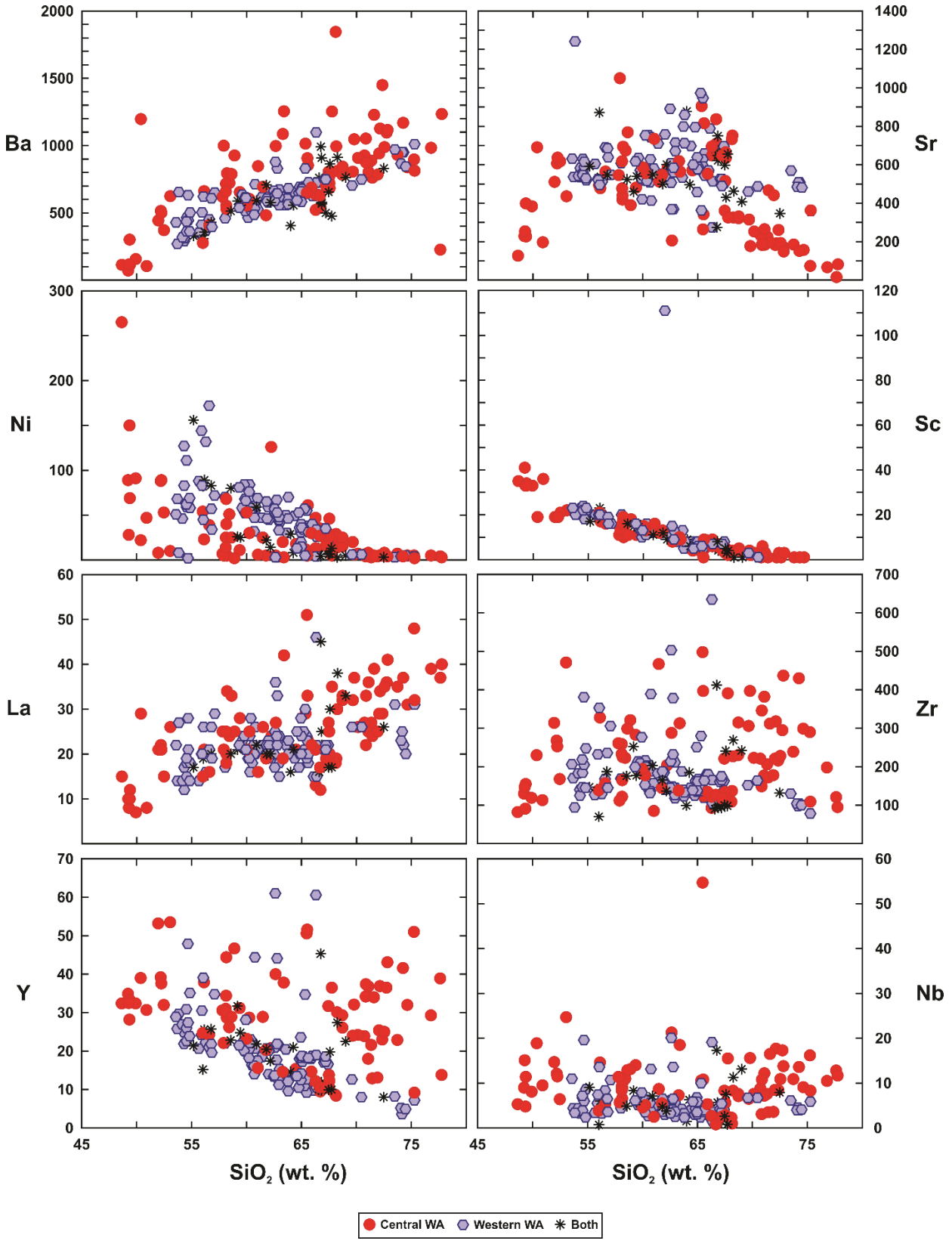

Figure 4.19 Harker diagrams showing trace element variations through space. Samples are coded based on their spatial location.

Table 4.7 Trace element ranges for each spatial and age category. Rocks older than WA age (~30 Ma) are not included here. Rocks with LOI values greater than 3.5 wt. % are included here.

		Spatial Divisions			*Age Divisions*					
	Total range (ppm) n = 220	**Central WA** n = 95	**Western WA** n = 101	**Both** n = 24	**<1Ma** n = 47	**1-3 Ma** n = 10	**3-5 Ma** n = 14	**5-8 Ma** n = 9	**8-13 Ma** n = 10	**17-28 Ma** n = 13
Rb	1.5 - 145.4	1.5 - 145.4	16.9 - 89.1	12.1 - 53.6	16.9 - 68.8	16.9 - 46.2	39.3 - 61	30.7 - 99.2	25.5 - 104.7	12.1 - 39
Sr	16 - 1241	16 - 1050	275 - 1241	275 - 878	413 - 973	516 - 891	503 - 595	67 - 582	174 - 816	622 - 905
Y	3.6 - 61	8.4 - 53.5	3.6 - 61	8 - 45.3	3.6 - 44.4	10.7 - 25.6	16.6 - 20.5	15.4 - 51	11.4 - 53.5	8.4 - 15.2
Zr	67 - 635	67 - 498	78 - 635	70 - 412	98 - 389	125 - 203	152 - 181	132 - 299	124 - 471	70 - 147
V	4 - 419	4 - 419	8 - 276	17 - 195	8 - 219	90 - 205	85 - 135	12 - 106	30 - 203	64 - 195
Ni	2 - 265	2 - 265	2 - 172	3 - 156	3 - 172	21 - 89	29 - 46	5 - 126	5 - 61	12 - 82
Cr	4 - 685	5 - 685	7 - 248	4 - 287	7 - 248	40 - 131	36 - 56	11 - 235	9 - 124	15 - 88
Nb	0.6 - 54.7	0.6 - 54.7	1.5 - 20.1	0.7 - 17.3	1.5 - 13.1	2.5 - 6.3	3.6 - 5.3	3.7 - 16.2	4.5 - 24.7	0.7 - 10.6
Ga	14.2 - 25.4	14.2 - 25.4	18.6 - 24.4	17 - 23.7	18.9 - 23.8	18.9 - 22.4	19.7 - 21	17.7 - 25.4	18.3 - 23.7	17 - 21.4
Cu	7 - 438	8 - 438	7 - 209	13 - 97	7 - 117	31- 126	27 - 55	12 - 59	8 - 60	12 - 89
Zn	14 - 309	14 - 309	32 - 115	48 - 91	32 - 87	56 - 83	53 - 72	38 - 61	39 - 138	27 - 91
Co	<1 - 66	<1 - 66	<1 - 33	<1 - 32	<1 - 33	4 - 28	5 - 16	<1 - 20	<1 - 30	2 - 29
Ba	21 - 1845	21 - 1845	269 - 1098	308 - 992	269 - 970	312 - 710	585 - 769	611 - 983	288 - 1126	308 - 1845
La	7 - 51	7 - 51	12 - 46	15 - 45	14 - 31	12 - 28	20 - 25	21 - 48	14 - 36	12 - 29
Ce	10 -104	10 - 104	22 - 90	19 - 89	22 - 54	23 - 40	29 - 41	38 - 104	30 - 78	18 - 48
U	<0.5 - 12.1	<0.5 - 12.1	<0.5 - 3.4	<0.5 - 2.2	<0.5 - 3.4	<0.5 - 2.5	<0.5 - 2.1	<0.5 - 2	<0.5 - 3.7	<0.5 - 1.2
Th	<0.5 - 41.7	<0.5 - 41.7	<0.5 - 12	<0.5 - 11.1	<0.5 - 8.5	<0.5 - 3.4	0.5 - 5.2	1.2 - 19	0.5 - 18	<0.5 - 1.6
Sc	<1 - 111	<1 - 41	<1 - 111	<1 - 23	<1 - 111	8 - 23	5 - 12	<1 - 11	<1 - 22	3 - 23
Pb	<1 - 45	<1 - 45	<1 - 28	<1 - 21	<1 - 28	<1 - 21	<1 - 17	<1 - 20	<1 - 20	<1 - 21

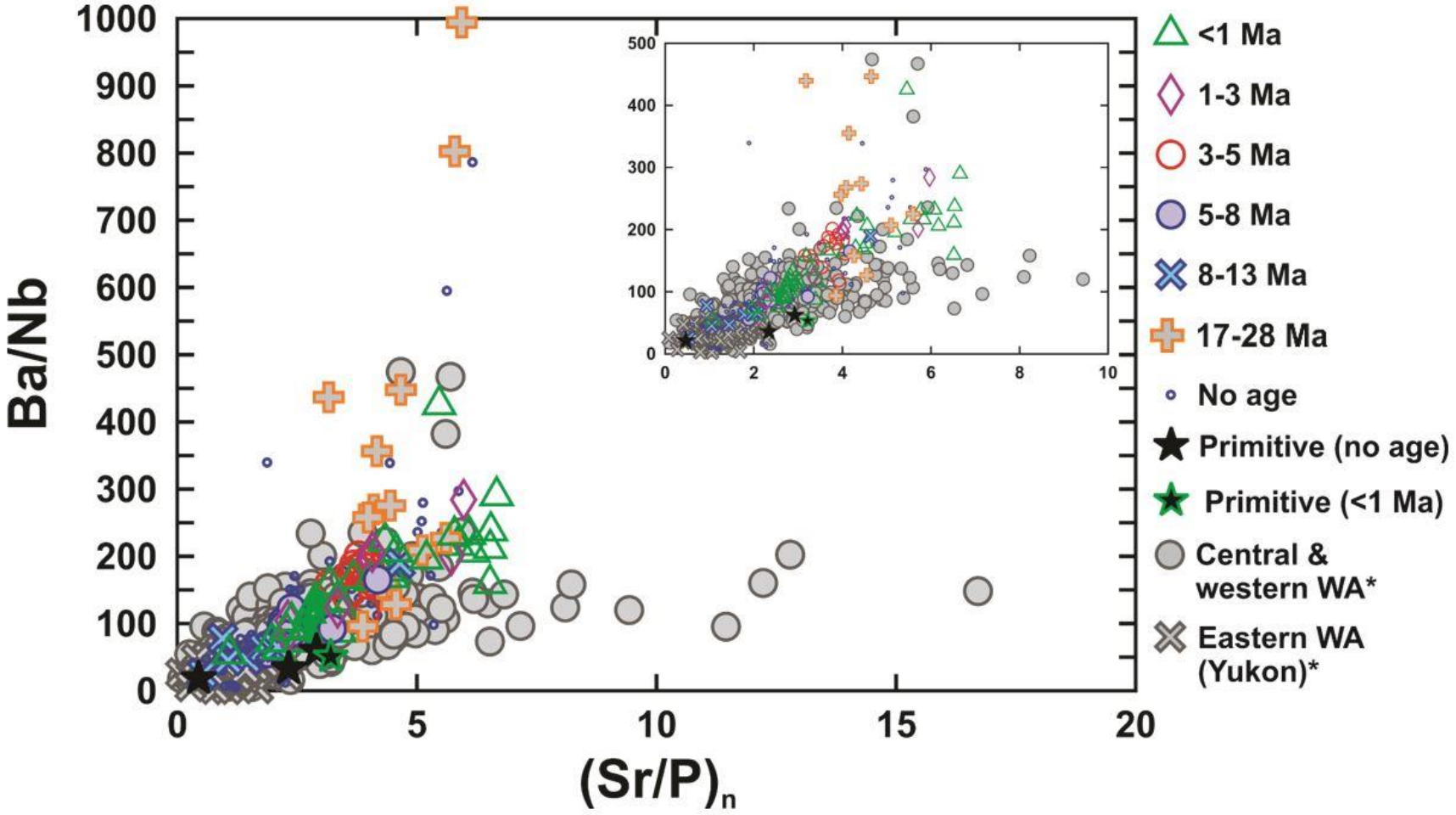

Figure 4.20 Ba/Nb versus $(Sr/P)_n$. Samples are coded based on their age. Primitive samples are defined as MgO > 6.0 wt.%, Ni > 100 ppm, and Cr > 200 ppm. Gray-scale samples comprise the existing WA bedrock record. *Central & western WA data are from Richter et al. (1990), Preece and Hart (2004), Trop et al. (2012); Eastern (Yukon) data are from Skulski et al. (1991; 1992).

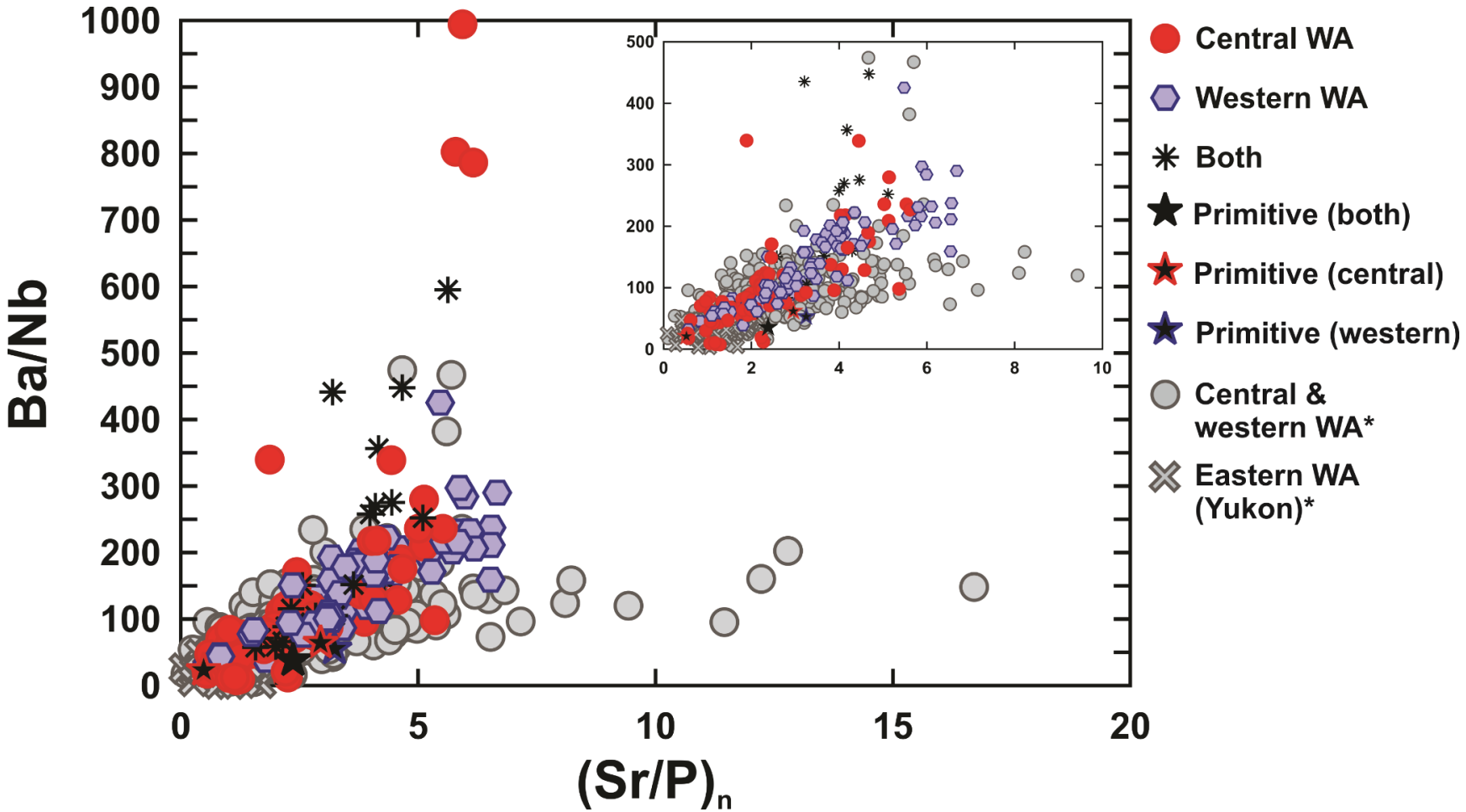

Figure 4.21 Ba/Nb versus $(Sr/P)_n$. Samples are coded based on their spatial location. Primitive samples are defined as MgO > 6.0 wt.%, Ni > 100 ppm, and Cr > 200 ppm. Gray-scale samples comprise the existing WA bedrock record. *Central & western WA data are from Richter et al. (1990), Preece and Hart (2004), Trop et al. (2012); Eastern (Yukon) data are from Skulski et al. (1991; 1992).

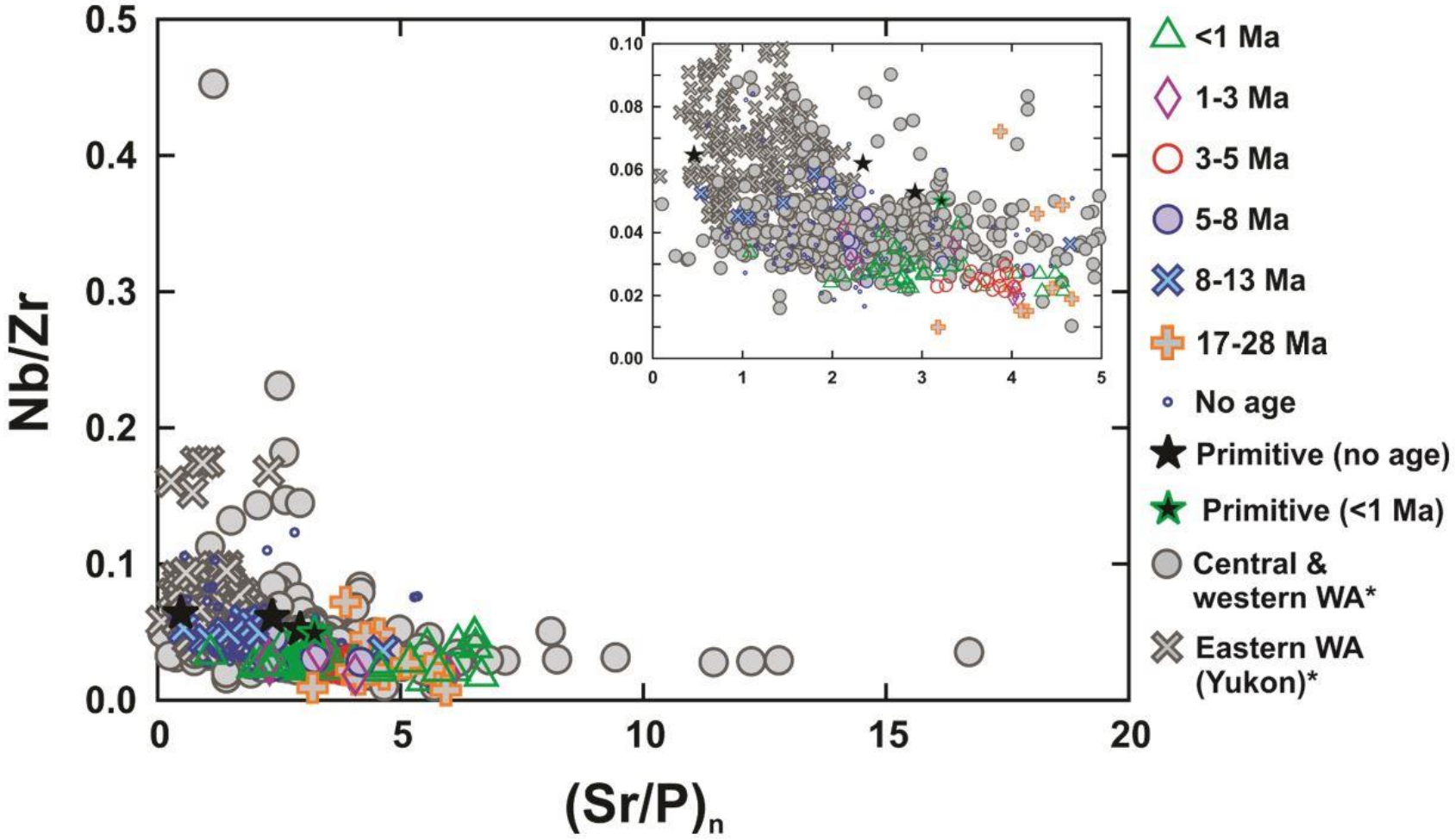

Figure 4.22 Nb/Zr versus $(Sr/P)_n$. Samples are coded based on their age. Primitive samples are defined as MgO > 6.0 wt.%, Ni > 100 ppm, and Cr > 200 ppm. Gray-scale samples comprise the existing WA bedrock record. *Central & western WA data are from Richter et al. (1990), Preece and Hart (2004), Trop et al. (2012); Eastern (Yukon) data are from Skulski et al. (1991; 1992).

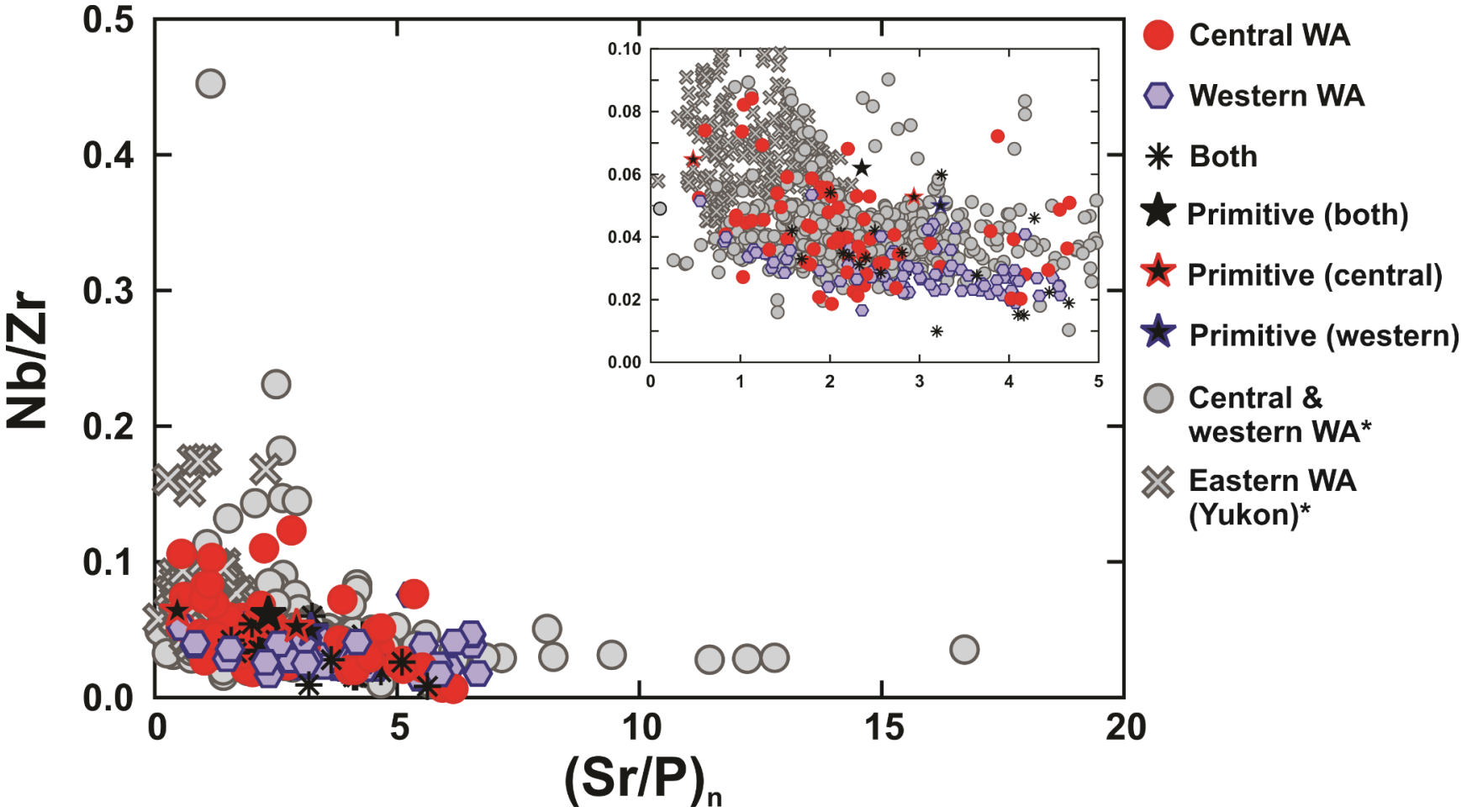

Figure 4.23 Nb/Zr versus $(Sr/P)_n$. Samples are coded based on their spatial location. Primitive samples are defined as MgO > 6.0 wt.%, Ni > 100 ppm, and Cr > 200 ppm. Gray-scale samples comprise the existing WA bedrock record. *Central & western WA data are from Richter et al. (1990), Preece and Hart (2004), Trop et al. (2012); Eastern (Yukon) data are from Skulski et al. (1991; 1992).

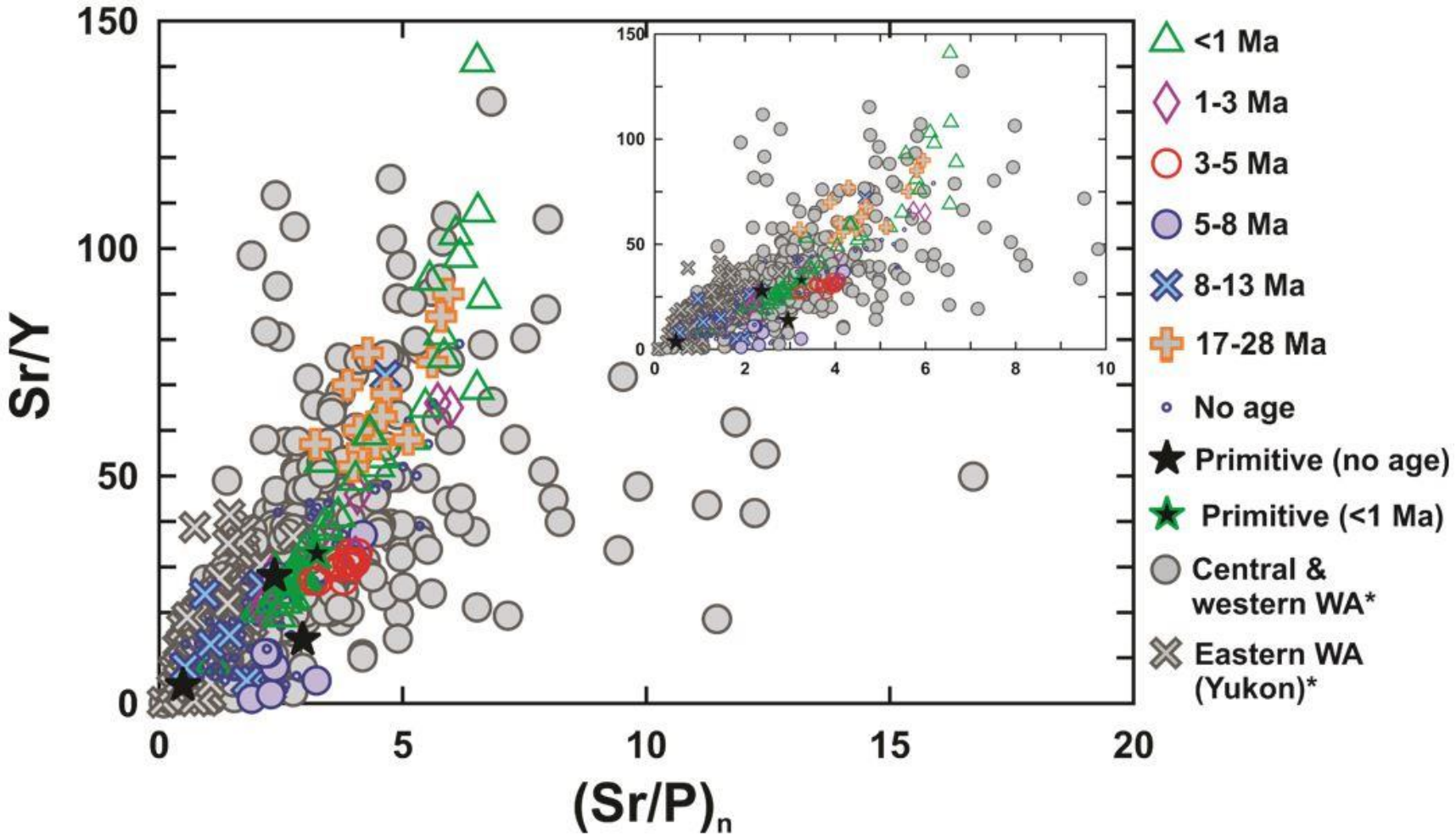

Figure 4.24 Sr/Y versus $(Sr/P)_n$. Samples are coded based on their age. Primitive samples are defined as MgO > 6.0 wt.%, Ni > 100 ppm, and Cr > 200 ppm. Gray-scale samples comprise the existing WA bedrock record. *Central & western WA data are from Richter et al. (1990), Preece and Hart (2004), Trop et al. (2012); Eastern (Yukon) data are from Skulski et al. (1991; 1992).

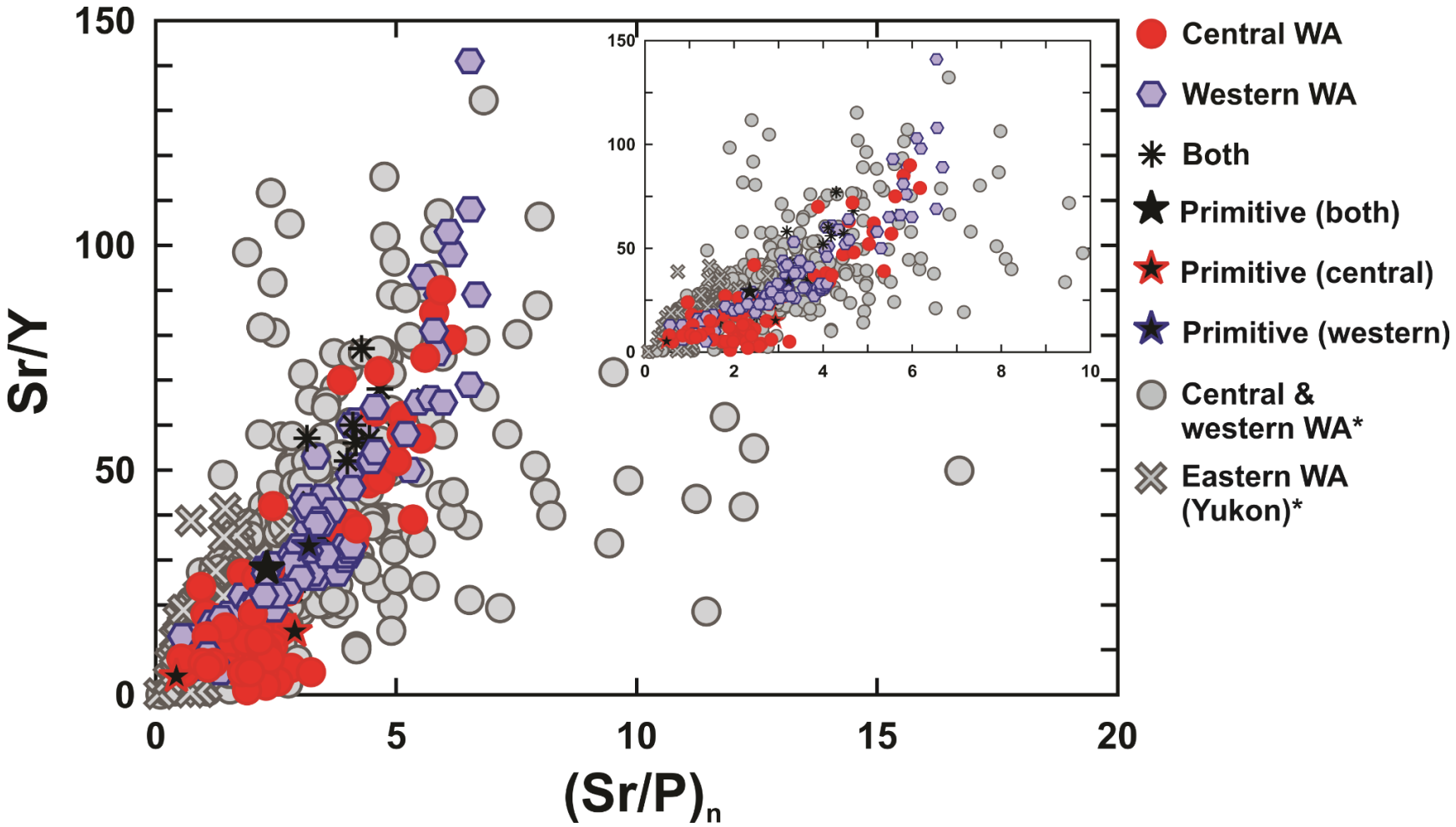

Figure 4.25 Sr/Y versus $(Sr/P)_n$. Samples are coded based on their spatial location. Primitive samples are defined as MgO > 6.0 wt.%, Ni > 100 ppm, and Cr > 200 ppm. Gray-scale samples comprise the existing WA bedrock record. *Central & western WA data are from Richter et al. (1990), Preece and Hart (2004), Trop et al. (2012); Eastern (Yukon) data are from Skulski et al. (1991; 199

Chapter 5 - Discussion

The geochemical and geochronological data collected for this study are combined to offer new insights into the spatial, temporal, and geochemical variations that have shaped the Wrangell arc since the time of its inception. Questions this work aims to address include the following:

1) Did the Wrangell arc initiate prior to the published date of ~26 Ma (Richter et al., 1990)? Additionally, what do new cobble, detrital sand, and bedrock ages reveal about the progression of WA magmatism through time?
2) Are specific time intervals during WA magmatism linked to eruptions and emplacement of different magma types? If so, what—if any—tectonic implications do these temporal trends reveal throughout the arc?
3) Are the controls on the occurrence of various magma types local or arc-wide?
4) What do the spatio-temporal trends of magmatism reveal about the tectonic regime(s) that formed the modern WA?
5) Are the compositions of the igneous cobbles in this study reflected in the existing bedrock record? What does this mean for the application of this indirect sampling strategy to other locations?

To address these questions, this discussion will establish a timeline for WA magmatism (1), consider geochemical variations through time and what tectonic implications those variations have (2), and consider those geochemical variations in a spatial context (3) to relate it back to tectonic processes influencing the migration of magmatism (4). Finally, since this is a novel technique, there will be a discussion of its usefulness in the Wrangell arc and potential to be utilized in other locations (5).

Did the Wrangell arc initiate prior to the published date of ~26 Ma (Richter et al., 1990? What do new ages reveal about the temporal progression of magmatism?

Prior to this study, the timing of WA inception was based on a single bedrock K-Ar age of ~26.3 Ma from the Sonya Creek volcanic field (SCVF; Fig 1.1, 2.1, and 2.3; Richter et al., 1990). However, the WA is huge (over 15,000 km^2) and there are many sample collection

limitations—ice cover, rugged terrain, and air travel—that impact where bedrock can and cannot be collected. These limitations make it difficult to constrain the timing of arc initiation in such a large continental arc setting. With the wide reach of this detrital cobble technique, we have been able to capture a larger area than would otherwise have been possible. As a result, this technique, along with other geochronologic data from detrital sand and zircons (Davis et al., 2017; Trop et al., 2017), has allowed for a better understanding of the age and migration patterns of the WA.

Data here, as well as new detrital data (Davis et al., 2017; Trop et al., 2017), suggest that WA magmatism initiated at ~29.0 Ma. One cobble sample from the White River yielded a single grain fusion age of 34.58 ± 0.47 Ma (Fig. 4.5), but we discount this age due to potential alteration. Trop et al. (2017) report less than 1% of more than 1600 new U/Pb detrital sand ages to be in the ~34.0 – ~29.0 Ma age range. This sparse evidence for magmatism from ~34.0 – ~29.0 Ma is not reflected in the current bedrock record: the oldest five bedrock ages are ~29.0 Ma (Berkelhammer, 2017; Davis et al., 2017) and hence the ~34.0 Ma to ~29.0 Ma single grain zircon ages maybe an artifact of the analytical accuracy of the ICPMS U/Pb dating technique. Alternatively, these single grain zircon ages maybe reflecting regional magmatism preceding the initiation of the WA or a nascent stage of the WA. Given the bedrock geochronology data set does not capture ~34.0 Ma to ~29.0 Ma magmatism in the region, we presently prefer to interpret these single grain zircon ages as reflecting analytical issues.

The next oldest age in the cobble record is 27.7 ± 0.2 Ma which is from the Nabesna River (Fig. 4.5). This leaves an age gap in the cobble record spanning roughly one million years, from ~29.0 Ma to ~28.0 Ma. However, new detrital sand data resolve the gap seen in the cobble record and show continuous arc activity began from ~29.0 Ma to present (Davis et al., 2017; Trop et al., 2017).

Samples in the cobble dataset demonstrate continuous magmatism from 27.7 Ma to ~0.0 Ma (Figs. 4.1 and 4.2) apart from absolutely no samples with ages between ~17.0 – ~13.0 Ma (Figs. 4.1, 4.2, and 5.1). This ~17.0 – ~13.0 Ma gap in magmatism is also observed in the bedrock of the western and central WA (Richter et al., 1990). Notably, the only occurrences of ages from 17.0 – 13.0 Ma are from bedrock in the eastern WA (Figs. 2.1 and 2.3; Skulski et al., 1991; 92) and from U/Pb ages of detrital zircons draining from the White and Nabesna Rivers in

the central WA (Figs. 2.3 and 4.4; Trop et al., 2017). The ~17.0 Ma to ~13.0 Ma single grain zircon ages may be an artifact of the analytical accuracy of the ICPMS U/Pb dating technique.

When considered with the detrital sand and bedrock age data, the cobble data fit in well with the overall history of the WA and reproduce the ~17.0 – ~13.0 Ma gap in magmatism seen in the western and central WA bedrock and detrital sand records. The cobble data are consistent with the hypothesis that WA magmatism began at least 3.0 m.y. earlier than previously thought, at ~29.0 Ma rather than ~26.0 Ma, and was continuous from ~29.0 to the present.

Are specific time intervals linked to magmatic events of different magma types and what tectonic implications do these magmatic events have?

It is possible to link magmatic events of different magma types (i.e., Trend 1, Trend 2a, Trend 2b) to specific time intervals throughout the history of the arc. Trend 1 defines a high TiO_2, transitional-tholeiitic suite, Trend 2a defines a low TiO_2 calc-alkaline suite, and Trend 2b defines a low TiO_2 calc-alkaline suite with adakitic characteristics (Preece and Hart, 2004). Trend 1 is associated with intra-arc extension, Trend 2a is formed by "normal" subduction, and Trend 2b is also formed by subduction, but has specific trace element (e.g., Sr > ~300 ppm and Y < ~10 ppm) geochemistry that may be attributed to partial melting of the subducting slab (i.e., adakite-like). Once divided into these trends, the data can also be considered on the basis of their respective ages to link magma types to specific time intervals. We will use the time intervals defined in the Results section throughout this consideration.

Figures 5.2 – 5.7 show that occurrences of cobbles defined as Trend 2a span the entire life of the arc. Cobbles defined as Trend 2b also occur throughout the entire life of the arc, but they are more abundant during the oldest (28.0 – 17.0 Ma) and youngest (3.0 – 0.0 Ma) periods of arc magmatism (Figs. 5.2, 5.3, and 5.7). Cobbles considered Trend 1 (transitional-tholeiitic) are temporally restricted to <1.0 Ma in the western WA and 10.8 – 5.9 Ma in the central WA (Figs. 5.2, 5.5, and 5.6).

Temporal occurrences of these trends in the cobble record are generally consistent with the existing bedrock record. It is well established in the literature that calc-alkaline (Trend 2a) magmas have erupted throughout the WA duration (Skulski et al., 1991, 1992; Richter et al., 1990; Preece and Hart, 2004; Trop et al., 2012; Keast et al., 2016; Berkelhammer, 2017; Trop et al., 2017; this study). Truly adakitic magmas have been recognized at <5 Ma (Preece and Hart,

2004) and between ~29.0 – ~20.0 Ma in the bedrock record (Berkelhammer, 2017; Weber et al., 2017). Adakite-like (Trend 2b) samples in the cobble dataset are consistent with these occurrences of Trend 2b in the bedrock record, but also show minor occurrences of Trend 2b throughout the entire history of the arc (Figs. 5.2 – 5.7).

Transitional-tholeiitic magmas (Trend 1) have been identified in the bedrock record at <1.0 Ma (Preece and Hart, 2004), at ~2.5 Ma (Keast et al., 2016), from ~12.5 – ~5.3 Ma (Trop et al., 2012), and from ~23.0 – ~18.0 Ma (Berkelhammer, 2017). Trend 1 magmas in the cobble record are only found from <1.0 Ma and from 10.8 – 5.9 Ma, which aligns well with the results of Preece and Hart (2004) and Trop et al., (2012), respectively.

Tectonic implications of geochemical timeline

Calc-alkaline magmas (Trend 2a) are signatures of "typical" subduction and, since the WA is a continental volcanic arc, are temporally ubiquitous throughout the bedrock and cobble record (Richter et al., 1990; Skulski et al., 1991; 92; Preece and Hart, 2004; Trop et al., 2012; Berkelhammer, 2017; Trop et al., 2017; this study). Additionally, the youngest (<5.0 Ma) and oldest (28.0 – 17.0 Ma) cobbles in our dataset have Ba/Nb ratios > 100, which is indicative of a subduction component (Fig. 4.20; Pearce et al., 2005). The tectonic implication of these cobble and bedrock occurrences through time is that subduction processes (e.g., melting of subduction-affected mantle wedge) have been continuous throughout the ~29.0 m.y. history of the arc.

Cobbles defined as Trend 2b occur throughout the entire history of the WA as well (Figs. 5.2 – 5.7), but are more abundant during the youngest (<1.0 Ma) and oldest (~28.0 – ~17.0 Ma) phases of WA magmatism, i.e. during modern magmatism and arc initiation, respectively (Figs. 5.2 and 5.7). Twelve of the thirteen oldest (28.0 – 17.0 Ma) cobbles in the dataset are considered Trend 2b, with only one cobble classified as Trend 2a (Fig. 5.7). The youngest (<5.0 Ma) and oldest (28.0 – 17.0 Ma) cobbles have the highest Sr/Y (> ~25; Fig. 4.24) in the dataset, which is consistent with partial slab melting. Furthermore, these same age groups (<1 Ma and ~28 – ~17 Ma) have Ba/Nb ratios > 100 (Fig. 4.20), which indicates a mantle wedge melt component ("normal" subduction) *in the same rocks* with a slab melt component. Trend 2b cobbles are referred to as "adakite-like" in this discussion since we do not have the all the necessary data to identify them as true adakites. La/Yb ratios are sometimes used to distinguish different types of adakites (Moyen, 2009), but we do not have Yb data, so the La/Yb ratio cannot be used to make this distinction. Since La/Yb ratios are not available, but there is evidence that Trend 2b cobbles

have components of partial slab melting and mantle wedge melting, it can be concluded this may have arisen from the mixing of an adakite-like magma and magma derived from melting of the mantle wedge. This explanation is consistent with that of Berkelhammer (2017) for similar compositions in the SCVF and by Weber et al., (2017) in locations across the north-central WA. In the bedrock record, occurrences of Trend 2b are only identified at <5.0 Ma (Preece and Hart, 2004) and ~29.0 – ~20.0 Ma (Berkelhammer, 2017; Weber et al., 2017). Trend 2b cobbles are more abundant during the time periods recognized in the bedrock (Figs. 5.2 and 5.7), but nonetheless occur throughout the entirety of WA magmatism (Figs. 5.2 – 5.7). The tectonic implication of this is that partial slab melting and mantle wedge melting occurred contemporaneously, and may have mixed to generate adakite-like compositions, throughout the entire history of WA magmatism.

Cobble data show that Trend 1 (transitional-tholeiitic) occurs during very young, 0.7 – 0.4 Ma, (Fig. 5.2) or intermediately aged magmatism, 10.8 – 5.9 Ma (Figs. 5.5 and 5.6). Additionally, many of the intermediate-aged cobbles and all of the very young cobbles considered Trend 1 have relatively high Nb/Zr (> ~0.03) when coupled with relatively low $(Sr/P)_n$ ratios (< ~2) compared to the rest of the dataset (Fig. 4.22). Note that some primitive samples in this dataset have Nb/Zr > ~0.06, but these samples do not yet have an age (Fig. 4.22). Overall, no cobble data show Nb/Zr ratios consistent with true intraplate character (Nb/Zr > 0.135; Sun and McDonough, 1989), but there is a clear difference between these 0.7 – 0.4 Ma and 10.8 – 5.9 Ma cobbles that show these relatively high Nb/Zr and low $(Sr/P)_n$ ratios versus the rest of the cobble dataset. In fact, all these relatively high Nb/Zr and low $(Sr/P)_n$ cobbles that are 0.7 – 0.4 Ma and 10.8 – 5.9 Ma plot as Trend 1 when data is coded according to Preece and Hart (2004) criteria (Fig. 5.8). Note that, even without primitive (i.e., MgO > 6.0 wt.%, Ni > 100ppm, and Cr >200 ppm) distinctions, there is a clear difference between transitional-tholeiitic Trend 1 chemistries and subduction-related Trend 2 chemistries: Trend 1 corresponds to relatively high Nb/Zr and low $(Sr/P)_n$, whereas Trends 2a and 2b are the opposite. While Trend 1 is not consistent with a true intraplate signature, it is consistent with less fluid-fluxed mantle wedge melting (lower $(Sr/P)_n$) and more decompression melting brought about by intra-arc extension (Preece and Hart, 2004; Trop et al., 2012).

These cobble data fit with previous studies that documented transitional-tholeiitic chemistries in the bedrock from these time periods (Preece and Hart, 2004; Trop et al., 2012).

Recent studies have also recognized transitional-tholeiitic (Trend 1) chemistries at ~2.5 Ma (Keast et al., 2016) and spanning ~23.0 – ~18.0 Ma in the SCVF (Berkelhammer, 2017) which were not captured in the cobble record. Notably, we did not collect any cobbles from the SCVF area, hence we acknowledge the geochemical and age data from this older region of the WA, but cannot compare the cobble dataset directly to the bedrock dataset for this region.

Transitional-tholeiitic (Trend 1) rocks are shown to be indicative of localized intra-arc extension in the western WA (Preece and Hart, 2004) and central WA (Trop et al., 2012; Keast et al., 2016; Berkelhammer, 2017). The tectonic implication of this is that intra-arc extension and subsequent basin formation has occurred in discrete time periods during WA magmatism: ~23.0 – ~18.0 Ma (Berkehlhammer, 2017); ~12.5 – ~5.3 Ma (Trop et al., 2012); ~2.5 Ma (Keast et al., 2016); <1.0 Ma (Preece and Hart, 2004). The youngest (< 5.0 Ma) and oldest (28.0 – 17.0 Ma) have low Nb/Zr ratios (< ~0.04) that indicate no intraplate component (i.e., decompression) went into the generation of these magmas (Fig. 4.22). These time periods were concurrent with eruptions of Trend 2a and Trend 2b (Figs. 5.2, 5.5, and 5.6), which suggests that intra-arc basins were forming concurrently with subduction and partial slab melting, but only during specific periods.

Are the controls on the occurrences of various magma types local or arc-wide?

Throughout the ~29.0 m.y. history of the WA, Trend 2a (calc-alkaline) and Trend 2b (adakite-like) cobbles are distributed evenly across the arc (Fig. 5.9). Virtually every study in the western (Richter et al., 1990; Preece and Hart, 2004) and central (Richter et al., 1990; Trop et al., 2012; Keast et al., 2016; Berkelhammer, 2017; Trop et al., 2017) has shown continuous spatial distribution of calc-alkaline (Trend 2a) rocks in the bedrock record. Trend 2b rocks have been recognized at Mt. Drum in the western WA and Mt. Churchill in the central WA (Fig. 1.1; Preece and Hart, 2004) and from the SCVF (Figs. 1.1, 2.1, and 2.3) in the north-central WA (Berkelhammer, 2017; Weber et al., 2017).

Trend 1 rocks, however, are more localized in occurrence. For example, no Trend 1 rocks have been observed in the cobble dataset from the Nadina to the Kuskulana Rivers of the western arc (Figs. 4.5 and 5.9). This absence of Trend 1 rocks in this area of the western WA is also seen in the bedrock record (Preece and Hart, 2004). While Preece and Hart (2004) show numerous occurrences of Trend 1 rocks within the WA, they sampled bedrock north of these

rivers (Fig. 5.9; Nadina, Dadina, Chetaslina, Kotsina, and Kuskulana) and outside the capture of the watersheds of these rivers, thereby avoiding the main bedrock contributors to each of these rivers (Mt. Wrangell, Mt. Blackburn; Table 4.2). Also, Preece and Hart (2004) point out that the locations of their Trend 1 occurrences are from Skookum Creek volcanic center (drained by the Nabesna and Jacksina Rivers; Table 4.2), the interior mesas (drained by the Nabesna and Jacksina Rivers; Table 4.2), and Mt. Sanford (drained by the Sanford River; Table 4.2), which are all locations where our data do show Trend 1 (Fig. 5.9). Trend 1 rocks are also observed in the SCVF (Fig. 1.1, 2.1, and 2.3; Berkelhammer, 2017) and as a basal unit at Eucher Mountain, adjacent to the Totschunda fault (Fig. 1.1, 2.1 and 2.3; Keast et al., 2016), as well as in the Yukon (Berkelhammer, 2017).

Tectonic implications spatial magmatic occurrences

Trend 2a (calc-alkaline) cobbles are universal across the western and central arc, which is unsurprising given that the WA is a continental volcanic arc. Cobbles draining from areas of the central and western WA have Ba/Nb ratios >100, consistent with a strong subduction signature (Pearce et al., 2005; Fig. 4.21). Some central WA and primitive cobbles are more heavily distributed at Ba/Nb < 100 (Fig. 4.21), indicating that some of the geochemistries in the central WA are controlled by upper plate processes, such as transtention along the Totschunda fault, rather than by subduction processes. Nonetheless, some central and western WA cobbles both show Ba/Nb ratios > 100, which is consistent with subduction fluid input (Pearce et al., 2005) across the entire arc since its inception.

Trend 2b cobbles are also found to drain from across the entire western and central arc (Fig. 5.9) and Trend 2b is recognized in the bedrock at Mt. Drum and Mt. Churchill (Preece and Hart, 2004). Mt Drum and Mt. Churchill are the northwestern- and southeastern-most volcanoes in the western and central WA, respectively (Fig. 1.1), and are coincident with the imaged leading and eastern edges of the subducting Yakutat microplate (Preece and Hart, 2004). Cobble data are consistent with these occurrences of Trend 2b because rivers draining from these two mountains (White, Dadina, Nadina, Sanford) capture cobbles recognized as Trend 2b (Fig. 5.9). Other occurrences of Trend 2b in the north-central bedrock and SCVF are thought to have been generated above the edge of the Yakutat microplate during early arc magmatism (i.e., ~29.0 – ~20.0 Ma; Berkelhammer, 2017; Weber et al., 2017). None of the rivers in this study drain the SCVF, but various rivers across the north-central WA (White, Chisana, Nabesna, and Copper;

Fig. 4.5) drain these mapped intrusives and captured Trend 2b cobbles (Fig. 5.9). Some cobbles from the central and western WA also have Sr/Y > ~25, which is consistent with our definition of adakite-like (Fig. 4.25). Again, there is a general difference between central and western rocks: most central WA rocks and primitive samples are grouped at Sr/Y < ~25, whereas most western WA have Sr/Y > ~25 (Fig. 4.25), indicating they are not adakite-like. Bedrock occurrences indicate Trend 2b is spatially restricted to the where the leading front of the Yakutat microplate was during early arc magmatism (Berkelhammer, 2017; Weber et al., 2017), or the current northwest and southeast edges of the subducting Yakutat (Preece and Hart, 2004). However, cobble data suggest an arc-wide distribution of Trend 2b (Fig. 5.9). There are Trend 2b cobbles from every river we sampled (except for Cross Creek, a tributary to the larger Chisana drainage; Fig. 5.9), some of which drain from areas where Trend 2b is *not* recognized in the bedrock (i.e., from rivers in the western WA that do not drain Mt. Drum: Chetaslina, Kotsina, Kuskulana; Figs. 1.1 and 4.5). These spatial occurrences indicate a component of partial slab melting across the entire arc. The fact that Trend 2b and Trend 2a cobbles are both spatially ubiquitous further supports the previous explanation that Trend 2b chemistries were generated from the mixing of an adakite-like magma, likely along a slab edge given the locations of Trend 2b occurrences in the bedrock (Preece and Hart, 2004; Berkelhammer, 2017; Weber et al., 2017), and a magma derived from melting of the mantle wedge (Trend 2a).

The most spatially restricted magma type in the cobble record is Trend 1, which is consistently absent from the Nadina River southward to the Kuskulana River (Fig. 5.9). Note that the Nabesna River and Cross Creek also have no cobble occurrences of Trend 1 (Fig. 5.9). However, the Jacksina River contains Trend 1 cobbles and the Jacksina is a tributary drainage to the Nabesna. This is reversed for the absence of Trend 1 cobbles from Cross Creek: Cross Creek is a tributary to the larger Chisana drainage, which *does* have Trend 1 cobbles (Fig. 5.9). Cross Creek also only has three available samples so it is entirely possible that Cross just missed the Trend 1 cobbles that were captured by the much larger Chisana drainage. Bedrock studies (Preece and Hart, 2004; Keast et al., 2016; Berkelhammer, 2017) show only localized occurrences of Trend 1, which stand in contrast to abundant spatial occurrences of Trends 2a and 2b. In summary, there are no Trend 1 cobbles draining from the Nadina, Dadina, Chetaslina, Kotsina, or Kuskulana Rivers and we hypothesize this is because there are no Trend 1 occurrences in the bedrock of each of these drainages. We conclude our sampling strategy did

not miss any Trend 1 cobbles that were in fact here. Rather, by using the known bedrock record, we can conclude that Trend 1 rocks do not exist here: Preece and Hart (2004) identified Trend 1 in the interior of the arc, with Trend 2a on either side. This is further highlighted by trace element ratio differences between the central and western WA. Some central WA cobbles have relatively high Nb/Zr ratios (> ~0.04) and low $(Sr/P)_n$ (< ~2) , which corresponds to Trend 1, while most western WA cobbles show the opposite (Fig. 4.23). These relatively high Nb/Zr and low $(Sr/P)_n$ are consistent with decompression melting brought about by intra-arc extension. Given the spatially isolated areas of Trend 1 throughout the bedrock and the nature of our sample collection, we cannot use our cobble data to make any significant spatio-tectonic implications about Trend 1.

What do spatio-temporal trends of magmatism reveal about tectonic regime(s) that formed the modern WA?

When cobble and bedrock geochemical, temporal, and spatial data are integrated, they show that similar magma-generation and tectonic processes have been ongoing over the past ~29.0 m.y. of WA magmatism, even though magmatism, and magma-generation processes, have migrated through time (Richter et al., 1990; Fig. 2.4). The following discussion will consider the spatial occurrences of each magma type (Trend 1, 2a, 2b) during the time intervals defined in the Results section (28.0 – 17.0 Ma, 17.0 – 13.0 Ma, 13.0 – 8.0 Ma, 8.0 – 5.0 Ma, 5.0 – 3.0 Ma, 3.0 – 1.0 Ma, and <1.0 Ma) in order to reveal spatio-temporal trends and their tectonic implications for WA magmatism.

28.0 to 17.0 Ma

The detrital sand and cobbles with ages of 28.0 – 17.0 Ma all came from the north-central WA—the Nabesna, Chisana, and White Rivers, and Cross Creek (Fig. 5.1)—and the oldest cobble (~28.0 Ma) drained from the Nabesna River (Figs. 4.2 and 5.1). In the cobble dataset, there are thirteen samples with ages that fall in the 28.0 – 17.0 Ma range. Twelve of these thirteen cobble samples of 28.0 – 17.0 Ma are defined by their geochemistry as Trend 2b. The one sample (Cross 7) not classified as Trend 2b is defined as Trend 2a (Figs. 5.7, 5.10, and Table 5.1).

The earliest WA magmatism recorded in the bedrock is from the SCVF also located in the north-central WA, but north of the White River and beyond the capture of its watershed (Berkelhammer, 2017; Figs. 1.1, 1.2, and 4.5). Magmatism began here at ~29.0 Ma and continued until 18 Ma (Figs. 1.1, 2.1, and 2.3; Berkelhammer, 2017). There are no cobble data from rivers draining the SCVF, but there are abundant detrital sand data from the area, that support the ~29.0 Ma start (Davis et al., 2017; Trop et al., 2017). In the SCVF, Trend 2a is documented from ~29.0 – 18.0, Trend 2b is documented from ~28.0 – ~23.0 Ma, and Trend 1 is documented from ~23.0 – 18.0 Ma (Berkelhammer, 2017). Various intrusions classified as Trend 2b are also found across the north-central WA, with ages of ~29.0 – ~20.0 Ma (Weber et al., 2017).

Tectonic implications of spatio-temporal trends, 28.0 – 17.0 Ma

These 28.0 – 17.0 Ma samples all drain from the White, Chisana, and Nabesna Rivers, and Cross Creek, located in the north-central WA (Fig. 5.7), which suggests that arc magmatism initiated by ~28.0 Ma in the north-central WA and remained relatively fixed in this area until ~18.0 – 17.0 Ma (Berkelhammer, 2017; Trop et al., 2017; this study). The fact that the oldest cobbles in the dataset are mostly Trend 2b and Trend 2a suggests that magmatism from 28.0 – 17.0 Ma in the north-central WA (areas drained by the White, Chisana, and Nabesna Rivers, and Cross Creek; Figs. 5.1 and 5.7) primarily resulted from concurrent subduction-driven processes: mantle wedge melting (Trend 2a) and partial slab melting (Trend 2b). These simultaneous processes likely led to magma mixing between the mantle wedge and partial slab melts, thereby generating the Trend 2b, adakite-like chemistries seen in the cobble record as well as in the SCVF (Berkelhammer, 2017; Weber et al., 2017). Bedrock data support this, given temporal and spatial occurrences of Trend 2a and Trend 2b in the SCVF (Berkelhammer, 2017) and occurrences of Trend 2b throughout the north-central WA (Weber et al., 2017). A majority of the cobbles from 28 – 17 Ma (i.e., 12 out of 13 cobbles) are Trend 2b, implying that partial slab melting was the dominant process during the time following the subduction initiation of the Yakutat microplate. During this early arc period (28.0 – 17.0 Ma), when subduction had just recently initiated, subducting slabs and slab edges are more prone to melting due to increased thermal gradients (Sajona et al., 1993), which may explain the widespread distribution of these old Trend 2b occurrences in the bedrock and cobbles, during ~29.0 – ~20.0 Ma and ~28.0 – 17.0 Ma, respectively.

A discrepancy between cobble and bedrock data arise from the lack of Trend 1 seen in the cobble record during 28.0 – 17.0 Ma, but the presence of Trend 1 in the bedrock of SCVF from ~23.0 – 18.0 Ma (Berkelhammer, 2017). However, as previously mentioned, no cobbles were collected from rivers that drain the SCVF, thereby not capturing the bedrock of the SCVF and any occurrences of Trend 1 there. Nevertheless, the fact that Trend 1 bedrock exists, with ages from ~23.0 – 18 Ma, suggests that decompression melting triggered by intra-arc extension was occurring in the SCVF (Berkelhammer, 2017) during the same time as subduction, but initiated ~6.0 m.y. after continuous arc activity began.

17.0 to 13.0 Ma

Cobble data show no samples with ages of ~17.0 – ~13.0 Ma. It is possible that our sampling technique missed samples from this age range. However, other studies of detrital material are consistent with our results. Davis et al. (2017) dated 862 sand grains using $^{40}Ar/^{39}Ar$ geochronology and found no ages in the range of 17.0 – 13.0 Ma. Trop et al. (2017) dated 2757 detrital zircons and found sixteen out of those 2757 total zircons (<0.006 %) with ages in the range of 17.0 – 13.0 Ma draining from the Nabesna, White, and Chitistone Rivers in the central WA (Fig. 4.5; Trop et al., 2017). Collectively, these studies suggest that rocks with an age of 17.0 – 13.0 Ma are either non-existent in most areas of the arc or very sparse (J. Trop, pers comm). This scarcity of samples means there was likely a significant reduction in the volume of magmatism in the central WA during 17.0 – 13.0 Ma. However, this age gap may also reflect mineral fertility differences between U/Pb (zircons) and $^{40}Ar/^{39}Ar$ (bedrock, cobbles, detrital sand) dating techniques. These scarce 17.0 – 13.0 Ma single grain zircon ages may be reflecting zircon rich felsic (i.e., zircon fertile) eruptions or intrusions and minor to no mafic/intermediate magmatism during this time. In contrast, magmatism in the eastern WA (Yukon) was active from 18.0 – 10.0 Ma, and notably during the 17.0 – 13.0 Ma the void presented by the current bedrock and cobble records of the western and central WA (Skulski et al., 1991; 92).

Tectonic implications of spatio-temporal trends, 17.0 – 13.0 Ma

The complete lack of cobbles and bedrock from 17.0 – 13.0 Ma would seem to imply that there was no magmatic activity in the western and central WA during this time. However, there are very scare detrital zircons from the central WA with ages from 17.0 – 13.0 Ma (Trop et al., 2017) that instead suggest the possibility of very little magmatic activity in the central WA

during this time. It is significant to note that no bedrock or cobble data corroborate these detrital sand data.

Meanwhile, the eastern WA was magmatically active from 17.0 – 13.0 Ma (Skulski et al., 1991; 92). Magmatic activity in the eastern WA was active and subparallel to the Denali and Duke River faults (Figs. 2.1 and 2.3), during 18.0 – 10.0 Ma, but only independent from western and central WA magmatism from 17.0 – 13.0 Ma. This suggests there was a migration of magmatism starting at ~18.0 – 17.0 Ma (last documented bedrock and cobble ages in the central WA) from the initial locus in the north-central WA (SCVF) towards the southeast (Yukon) that lasted until ~10.0 Ma. Bedrock from the eastern WA during this 18.0 – 10.0 Ma span varies from calc-alkaline to transitional to alkaline in composition (Skulski et al., 1991; 1992). However, Berkelhammer (2017) show that these calc-alkalic compositions found in the Yukon should actually be considered Trend 1 (transitional-tholeiitic). Therefore, all magmas from the 17.0 – 13.0 Ma period are, to some extent, related to extension which allowed various degrees of decompression melting. Given the proximity of eastern WA volcanic fields to the Denali and Duke River faults and the southeastward progression of magmatism from the north-central starting at ~18.0 Ma (Figs. 2.1 and 2.3), there is likely a link between fault movement and magmatism (Skulski et al., 1991; 1992). Magmatism became dormant in the eastern WA at ~10.0 Ma (Skulski et al., 1991; 1992). Given the genetic link between movement along the faults and magmatism, the complete lack of central and western WA bedrock and cobbles during 17.0 – 13.0 Ma, and the occurrences of Trend 1 (Berkelhammer, 2017) and transitional to alkaline magmas (Skulski et al., 1991; 1992) in the eastern WA, we hypothesize that from 17.0 – 13.0 Ma the dominant tectonic regime responsible for magmatism was a combination of extensional motion along strike-slip faults *and* subduction, which can be explained by the migration of magmatism and chemical progression to extensional-dominated magmas. This halt of central and western WA magmatism and southeastward migration of magmatism was likely accomplished by slab rollback, to diminish the subduction component of melting and to move the locus of magmatism to the south, coupled with dextral movement along the Denali and Duke River faults, which provided conduits for magmas (most magmas from this period show some component of decompression melting; Skulski et al., 1991; 1992; Berkelhammer, 2017), acting simultaneously.

13.0 to 8.0 Ma

Magmatism returned across the international border to the central WA starting at ~13.0 Ma, as is evident explicitly in the cobble record: one sample, classified as Trend 2a, with an age of 12.63 ± 0.28 Ma comes from the White River, followed by continuous magmatism until ~8.0 Ma (Figs. 5.1 and 5.11). During this 13.0 – 8.0 Ma time, Trend 1, 2a, and 2b chemistries draining from the White and Chisana rivers are observed in the cobble record (Figs. 5.6 and 5.11). Detrital sand and zircons are consistent with and support this cobble temporal progression from 13.0 – 8.0 Ma (Trop et al., 2017).

Contemporaneous magmatic activity between the eastern and central WA continued until ~10.0 Ma, when the eastern WA became dormant (Skulski et al., 1991; 92). The bedrock record documents a return of magmatism to the central WA at ~12.5 – ~11 Ma (Trop et al., 2012) that is south of the location of initial arc magmatism in the north-central WA (see location of "Late Miocene arc volcanism" in Fig 1.1). Magmatism in the central WA bedrock during 13.0 – 8.0 Ma is classified as primarily Trend 1 and Trend 2a, with very minor Trend 2b (Trop et al., 2012).

Tectonic implications of spatio-temporal trends, 13.0 – 8.0 Ma

The bedrock and cobble records imply that magmatism during this 13.0 – 8.0 Ma period was focused in the central WA (Figs. 5.6 and 5.9), with ~3.0 m.y. of overlapping magmatic activity between the central and eastern WA (eastern WA magmatism concluded at ~10.0 Ma). All three magma types (Trend 1, 2a, and 2b) are found in the bedrock and cobble record during this time. After the return of magmatism in this region starting at ~13.0 Ma, ~2.0 – 3.0 m.y. went by before Trend 1 appeared in the cobble record, and these Trend 1 occurrences are confined to the a ~1.0 m.y., period, from 11.0 – 10.0 Ma (Fig. 5.11). Despite this temporal restriction in the cobble record, the bedrock record shows occurrences of Trend 1 from 13.0 – 8.0 Ma (Trop et al., 2012). This implies that subduction (Trend 2a), likely slab melting (Trend 2b), and intra-arc extension (Trend 1) were all acting concurrently during this 13.0 – 8.0 Ma period.

However, one vital question remains: What caused magmatism to migrate back to the central WA and eastern WA magmatism to become dormant? Significantly, the eastern WA went dormant at ~10.0 Ma but magmatism returned to the central WA at ~13.0 Ma, suggesting overlapping tectonic activity between the two regions. The geochemistries during this time period may help explain a change in tectonics. Recall that the geochemistries in the eastern WA all have an extensional component: Trend 1, transitional, and alkaline chemistries (Skulski et al. (1991; 1992) all indicate a component of decompression melting, but there is less subduction

input in all of these rocks. The return of magmatism to the central WA at ~13.0 Ma is marked by a return to a subduction component (Trend 2a; Fig. 5.11), suggesting a change with the subducting slab took place at ~13.0 Ma. Given the northwestward progression of magmatism, we hypothesize a halt in slab rollback, and a change in plate orientation and/or subduction direction (towards the northwest) of the subducting Yakutat microplate to cause this northwest migration.

8.0 to 5.0 Ma

Cobbles with ages of 8.0 – 5.0 Ma are only observed from Chisana River (Fig. 5.1) and are primarily Trend 2a with relatively less occurrences of Trend 2b and Trend 1 (Figs. 5.5 and 5.12). Cobbles show a progression of Trend 2a to Trend 2b with a conclusion of Trend 1 (Fig. 5.12). Detrital sand data show ages of 8.0 – 5.0 Ma focused primarily in the central WA, but with some from data the Kuskulana, Kotsina, Chetaslina, and Boulder Rivers in the western WA (Fig. 4.5; Davis et al., 2017; Trop et al., 2017). The bedrock record contains Trend 1 and Trend 2a located at the Green Hills area in the central WA with ages from ~7.0 – ~4.5 Ma, ~4.5 Ma being the youngest age documented in the central WA (Fig. 1.1; Fitzgerald et al., 2016).

Tectonic implications of spatio-temporal trends, 8.0 – 5.0 Ma

The bedrock and cobble record reiterate that magmatism was relatively fixed in the central WA (Fig. 1.1) from 8.0 – 5.0 Ma. The dominant occurrences of Trend 2a suggests a subduction regime, with partial slab melting and intra-arc extension (Trends 2b and 1, respectively) being less dominant processes but nevertheless present. During 8.0 – 5.0 Ma, there are no major migrations or transitions between geochemical signatures to account for, so we hypothesize tectonic processes were relatively consistent with the previous time division.

5.0 to 3.0 Ma

Cobbles with ages of 5.0 – 3.0 Ma are only seen from the Kuskulana River, which is consistent with draining the 4.2 – 3.4 Ma Mt. Blackburn in the western WA (Figs. 1.1, 4.5, and Table 4.2). Detrital data show ages of 5.0 – 3.0 Ma from across the western WA (Davis et al., 2017; Trop et al., 2017). The cobbles are Trend 2a and Trend 2b (Fig. 5.13), suggesting subduction and partial slab melting but no intra-arc extension during 5.0 – 3.0 Ma. Bedrock from this time are consistent with Trend 2a in the western WA, but Trend 2b is not recorded in the bedrock from 5.0 – 3.0 Ma (Preece and Hart, 2004).

Tectonic implications of spatio-temporal trends, 5.0 – 3.0 Ma

Between the period of 8.0 – 5.0 Ma and 5.0 – 3.0 Ma, the locus of magmatism continued to migrate towards the northwest, from the central WA to Mt. Blackburn in the western WA (Figs. 1.1 and 2.4). The migration from the central WA to the western WA was accompanied by a halt in Trend 1 (no Trend 1 occurrences in the cobbles (Fig. 5.13) or the bedrock during this period), suggesting no intra-arc extension after the initial migration, from 5.0 – 3.0 Ma. Rather, given the geochemical data that exist in the cobble and bedrock record, this period was dominated by subduction-processes.

3.0 to 1.0 Ma

Cobbles with ages of 3.0 – 1.0 Ma drain from the Kuskulana, Kotsina, Dadina, Sanford, and Nabesna Rivers (Fig. 5.1 and 5.3). The Kuskulana, Kotsina, Dadina, and Sanford Rivers drain the western WA, whereas the Nabesna River drains portions of both the central and western WA (Fig. 4.5). This young (3.0 – 1.0 Ma) Nabesna sample is the only sample draining from the Nabesna River that is not in the 28.0 – 17.0 Ma age group (Fig. 5.7). These cobble occurrences are consistent with detrital (Davis et al., 2017; Trop et al., 2017) and most bedrock data (Preece and Hart, 2004; Keast et al., 2016). The one disagreement is the 2.4 – 2.0 Ma Mt. Eucher Mountain, truncated by the Totschunda fault on its west side, in the central WA (Fig. 1.1, 2.1, and 2.3; Keast et al., 2016). Eucher Mountain is within the Chisana River watershed (Figs. 1.1 and 4.5; Table 4.2), but there are no Chisana samples with ages of 2.4 – 2.0 Ma (Figs. 5.1 and 5.3), which indicates cobble sampling missed Eucher samples. This is not surprising given the Chisana cobbles were collected along a morainal bench sourcing bedrock up glacier from Eucher Mountain. Cobbles during this time are Trend 2a and Trend 2b (Figs. 5.3 and 5.14). Western WA bedrock data during 3.0 – 1.0 Ma are primarily Trend 2a (Preece and Hart, 2004), but Eucher Mountain contains a basal unit classified as Trend 1 (Keast et al., 2016). Again, since no cobbles are Trend 1 (Fig. 5.14), the cobble sampling missed Eucher Mountain samples.

Tectonic implications of spatio-temporal trends, 3.0 – 1.0 Ma

The locus of magmatism in the western WA during 3.0 – 1.0 Ma is consistent across cobble, detrital, and bedrock datasets (Preece and Hart, 2004; Davis et al., 2017; Trop et al., 2017). However, cobbles reveal Trend 2b during this 3.0 – 1.0 Ma period from the Kuskulana, Dadina, and Sanford Rivers (Figs. 5.3 and 5.14) that are not documented in the bedrock during this time (Preece and Hart, 2004). Trend 2b bedrock has been documented at Mt. Drum (Fig.

1.1) in the western WA, which the Dadina and Sanford Rivers drain (Fig. 4.5 and Table 4.2), but Trend 2b bedrock ages here are 0.7 -0.2 Ma (Preece and Hart, 2004). It is possible that the Sanford and Dadina Rivers have captured 3.0 – 1.0 m.y. old Trend 2b bedrock that is unrecognized in the literature. Or it is possible that all these Trend 2b samples are not the same suite identified by Preece and Hart (2004), but rather the product of mixing of an adakite-like magma and a magma derived from melting of the mantle wedge (Trend 2a).

Eucher Mountain may seem like a spatial and geochemical abnormality (it has Trend 1 whereas no bedrock or cobbles show Trend 1 from 3.0 – 1.0 Ma), but it is not. When slip rates along the Totschunda fault are extrapolated, they are consistent with the hypothesis that Eucher Mountain was translated along the Totschunda fault from an initial location in the western WA, adjacent to the Skookum Creek volcanic center, beginning at ~2.5 Ma (Keast et al., 2016), where its age is consistent with surrounding bedrock (Preece and Hart, 2004), cobbles (this study), and detrital sand (Davis et al., 2017; Trop et al., 2017). The Trend 1 basal unit at Eucher (Keast et al., 2016) also suggests that magmatism initiated with extension (i.e., transtension) along the Totschunda fault, triggering decompression melting.

Less than 1.0 Ma

Cobbles with ages of <1.0 Ma (i.e., modern WA magmatism) are spatially restricted to the western WA—the Kotsina, Chetaslina, Dadina, Nadina, and Sanford Rivers (Figs. 5.1). This is consistent with detrital data (Davis et al., 2017; Trop et al., 2017) and the bedrock record (Preece and Hart, 2004). Cobbles occur as Trends 1, 2a, and 2b (Figs. 5.2 and 5.15), which is consistent with the compositions also seen in the bedrock (Preece and Hart, 2004). Note that this age group of <1.0 Ma has, by far, the most cobbles (Figs. 5.2 and 5.15). The fact that a majority of cobbles are <1.0 Ma does not necessarily correlate to the most voluminous period of magmatism in the arc's history (although it could, but it is impossible to tell from our data). Rather, these samples are less weathered, they look the freshest in the field and may had biased the sample collector, and six out of the ten rivers with ages drain the western WA, which may artificially inflate the number of younger samples. Additionally with time, younger volcanic products can cover older volcanic products in a magmatic belt, leading to under representation of older units in the modern sedimentary system.

Tectonic implications of spatio-temporal trends, <1.0 Ma

The location of modern WA magmatism fits with the conclusion by Richter et al., (1990) that WA magmatism has migrated generally northwestward through time, though it was punctuated by a number of geographic shifts that were unrecognized by Richter et al. (1990). Cobble data and detrital sand and zircon data (Davis et al., 2017; Trop et al., 2017) also show a northwestward younging trend (Fig. 5.1). Trends 2a, 2b, and 1 cobbles and bedrock suggest concurrent subduction, partial slab melting, and intra-arc extension. Aside from the ~2.5 Ma Eucher Mountain, these Trend 1 occurrences are the first in the cobble and bedrock records since the northwest migration to the western WA took place at ~5.0 Ma.

Cobble occurrences of Trend 2b during this <1.0 Ma period are consistent with bedrock occurrences of Trend 2b at Mt. Drum and Mt Churchill (Fig. 1.1; Preece and Hart, 2004). Recall the widespread distribution of Trend 2b bedrock during early arc magmatism in the north-central WA (~29.0 – ~20.0 Ma; Berkelhammr, 2017; Weber et al., 2017) that is attributed to an increased thermal gradient along the newly subducted slab edges, causing slab edge melting on a relatively large scale (Trend 2b intrusions outcrop in the north-central WA for ~65 – 80 km). The formation of young (<1.0 Ma) Trend 2b magmas is thought to have occurred on a more localized scale, when wholesale slab edge melting was not as feasible because subduction has been ongoing for the past ~29.0 m.y.. The Trend 2b adakites identified by Preece and Hart (2004) are restricted to Mt. Drum and Mt. Churchill (Fig. 1.1) and therefore must be attributed to a more localized process than older adakite-like magmas recognized by Berkelhammer (2017), Weber et al. (2017), and this study. Preece and Hart (2004) and Fuis et al, (2008) suggest a slab tear on the northwest boundary of the Yakutat, underneath Mt. Drum. This slab tear, if present, may have created a slab window, allowing mantle flow along the slab's edge and subsequent slab melting (Preece and Hart, 2004; Thorkelson et al., 2011), thereby generating adakites. There is no geophysical evidence for a slab tear on the southeast edge of the Yakutat, underneath Mt. Churchill, so it requires a different explanation. Preece and Hart (2004) suggest a physical transition, between the down going Pacific Plate coupled with the Yakutat and the Pacific Plate, that increases shear stresses, thereby increasing the thermal gradient, which could lead to slab melting.

This leads to the question: what about Trend 2b cobbles? They drain from every river we sampled around the arc (Fig. 5.9) and exist outside of the time limits established by bedrock

occurrences, ~29.0 – ~20.0 Ma and <1.0 Ma (Figs. 5.2-5.7). The fact is, most Trend 2b cobbles may not be true adakites, especially if they are from rivers that don't drain Mt. Drum and Mt. Churchill. Trend 2b cobbles draining from rivers consistent with bedrock locations may be true adakites, but we have no way of knowing given that we do not have Yb concentrations. The best we can do it match bedrock occurrences with Trend 2b cobbles from rivers that drain those locations and that are the appropriate age. Otherwise, we resort back to the hypothesis that, since Trend 2b cobbles have components of partial slab melting and mantle wedge melting, these magmas may have arisen from the mixing of an adakite-like magma and a magma derived from melting of the mantle wedge.

Do cobbles reflect the existing bedrock record? Did this novel technique "work"?

The results from this study show that the sampled cobble lithologies largely reproduce the known bedrock record in geochemical (Figs. 5.16-5.18, Fig. 5.19a, and Fig. 5.20a), temporal (Figs. 5.19b and 5.20b), and spatial contexts (Figs. 5.19c and 5.20c). We did not discover any undocumented bedrock lithologies. Conversely, the known bedrock record doesn't contain any lithologies that are not present in the cobble record. The ages represented in the cobble record span the lifetime of the arc (~28.0 Ma to present) as known from the bedrock record and detrital sand/zircons ages (Figs. 2.5, 4.1, and 4.2; Davis et al., 2017; Trop et al., 2017). The cobble age data reproduce one key observation from other datasets: 1) The ~17.0 – ~13.0 Ma gap in volcanism in the bedrock and detrital sand records. This agreement serves to further solidify the robust nature of the cobble data in this study and indicate its validity and usefulness.

Within our dataset, cobble dates are more heavily distributed toward younger ages. Nearly half of the ages are <1.0 Ma, and samples become sparser the older they get (Fig. 4.1). In fact, the age category of 28.0 – 17.0 Ma only has 13 samples in it, but it covers the largest age range in our classifications. This could be due to sampling bias during collection but it's more likely that there just are not as many old samples in the form of cobbles (or exposed bedrock). Nearly 30.0 m.y. is a long time for rocks not to be tremendously weathered when they are exposed to high elevations, glaciers, ice fields, snow/rain, and large rivers. Therefore, it is more likely that older samples have been weathered, eroded, or covered by younger volcanic products whereas younger samples are still around for collecting. Nevertheless, the older samples (28.0 – 17.0 Ma) are still present in the cobble record and provide meaningful and significant data with implications for the inception of WA magmatism.

The ability of the cobble data to reproduce the geochronology and geochemistry based on more detailed field mapping and bedrock sample analysis is encouraging, because it suggests the methodology applied here can be successfully translated to other localities. In particular, it can be an efficient and cost effective way of indirectly sampling bedrock in locations where field conditions may limit sampling capabilities. It has the potential to provide access to lithologies that are otherwise inaccessible due to ice cover or another hindrance that restricts bedrock sampling. This type of sample collection method can also be easily added on to a more ambitious field study with relative ease to complement any bedrock record and increase the robustness of an entire dataset, and we suggest it will work in any arc-setting, or other igneous-hosted terrains, that are dissected by fluvial systems.

Future Work

The novel approach developed here of using stream cobbles as a reconnaissance tool has successfully contributed new results to an ongoing effort to gather data on the WA and expanded our understanding of the origin and evolution of the WA. The area under investigation is large (17 drainage basins encompassing more than 15,000 km^2 of the arc), remote, and relatively understudied. The fluvial cobble method employed here allowed for large swathes of land to be surveyed by collecting rocks from all over a drainage in a single location.

An alternative approach for future studies could be to focus on smaller areas by collecting cobbles from multiple sites along the same river, especially rivers that are known to drain regions of interest, moving closer to areas of interest. Standard sedimentological methodologies could also be used to obtain a petrological outcome. For example, the distribution of sample lithologies could be statistically analyzed within a grid system at each collection site to discourage over or underrepresentation of a particular lithology.

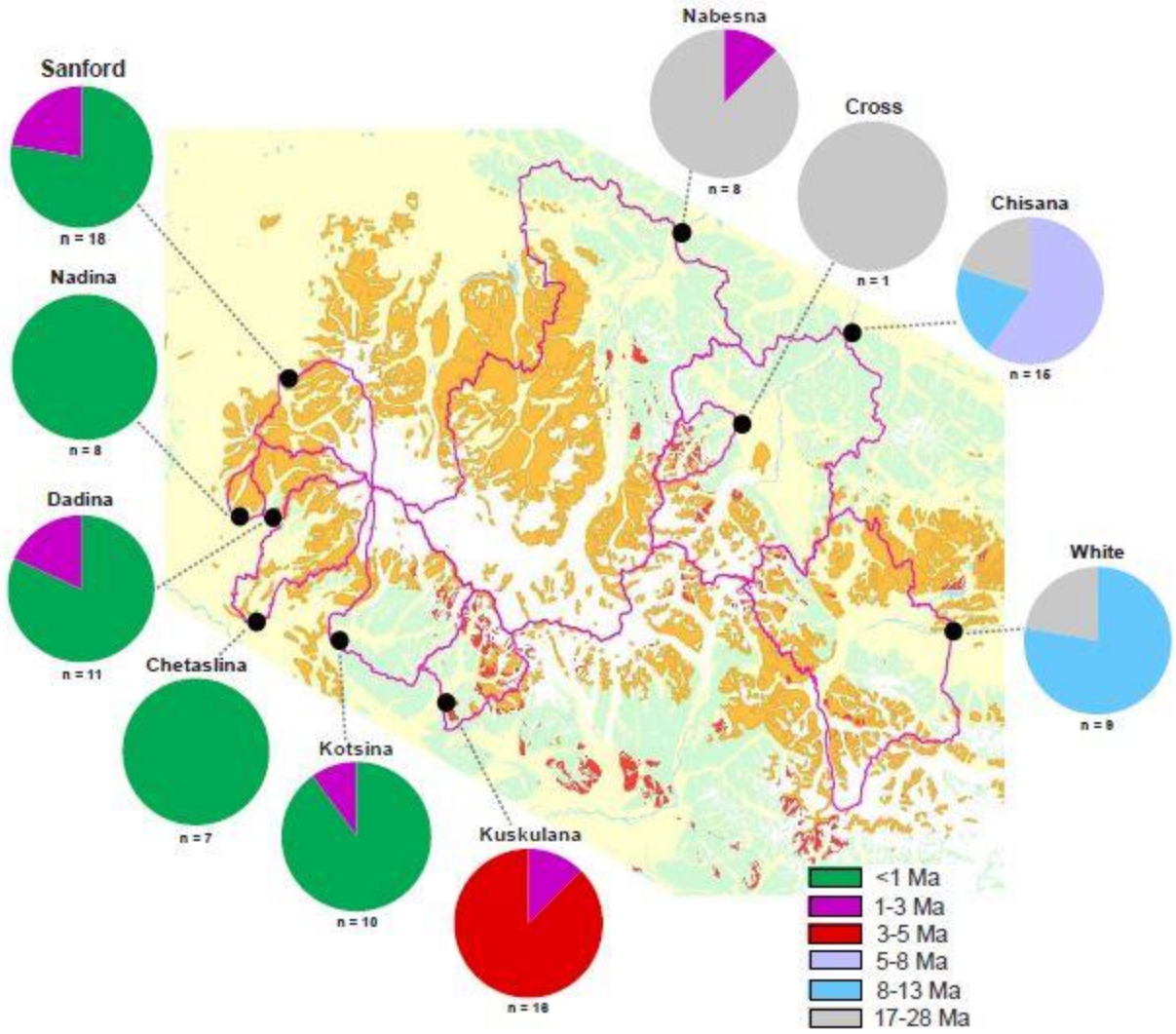

Figure 5.1 Watershed map showing the spatial distribution of different cobble ages throughout the WA. Note there are no cobbles in the 17 – 13 Ma age range.

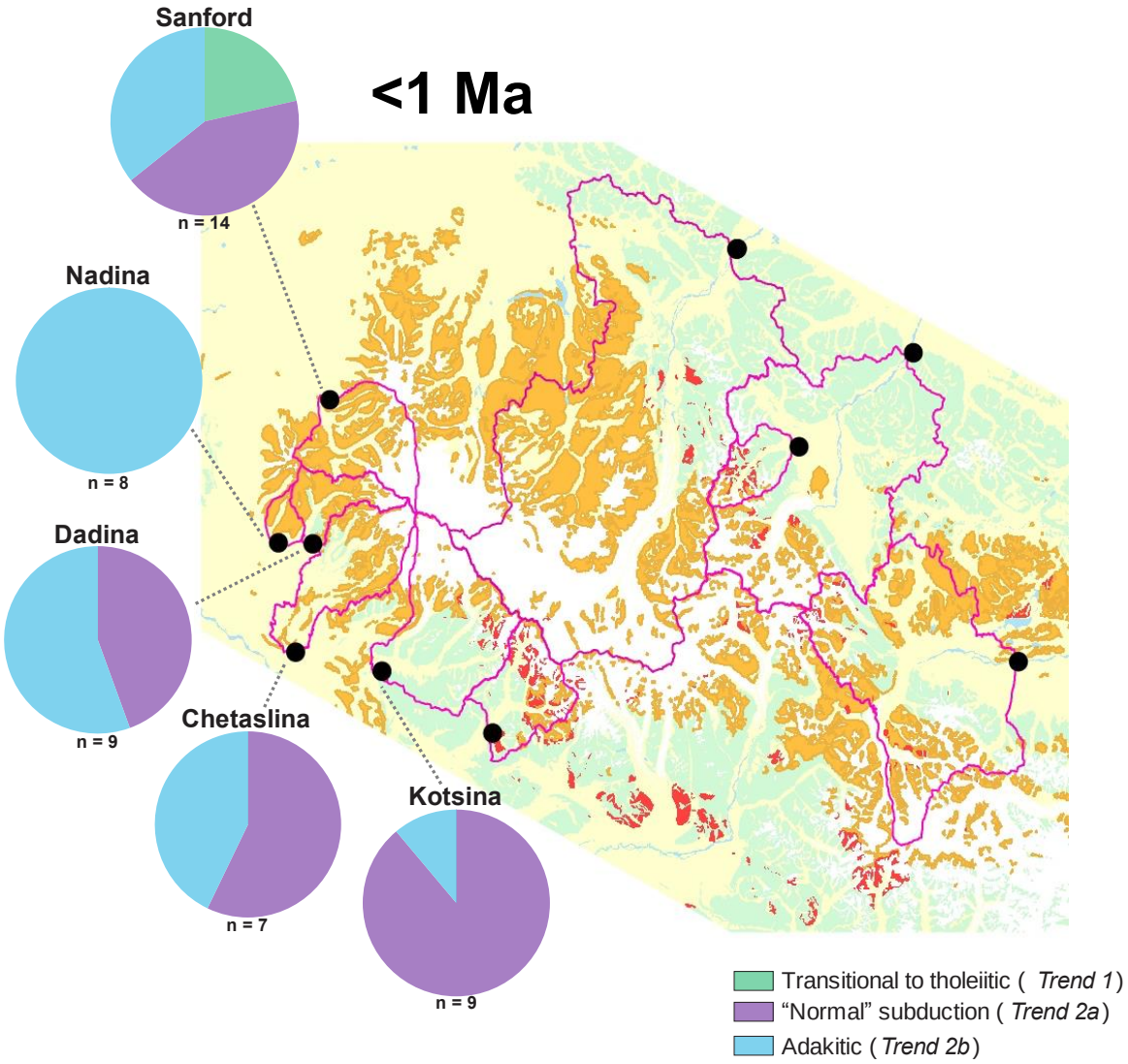

Figure 5.2 Cobble geochemical data, divided into Preece and Hart (2004) trends, showing the distribution of magma types at <1 Ma.

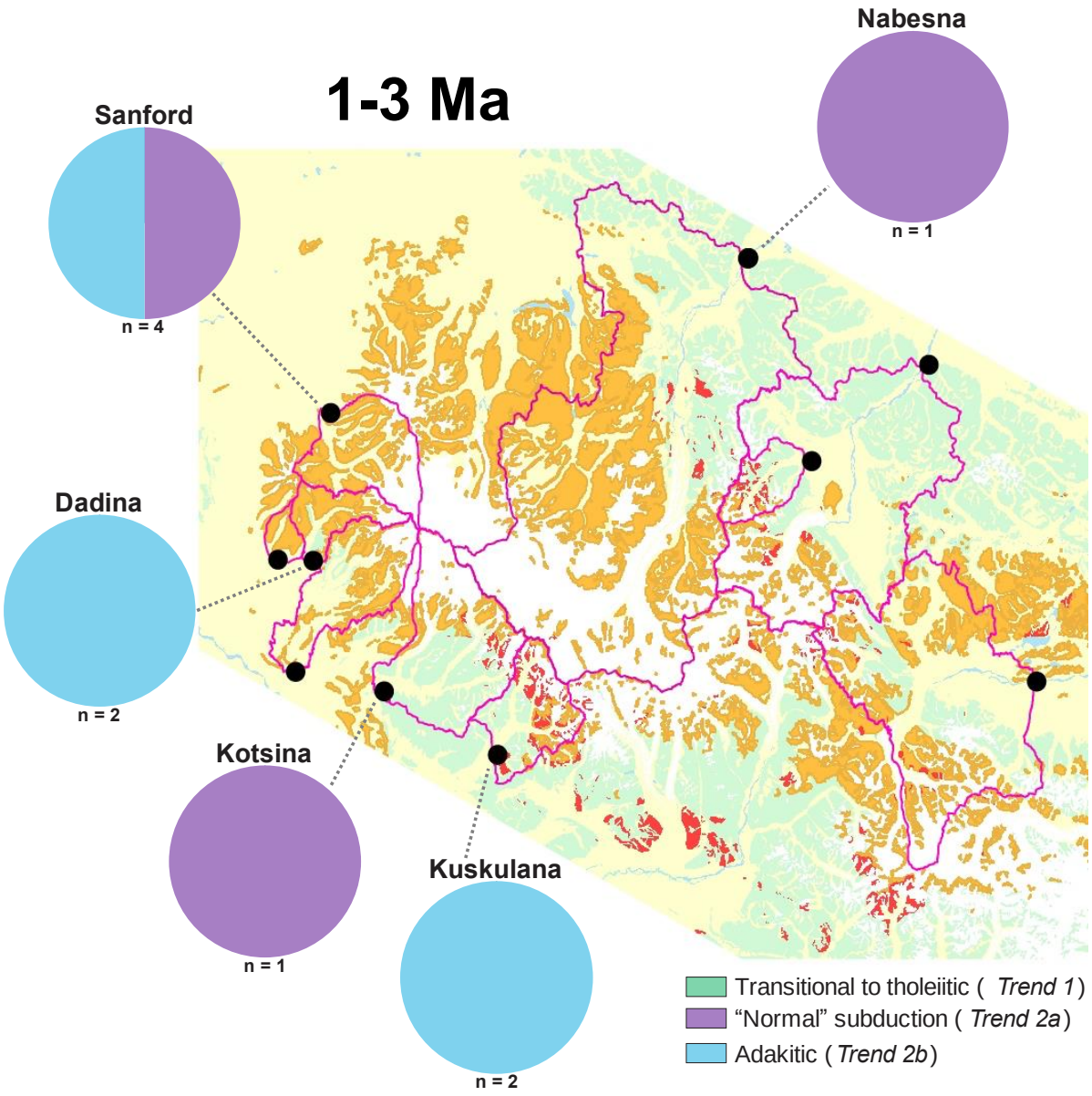

Figure 5.3 Cobble geochemical data, divided into Preece and Hart (2004) trends, showing the distribution of magma types at 1-3 Ma.

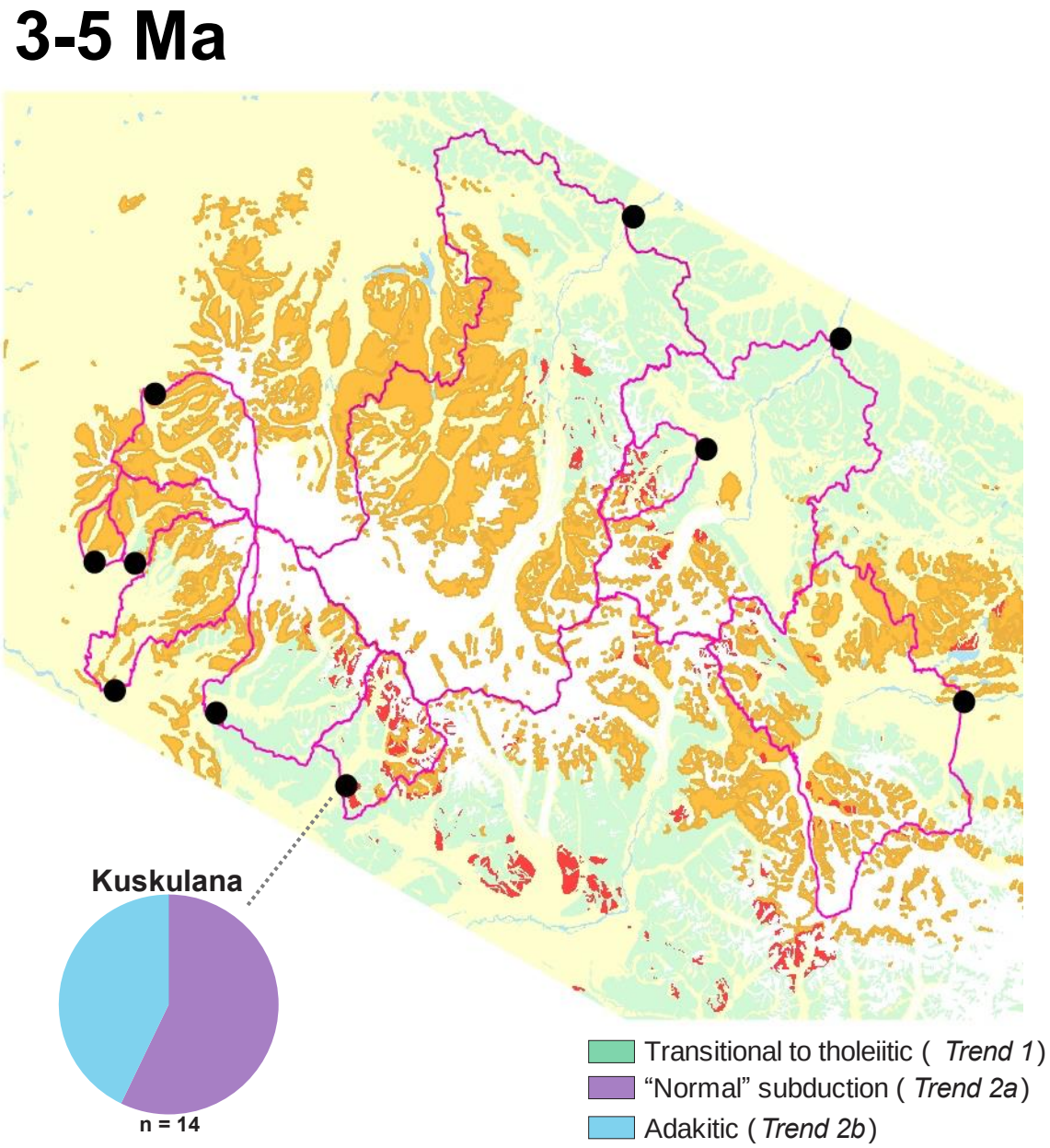

Figure 5.4 Cobble geochemical data, divided into Preece and Hart (2004) trends, showing the distribution of magma types at 3 - 5 Ma.

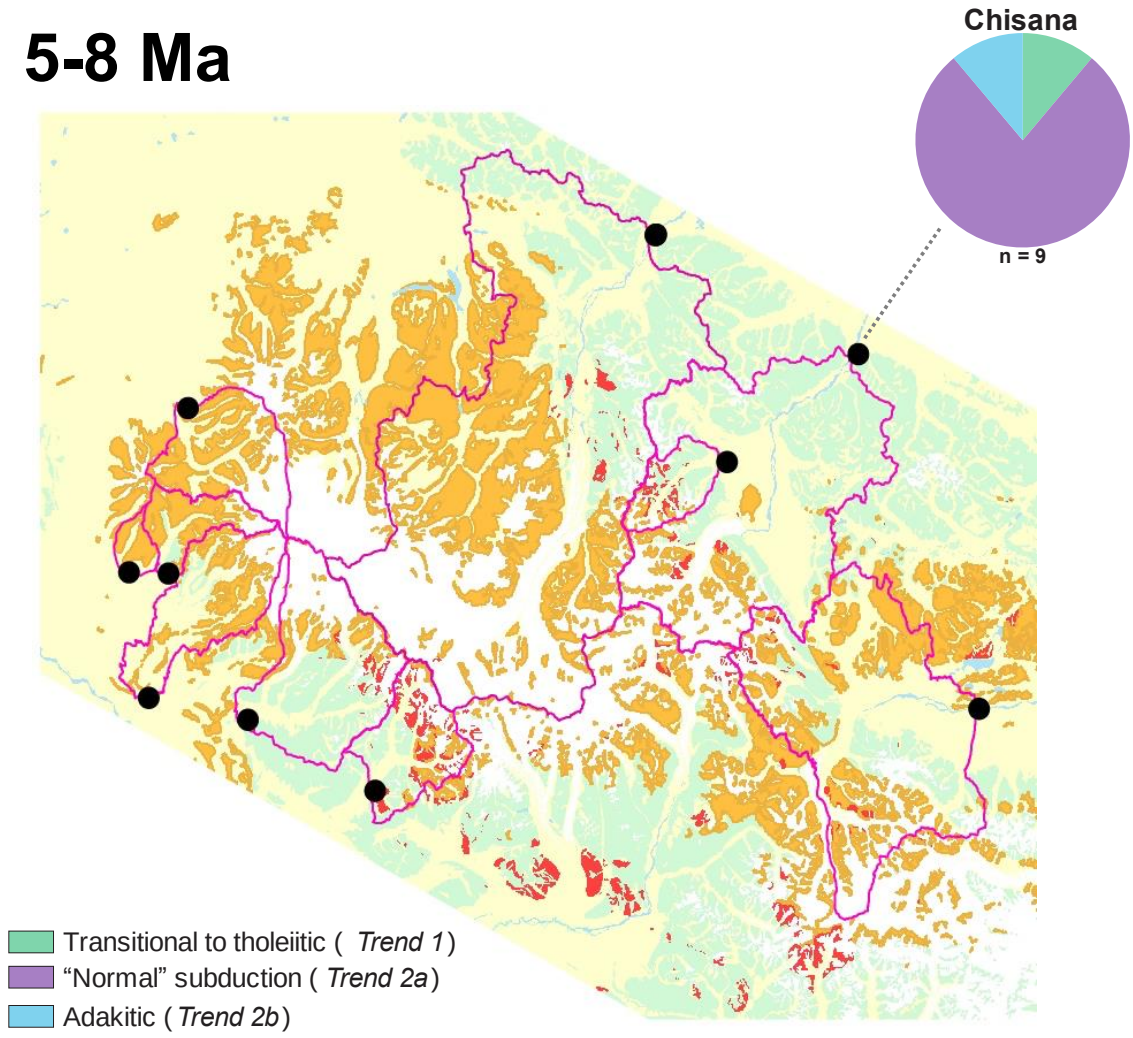

Figure 5.5 Cobble geochemical data, divided into Preece and Hart (2004) trends, showing the distribution of magma types at 5 - 8 Ma.

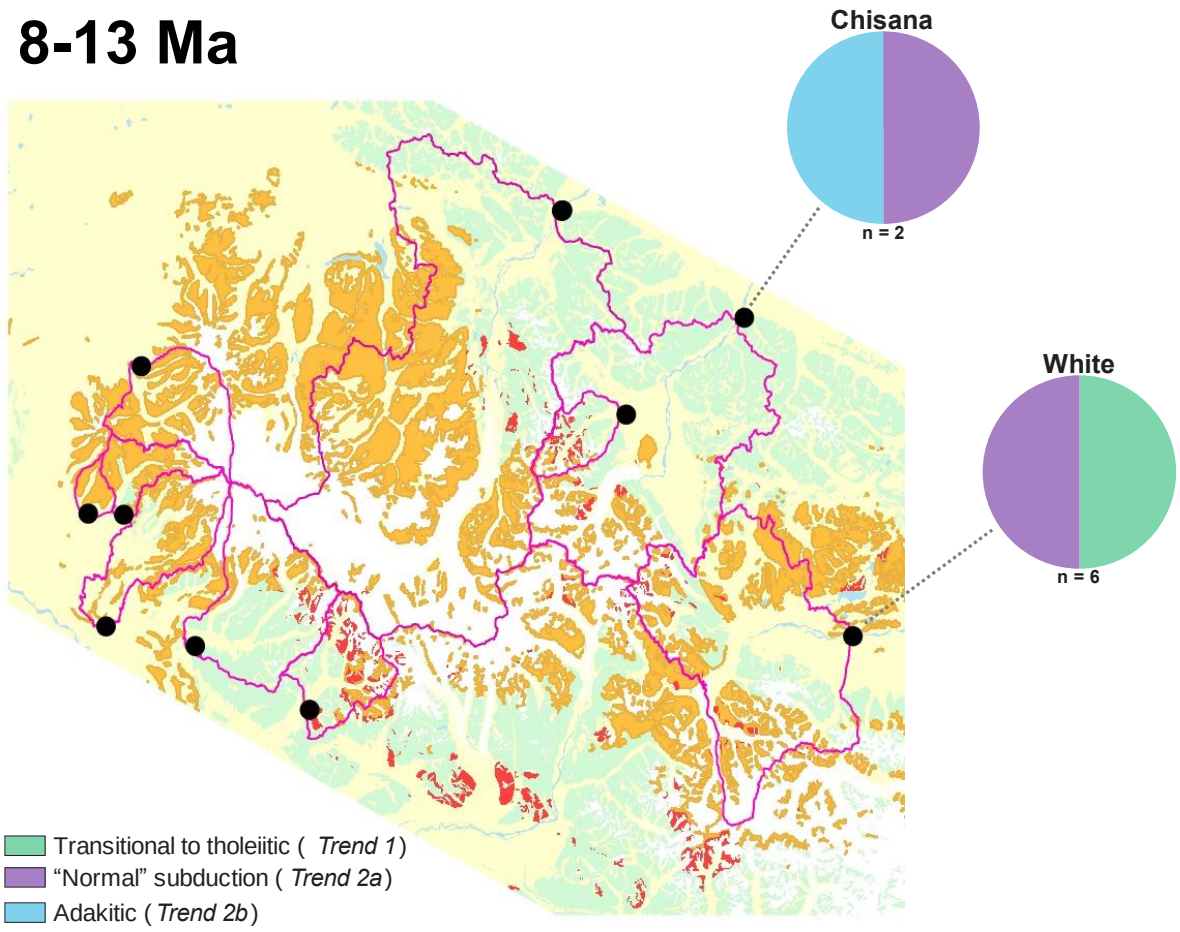

Figure 5.6 Cobble geochemical data, divided into Preece and Hart (2004) trends, showing the distribution of magma types at 8 – 13 Ma.

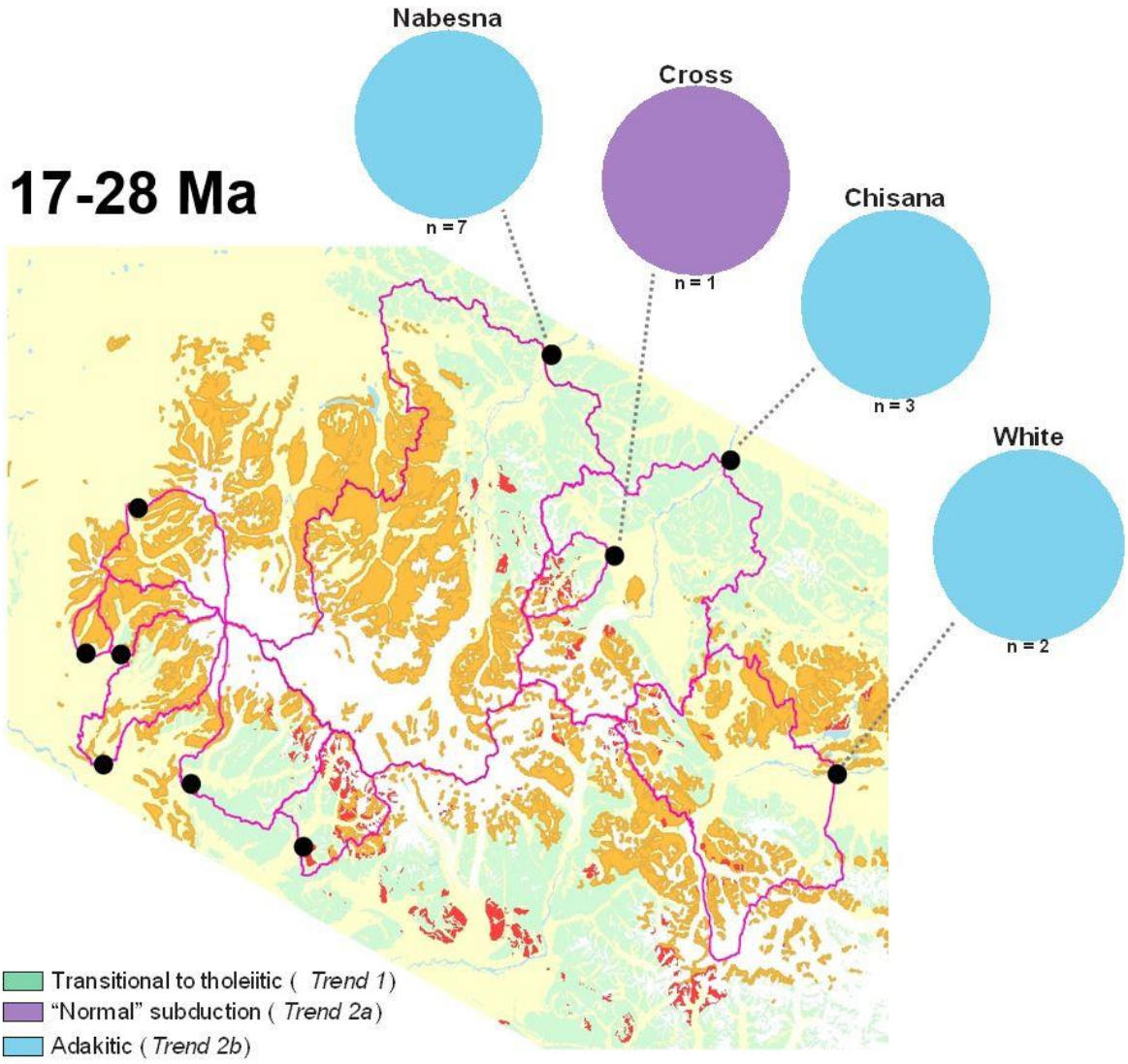

Figure 5.7 Cobble geochemical data, divided into Preece and Hart (2004) trends, showing the distribution of magma types at 17 - 28 Ma.

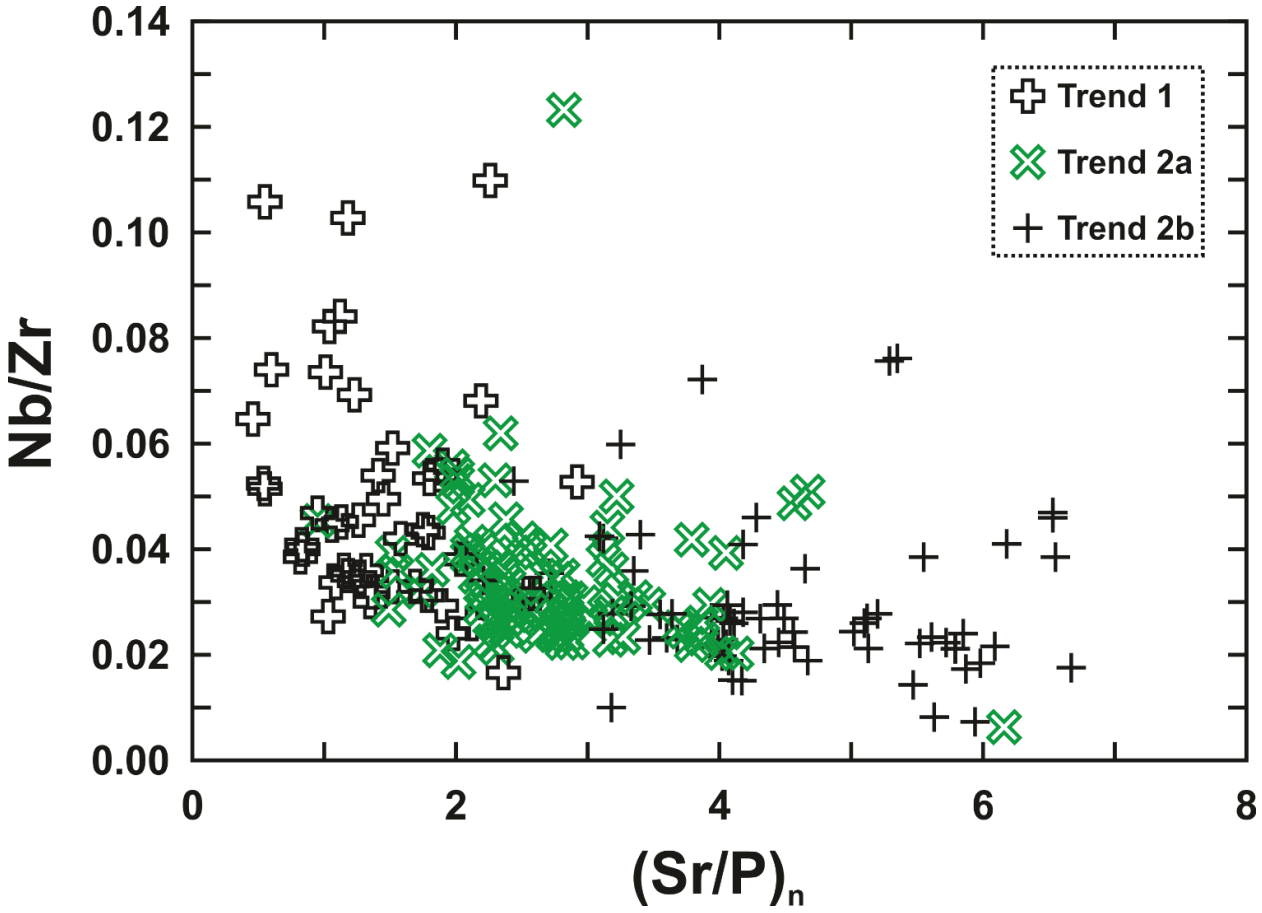

Figure 5.8 Nb/Zr vs. $(Sr/P)_n$ diagram with cobble data coded according to Preece and Hart (2004) trends. Note that, even without primitive (i.e., MgO > 6.0 wt.%) distinctions, there is a clear difference between transitional-tholeiitic Trend 1 chemistries and subduction-related Trend 2 chemistries: Trend 1 corresponds to relatively high Nb/Zr and low $(Sr/P)_n$, while Trends 2a and 2b are the opposite. While Trend 1 is not consistent with a true intraplate signature (Nb/Zr > 0.135; Sun and McDonough, 1989), it is consistent with less fluid-fluxed mantle wedge melting and more decompression melting due to intra-arc extension.

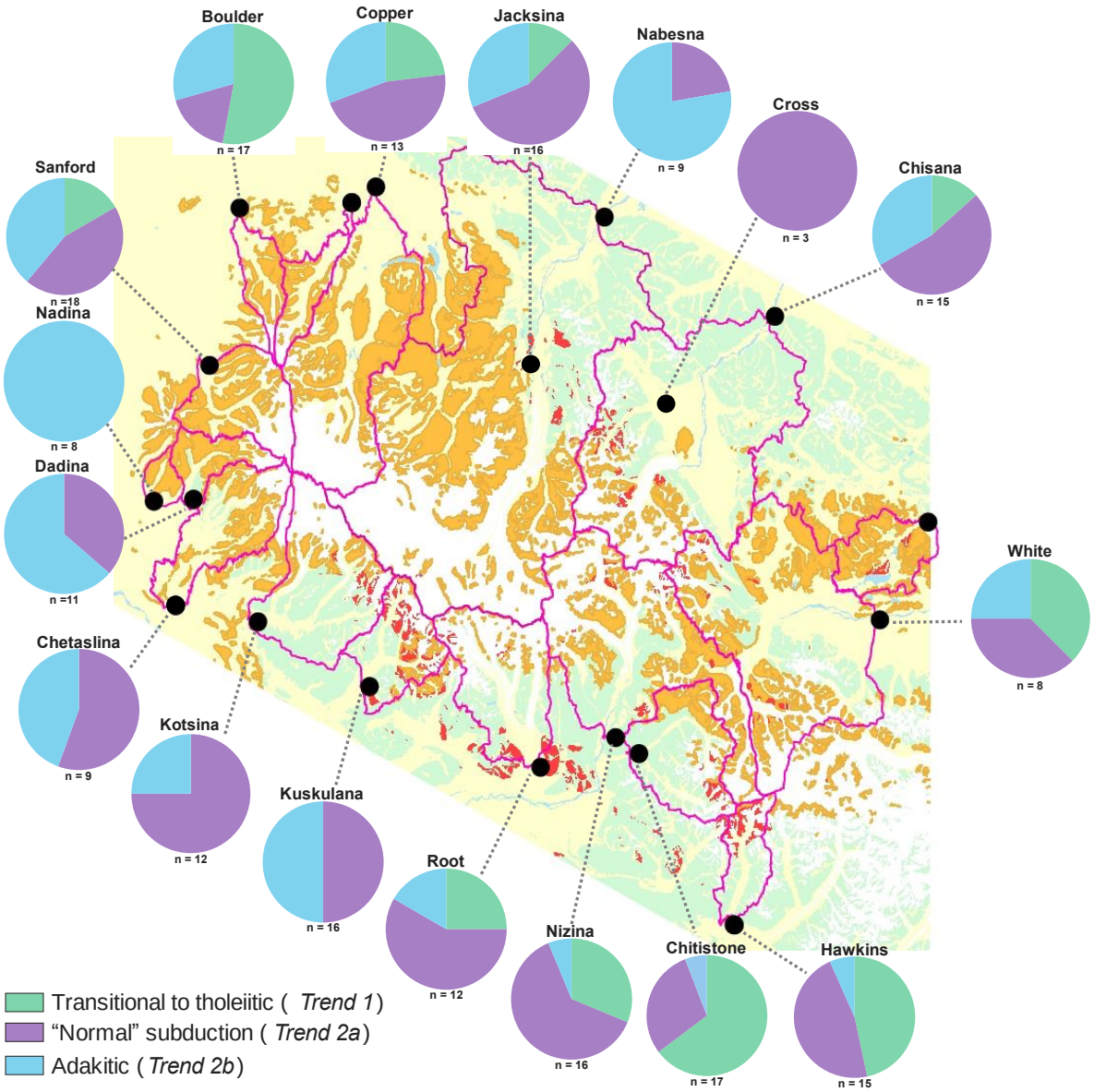

Figure 5.9 Cobble geochemical data, divided into Preece and Hart (2004) trends, showing the distribution of magma types in space with no regard to time.

Table 5.1 All cobbles in our dataset that fall into the 28 – 17 Ma age range. Note they all drain from rivers in the north-central WA and that all samples except Cross 7 are considered as Trend 2b. The age of sample White 14 is questionable (hence the strikethrough) but we still consider it in the oldest cobble group of 28 – 17 Ma.

Sample	Age (Ma)	Magma type
Nabesna 1	17.72 ± 0.36	Trend 2b
Nabesna 2	23.9 ± 0.4	Trend 2b
Nabesna 4	19.21 ± 0.22	Trend 2b
Nabesna 7	20.35 ± 0.36	Trend 2b
Nabesna 8	18.8 ± 0.23	Trend 2b
Nabesna 13	27.7 ± 0.2	Trend 2b
Nabesna 14	22.63 ± 0.28	Trend 2b
Chisana 2	22.9 ± 0.4	Trend 2b
Chisana 3	25.12 ± 0.26	Trend 2b
Chisana 11	20.6 ± 0.5	Trend 2b
White 5	23.5 ± 0.7	Trend 2b
White 14	~~34.58 ± 0.47~~	Trend 2b
Cross 7	26.6 ± 0.31	Trend 2a

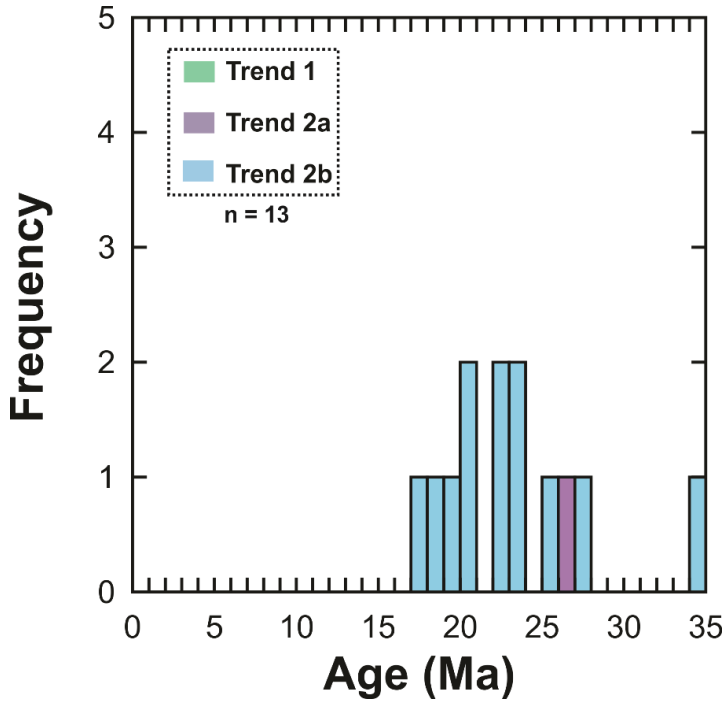

Figure 5.10 Histogram showing the geochemical distribution (Trend 1, Trend 2a, Trend 2b) of magmatism from 28 – 17 Ma. All samples here drained from the Nabesna, Chisana, and White Rivers, and Cross Creek (Fig. 5.7). The ~35 Ma cobble is sample White 14 and we note this age is questionable.

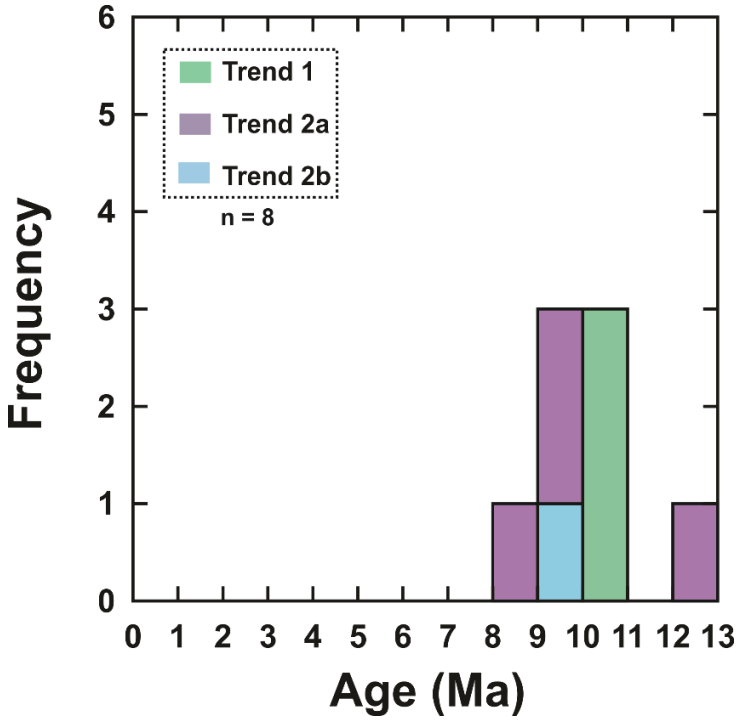

Figure 5.11 Histogram showing the return of magmatism to the central WA at ~13 Ma and the temporal distribution of different magma types (Trend 1, 2a, and 2b) at 13 - 8 Ma. All samples here drained from the White and Chisana Rivers (Fig. 5.6).

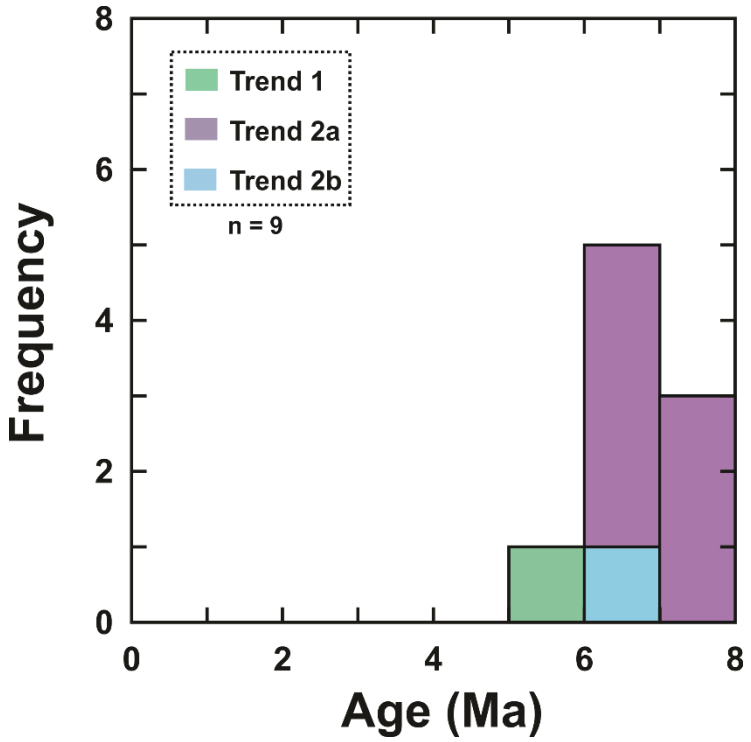

Figure 5.12 Histogram showing the geochemical distribution (Trend 1, Trend 2a, Trend 2b) of magmatism from 8 - 5 Ma. All samples here drained from the Chisana River (Fig. 5.5).

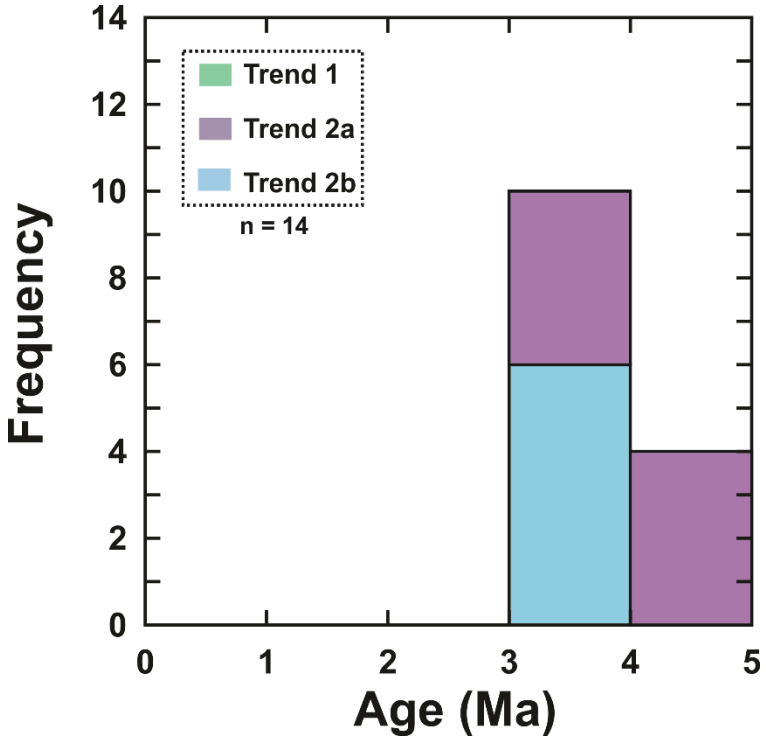

Figure 5.13 Histogram showing the geochemical distribution (Trend 1, Trend 2a, Trend 2b) of magmatism from 5 – 3 Ma. All samples drained here are from the Kuskulana River (Fig. 5.4).

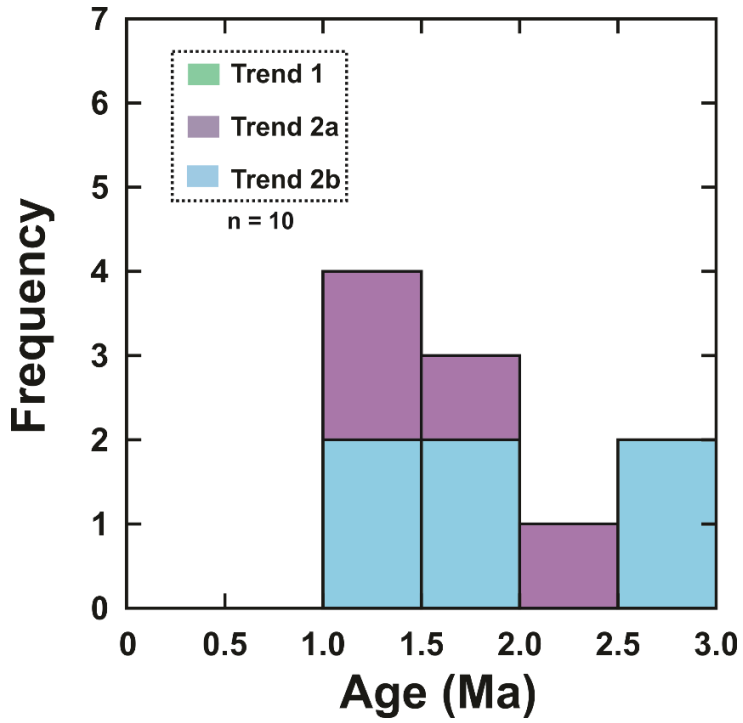

Figure 5.14 Histogram showing the geochemical distribution (Trend 1, Trend 2a, Trend 2b) of magmatism from 3 – 1 Ma. All samples drained here are from the Nabesna, Sanford, Dadina, Kotsina, and Kuskulana Rivers (Fig. 5.3).

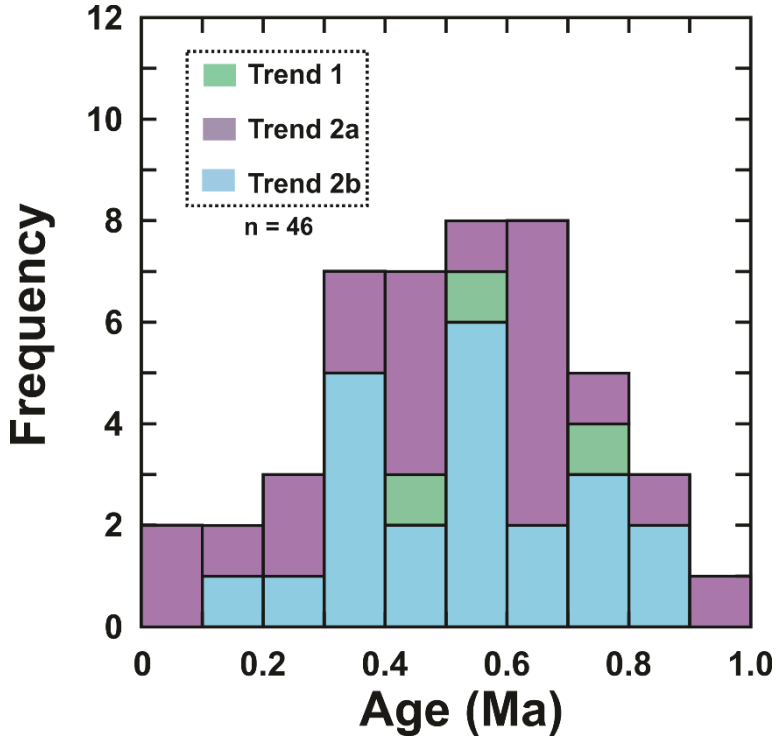

Figure 5.15 Histogram showing the geochemical distribution (Trend 1, Trend 2a, Trend 2b) of magmatism from 1 Ma to the present. All samples drained here are from the Sanford, Nadina, Dadina, Chetaslina, and Kotsina Rivers (Fig. 5.2).

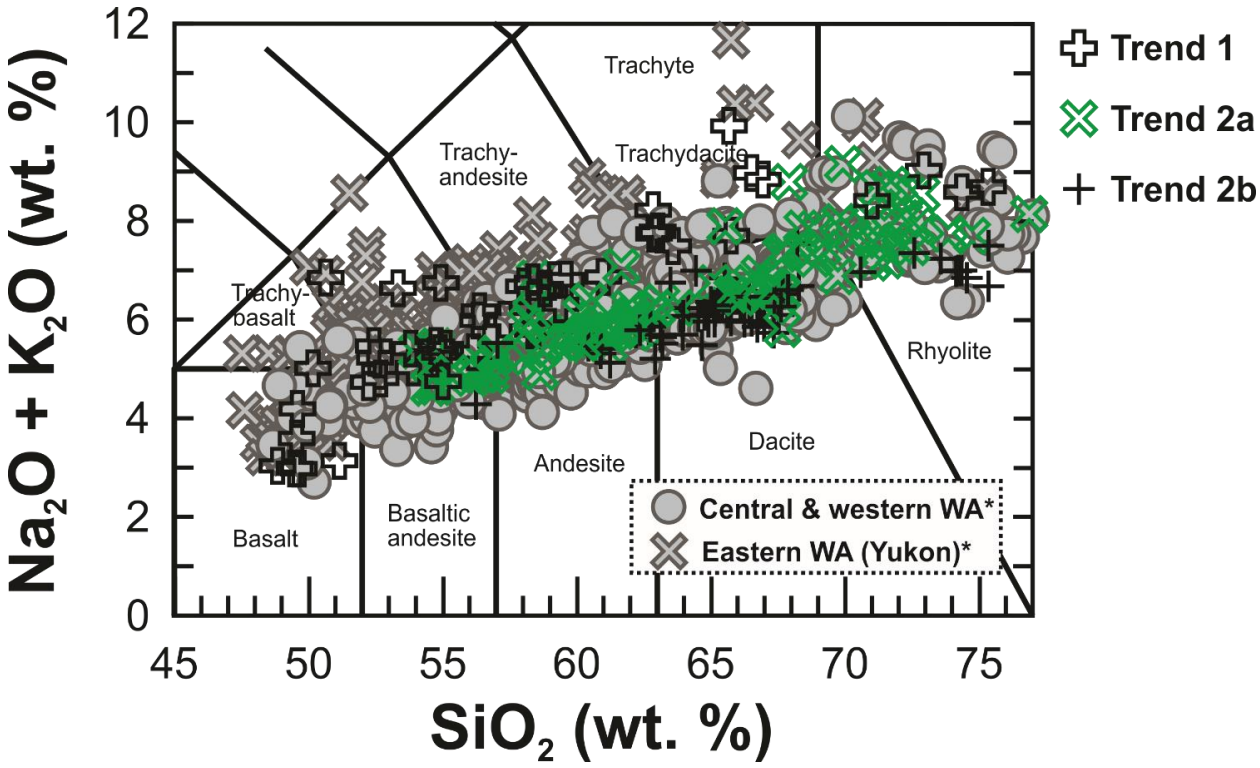

Figure 5.16 Total alkalis versus silica diagram showing cobble data, coded by geochemical parameters that define the Preece and Hart (2004) trends, overlain on existing bedrock record. Significantly, all cobble compositions overlap with existing bedrock samples. Gray-scale samples comprise the existing WA bedrock record. *Central & western WA data are from Richter et al. (1990), Preece and Hart (2004), Trop et al. (2012); Eastern (Yukon) data is from Skulski et al. (1991; 1992).

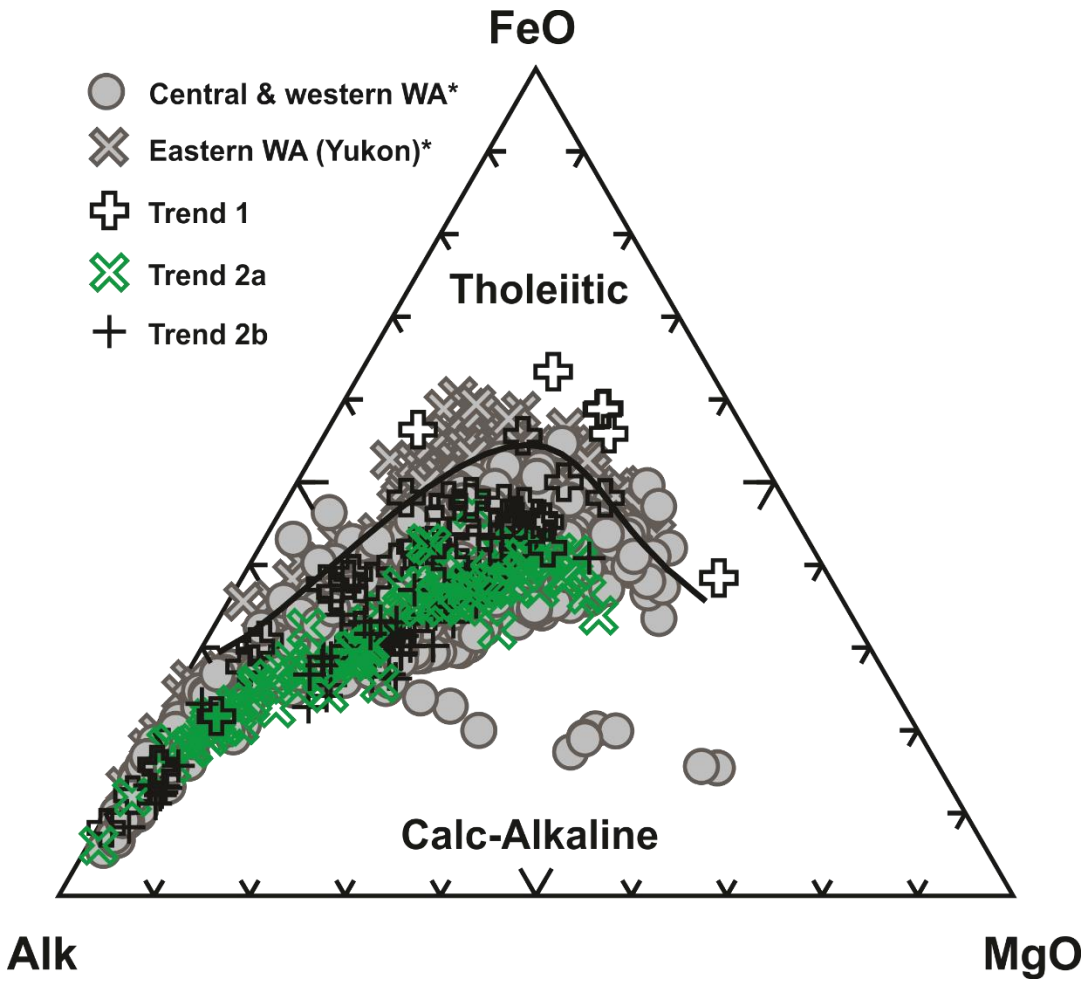

Figure 5.17 AFM diagram showing cobble data, coded by geochemical parameters that define the Preece and Hart (2004) trends, overlain on existing bedrock record. Significantly, all cobble compositions overlap with existing bedrock samples except a few minor occurrences that plot as slightly more tholeiitic. These samples either do not yet have an age or have alteration material that may have enriched them in iron. Gray-scale samples comprise the existing WA bedrock record. *Central & western WA data are from Richter et al. (1990), Preece and Hart (2004), Trop et al. (2012); Eastern (Yukon) data is from Skulski et al. (1991; 1992).

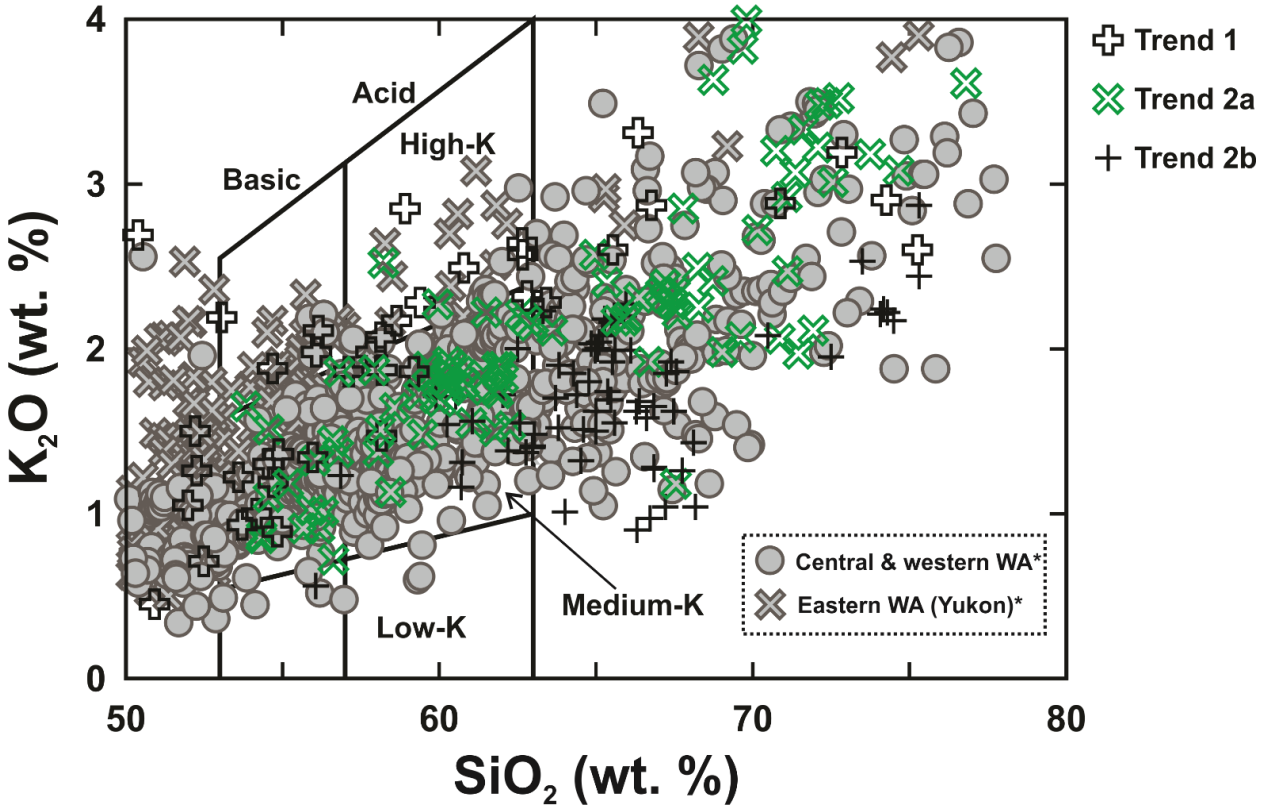

Figure 5.18 Andesite type diagram showing cobble data, coded by geochemical parameters that define the Preece and Hart (2004) trends, overlain on existing bedrock record. Significantly, all cobble compositions overlap with existing bedrock samples. Gray-scale samples comprise the existing WA bedrock record. *Central & western WA data are from Richter et al. (1990), Preece and Hart (2004), Trop et al. (2012); Eastern (Yukon) data is from Skulski et al. (1991; 1992).

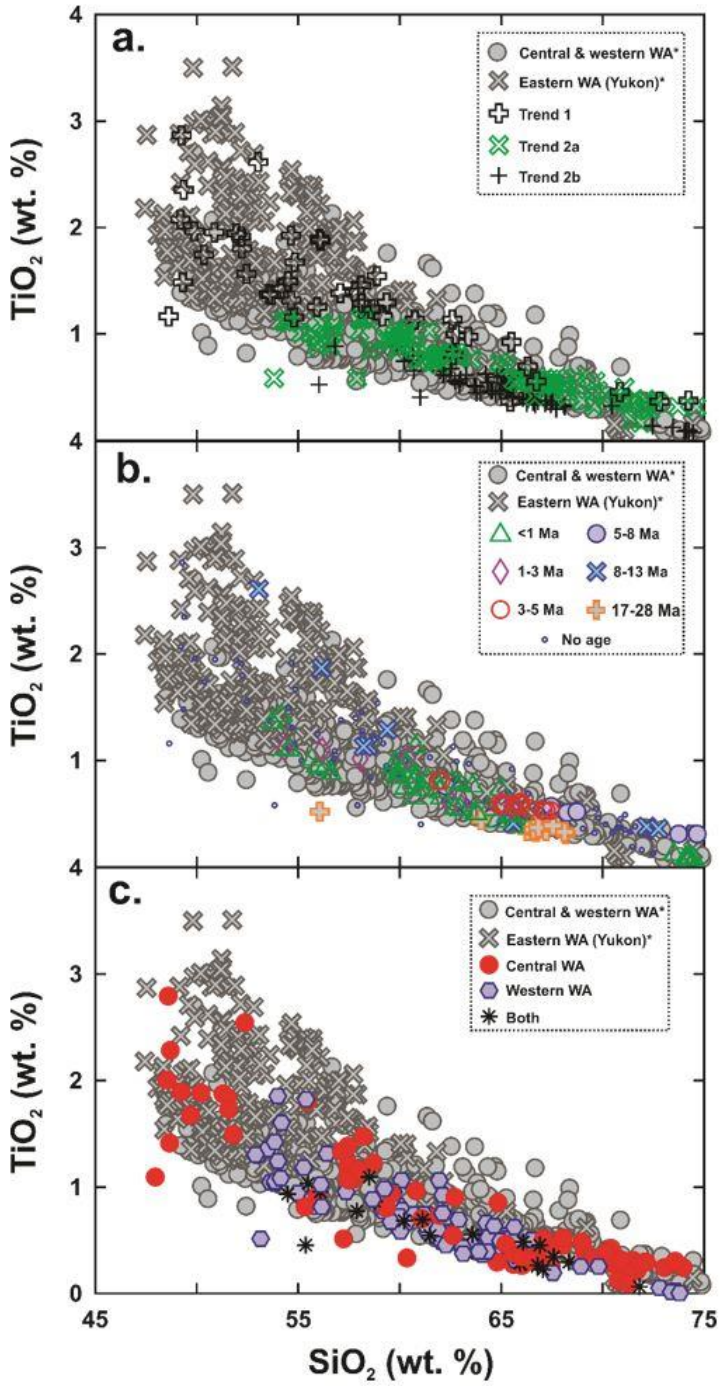

Figure 5.19 TiO_2 vs. SiO_2 diagrams with cobble data overlain on existing bedrock data. Gray-scale samples comprise the existing WA bedrock record. *Central & western WA data are from Richter et al. (1990), Preece and Hart (2004), Trop et al. (2012); Eastern (Yukon) data is from Skulski et al. (1991; 1992). (a) Samples are coded based on geochemical parameters defined by Preece and Hart (2004) criteria. (b) Samples coded based on respective ages. (c) Samples coded based on spatial divisions outlined in the Results section (Fig. 4.5).

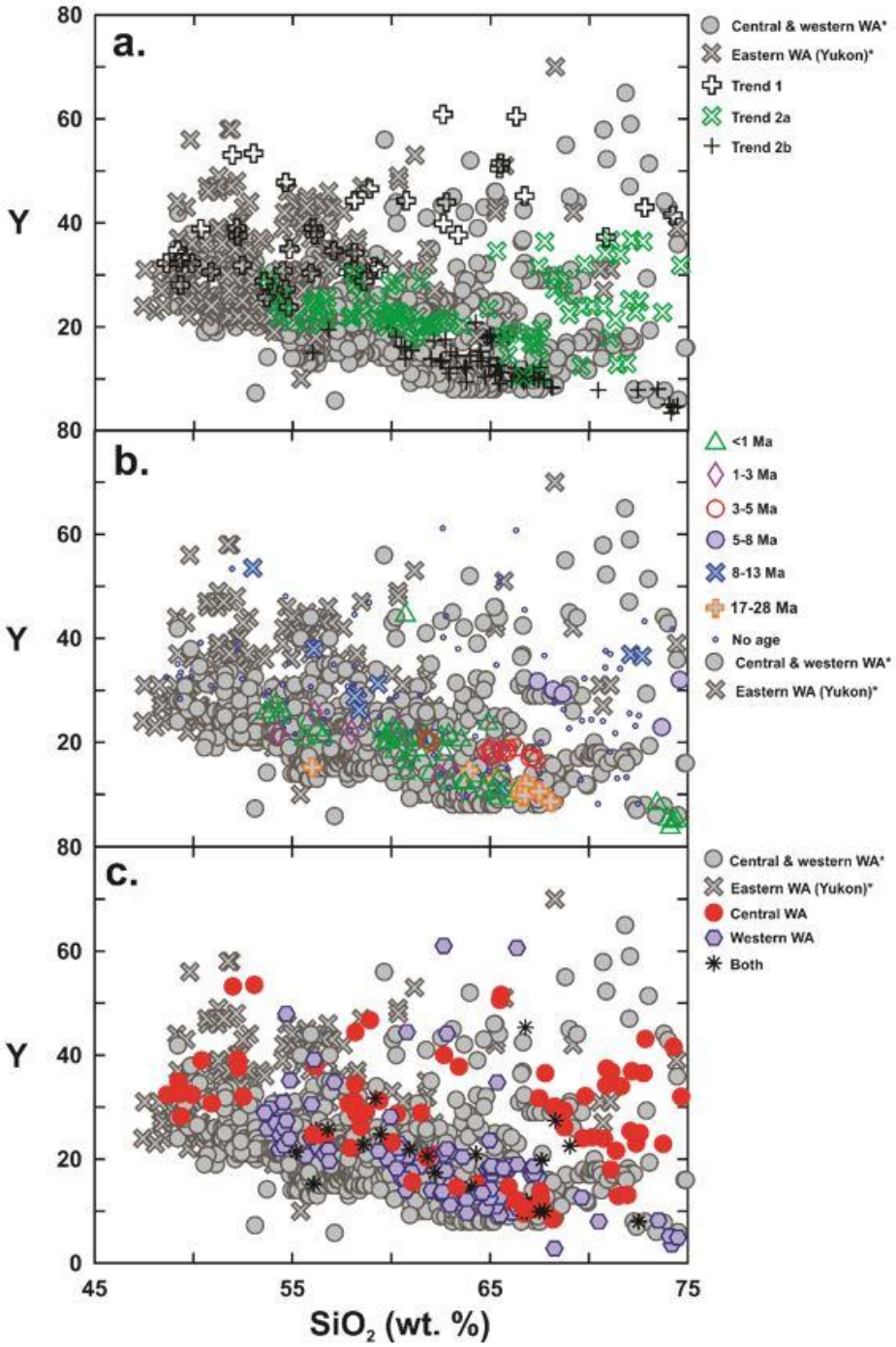

Figure 5.20 Y vs. SiO_2 diagrams with cobble data overlain on existing bedrock data. Gray-scale samples comprise the existing WA bedrock record. *Central & western WA data are from Richter et al. (1990), Preece and Hart (2004), Trop et al. (2012); Eastern (Yukon) data is from Skulski et al. (1991; 1992). (a) Samples are coded based on geochemical parameters defined by Preece and Hart (2004) criteria. (b) Samples coded based on respective ages. (c) Samples coded based on spatial divisions outlined in the Results section (Fig. 4.5).

Chapter 6 - Conclusions

1. Similar tectonic processes of subduction and slab melting have been ongoing over the past ~29.0 m.y. in the western and central WA, although these processes have migrated through time due to subducting slab processes (i.e., slab rollback and change in subduction direction) and shifting upper plate processes (i.e., transtensional and dextral movement along the Totschunda, Denali, and Duke River faults).
2. Mantle wedge melting due to subduction has been ongoing over the ~29.0 m.y. of WA magmatism and is spatially ubiquitous. From ~17.0 – ~13.0 Ma, mantle wedge melting was a less dominant process due to slab rollback and extensional and dextral movement along the Totschunda, Denali, and Duke River faults.
3. Melting due to intra-arc extension has occurred in discrete time periods over the ~29.0 m.y. of WA magmatism, but is not a temporally or spatially ubiquitous in the WA.
4. Trend 2b cobbles are spatially and temporally ubiquitous, suggesting that Trend 2b cobbles are, in most instances, the result of a magma mixing of an adakite-like melt (likely due to slab edge effects) and a magma derived from melting of the mantle wedge. Trend 2b cobbles may reflect true adakites if their ages are consistent with ages of adakites documented in the bedrock, ~29.0 – ~20.0 Ma and <1.0 Ma, and if they were collected from rivers that drain bedrock occurrences of true adakites. However, this may be complicated by dynamic fluvial systems changing over the course of ~29.0 m.y. and, when coupled with the fact that we have no Yb, should not be considered definitive.
5. This igneous clast technique is novel but has proven successful in this location. It can possibly be applied in other arc settings where access to bedrock sample may be difficult but river-to-river transportation is (relatively) easy. At the same time, it also allows us to gather important arc data from rocks that have never been—and likely never would have been—sampled. Therefore, the results from this project are twofold: 1) a novel technique was tested and proven effective, and 2) knowledge was gained and data contributed to a growing body of work on the Wrangell arc.

References

Ayers, J.C., and E.B., Watson, 1993, Rutile solubility and mobility in supercritical aqueous fluids, Contributions to Mineralogy and Petrology, v. 114, p. 321-330.

Bauer, M.A., Pavlis, G.L., and Landes, M., 2014, Subduction geometry of the Yakutat terrane, southeastern Alaska: Geosphere, v. 10, np. 6, p. 1161-1176.

Beate, B., Monzier, M., Spikings, R., Cotten, J., Silva, J., Bourdon, E., Eissen, J.-P., 2001. Mio-Pliocene adakite generation related to flat subduction in southern Ecuador: the Quim-sacocha volcanic center. Earth and Planetary Science Letters 192, 561–570.

Benowitz, J.A., Layer, P., Armstrong, P., Perry, S., Haeussler, P., Fitzgerald, P., and VanLaningham, S., 2011, Spatial variations in focused exhumation along a continental-scale strike-slip fault: The Denali fault of the eastern Alaska Range: Geosphere, v. 7, p. 455–467.

Benowitz, J.A., Davis, K.N., Brueseke, M.E., Trop, J.M., and Layer, P., 2014, Investigating the Lost Arc: geological constraints of ~25 million years of magmatism along an arc-transform junction, Wrangell volcanic belt, Alaska: Abstracts with Programs, 2014 Annual Meeting, Geological Society of America.

Benowitz, J. A., Layer, P. W., & Vanlaningham, S., 2014, Persistent long-term (c. 24 Ma) exhumation in the Eastern Alaska Range constrained by stacked thermochronology, *in*, Jourdan, F., Mark, D. F. & Verati, C., eds., Advances in 40Ar/39Ar Dating: from Archaeology to Planetary Sciences: Geological Society, London, Special Publications, 385, p. 225-243.

Berkelhammer, S.E., 2017, Initiation of the Wrangell arc: A record of tectonic changes in an arc-transform junction revealed by new geochemistry and geochronology of the ~29-18 Ma Sonya Creek volcanic field, Alaska: Kansas State University, Manhattan, Kansas. M.S. Thesis, 217 p.

Borg, L.E., Clynne, M.A., and Bullen, T.D., 1997, The variable role of slab-derived fluids in the generation of a suite of primitive calc-alkaline lavas from the southernmost Cascades, California: The Canadian Mineralogist, v. 35, p. 425-452.

Bourdon, E., Eissen, J.-P., Monzier, M., Robin, C., Martin, H., 2002. Adakite-like lavas from Antisana volcano (Ecuador): evidence from slab melt metasomatism beneath the Andean Northern volcanic zone. Journal of Petrology 43, 99–217.

Brenan, J.M., Shaw, H.F., Phinney, D.L., and Ryerson, F.J., 1994, Rutile aqueous fluid partitioning of Nb, Ta, Hf, Zr, U, and Th: Implications for high field strength element depletions in island arc basalts, Earth and Pleanetary Science Letters, v. 128, p. 327-339.

Brueseke, M. E., Benowitz., J.A., Trop, J.M., Davis, K.D., and Layer, P.W., 2015, New geochemical and age constraints on the initiation of the lost arc, Wrangell Volcanic Belt, Alaska: Abstracts with Programs, 2015 Cordilleran Meeting, Geological Society of America.

Bruns, T.R., 1983, Model for the origin of the Yakutat block, an accreting terrane in the northern Gulf of Alaska: Geology, v. 11, p. 718–721, doi:10.1130/0091-7613 (1983)11<718:MFTOOT>2.0.CO;2.

Calmus, T., Aguillon-Robles, A., Maury, R.C., Bellon, H., Benoit, M., Cotten, J., Bourgois, J., Michaud, F., 2003. Spatial and temporal evolution of basalts and magnesian andesites (bajaites) from Baja California, Mexico: the role of slab melts. Lithos 66, 77–105.

Castillo, P.R., 2012, Adakite petrogenesis: Lithos, v. 134-135, p. 304-316.

Davis, A.S., and Plafker, G., 1986, Eocene basalts from the Yakutat terrane: Evidence for the origin of an accreting terrane in southern Alaska: Geology, v. 14, p. 963–966, doi:10.1130/0091-7613(1986)14<963:EBFTYT>2.0 .CO;2.

Davis, K.N., Benowitz, J., Layer, P.W., Trop, J., and Brueseke, M., 2017, Dating the lost arc of Alaska: constraining the timing of initiation of the Wrangell arc with a new $^{40}Ar/^{39}Ar$ geochronology approach on modern river detrital lithic grains: Geological Sociery of America Abstracts with Programs, v. 49, no. 4.

Defant, M.J., and Drummond, M.S., 1990, Derivation of some modern arc magmas by melting of young subducted lithosphere: Nature, v. 347, p. 662-665.

Eberhart-Phillips, D., Christensen, D.H., Brocher, T.M., Hansen, R., Ruppert, N.A., Haeussler, P.J., and Abers, G.A., 2006, Imaging the transition from Aleutian subduction to Yakutat collision in central Alaska with local earthquakes and active source data: Journal of Geophysical Research, v. 111.

Ehlers, T.A., Szameitat, A., Enkelmann, E., Yanites, B.J., and Woodsworth, G.J., 2015, Identifying the spatial variations in glacial catchment erosion with detrital thermochronology: Journal of Geophysical Research: Earth Surface, v. 120, p. 1023-1039.

Enkelmann, E. and Ehlers, T.A., 2015, Evaluation of detrital thermochronology for quantification of glacial catchment denudation and sediment mixing: Chemical Geology, v.411, p. 299-309.

Falkowski, S., Enkelmann, E., Drost, K., Pfander, J.A., Stubner, K., and Ehlers, T.A., 2016, Cooling history of the St. Elias syntaxis, southeast Alaska, revealed by geochronology and thermochronology of cobble-sized glacial detritus: Tectonics, v. 35, p. 447-468.

Fitzgerald, V.T., Brueske, M.E., Berkelhammer, S.E., Trop, J.M., Benowitz, J., Layer, P.W., and Davis, K., Stuck in the middle: stratigraphy and geochemistry of volcanic rocks from the Green Hills in the central Wrangell arc, Alaska, : Abstracts with Programs, 2016 Annual Meeting, Geological Society of America.

Fuis, G.S., Moore, T.E., Plafker, G., Brocher, T.M., Fisher, M.A., Mooney, W.D., Nokleberg, W.J., Page, R.A., Beaudoin, B.C., Christensen, N.I., Levander, A.R., Lutter, W.J., Saltus, R.W., and Ruppert, N.A., 2008, Trans-Alaska Crustal Transect and continental evolution involving subduction underplating and synchronous foreland thrusting: Geology, v. 36, p. 267–270.

Gill, J.B., 1981, Orogenic andesite and plate tectonics: Springer-Verlag, New York, 390 pp.

Grabowski, D.M., Enkelmann, E., and Ehlers, T.A., 2013, Spatial extent of rapid denudation in the glaciated St. Elias syntaxis region, SE, Alaska: Journal of Geophysical Research: Earth Surface, vol. 118, p. 1921-1938.

Gulick, S.P.S., Reece, R.S., Christeson, G.L., van Avendonk, H., Worthington, L.L., and Pavlis, T.L., 2013, Seismic images of the Transition fault and the unstable Yakutat-Pacific-North American triple junction: Geology, v. 41, p. 571-574.

Gutscher, M.-A., Maury, F., Eissen, J.-P., Bourdon, E., 2000. Can slab melting be caused by flat subduction? Geology 28, 535–538.

Haeussler, P.J., 2008, An overview of the neotectonics of interior Alaska: Far-field deformation from the Yakutat microplate collision, *in* Freymueller, J.T., et al., eds., Active tectonics and seismic potential of Alaska: American Geophysical Union Geophysical Monograph 179, p. 269-285.

Kay, R.W., 1978, Aleutian magnesian andesites: melts from subducted Pacific Ocean crust: Journal of Volcanology and Geothermal Research, v. 4, p. 117-132.

Keast, R.T., Brueseke, M.E., Trop, J.M., Berkelhammer, S.E., and Benowitz, J., Volcanic stratigraphy of the ~2.4 Ma Eucher Mountain volcano, Wrangell arc, Alaska (U.S.A.): Abstracts with Programs, 2016 Annual Meeting, Geological Society of America.

Kortyna, C., Donaghy, E., Trop, J.M., and Idleman, B., 2014, Integrated provenance record of a forearc basin modified by slab-window magmatism: detrital-zircon geochronology and sandstone compositions of the Paleogene Arkose Ridge Formation, south-central Alaska: Basin Research, v. 26, p. 436-460.

Layer, P.W., Hall, C.M. and York, D., 1987, The derivation of 40Ar/39Ar age spectra of single grains of hornblende and biotite by laser step heating: Geophysical Research Letters, v. 14, p. 757-760.

Lease, R.O., Haeussler, P.J., and O'Sullivan, P., 2016, Changing exhumation patterns during Cenozoic growth and glaciation of the Alaska Range: Insights from detrital thermochronology and geochronology: Tectonics, v. 35, doi:10.1002/2015TC004067.

LeBas, M.J., Le Maitre, R.W., Streckeiser, A., Zanettin, B., 1986. Chemical classification of volcanic rocks based on total alkali-silica diagram. Journal of Petrology 27, 745–750.

LeMaitre, R.W., 1976. The chemical variability of some common igneous rocks. Journal of Petrology 17, 589-637.

Martin, H., Smithies, R.H., Rapp, R., Moyen, J.F., Champion, D., 2005, An overview of adakite, tonalite-tronhjemite-granodiorite (TTG) and sanukitoid: relationships and some implications for crustal evolution: Lithos, v. 79, p. 1-24.

McDougall, I. and Harrison, T.M., 1999, Geochronology and Thermochronology by the 40Ar/39Ar method-2nd ed, Oxford University Press, New York, 269pp.

Mertzman, S.A., 2000. K/Ar results from the southern Oregon-northern California Cascade Range. Oregon Geology 62, 99-122.

Mertzman, S.A., 2015. XRF laboratory: overview and analytical procedures. http://www.fandm.edu/earth-environment/laboratory-facilities/instrument-use-and-instructions (Accessed 3/30/2017).

Moyen, J.F., 2009. High Sr/Y and La/Yb ratios: the meaning of the "adakitic signature". Lithos 112, 556-574.

Peacock, S.M., Rushmer, T, Thompson, A.B., 1994, Partial melting of subducting oceanic crust: Earth and Planetary Science Letters, v. 121, p. 227-244.

Pearce, J.A., Stern, R.J., Bloomer, S.H., and Fryer, P., 2005, Geochemical mapping of the Mariana arc-basin system: Implications for the nature and distribution of subduction components: Geochemistry Geophysics Geostystems, v. 6, no. 7.

Plafker, G., and Berg, H.C., 1994, Overview of the geology and tectonic evolution of Alaska, in Plafker, G., and Berg, H. C., eds., The Geology of Alaska: Boulder, Colorado, Geological Society of America, The Geology of North America, v. G-1, pp. 989-1021.

Preece, S.J., and Hart, W.K., 2004, Geochemical variations in the <5 Ma Wrangell Volcanic Field Alaska: implications for the magmatic and tectonic development of a complex continental arc system: Tectonophysics, v. 392, p. 165-191.

Preece, S.J., McGimsey, R.G., Westgate, J.A., Pearce, N.J.G., Hart, W.K., and Perkins, W.T., 2014, Chemical complexity and source of the White River Ash, Alaska and Yukon: Geosphere, v. 10, p. 1020-1042.

Renne, P. R., Mundil, R., Balco, G., Min, K., and Ludwig, K. R., 2010, Joint determination of 40K decay constants and 40Ar∗/40K for the Fish Canyon sanidine standard, and improved accuracy for 40Ar/39Ar geochronology: Geochimica et Cosmochimica Acta, v. 74, p. 5349.

Richter, D.H., Smith, J.G., Lanphere, M.A., Dalrymple, G.B., Reed, B.L., and Shew, N., 1990, Age and progression of volcanism, Wrangell volcanic field, Alaska: Bulletin of Volcanology, v. 53, p. 29-44.

Richter, D.H., Rosenkrans, D.S., and Steigerwald, M.J., 1994, Guide to the Volcanoes the Western Wrangell Mountains, Alaska: Wrangel-St. Elias National Park and Preserve: U.S. Geological Survey Bulletin 2072.

Richter, D.H., Preller, C.C., Labay, K.A., and Shew, N.B., 2006, Geologic map of the Wrangell–Saint Elias Park and Preserve, Alaska: U.S. Geological Survey Scientific Investigations Map 2877, scale 1: 350,000.

Roddick, J.C., 1978, The application of isochron diagrams in 40Ar/39Ar dating: A discussion: Earth and Planetary Science Letters, v. 41, p. 233-244.

Roddick, J.C., Cliff, R.A., and Rex, D.C., 1980, The evolution of excess argon in alpine biotites – a 40Ar/39Ar analysis: Earth and Planetary Science Letters, v. 48, p. 185-208.

Rollinson, H., and Martin, H., 2005, Geodynamic controls on adakite, TTG, and sanukitoid genesis: implications for models of crust formation, introduction to the special issue: Lithos, v. 79, ix-xii.

Ryerson, F.J., and Watson, E.B., 1987, Rutile saturation in magmas: Implications for Ti-Nb-Ta depletion in island arc basalts, Earth and Planetary Science Letters, v. 86, p. 225-239.

Sajona, F.G., Maury, R.C., Bellon, H., Cotten, J., Defant, M.J., Pubellier, M., Rangin, C., 1993. Initiation of subduction and the generation of slab melts in western and eastern Mindanao, Philippines. Geology 21, 1007–1010.

Sajona, F.G., Maury, R.C., Bellon, H., Cotten, J., Defant, M., 1996. High field strength ele- ment enrichment of Pliocene–Pleistocene island arc basalts, Zamboanga Peninsula, western Mindanao (Philippines). Journal of Petrology 37, 693–726.

Skulski, T., Francis, D., and Ludden, J., 1991, Arc-transform magmatism in the Wrangell volcanic belt: Geology, v. 19, p. 11–14.

Skulski, T., Francis, D., and Ludden, J., 1992, Volcanism in an arc-transform transition zone: the stratigraphy of the Saint Clare Creek volcanic field, Wrangell volcanic belt, Yukon, Canada: Canadian Journal of Earth Science, v. 29, p. 446–461.

Śliwiński, M., Bąbel, M., Nejbert, K., Olszeska-Nejbert, D., Gąsiewicz, A., Schreiber, B.C., Benowitz, J.A., and Layer, P.W., 2012, Badenian-Sarmatian chronostratigraphy in the Polish Carpathian Foredeep: Paleogeography, Paleoclimatology, Paleoecology, p. 326-328, 12-29.

Sun, S., and McDonough, W.F., 1989, Chemical and isotopic systematics of oceanic basalts: Implications for mantle composition and processes, in Saunders, A.D., and Norry, M.J., eds., Magmatism in the ocean basins: Geological Society of London Special Publication 42, p. 313-345, doi: 10.1144/GSL.SP.1989.042.01.19.

Thorkelson, D.J., Breitsprecher, K., 2005. Partial melting of slab window margins: gen- esis of adakitic and non-adakitic magmas. Lithos 79, 25–41.

Trop, J.M**.,** Snyder, D., Hart, W.K., and Idleman, B.D., 2012, Miocene basin development and volcanism along a strike-slip to flat-slab subduction transition: stratigraphy, geochemistry, and geochronology of the central Wrangell volcanic belt, Yakutat-North America collision zone: Geosphere, v. 8, p. 805–834.

Trop, J.M., Benowitz, J., Brueseke, M., Davis, K., Berkelhammer, S.E., Morter, B.K., Layer, P.W., Weber, M., Fitzgerald, V.T., Keast, R.T., and Moretti, B., 2017, Investigating the lost arc: geologic constraints on ~29 million years of continuous magmatism along an arc-transform junction, Wrangell arc, Alaska: Geological Society of America Abstracts with Programs, v. 49, no. 4.

Weber, M.A., Brueseke, M.E., Benowitz, J.A., Trop, J.M., Berkelhammer, S.E., Davis, K.N., Layer, P.W., Morter, B.K., and Mertzman, S.A., 2017, Geological and geochemical constraints on Oligo-Miocene hypabyssal intrusive bodies from the Wrangell Arc, Alaska: Abstracts with Programs, 2017 Cordilleran Meeting, Geological Society of America.

Wilson, F.H., Hults, C.P., Mull, C.G., and Karl, S.M., 2015, Geologic map of Alaska: U.S. Geological Survey Scientific Investigations Map 3340, scale 1: 1,584,000.

Worthington, L.L., Van Avendonk, H.J.A., Gulick, S.P.S., Christeson, G.L., and Pavlis, T.L., 2012, Crustal structure of the Yakutat terrane and the evolution of subduction and collision in southern Alaska: Journal of Geophysical Research, v. 117, B01102.

Yogodzinski, G.M., Kay, R.W., Volynets, O.N., Koloskov, A.V., Kay, S.M., 1995. Magnesian andesite in the western Aleutian Komandorsky region: implications for slab melt- ing and processes in the mantle wedge. Geological Society of America Bulletin 107, 505–519.

Yogodzinski, G.M., Lees, J.M., Churikova, T.G., Dorendorf, F., Woerner, G., Volynets, O.N., 2001. Geochemical evidence for the melting of subducting oceanic lithosphere at plates edges. Nature 409, 500–504.

York, D., Hall, C.M., Yanase, Y., Hanes, J.A. & Kenyon, W.J., 1981, 40Ar/39Ar dating of terrestrial minerals with a continuous laser: Geophysical Research Letters, v. 8., p. 1136-1138.

Appendix A - Hand Sample Descriptions

*Samples with LOI > 3.5 wt. %

Chisana (5.88 – 162.45 Ma)

Chisana 1

Mafic; porphyritic plutonic texture with black aphanitic groundmass and small anhedral feldspar phenocrysts. (*Basalt**. 51.88 ± 2.01 Ma)

Chisana 2

Felsic; porphyritic plutonic texture with aphanitic gray groundmass, abundant euhedral plagioclase phenocrysts, and lesser amounts of elongate and equant amphibole phenocrysts; minor sulfide mineralization. (*Dacite*. 22.9 ± 0.4 Ma)

Chisana 3

Felsic; porphyritic plutonic texture with aphanitic gray groundmass, subhedral plagioclase phenocrysts, and subhedral amphibole phenocrysts. Amphibole-rich xenoliths are also present. (*Dacite*. 25.12 ± 0.26 Ma)

Chisana 4

Felsic; porphyritic plutonic texture with gray, waxy-looking aphanitic groundmass, subhedral plagioclase phenocrysts, and pervasive green alteration material. (*Dacite**. 9 ± 0.13 Ma)

Chisana 5

Mafic; porphyritic volcanic texture with aphanitic groundmass and sparse subhedral to euhedral plagioclase phenocrysts. (*Andesite*. 6.36 ± 0.46 Ma)

Chisana 6

Felsic; crystal- and lithic-rich volcanic tuff. Brown aphanitic groundmass contains lithics, subhedral quartz, subhedral feldspar (sanidine?), and subhedral biotite. Presence

of fiamme and hefty rock density indicate a high degree of welding. (*Rhyolite*. 6.23 ± 0.09 Ma)

Chisana 7

Felsic; crystal- and lithic-rich volcanic tuff. Gray aphanitic groundmass contains lithics, pumice fragments, subhedral biotite, subhedral amphibole, and subhedral feldspar (sanidine?). Pumice fragments are slightly flattened, indicating a moderate degree of welding. (*Dacite*. 7.43 ± 0.15 Ma.)

Chisana 8

Felsic; crystal-rich volcanic tuff. Gray aphanitic groundmass contains pumice fragments, subhedral amphibole, and subhedral feldspar (sanidine?). Pumice fragments are slightly flattened, indicating a moderate degree of welding. (*Dacite*. 6.93 ± 0.15 Ma)

Chisana 9

Felsic; porphyritic volcanic texture with tan, aphanitic groundmass and elongate amphibole phenocrysts. Contains vugs lined with rust-colored alteration material. (*Dacite*. 6.25 ± 0.15 Ma)

Chisana 11

Felsic; porphyritic plutonic texture with light gray groundmass, abundant subhedral plagioclase phenocrysts, sparse biotite, and sparse xenoliths. (*Dacite*. 20.6 ± 0.5 Ma)

Chisana 12

Felsic; porphyritic volcanic texture with light gray, aphanitic groundmass, euhedral to subhedral plagioclase laths, elongate amphibole, and sparse biotite. (*Rhyolite*. 5.88 ± 0.12 Ma)

Chisana 13

Felsic; porphyritic plutonic texture with light gray groundmass, abundant euhedral to subhedral plagioclase laths, and euhedral elongate amphibole. (*Dacite*. 7.9 ± 0.38 Ma)

Chisana 14

Felsic; porphyritic plutonic texture with light gray groundmass, subhedral to anhedral plagioclase phenocrysts and elongate to equant amphibole. (*Dacite*. 9.15 ± 0.21 Ma)

Chisana 15

Felsic; porphyritic volcanic texture with gray aphanitic groundmass andpo sparse feldspar phenocrysts (sanidine?). Rock has prevalent flow banding throughout. (*Rhyolite.* 6.55 ± 0.04 Ma)

Chisana 16

Mafic; porphyritic volcanic texture with dark gray/green groundmass and subhedral to anhedral plagioclase phenocrysts. (*Basalt*. 162.45 ± 1.43 Ma)

Chisana 17

Felsic; porphyritic volcanic texture with white/tan groundmass and subhedral to euhedral plagioclase laths. Pervasive alteration throughout: most micas have been replaced by green alteration product. (*Rhyolite*. 7.06 ± 0.08 Ma)

Chisana 18

Intermediate; fine-grained phaneritic. Roughly even distributions of light to dark minerals, but most grains are too small to be identified using a hand lens. (*Trachyandesite*. 8.02 ± 0.18 Ma)

White (9.31-300.97 Ma)

White 2

Mafic; black aphanitic rock with pervasive orange alteration material. (*Rhyolite**. 262.66 ± 1.66 Ma)

White 3

Mafic; porphyritic volcanic texture with dark red aphanitic groundmass, abundant subhedral plagioclase phenocrysts, and patches of green alteration. (*Andesite**. 11.49 ± 0.26 Ma)

White 5

Felsic; porphyritic plutonic texture with aphanitic gray groundmass, abundant subhedral plagioclase phenocrysts, and lesser elongate and equant amphibole phenocrysts. (*Dacite*. 23.5 ± 0.7 Ma)

White 6

Mafic; porphyritic volcanic texture with aphanitic dark gray groundmass and round and flattened feldspar phenocrysts. Sparse amygdules are filled with red material. (*Basaltic trachy-andesite*. 10.25 ± 0.19 Ma)

White 7

Mafic; porphyritic plutonic texture with dark gray aphanitic groundmass, anhedral feldspar phenocrysts, and unidentifiable black phenocrysts. (*Basalt**. 93.48 ± 1.11 Ma)

White 8

Mafic; porphyritic volcanic texture with dark gray aphanitic groundmass and subhedral to anhedral feldspar phenocrysts (plagioclase?). (*Andesite*. 12.63 ± 0.28 Ma)

White 11

Felsic; phaneritic texture with gradation of crystal sizes (smallest to largest): pink/gray tabular crystals (feldspar?), subhedral to anhedral amphibole, and relatively large, subhedral plagioclase. Dissolution vugs are ubiquitous. (*Rhyolite*. 9.31 ± 0.12 Ma)

White 13

Mafic; black aphanitic rock with pervasive orange alteration material. (*Dacite**. 300.86 ± 4.16 Ma)

White 14

Felsic; porphyritic plutonic texture with light gray aphanitic groundmass, subhedral to euhedral plagioclase phenocrysts, relatively small subhedral to anhedral amphibole phenocrysts. (*Dacite*. 34.58 ± 0.47 Ma)

White 15

Mafic; porphyritic volcanic texture with dark gray aphanitic groundmass and subhedral to anhedral elongate feldspar phenocrysts. (*Basaltic trachyandesite*. 10.4 ± 0.3 Ma)

White 16

Felsic; phaneritic texture with gradation of crystal sizes (smallest to largest): pink/white tabular crystals (feldspar?), subhedral to anhedral amphibole, and relatively large, subhedral to anhedral plagioclase. Dissolution vugs are ubiquitous. Xenoliths also present. (*Rhyolite*. 9.92 ± 0.23 Ma)

White 17

Mafic; porphyritic volcanic texture with dark gray aphanitic groundmass and subhedral rounded and flattened feldspar phenocrysts. (*Trachyandesite*. 10.84 ± 0.08 Ma)

White 18

Mafic; black, aphanitic rock. (*Basaltic andesite**. 300.97 ± 4.16 Ma)

Nabesna (1.37 – 153.31 Ma)

Nabesna 1

Felsic; porphyritic plutonic texture with light gray aphanitic groundmass, subhedral feldspar phenocrysts, and subhedral amphibole phenocrysts. (*Dacite*. 17.72 ± 0.36 Ma)

Nabesna 2

Mafic; phaneritic texture with plagioclase crystals and unidentifiable black crystals. (*Basaltic andesite*. 23.9 ± 0.4 Ma)

Nabesna 4

Felsic; porphyritic plutonic texture with light gray aphanitic groundmass, subhedral plagioclase phenocrysts, subhedral amphibole phenocrysts, and sparse subhedral biotite phenocrysts. (*Dacite*. 19.21 ± 0.22 Ma)

Nabesna 5

Felsic; porphyritic plutonic texture with gray aphanitic groundmass, subhedral plagioclase phenocrysts, and an unidentifiable dark phase that has been heavily altered to a green material. Minor sulfide mineralization. (*Andesite*. 69.87 ± 0.29 Ma)

Nabesna 7

Felsic; porphyritic plutonic texture with gray aphanitic groundmass, subhedral plagioclase phenocrysts, subhedral amphibole phenocrysts, and spare subhedral biotite phenocrysts. (*Dacite.* 20.35 ± 0.36 Ma)

Nabesna 8

Felsic; porphyritic plutonic texture with tan aphanitic groundmass, subhedral feldspar phenocrysts, subhedral amphibole phenocrysts, and sparse subhedral biotite phenocrysts. Dissolution vugs are ubiquitous. (*Dacite*. 18.8 ± 0.23 Ma)

Nabesna 11

Mafic; porphyritic volcanic texture with dark gray aphanitic groundmass, small subhedral to anhedral feldspar phenocrysts, and patches of green alteration. (*Basaltic andesite**. 153.31 ± 1.39 Ma)

Nabesna 12

Mafic; dark gray aphanitic rock with ubiquitous vesicles. (*Basaltic andesite*. 1.37 ± 0.32 Ma)

Nabesna 13

Felsic; porphyritic plutonic texture with light gray aphanitic groundmass, subhedral feldspar phenocrysts, and relatively smaller subhedral amphibole and biotite phenocrysts. (*Dacite*. 27.7 ± 0.2 Ma)

Nabesna 14

Felsic; porphyritic plutonic texture with light gray aphanitic groundmass, subhedral to anhedral feldspar phenocrysts, and relatively smaller subhedral amphibole phenocrysts. (*Dacite*. 22.63 ± 0.28 Ma)

Dadina (0.31 – 1.86 Ma)

Dadina 1A-1

Mafic; porphyritic volcanic texture with dark gray aphanitic groundmass and subhedral to anhedral plagioclase phenocrysts. Dissolution vugs are ubiquitous. (*Andesite*. 0.49 ± 0.11 Ma)

Dadina 1A-2

Felsic; porphyritic volcanic texture with tan/light red aphanitic groundmass, subhedral to anhedral feldspar phenocrysts, and relatively small amphibole phenocrysts that have been altered to dark red. (*Dacite*. 0.31 ± 0.12 Ma)

Dadina 1B-1

Felsic; porphyritic volcanic texture with light gray aphanitic groundmass and small subhedral amphibole phenocrysts, some of which have been heavily altered. (*Dacite*. 1.86 ± 0.12 Ma)

Dadina 1B-2

Mafic; porphyritic volcanic texture with black aphanitic groundmass and subhedral to euhedral plagioclase phenocrysts. (*Andesite*. 0.48 ± 0.09 Ma)

Dadina 1B-3

Felsic; porphyritic volcanic texture with light gray aphanitic groundmass and sparse subhedral feldspar and biotite phenocrysts. (*Dacite*. 0.49 ± 0.09)

Dadina 1B-4

Mafic; porphyritic volcanic texture with black aphanitic groundmass, subhedral to anhedral plagioclase phenocrysts, and sparse heavily altered biotite phenocrysts. Sparse dissolution vugs are present. (*Andesite*. 0.68 ± 0.09 Ma)

Dadina 1C-1

Mafic; porphyritic volcanic texture with black aphanitic groundmass and subhedral to anhedral plagioclase phenocrysts. (*Andesite/dacite*. 0.74 ± 0.11)

Dadina 1C-2

Mafic; porphyritic plutonic texture with gray aphanitic groundmass anhedral feldspar phenocrysts, and relatively smaller subhedral amphibole phenocrysts. (*Andesite*. 1.46 ± 0.09 Ma)

Dadina 1C-3

Felsic; porphyritic volcanic texture with pink aphanitic groundmass, anhedral feldspar phenocrysts, and anhedral biotite phenocrysts that have been heavily altered. Dissolution vugs are present. (*Rhyolite*. 0.56 ± 0.08 Ma)

Dadina 1C-4

Felsic; porphyritic volcanic texture with tan/white aphanitic groundmass and sparse subhedral feldspar and biotite phenocrysts. (*Rhyolite*. 0.65 ± 0.09 Ma)

Dadina 1C-5

Felsic; porphyritic plutonic texture with light gray aphanitic groundmass, anhedral feldspar phenocrysts, and relatively smaller subhedral amphibole phenocrysts. The entire rock has a yellowish tinge. (*Dacite*. 0.76 ± 0.16 Ma)

Sanford (-0.38 – 2.3 Ma)

Sanford 1

Mafic; porphyritic volcanic texture with red/gray groundmass, subhedral plagioclase phenocrysts, and vesicles. (*Basaltic andesite*. 0.07 ± 0.34 Ma)

Sanford 2

Mafic; porphyritic volcanic texture with dark gray aphanitic groundmass, anhedral plagioclase phenocrysts, and vesicles. Some red vesicle fill exists but only within about 2cm from the edge of the rock. (*Basaltic andesite*. 2.3 ± 0.64 Ma)

Sanford 3

Felsic; porphyritic plutonic texture with light gray aphanitic groundmass, subhedral to anhedral feldspar phenocrysts, and sparse black mineral grain that is unidentifiable in hand sample. (*Andesite*. 1.29 ± 0.05 Ma)

Sanford 4

Mafic; porphyritic volcanic texture with black aphanitic groundmass, subhedral plagioclase phenocrysts, and vesicles. (*Basaltic andesite*. 0.83 ± 0.15 Ma)

Sanford 5

Intermediate; lithic-rich volcanic tuff. Black and dark red aphanitic groundmass contains abundant lithics and anhedral feldspar crystals. Presence of fiamme and hefty rock density indicate a high degree of welding. (*Andesite/dacite*. 1.69 ± 0.62 Ma)

Sanford 6

Mafic; porphyritic volcanic texture with black aphanitic groundmass, subhedral to anhedral plagioclase phenocrysts, and sparse olivine(?) phenocrysts. (*Basaltic andesite*. 0.59 ± 0.18 Ma)

Sanford 7

Mafic; porphyritic volcanic texture with gray/dark red aphanitic groundmass and subhedral plagioclase phenocrysts. Dissolution vugs are ubiquitous. (*Basaltic andesite*. 0.7 ± 0.35 Ma)

Sanford 8

Mafic; porphyritic volcanic texture with gray aphanitic groundmass and subhedral to anhedral plagioclase phenocrysts. Spare vesicles are also present. (*Basaltic andesite*. 0.34 ± 0.21 Ma)

Sanford 9

Mafic; porphyritic volcanic texture with dark red aphanitic groundmass and subhedral to anhedral feldspar phenocrysts. (*Andesite*. 0.54 ± 0.16 Ma)

Sanford 11

Mafic; porphyritic volcanic texture with black aphanitic groundmass and subhedral to anhedral plagioclase phenocrysts. Vesicles are ubiquitous. Sparse orange vesicle fill is present. (*Basaltic andesite*. 0.67 ± 0.1 Ma)

Sanford 12

Mafic; dark gray aphanitic rock. (*Basaltic andesite*. -0.38 ± 0.39 Ma)

Sanford 13

Mafic; porphyritic volcanic texture with black aphanitic groundmass and subhedral to anhedral feldspar phenocrysts. Sparse vugs are present and some are filled with tan alteration material. (*Andesite*. 0.24 ± 0.08 Ma)

Sanford 14

Mafic; porphyritic volcanic texture with dark gray aphanitic groundmass and subhedral to anhedral feldspar phenocrysts. (*Trachyandesite*. 0.4 ± 0.05 Ma)

Sanford 15

Felsic; porphyritic volcanic texture with tan aphanitic groundmass, anhedral feldspar phenocrysts, and sparse heavily altered amphibole phenocrysts. (*Dacite*. 0.35 ± 0.13 Ma)

Sanford 16

Felsic; porphyritic volcanic rock with white aphanitic groundmass, subhedral biotite phenocrysts, and ubiquitous heavily altered feldspar phenocrysts. (*Rhyolite*. 0.56 ± 0.04 Ma)

Sanford 17

Mafic; porphyritic volcanic texture with dark gray aphanitic groundmass, subhedral plagioclase phenocrysts, and sparse vesicles. (*Andesite*. 1.46 ± 0.15 Ma)

Sanford 18

Felsic; porphyritic volcanic texture with tan aphanitic groundmass, subhedral to anhedral feldspar phenocrysts, and heavily altered amphibole phenocrysts. Dissolution vugs and heavily altered xenoliths are sparse. (*Dacite*. 0.64 ± 0.06 Ma)

Sanford 19

Felsic; porphyritic volcanic texture with light gray, aphanitic groundmass and subhedral biotite phenocrysts. (*Rhyolite*. 0.58 ± 0.08 Ma)

Kotsina (0.02 – 215.07 Ma)

Kotsina 1A-1

Mafic; porphyritic volcanic texture with black aphanitic groundmass, abundant subhedral plagioclase phenocrysts, and less anhedral olivine (?) phenocrysts (could be an altered mineral?). (*Andesite*. 0.43 ± 0.38 Ma)

Kotsina 1A-2

Mafic; porphyritic volcanic texture with black aphanitic groundmass, abundant subhedral plagioclase phenocrysts, and less anhedral olivine (?) phenocrysts (could be an altered mineral?). (*Andesite*. 0.64 ± 0.21 Ma)

Kotsina 1B-1

Intermediate; phaneritic texture with roughly equal proportions of subhedral feldspar and subhedral to euhedral amphibole crystals. The amphibole crystals show planar alignment. (*Andesite*. 152.31 ± 1.09 Ma)

Kotsina 1B-2

Mafic; porphyritic volcanic texture with black aphanitic groundmass and subhedral to anhedral plagioclase phenocrysts. (*Andesite*. 0.49 ± 0.18 Ma)

Kotsina 1B-3

Felsic; porphyritic volcanic texture with light red aphanitic groundmass, abundant subhedral feldspar phenocrysts, minor amounts of subhedral amphibole and biotite phenocrysts, and ubiquitous dissolution vugs. (*Andesite*. 1.54 ± 0.45 Ma)

Kotsina 1B-4

Felsic; porphyritic plutonic texture with light gray aphanitic groundmass, anhedral feldspar phenocrysts, and a black phenocryst phase that has been heavily altered to a green mineral. Dissolution vugs are sparse. (*Dacite*. 0.55 ± 0.17 Ma)

Kotsina 1B-5

Mafic; porphyritic volcanic texture with black aphanitic groundmass, abundant euhedral to subhedral plagioclase phenocrysts, and ubiquitous vesicles. (*Andesite*. 0.68 ± 0.16 Ma)

Kotsina 1B-6

Felsic; porphyritic plutonic texture with gray groundmass, abundant and large subhedral feldspar phenocrysts, and sparse quartz phenocrysts. (*Dacite*. 150.27 ± 0.39 Ma)

Kotsina 11 7/23

Mafic; porphyritic volcanic texture with black aphanitic groundmass, abundant euhedral to subhedral plagioclase phenocrysts, and ubiquitous vesicles. Some vesicles are filled with a rust-colored alteration material. (*Andesite*. 0.66 ± 0.12 Ma)

Kotsina 12 7/23

Felsic; porphyritic volcanic texture with red aphanitic groundmass, subhedral plagioclase phenocrysts, unidentifiable black phenocrysts, and dissolution vugs. (*Andesite*. 0.02 ± 0.32 Ma)

Kotsina 14 7/23

Intermediate; porphyritic plutonic texture with gray aphanitic groundmass, subhedral to anhedral feldspar phenocrysts, and anhedral unidentifiable black phenocrysts. (*Andesite*. 0.85 ± 0.12 Ma)

Kotsina 15 7/23

Felsic; porphyritic volcanic texture with gray aphanitic groundmass, heavily altered amphibole phenocrysts, and sparse anhedral phenocrysts. (*Dacite*. 0.11 ± 0.1 Ma)

Kotsina 16 7/23

Mafic; porphyritic volcanic texture with dark gray aphanitic groundmass, anhedral waxy-looking feldspar phenocrysts that are rimmed with a green alteration material, and patches of green alteration material. (*Basalt**. 215.07 ± 14.23 Ma)

Nadina (0.17 – 0.88 Ma)

Nadina 1A-1

Mafic; porphyritic volcanic texture with dark gray aphanitic groundmass and anhedral feldspar phenocrysts. (*Andesite*. 0.57 ± 0.17 Ma)

Nadina 1A-2

Felsic; porphyritic volcanic texture with light gray aphanitic groundmass, abundant subhedral amphibole phenocrysts, and sparse subhedral biotite phenocrysts. (*Dacite*. 0.47 ± 0.1 Ma)

Nadina 1A-3

Felsic; porphyritic volcanic texture with red aphanitic groundmass with abundant subhedral plagioclase phenocrysts. (*Andesite/Dacite.* 0.77 ± 0.33 Ma)

Nadina 1A-4

Mafic; porphyritic volcanic texture with black aphanitic groundmass and subhedral feldspar phenocrysts. (*Andesite*. 0.36 ± 0.16 Ma)

Nadina 1A-5

Felsic; porphyritic plutonic texture with light gray aphanitic groundmass and subhedral feldspar, amphibole, and sparse biotite phenocrysts. (*Dacite*. 0.17 ± 0.13 Ma)

Nadina 1A-6

Mafic; dark red and black aphanitic rock. (*Andesite/Dacite*. 0.29 ± 0.18 Ma)

Nadina 1B-1

Felsic; porphyritic plutonic texture with light gray aphanitic groundmass, subhedral to anhedral feldspar phenocrysts, subhedral amphibole phenocrysts, and subhedral to euhedral biotite phenocrysts. (*Dacite*. 0.39 ± 0.29 Ma)

Nadina 1B-2

Mafic; dark gray, aphanitic rock. (*Andesite*. 0.88 ± 0.11 Ma)

Chetaslina (0.23 – 152.42 Ma)

Chetaslina 1A-1

Felsic; porphyritic volcanic texture with purple aphanitic groundmass and amphibole and biotite phenocrysts that have been completely altered to a maroon mineral. (*Dacite*. 0.39 ± 0.11 Ma)

Chetaslina 1A-2

Mafic; porphyritic volcanic texture with black aphanitic groundmass and abundant subhedral to euhedral plagioclase phenocrysts. (*Andesite*. 0.62 ± 0.11 Ma)

Chetaslina 1A-3

Felsic; crystal- and lithic-rich volcanic tuff. Light red aphanitic groundmass contains lithics, subhedral quartz, subhedral feldspar (sanidine?), and fiamme. (*Andesite*. 0.92 ± 0.54 Ma)

Chetaslina 1B-1

Intermediate; phaneritic texture with subhedral feldspar and amphibole crystals and books of biotite. (*Andesite.* 150.24 ± 0.48 Ma)

Chetaslina 1B-2

Intermediate; phaneritic texture with anhedral feldspar and pyroxene crystals. (*Basaltic trachyandesite.* 152.42 ± 0.96 Ma)

Chetaslina 1C-2

Intermediate; porphyritic volcanic texture with gray aphanitic groundmass, anhedral feldspar phenocrysts, and spare unidentifiable black phenocrysts. (*Basaltic andesite*. 0.35 ± 0.11 Ma)

Chetaslina 1C-3

Felsic; porphyritic volcanic texture with tan aphanitic groundmass and sparse subhedral biotite phenocrysts. (*Rhyolite*. 0.51 ± 0.08 Ma)

Chetaslina 1C-5

Intermediate; porphyritic volcanic texture with gray aphanitic groundmass and abundant subhedral to euhedral amphibole and biotite phenocrysts. (*Dacite*. 0.76 ± 0.24 Ma)

Chetaslina 1C-6

Mafic; porphyritic volcanic texture with black aphanitic groundmass and subhedral plagioclase phenocrysts. (*Andesite*. 0.23 ± 0.07 Ma)

Cross (26.6 – 147.97 Ma)

Cross 3

Intermediate; phaneritic texture with feldspar and pyroxene crystals. (*Andesite*. 118.19 ± 0.37 Ma)

Cross 5

Felsic; heavily altered porphyritic volcanic rock with red aphanitic groundmass and unidentifiable white and black phenocrysts. (*Rhyolite**. 147.97 ± 0.93 Ma)

Cross 6

Intermediate; porphyritic plutonic texture with gray aphanitic groundmass, subhedral plagioclase phenocrysts, and subhedral relatively small amphibole phenocrysts. (*Trachyandesite*. 87.65 ± 0.65 Ma)

Cross 7

Intermediate; porphyritic plutonic texture with gray aphanitic groundmass, subhedral to anhedral plagioclase phenocrysts, and unidentifiable black phenocrysts. (*Dacite*. 26.6 ± 0.31 Ma)

Kuskulana (2.79 – 4.55 Ma)

Kuskulana 1A-1

Intermediate; porphyritic plutonic texture with dark gray aphanitic groundmass, subhedral feldspar phenocrysts, and subhedral amphibole phenocrysts. (*Dacite*. 3.08 ± 0.12 Ma)

Kuskulana 1B-1

Mafic; porphyritic plutonic texture with black aphanitic groundmass and subhedral feldspar and amphibole phenocrysts. (*Dacite*. 3.04 ± 0.51 Ma)

Kuskulana 1B-2

Mafic; porphyritic plutonic texture with black aphanitic groundmass, subhedral feldspar phenocrysts, and unidentifiable black phenocrysts. (*Dacite*. 3.16 ± 0.16 Ma)

Kuskulana 1B-3

Felsic; porphyritic plutonic texture with gray aphanitic groundmass and subhedral to anhedral plagioclase phenocrysts. (*Dacite*. 2.79 ± 0.14 Ma)

Kuskulana 1B-4

Mafic; porphyritic plutonic texture with black aphanitic groundmass and subhedral plagioclase and amphibole phenocrysts. (*Dacite*. 2.89 ± 0.19 Ma)

Kuskulana 1B-5

Mafic; porphyritic plutonic texture with dark gray aphanitic groundmass, subhedral to anhedral feldspar phenocrysts, and subhedral amphibole phenocrysts. (*Dacite*. 3.77 ± 0.25 Ma)

Kuskulana 1B-6

Mafic; porphyritic plutonic texture with black aphanitic groundmass and subhedral plagioclase phenocrysts. (*Dacite*. 3.45 ± 0.17 Ma)

Kuskulana 1B-7

Mafic; porphyritic plutonic texture with black aphanitic groundmass and subhedral plagioclase phenocrysts. (*Dacite*. 3.31 ± 0.27 Ma)

Kuskulana 1B-8

Mafic; porphyritic volcanic texture with black aphanitic groundmass and sparse subhedral plagioclase phenocrysts. (*Andesite*. 3.12 ± 0.18 Ma)

Kuskulana 1C-1

Felsic; phaneritic texture with abundant feldspar crystals and relatively less unidentifiable dark crystals. (*Dacite*. 3.72 ± 0.31 Ma)

Kuskulana 1C-2

Felsic; phaneritic texture with abundant feldspar crystals and relatively less amphibole crystals that have been altered to a green mineral. (*Dacite*. 4.47 ± 0.41 Ma)

Kuskulana 1C-3

Felsic; phaneritic texture with abundant feldspar crystals, relatively less amphibole crystals, and an unidentifiable green mineral. (*Dacite*. 4.55 ± 0.23 Ma)

Kuskulana 1C-4

Felsic; phaneritic texture with abundant feldspar crystals, relatively less amphibole crystals, and an unidentifiable green mineral. (*Dacite*. 4.06 ± 0.4 Ma)

Kuskulana 1C-5

Felsic; phaneritic texture with abundant feldspar and amphibole crystals. (*Dacite*. 4.03 ± 0.15 Ma)

Kuskulana 1C-6

Felsic; phaneritic texture with abundant feldspar crystals, relatively less amphibole crystals, and an unidentifiable green mineral. (*Dacite*. 3.61 ± 0.47 Ma)

Kuskulana 1D

Mafic; porphyritic volcanic rock with dark gray aphanitic groundmass and anhedral feldspar phenocrysts. (*Andesite*. 3.31 ± 0.18 Ma)

Chitistone (No ages yet)

Chitistone 1

Mafic; dark gray phaneritic rock. Minerals present include subhedral pink feldspar (orthoclase?), subhedral to anhedral gray feldspar, and black to dark gray phase that cannot be identified in hand sample. (*Basaltic trachyandesite*)

Chitistone 2

Mafic; porphyritic volcanic texture with black aphanitic groundmass and subhedral rounded and flattened feldspar phenocrysts. (*Basaltic trachyandesite*)

Chitistone 3

Mafic; porphyritic plutonic texture with dark gray/green aphanitic groundmass and anhedral feldspar phenocrysts. (*Trachybasalt/Basalt*)

Chitistone 4

Felsic; porphyritic volcanic texture with pink aphanitic groundmass and subhedral to anhedral feldspar phenocrysts, many of which have been replaced by an orange material. (*Dacite**)

Chitistone 6

Mafic; porphyritic volcanic texture with dark gray aphanitic groundmass and subhedral to anhedral feldspar phenocrysts. (*Basaltic trachyandesite**)

Chitistone 7

Felsic; phaneritic texture with abundant subhedral feldspars and quartz. Relatively lesser amounts of anhedral black/dark green phase also exists but is unidentifiable in hand sample. Minor sulfide mineralization is present. (*Dacite*)

Chitistone 8

Felsic; porphyritic volcanic texture with dark red aphanitic groundmass and abundant subhedral plagioclase and quartz phenocrysts. (*Rhyolite**)

Chitistone 9

Intermediate; phaneritic texture with dark and light phases present. Dark phase is subhedral to anhedral, black, and ranges from equant to elongate (amphibole?). Light phase includes subhedral elongate plagioclase and other unidentifiable feldspars. (*Trachyandesite*)

Chitistone 10

Mafic; porphyritic plutonic texture with dark gray aphanitic groundmass, subhedral plagioclase laths, and minor sulfide mineralization. (*Basalt*)

Chitistone 11

Mafic; porphyritic volcanic texture with dark red aphanitic groundmass and subhedral to anhedral feldspar phenocrysts. (*Basaltic trachyandesite**)

Chitistone 12

Felsic; porphyritic volcanic texture with white aphanitic groundmass and small unidentifiable phenocrysts. (*Rhyolite*)

Chitistone 13

Felsic; phaneritic texture with abundant subhedral plagioclase, orthoclase, and quartz crystals and relatively lesser amounts of an unidentifiable anhedral black/dark green mineral. (*Rhyolite*)

Chitistone 14

Mafic; phaneritic texture with subhedral plagioclase laths, elongate amphibole crystals, and anhedral pyroxene crystals. The plagioclase and amphibole crystals show a strong alignment. (*Basalt*)

Chitistone 15

Felsic; phaneritic texture with abundant white and pink feldspar crystals and unidentifiable anhedral black crystals. (*Rhyolite*)

Chitistone 17

Mafic; porphyritic volcanic texture with dark gray aphanitic groundmass and subhedral plagioclase phenocrysts. (*Basalt*)

Chitistone 18

Intermediate; phaneritic texture with light and dark mineral phases. The light phase is subhedral plagioclase crystals. The dark phases include subhedral biotite and a dark mineral that is unidentifiable in hand sample. (*Andesite*)

Chitistone 19

Mafic; porphyritic volcanic texture with black aphanitic groundmass with abundant subhedral plagioclase phenocrysts. (*Basaltic andesite*)

Chitistone 20

Mafic; porphyritic volcanic texture with black aphanitic groundmass and subhedral rounded and flattened feldspar phenocrysts. (*Trachyandesite*)

Chitistone 21

Intermediate; phaneritic texture with roughly equal amounts of light and dark mineral phases. The light phase is subhedral plagioclase. The dark phases include subhedral to euhedral elongate amphibole crystals and subhedral equant pyroxene. (*Andesite*)

Chitistone 22

Mafic; porphyritic volcanic texture with dark gray aphanitic groundmass and light colored anhedral phenocrysts (plagioclase) that show a very strong planar alignment. (*Trachydacite*)

Chitistone 24

Mafic; porphyritic volcanic texture with dark gray aphanitic groundmass and subhedral rounded and flattened feldspar phenocrysts. (*Basaltic trachyandesite*)

Copper (No ages yet)

Copper 2

Mafic; porphyritic volcanic texture with dark gray aphanitic groundmass, subhedral to anhedral plagioclase phenocrysts, and dissolution vugs. Some cavities are lined with tan alteration material. (*Andesite*)

Copper 3

Mafic; black aphanitic rock. (*Basaltic trachyandesite*)

Copper 4

Felsic; porphyritic volcanic texture with light gray/pink aphanitic groundmass and subhedral to anhedral feldspar phenocrysts, some of which have been altered to a rusty orange material. Dissolution vugs are sparse. (*Dacite)*

Copper 5

Mafic; porphyritic volcanic texture with dark red aphanitic groundmass, unidentifiable black phenocrysts, and subhedral plagioclase phenocrysts. (*Andesite/Dacite)*

Copper 6

Felsic; porphyritic volcanic texture with tan/pink aphanitic groundmass, anhedral feldspar phenocrysts, and dissolution vugs. (*Rhyolite)*

Copper 8

Mafic; porphyritic volcanic texture with dark gray aphanitic groundmass, subhedral to anhedral feldspar phenocrysts, and irregular/angular vesicles. (*Basaltic andesite/Andesite)*

Copper 10

Mafic; dark red, aphanitic rock with ubiquitous vesicles. (*Basaltic andesite)*

Copper 11

Mafic; porphyritic volcanic texture with black aphanitic groundmass, anhedral feldspar phenocrysts, and ubiquitous dissolution vugs. (*Trachydacite)*

Copper 12

Mafic; porphyritic volcanic texture with black/dark red aphanitic groundmass and anhedral feldspar phenocrysts. (*Basaltic andesite/Andesite)*

Copper 13

Mafic; porphyritic volcanic texture with black aphanitic groundmass, subhedral plagioclase phenocrysts, and sparse vesicles. There are also patches of bright orange alteration material. (*Andesite)*

Copper 14

Felsic; porphyritic volcanic texture with light red aphanitic groundmass, anhedral feldspar phenocrysts, and amphibole phenocrysts that have been completely altered to a dark red material. Some vugs also exist. (*Dacite)*

Copper 15

Intermediate; porphyritic volcanic texture with gray aphanitic groundmass, anhedral feldspar phenocrysts, and much smaller subhedral amphibole phenocrysts. Vugs are sparse throughout. (*Dacite)*

Copper 16

Felsic; porphyritic volcanic texture with light gray aphanitic groundmass, subhedral to anhedral plagioclase phenocrysts, and pervasive green alteration material. (*Trachydacite)*

Boulder (No ages yet)

Boulder 1

Felsic; porphyritic plutonic texture with light gray aphanitic groundmass, subhedral feldspar, amphibole, and biotite phenocrysts. (*Dacite*)

Boulder 2

Felsic; porphyritic volcanic texture with pinkish gray aphanitic groundmass and anhedral amphibole phenocrysts. There is another phenocryst phase but it cannot be identified in hand sample. (*Trachydacite*)

Boulder 4

Mafic; phaneritic texture with amphibole, pyroxene, and feldspar crystals. (*Basaltic andesite/Basaltic trachyandesite*)

Boulder 6

Mafic; porphyritic volcanic texture with black aphanitic groundmass, subhedral plagioclase phenocrysts, and sparse dissolution vugs. (*Trachyandesite/Trachydacite**)

Boulder 7

Felsic; porphyritic volcanic texture with light gray aphanitic groundmass, anhedral feldspar phenocrysts, and minor amounts of very small biotite phenocrysts. (*Rhyolite*)

Boulder 8

Felsic; porphyritic volcanic texture with red aphanitic groundmass, abundant euhedral to subhedral plagioclase phenocrysts, and an unidentifiable black phenocryst phase. Looks like a crystal-rich volcanic tuff or air fall deposit. (*Dacite*)

Boulder 9

Mafic; porphyritic volcanic texture with dark gray aphanitic groundmass, abundant very small feldspar phenocrysts, and ubiquitous dissolution vugs. (*Basaltic andesite*)

Boulder 10

Mafic; porphyritic volcanic texture with dark gray aphanitic groundmass, abundant subhedral to anhedral feldspar phenocrysts, spare olivine (?) phenocrysts, and ubiquitous vesicles. Some vesicles are lined with tan alteration material. (*Basaltic andesite/Basaltic trachyandesite*)

Boulder 11

Felsic; porphyritic volcanic texture with pink aphanitic groundmass, subhedral feldspar phenocrysts, and an unidentifiable black phenocryst phase. (*Andesite/Dacite*)

Boulder 12

Mafic; porphyritic volcanic texture with black aphanitic groundmass and subhedral to anhedral feldspar phenocrysts. (*Basaltic andesite/Basaltic trachyandesite*)

Boulder 13

Felsic; porphyritic volcanic texture with light gray aphanitic groundmass, abundant very small feldspar phenocrysts, sparse olivine (?) phenocrysts, and sparse dissolution vugs. (*Basaltic andesite*)

Boulder 14

Felsic; porphyritic plutonic texture with light gray aphanitic groundmass, abundant subhedral plagioclase phenocrysts, lesser black phenocrysts that are unidentifiable, and ubiquitous dissolution vugs. (*Dacite*)

Boulder 15

Mafic; black aphanitic rock with abundant very small dissolution vugs. (*Basaltic andesite/Basaltic trachyandesite*)

Boulder 16

Felsic; porphyritic plutonic texture with red aphanitic groundmass, subhedral plagioclase phenocrysts, and an unidentifiable black phenocryst phase. Looks like a crystal-rich volcanic tuff. (*Andesite*)

Boulder 17

Mafic; porphyritic volcanic texture with black aphanitic groundmass and subhedral to anhedral feldspar phenocrysts. (*Trachydacite*)

Boulder 18

Mafic; porphyritic plutonic texture with dark gray aphanitic groundmass, subhedral feldspar phenocrysts, and unidentifiable black phenocrysts. (*Andesite/Trachyandesite*)

Boulder 20

Mafic; dark red aphanitic groundmass contains flattened black lithic fragments. Presence of flattened lithics and hefty rock density indicate a high degree of welding. (*Basaltic trachyandesite*)

Boulder 21

Mafic; porphyritic volcanic texture with dark red aphanitic groundmass and abundant subhedral unidentifiable black phenocrysts. (*Basaltic andesite/Basaltic trachyandesite*)

Root (No ages yet)

Root 1

Felsic; porphyritic plutonic texture with pink aphanitic groundmass and abundant subhedral plagioclase phenocrysts. (*Dacite*)

Root 3

Felsic; phaneritic texture with plagioclase, amphibole, and biotite crystals. (*Trachyandesite*)

Root 4

Felsic; phaneritic texture with abundant plagioclase, relatively less amphibole, and sparse, heavily altered biotite crystals. (*Dacite*)

Root 6

Intermediate; phaneritic texture with roughly equal proportions of plagioclase and unidentifiable black crystals. (*Andesite*)

Root 7

Felsic; porphyritic plutonic texture with white aphanitic groundmass, abundant subhedral to anhedral feldspar phenocrysts, and lesser amounts of subhedral biotite and amphibole phenocrysts. (*Dacite*)

Root 8

Mafic; black, aphanitic rock. (*Basalt*)

Root 9

Felsic; porphyritic plutonic texture with pink aphanitic groundmass and abundant subhedral plagioclase phenocrysts. (*Dacite*)

Root 10

Felsic; porphyritic plutonic texture with light gray aphanitic groundmass, abundant subhedral plagioclase phenocryst, and minor amounts of subhedral amphibole, biotite, and other unidentifiable black phenocrysts. (*Dacite*)

Root 11

Mafic; porphyritic volcanic texture with dark gray aphanitic groundmass, anhedral feldspar phenocrysts, and pervasive green alteration material. (*Basaltic trachyandesite**)

Root 12

Mafic; black, aphanitic rock. (*Basaltic andesite*)

Root 13

Felsic; porphyritic plutonic texture with light gray aphanitic groundmass and roughly equal proportions of feldspar, amphibole, and biotite phenocrysts. (*Dacite*)

Root 14

Felsic; light gray, aphanitic rock. (*Trachydacite**)

Root 15

Felsic; light gray, aphanitic rock. (*Basaltic andesite*)

Root 16

Mafic; porphyritic volcanic texture with dark gray aphanitic groundmass, subhedral tiny but abundant feldspar phenocrysts, and minor sulfide mineralization. (*Trachyandesite*)

Hawkins (No ages yet)

Hawkins 1

Intermediate; porphyritic plutonic texture with dark gray aphanitic groundmass, large subhedral feldspar phenocrysts, and relatively small but more abundant amphibole phenocrysts. (*Dacite*)

Hawkins 2

Intermediate; porphyritic volcanic texture with gray aphanitic groundmass and anhedral unidentifiable white phenocrysts. (*Dacite**)

Hawkins 3

Felsic; phaneritic texture with abundant feldspar crystals and relatively less biotite and amphibole phenocrysts. (*Rhyolite*)

Hawkins 4

Felsic; porphyritic volcanic texture with white aphanitic groundmass and very small biotite phenocrysts. (*Rhyolite*)

Hawkins 5

Felsic; phaneritic texture with abundant feldspar crystals and relatively less amphibole crystals. (*Rhyolite*)

Hawkins 6

Felsic; phaneritic texture with abundant feldspar crystals, abundant unidentifiable black crystals, and sparse and relatively large biotite phenocrysts. (*Rhyolite*)

Hawkins 7

Felsic; phaneritic texture with abundant pink/red feldspar crystals, heavily altered plagioclase crystals, and heavily altered hornblende. (*Trachydacite/Trachyte)*

Hawkins 8

Felsic; phaneritic texture with abundant feldspar, quartz, biotite, and amphibole crystals. (*Rhyolite*)

Hawkins 9

Felsic; phaneritic texture with abundant feldspar, quartz, biotite, and amphibole crystals. (*Rhyolite*)

Hawkins 10

Mafic; black, aphanitic rock. (*Basalt*)

Hawkins 11

Mafic; porphyritic plutonic texture with dark red aphanitic groundmass and anhedral unidentifiable black and white phenocrysts. (*Dacite/Trachydacite**)

Hawkins 12

Mafic; porphyritic plutonic texture with black aphanitic groundmass and small anhedral feldspar phenocrysts. (*Basalt*)

Hawkins 13

Mafic; porphyritic volcanic texture with black aphanitic groundmass and small and sparse feldspar phenocrysts. (*Trachydacite*)

Hawkins 14

Mafic; porphyritic volcanic texture with black aphanitic groundmass, small feldspar phenocrysts, and relatively large olivine phenocrysts. (*Basaltic andesite*)

Hawkins 15

Felsic; phaneritic texture with abundant feldspar, quartz, biotite, and amphibole crystals. (*Rhyolite*)

Hawkins 17

Felsic; phaneritic texture with abundant feldspar, quartz, biotite, and amphibole crystals. (*Rhyolite*)

Hawkins 18

Intermediate; phaneritic texture with roughly equal proportions of plagioclase, amphibole, and pyroxene crystals. (*Andesite*)

Jacksina (No ages yet)

Jacksina 1

Felsic; porphyritic volcanic texture with pink aphanitic groundmass and subhedral heavily altered feldspar phenocrysts. (*Dacite*)

Jacksina 2

Felsic; porphyritic volcanic texture with red aphanitic groundmass and sparse subhedral to anhedral feldspar phenocrysts. (*Dacite*)

Jacksina 3

Mafic; porphyritic volcanic texture with black aphanitic groundmass, abundant subhedral plagioclase phenocrysts, and ubiquitous dissolution vugs. (*Andesite*)

Jacksina 4

Felsic; porphyritic volcanic texture with gray aphanitic groundmass, small subhedral to anhedral feldspar phenocrysts, and sparse dissolution vugs. (*Dacite/Trachydacite*)

Jacksina 5

Felsic; porphyritic volcanic texture with pink aphanitic groundmass and small rounded phenocrysts that have been completely replaced by a rust-colored material. (*Rhyolite*)

Jacksina 6

Mafic; porphyritic volcanic texture with black aphanitic groundmass, anhedral feldspar phenocrysts (some have been replaced by orange material), and sparse vesicles. (*Andesite/Trachyandesite*)

Jacksina 7

Mafic; porphyritic volcanic texture with gray aphanitic groundmass, subhedral plagioclase phenocrysts, subhedral olivine phenocrysts, and ubiquitous vesicles. (*Basaltic andesite*)

Jacksina 8

Mafic; dark red and black aphanitic rock. The black areas are angular and give it the appearance of breccia. (*Andesite*)

Jacksina 9

Mafic; porphyritic volcanic texture with dark gray aphanitic groundmass and abundant small anhedral feldspar phenocrysts. (*Andesite*)

Jacksina 10

Felsic; porphyritic volcanic texture with light gray aphanitic groundmass and sparse unidentifiable dark-colored phenocrysts. (*Dacite*)

Jacksina 11

Felsic; phaneritic texture with abundant feldspar and relatively less and smaller amphibole crystals. (*Dacite*)

Jacksina 12

Mafic; porphyritic volcanic texture with black aphanitic groundmass and abundant subhedral plagioclase phenocrysts. (*Andesite*)

Jacksina 13

Felsic; porphyritic volcanic texture with tan aphanitic groundmass and small amphibole and biotite phenocrysts. (*Dacite*)

Jacksina 14

Mafic; porphyritic volcanic texture with gray aphanitic groundmass, subhedral feldspar phenocrysts, and ubiquitous dissolution vugs. (*Andesite*)

Jacksina 15

Mafic; porphyritic volcanic texture with dark gray aphanitic groundmass, subhedral plagioclase and amphibole phenocrysts, and pervasive red material throughout. (*Basaltic andesite/Andesite*)

Jacksina 16

Felsic; porphyritic volcanic texture with light gray aphanitic groundmass and subhedral to anhedral plagioclase phenocrysts. (*Trachydacite*)

Nizina (No ages yet)

Nizina 1

Felsic; porphyritic volcanic texture with pink aphanitic groundmass and unidentifiable phenocrysts that have been completely replaced with a rust-colored material. (*Rhyolite*)

Nizina 3

Mafic; porphyritic volcanic texture with black aphanitic groundmass and sparse and small anhedral feldspar phenocrysts. (*Andesite*)

Nizina 4

Felsic; phaneritic texture with abundant feldspar crystals and relatively less amphibole crystals. (*Trachydacite*)

Nizina 6

Mafic; porphyritic volcanic texture with black aphanitic groundmass and abundant subhedral plagioclase phenocrysts. (*Trachydacite*)

Nizina 7

Felsic; porphyritic volcanic texture with light gray aphanitic groundmass, subhedral plagioclase phenocrysts, and unidentifiable dark green phenocrysts. (*Rhyolite*)

Nizina 8

Felsic; lithic- and crystal-rich volcanic tuff. Light gray aphanitic groundmass contains lithics, subhedral plagioclase, subhedral quartz, subhedral biotite, and fiamme. (*Rhyolite*)

Nizina 9

Felsic; porphyritic volcanic texture with pink aphanitic groundmass, subhedral plagioclase phenocrysts, and ubiquitous dissolution vugs that are lined with orang alteration material. (*Rhyolite*)

Nizina 11

Mafic; porphyritic volcanic texture with dark gray aphanitic groundmass and sparse and small anhedral feldspar phenocrysts. (*Andesite**)

Nizina 12

Mafic; porphyritic volcanic texture with dark gray aphanitic groundmass and abundant subhedral plagioclase phenocrysts. (*Rhyolite*)

Nizina 13

Felsic; phaneritic texture with abundant feldspar crystals, relatively less amphibole crystals, unidentifiable dark green crystals, and sparse dissolution vugs. (*Rhyolite*)

Nizina 14

Felsic; porphyritic plutonic texture with gray aphanitic groundmass, subhedral plagioclase phenocrysts, and unidentifiable dark green phenocrysts. (*Rhyolite*)

Nizina 15

Intermediate; fine-grained phaneritic texture with roughly equal proportions of feldspar and amphibole crystals. (*Andesite)*

Nizina 16

Intermediate; phaneritic texture with roughly equal proportions of feldspar and amphibole crystals with the occasional biotite crystal. (*Andesite*)

Nizina 17

Felsic; porphyritic volcanic texture with white aphanitic groundmass and very sparse quartz and biotite phenocrysts. (*Rhyolite*)

Nizina 18

Mafic; porphyritic volcanic texture with dark brown aphanitic groundmass, small anhedral feldspar phenocrysts, unidentifiable black phenocrysts, and patches of orange alteration material. (*Basaltic andesite**)

Nizina 19

Felsic; crystal-rich volcanic tuff. Light gray aphanitic groundmass contains subhedral plagioclase and abundant fiamme. Pervasive orange alteration material is present. (*Rhyolite*)

Nizina 20

Mafic; porphyritic volcanic texture with dark gray aphanitic groundmass, sparse and small anhedral feldspar phenocrysts, and patches of orange alteration material. (*Andesite/Trachyandesite*)

Nizina 24

Mafic; porphyritic volcanic texture with dark gray aphanitic groundmass, abundant subhedral plagioclase phenocrysts, and sparse amphibole phenocrysts. (*Trachyandesite*)

Appendix B - Raw Geochemical Data

Major and trace elements were analyzed at Franklin and Marshall College using XRF spectroscopy. $^{40}Ar/^{39}Ar$ ages were analyzed at University of Alaska, Fairbanks. All major element data are expressed as raw wt.% and all trace element data are expressed in ppm. Fe_2O_3* is total Fe. N.D. indicates "not determined", and applies to samples that do not yet have ages. If there are sample numbers that appear to be missing (e.g., White 3 is followed by White 5), this simply indicates the missing sample was discarded in the sample preparation step due to intensive alteration and was therefore not analyzed using XRF spectroscopy.

Sample	Sanford 1	Sanford 2	Sanford 3	Sanford 4	Sanford 5	Sanford 6	Sanford 7	Sanford 8	Sanford 9	Sanford 11
Age (Ma)	0.07	2.3	1.29	0.83	1.69	0.59	0.7	0.34	0.54	0.67
± Ma	0.34	0.64	0.05	0.15	0.62	0.18	0.35	0.21	0.16	0.1
SiO_2	53.83	53.88	60.12	55.84	62.75	53.36	53.76	55.43	61.66	54.03
TiO_2	1.1	1.1	0.75	0.92	0.57	1.35	1.41	0.94	0.65	1.09
Al_2O_3	17.43	18.04	17.08	16.76	16.86	17.88	18	16.8	16.83	17.03
Fe_2O_3*	8.04	7.84	6.17	7.38	5.16	8.98	8.79	7.49	5.52	8.3
MnO	0.14	0.13	0.1	0.13	0.11	0.15	0.14	0.14	0.11	0.14
MgO	6.24	5.4	3.54	5.86	3.05	5.1	4.49	6	3.45	6.07
CaO	8.04	8.46	6.13	7.73	5.7	7.87	7.72	7.82	5.64	8.08
Na_2O	3.75	3.71	3.93	3.84	4.01	4.06	4.23	3.76	3.99	3.5
K_2O	0.84	0.86	1.7	1	1.47	0.92	0.99	1.01	1.71	1.09
P_2O_5	0.21	0.26	0.19	0.19	0.18	0.26	0.28	0.21	0.17	0.25
LOI	0.03	0.22	0.66	0.28	0.24	0.13	-0.15	-0.01	0.39	0.37
Total	99.62	99.68	99.71	99.65	99.86	99.93	99.81	99.6	99.73	99.58
Rb	16.9	19..5	30.5	22.9	33.7	20.0	20.6	22.5	28.8	22.9
Sr	535	583	755	512	587	537	542	525	758	560
Y	24.9	21.9	16.4	22.3	15.3	25.8	26.9	24.2	14.0	26.0
Zr	140	125	143	129	145	170	183	137	140	147
V	170	205	151	181	111	218	205	170	99	219
Ni	127	83	56	132	42	68	46	144	45	111
Cr	155	105	80	136	70	54	40	134	73	163
Nb	3.3	3.7	2.7	3.2	5.2	4.4	4.4	5.5	3.0	3.9
Ga	19.1	19.5	20.4	18.9	20.2	19.6	20.1	19.1	20.9	19.1
Cu	58	58	48	88	38	80	75	72	62	109
Zn	67	68	56	68	58	77	73	64	57	74
Co	31	27	17	29	13	33	30	30	13	33
Ba	289	312	557	369	642	269	318	412	619	361
La	17	12	18	16	19	14	14	20	19	15
Ce	24	23	30	24	33	23	22	33	29	26
U	<0.5	<0.5	<0.5	1.0	<0.5	<0.5	<0.5	2.2	0.6	<0.5
Th	<0.5	<0.5	1.3	0.8	1.7	<0.5	<0.5	<0.5	1.7	<0.5
Sc	22	23	14	20	12	22	22	19	12	24
Pb	<1	<1	9	11	<1	<1	<1	13	17	11

***Note*: All major element data expressed as raw weight % oxides; all other concentrations in ppm. Fe_2O_3* is total Fe, N.D. = not determined. Dad = Dadina, Che = Chetaslina, Kot = Kotsina, Nad = Nadina, Kusk = Kuskulana.**

Sample	Sanford 12	Sanford 13	Sanford 14	Sanford 15	Sanford 16	Sanford 17	Sanford 18	Sanford 19	White 2	White 3
Age (Ma)	-0.38	0.24	0.4	0.35	0.56	1.46	0.64	0.58	262.66	11.49
± Ma	0.39	0.08	0.05	0.13	0.04	0.15	0.06	0.08	1.66	0.26
SiO_2	55.31	59.78	60.39	65.35	74.1	57.65	65.79	73.95	74.89	56.50
TiO_2	1.0	0.88	1.12	0.4	0.09	1.01	0.39	0.09	0.50	1.10
Al_2O_3	17.74	16.73	15.74	16.77	15.08	17.16	16.76	15.14	11.31	16.60
Fe_2O_3*	7.87	6.29	7.31	4.09	1.13	7.29	3.85	1.16	6.64	8.23
MnO	0.13	0.11	0.13	0.07	0.06	0.12	0.06	0.06	0.04	0.17
MgO	5.03	3.89	2.97	2.32	0.4	4.18	2.1	0.4	2.40	5.72
CaO	7.63	6.18	4.93	4.76	1.9	6.89	4.73	1.92	1.14	6.11
Na_2O	3.99	3.92	4.33	3.97	4.77	3.84	3.94	4.75	1.49	4.04
K_2O	0.9	1.79	2.47	1.98	2.21	1.36	1.98	2.23	1.60	0.92
P_2O_5	0.26	0.2	0.39	0.13	0.08	0.27	0.14	0.08	0.08	0.24
LOI	0.03	0.26	-0.11	2.72	0.6	0.61	2.27	0.64	4.14	6.83
Total	99.86	99.77	99.78	99.84	99.82	99.77	99.74	99.78	100.09	99.63
Rb	18.8	47.0	59.9	43.0	62.7	30.2	46.0	60.9	55.6	25.5
Sr	605	518	413	658	509	608	789	508	231	328
Y	20.6	22.8	44.4	11.4	4.7	22.0	9.7	3.6	26.5	29.1
Zr	127	202	389	119	104	169	128	98	174	144
V	191	151	133	94	12	187	81	10	109	155
Ni	88	61	55	38	5	70	29	5	56	23
Cr	122	78	72	54	9	93	43	12	101	123
Nb	3.4	5.0	13.1	3.3	4.0	4.4	2.7	4.5	15.2	5.5
Ga	20.1	19.8	21.6	20.7	20.4	19.9	21.1	20.1	14.7	18.3
Cu	78	66	65	59	7	126	54	8	32	17
Zn	73	59	87	49	32	74	50	33	160	91
Co	29	17	17	6	<1	23	6	<1	11	30
Ba	352	463	712	645	950	459	624	950	325	288
La	14	19	26	18	22	17	15	25	25	14
Ce	26	29	53	25	33	35	38	33	44	30
U	<0.5	2.4	0.8	<0.5	<0.5	<0.5	1.5	<0.5	2.2	<0.5
Th	<0.5	6.2	8.5	2.0	7.1	<0.5	2.8	6.8	16.7	8.3
Sc	20	14	15	9	<1	20	8	<1	6	21
Pb	<1	8	7	<1	8	15	18	17	10	<1

***Note*: All major element data expressed as raw weight % oxides; all other concentrations in ppm. Fe_2O_3* is total Fe, N.D. = not determined. Dad = Dadina, Che = Chetaslina, Kot = Kotsina, Nad = Nadina, Kusk = Kuskulana.**

Sample	White 5	White 6	White 7	White 8	White 11	White 13	White 14	White 15	White 16	White 17
Age (Ma)	23.5	10.25	93.48	12.63	9.31	300.86	34.58	10.4	9.92	10.84
± Ma	0.7	0.19	1.11	0.28	0.12	4.16	0.47	0.3	0.23	0.08
SiO_2	65.94	52.56	48.73	57.97	72.08	64.74	66.39	55.56	72.82	59.06
TiO_2	0.34	2.59	1.33	1.13	0.38	0.43	0.33	1.85	0.36	1.28
Al_2O_3	16.56	16.20	15.11	16.39	14.51	9.46	16.62	17.19	14.23	17.38
Fe_2O_3*	3.51	12.03	11.65	6.97	2.25	9.26	3.37	8.59	2.19	6.81
MnO	0.08	0.13	0.17	0.12	0.08	0.06	0.07	0.12	0.07	0.12
MgO	2.54	1.86	8.05	4.59	0.58	2.43	2.27	2.94	0.57	2.35
CaO	4.43	7.04	10.41	7.22	1.42	11.30	4.36	6.68	1.31	5.73
Na_2O	5.24	4.38	3.55	3.77	5.13	0.94	5.20	4.01	5.04	4.50
K_2O	0.90	2.17	0.49	1.12	3.48	0.84	0.97	2.09	3.52	2.27
P_2O_5	0.13	0.83	0.13	0.33	0.10	0.10	0.13	0.46	0.10	0.34
LOI	1.29	3.12	4.01	1.84	0.30	10.51	2.44	3.06	0.40	0.85
Total	99.67	99.79	99.62	99.61	100.01	99.56	99.71	99.49	100.21	99.84
Rb	24.0	56.5	8.1	47.5	104.7	21.9	26.2	54.2	97.3	65.8
Sr	648	436	258	674	191	702	710	478	174	481
Y	11.2	53.5	27.6	26.2	36.9	25.2	9.5	37.9	36.5	31.2
Zr	93	471	93	223	318	136	103	328	295	283
V	82	203	309	142	30	100	74	164	31	123
Ni	47	10	120	51	5	52	35	23	5	11
Cr	88	16	265	124	9	77	51	44	9	26
Nb	2.5	24.7	5.6	11.0	17.7	6.7	2.4	14.6	17.3	14.0
Ga	20.3	23.7	16.7	19.7	21.0	10.9	20.1	20.5	20.9	21.8
Cu	13	60	21	36	8	22	12	47	8	29
Zn	46	138	100	77	51	122	44	96	39	79
Co	8	28	52	20	<1	8	7	24	<1	16
Ba	522	624	61	722	1126	251	545	661	1096	654
La	13	26	8	24	34	24	12	21	36	28
Ce	20	43	15	55	78	39	18	46	70	49
U	<0.5	3.7	<0.5	<0.5	3.5	1.3	<0.5	3.2	0.6	0.6
Th	1.3	12.8	<1	4.5	18.0	4.8	1.6	11.2	17.8	7.2
Sc	9	22	39	16	1	18	7	17	<1	11
Pb	2	1	<1	9	6	8	1	13	13	1

***Note*: All major element data expressed as raw weight % oxides; all other concentrations in ppm. Fe_2O_3* is total Fe, N.D. = not determined. Dad = Dadina, Che = Chetaslina, Kot = Kotsina, Nad = Nadina, Kusk = Kuskulana.**

Sample	White 18	Chisana 1	Chisana 2	Chisana 3	Chisana 4	Chisana 5	Chisana 6	Chisana 7	Chisana 8	Chisana 9
Age (Ma)	300.97	51.88	22.9	25.12	9	6.36	6.23	7.43	6.93	6.25
± Ma	1.81	2.01	0.4	0.26	0.13	0.46	0.09	0.15	0.15	0.15
SiO_2	56.19	47.02	67.83	65.07	69.71	61.75	73.51	67.94	68.48	64.1
TiO_2	0.26	0.44	0.31	0.46	0.40	0.75	0.31	0.51	0.52	0.46
Al_2O_3	6.40	17.21	16.44	17.15	15.62	15.54	13.82	15.56	15.33	17.22
Fe_2O_3*	3.30	11.30	2.98	3.97	2.92	5.42	2.21	3.59	3.54	4.38
MnO	0.06	0.16	0.06	0.10	0.05	0.11	0.07	0.08	0.09	0.08
MgO	1.23	8.53	1.80	1.76	1.16	4.57	0.65	1.46	1.45	2.37
CaO	30.33	12.93	3.48	4.22	3.44	5.35	1.44	3.06	3.07	5.42
Na_2O	0.63	2.16	5.61	5.07	3.91	4.25	4.55	4.92	4.8	4.13
K_2O	1.08	0.13	1.03	1.73	2.53	1.52	3.17	2.48	2.4	1.31
P_2O_5	0.08	0.07	0.13	0.24	0.12	0.25	0.08	0.15	0.15	0.14
LOI	19.66	4.69	1.22	1.52	3.62	1.72	0.8	1.51	1.46	2.73
Total	99.56	99.95	99.67	99.77	99.86	99.51	99.81	99.75	99.83	99.61
Rb	19.8	3.1	18.3	37.6	68.9	42.6	61.3	61.0	61.3	30.7
Sr	769	163	752	905	376	582	185	326	322	571
Y	13.1	17.0	8.4	12.9	15.7	20.8	22.9	30.1	29.3	15.4
Zr	130	20	137	147	162	204	239	227	230	132
V	57	251	71	73	63	106	35	65	66	88
Ni	17	207	29	12	14	126	7	14	15	18
Cr	44	229	51	18	26	235	14	26	31	31
Nb	5.7	<1	1.0	10.6	5.8	5.0	10.9	8.3	7.6	3.7
Ga	7.3	13.5	19.6	20.8	18.5	19.1	19.5	21.1	20.5	18.4
Cu	8	88	18	17	30	59	15	23	27	33
Zn	41	70	27	57	45	61	43	55	55	54
Co	<1	55	4	6	3	20	<1	2	2	9
Ba	143	61	994	1014	815	611	931	811	783	611
La	21	11	19	29	25	24	35	30	32	21
Ce	34	16	28	48	48	49	60	54	58	38
U	0.6	<0.5	0.5	1.2	1.3	<0.5	2.0	0.7	1.3	<0.5
Th	<0.5	<0.5	0.5	1.6	11.4	2.6	12.1	8.0	8.8	1.2
Sc	25	37	4	3	5	11	1	4	5	4
Pb	<1	<1	3	5	6	1	2	5	3	<1

***Note*: All major element data expressed as raw weight % oxides; all other concentrations in ppm. Fe_2O_3* is total Fe, N.D. = not determined. Dad = Dadina, Che = Chetaslina, Kot = Kotsina, Nad = Nadina, Kusk = Kuskulana.**

Sample	Chisana 11	Chisana 12	Chisana 13	Chisana 14	Chisana 15	Chisana 16	Chisana 17	Chisana 18	Dad 1A-1	Dad 1A-2
Age (Ma)	20.6	5.88	7.9	9.15	6.55	162.45	7.06	8.02	0.49	0.31
± Ma	0.5	0.12	0.38	0.21	0.04	1.43	0.08	0.18	0.11	0.12
SiO_2	67.82	74.9	67.13	65.19	76.6	48.2	74.42	57.73	60.19	64.17
TiO_2	0.33	0.22	0.57	0.41	0.15	2.61	0.31	1.12	0.88	0.54
Al_2O_3	16.3	13.72	15.74	16.47	12.82	15.25	13.99	16.76	16.46	16.62
Fe_2O_3*	3.05	1.36	3.81	3.69	1.24	13.92	1.68	7.4	6.23	4.61
MnO	0.06	0.06	0.08	0.08	0.05	0.18	0.04	0.15	0.11	0.09
MgO	1.8	0.19	1.64	2.83	0.18	5.74	0.39	3.01	3.82	2.78
CaO	2.75	0.47	3.27	4.23	0.62	9.41	1.23	5.91	5.99	4.94
Na_2O	6.08	6.06	5.03	4.98	4.52	3.51	4.61	4.26	3.9	4.33
K_2O	1.42	2.59	2.26	1.54	3.6	0.58	3.07	2.5	1.85	1.71
P_2O_5	0.13	0.04	0.17	0.18	0.03	0.26	0.05	0.75	0.2	0.16
LOI	1.33	0.41	1.24	1.22	0.33	2.12	1.78	1.3	0.27	0.17
Total	99.74	99.61	99.7	99.6	99.81	99.66	99.79	99.59	99.63	99.95
Rb	31.1	62.2	58.2	32.5	99.2	7.3	97.9	53.4	45.6	41.2
Sr	733	74	361	816	67	314	157	694	508	698
Y	8.6	51.0	31.7	11.4	29.3	39.3	32.0	28.7	22.0	13.5
Zr	109	290	221	124	198	163	299	225	204	145
V	67	16	72	78	12	402	21	154	135	79
Ni	26	5	17	61	5	84	5	5	56	49
Cr	47	14	24	69	11	138	15	9	81	68
Nb	2.3	16.2	8.3	4.5	10.5	14.6	9.1	10.2	5.6	3.9
Ga	19.4	25.4	21.0	20.5	17.7	19.3	18.1	21.6	19.7	20.5
Cu	49	13	26	39	12	152	16	43	75	57
Zn	34	44	41	63	38	86	41	82	63	62
Co	5	<1	3	9	<1	44	<1	18	16	12
Ba	1845	897	805	853	983	97	838	794	497	656
La	18	48	27	23	39	12	31	34	22	19
Ce	27	104	48	37	75	18	64	65	37	37
U	<0.5	0.5	0.7	0.5	2.0	<0.5	1.5	0.5	<0.5	<0.5
Th	0.5	15.7	6.7	0.5	19.0	<0.5	15.5	2.3	1.5	0.8
Sc	4	<1	3	5	<1	36	1	10	12	8
Pb	3	20	1	20	16	<1	14	8	<1	2

***Note*: All major element data expressed as raw weight % oxides; all other concentrations in ppm. Fe_2O_3* is total Fe, N.D. = not determined. Dad = Dadina, Che = Chetaslina, Kot = Kotsina, Nad = Nadina, Kusk = Kuskulana.**

Sample	Dad 1B-1	Dad 1B-2	Dad 1B-3	Dad 1B-4	Dad 1C-1	Dad 1C-2	Dad 1C-3	Dad 1C-4	Dad 1C-5	Nabesna 1
Age (Ma)	1.86	0.48	0.49	0.68	0.74	1.46	0.56	0.65	0.76	17.72
± Ma	0.12	0.09	0.09	0.09	0.11	0.09	0.08	0.09	0.16	0.36
SiO_2	67.31	59.57	63.4	59.24	62.66	62.22	73.56	73.99	66.08	66.9
TiO_2	0.42	0.84	0.51	0.92	0.78	0.6	0.12	0.08	0.38	0.34
Al_2O_3	15.78	16.98	17.16	16.32	16.57	16.68	15.52	15.19	16.59	16.63
Fe_2O_3*	3.75	6.35	4.65	6.58	5.4	5.18	1.28	1.24	3.8	3.68
MnO	0.08	0.11	0.09	0.11	0.1	0.1	0.07	0.07	0.06	0.08
MgO	2.19	3.99	2.54	4.39	2.69	3.51	0.43	0.39	2.2	1.71
CaO	4.36	6.28	5.24	6.4	5.11	5.51	1.85	1.93	4.59	4.54
Na_2O	4.17	3.89	4.33	3.69	4.18	3.91	4.71	4.77	4.27	4.67
K_2O	1.92	1.69	1.69	1.88	2.13	1.99	2.53	2.21	1.67	1.04
P_2O_5	0.12	0.19	0.18	0.23	0.2	0.16	0.09	0.09	0.13	0.16
LOI	0.55	0.93	-0.03	0.28	0.84	-0.03	1.46	1.13	1.79	1.69
Total	100.1	99.89	99.79	99.76	99.82	99.86	100.16	99.96	99.77	99.75
Rb	40.8	44.1	35.7	46.8	57.3	35.0	58.2	57.7	39.3	22.4
Sr	696	558	799	636	586	891	569	485	692	649
Y	10.7	21.5	12.4	22.0	21.4	13.4	8.2	5.2	10.6	11.5
Zr	136	189	140	214	211	148	130	104	105	93
V	90	145	106	170	121	132	8	11	85	74
Ni	21	68	30	58	33	55	3	4	26	13
Cr	54	77	38	143	39	96	7	7	28	23
Nb	2.5	5.0	3.4	5.1	5.7	3.3	6.1	4.0	1.5	1.4
Ga	20.3	19.6	22.5	19.6	20.6	22.4	20.5	20.0	20.6	20.1
Cu	64	88	85	96	66	91	11	13	67	18
Zn	57	73	67	71	64	66	67	46	57	48
Co	4	19	10	20	11	14	<1	<1	7	5
Ba	710	514	604	635	674	665	970	866	638	499
La	18	24	22	23	24	20	31	23	15	20
Ce	26	37	28	44	44	32	54	39	23	30
U	0.5	<0.5	<0.5	<0.5	<0.5	<0.5	0.5	0.5	<0.5	<0.5
Th	<0.5	0.5	<0.5	1.8	0.5	<0.5	7.4	1.2	<0.5	<0.5
Sc	8	13	5	14	8	10	<1	<1	7	6
Pb	21	1	<1	12	5	15	28	4	7	10

***Note*: All major element data expressed as raw weight % oxides; all other concentrations in ppm. Fe_2O_3* is total Fe, N.D. = not determined. Dad = Dadina, Che = Chetaslina, Kot = Kotsina, Nad = Nadina, Kusk = Kuskulana.**

Sample	Nabesna 2	Nabesna 4	Nabesna 5	Nabesna 7	Nabesna 8	Nabesna 11	Nabesna 12	Nabesna 13	Nabesna 14	Che 1A-1
Age (Ma)	23.9	19.21	69.87	20.35	18.8	153.31	1.37	27.7	22.63	0.39
± Ma	0.4	0.22	0.29	0.36	0.23	1.39	0.32	0.2	0.28	0.11
SiO_2	55.46	66.63	60.11	66.42	66.37	52.95	55.82	66.59	63.73	65.33
TiO_2	0.51	0.36	0.68	0.36	0.35	0.66	1.09	0.37	0.44	0.48
Al_2O_3	15.79	16.82	16.36	16.71	16.81	17.39	17.23	16.84	17.65	15.98
Fe_2O_3*	8.04	3.74	7.23	3.84	3.84	9.22	7.77	3.15	4.49	4.07
MnO	0.13	0.09	0.15	0.08	0.09	0.2	0.15	0.08	0.11	0.08
MgO	6.27	1.73	3.15	1.75	1.78	5.66	5.41	1.78	2.64	2.7
CaO	8.74	4.47	6.27	4.44	4.65	9.72	7.27	4.27	4.34	4.96
Na_2O	3.68	4.63	3.39	4.56	4.26	1.76	3.96	4.91	5.2	4.08
K_2O	0.55	1.27	2.06	1.27	1.57	1.71	0.9	1.64	1.01	2.15
P_2O_5	0.28	0.15	0.18	0.16	0.15	0.28	0.26	0.18	0.22	0.16
LOI	0.97	2.05	1.57	2.02	2.74	7.94	0.29	1.24	2.18	0.17
Total	99.45	99.89	99.58	99.59	99.87	99.55	99.86	99.81	99.83	99.99
Rb	12.1	25.0	43.7	24.5	29.9	22.0	16.9	39.0	16.1	34.1
Sr	872	649	400	622	681	648	538	750	878	947
Y	15.2	11.4	29.9	11.9	10.0	21.5	25.6	9.8	14.6	9.2
Zr	70	94	152	100	90	75	145	124	99	139
V	195	72	181	76	77	231	164	64	96	101
Ni	82	13	11	15	13	25	89	15	29	55
Cr	70	16	15	22	15	61	131	26	24	60
Nb	0.7	2.1	3.1	2.2	1.7	2.6	6.0	5.7	1.5	3.0
Ga	17.0	20.2	17.8	20.4	19.7	14.8	18.9	20.2	21.4	22.7
Cu	89	31	80	26	24	137	68	18	37	117
Zn	91	65	68	62	59	123	83	55	75	67
Co	29	4	18	5	3	29	28	2	9	7
Ba	308	578	475	567	761	1034	357	909	404	696
La	19	21	19	22	16	16	15	25	16	19
Ce	32	27	27	28	19	28	27	42	29	30
U	<0.5	<0.5	<0.5	1.0	<0.5	<0.5	<0.5	0.7	<0.5	0.5
Th	<0.5	<0.5	<0.5	0.5	<0.5	<0.5	<0.5	0.5	<0.5	<0.5
Sc	23	5	19	6	5	31	18	4	9	7
Pb	<1	8	<1	21	9	11	5	7	6	20

***Note*: All major element data expressed as raw weight % oxides; all other concentrations in ppm. Fe_2O_3* is total Fe, N.D. = not determined. Dad = Dadina, Che = Chetaslina, Kot = Kotsina, Nad = Nadina, Kusk = Kuskulana.**

Sample	Che 1A-2	Che 1A-3	Che 1B-1	Che 1B-2	Che 1C-2	Che 1C-3	Che 1C-5	Che 1C-6	Cross 3	Cross 5
Age (Ma)	0.62	0.92	150.24	152.42	0.35	0.51	0.76	0.23	118.19	147.97
± Ma	0.11	0.54	0.48	0.96	0.11	0.08	0.24	0.07	0.37	0.93
SiO_2	62.28	61.69	60.99	51.45	56.21	74.24	65.05	60.49	58.82	70.07
TiO_2	0.8	0.71	0.41	0.64	0.87	0.07	0.48	0.85	0.72	0.16
Al_2O_3	16.18	16.54	17.87	19.46	16.29	14.99	16.17	17.29	16.62	15.6
Fe_2O_3*	5.59	5.54	5.36	8.59	6.9	1.2	4.1	5.68	7.84	2.57
MnO	0.11	0.12	0.14	0.24	0.12	0.06	0.08	0.1	0.15	0.13
MgO	3.23	3.57	3.12	3.34	7.31	0.25	2.7	3.07	3.53	0.93
CaO	5.32	5.79	6.21	9.93	6.98	2.02	4.93	6.29	6.88	3.02
Na_2O	3.92	3.82	4.05	3.5	3.41	4.67	4.05	4.08	3.18	4.07
K_2O	2.2	1.88	1.48	2.13	1.43	2.16	2.17	1.78	1.83	2.99
P_2O_5	0.21	0.2	0.2	0.49	0.22	0.08	0.15	0.21	0.17	0.13
LOI	1.07	0.47	1.24	0.55	0.25	1.41	0.88	0.84	0.9	5.27
Total	99.84	99.86	99.83	99.77	99.74	99.74	99.88	99.84	99.74	99.67
Rb	54.2	49.6	31.5	33.0	38.2	54.5	36.4	45.3	40.3	68.9
Sr	507	554	1200	1436	691	481	973	579	366	569
Y	20.9	20.2	10.8	22.2	21.0	4.9	10.9	20.6	29.9	8.6
Zr	214	185	73	93	168	100	137	188	158	98
V	132	124	141	208	169	15	109	148	200	53
Ni	53	59	17	5	172	5	57	60	13	4
Cr	67	76	47	7	248	13	63	49	26	9
Nb	6.2	5.4	1.7	1.9	8.4	4.1	2.4	5.8	3.1	8.3
Ga	19.6	19.8	18.6	18.7	19.1	19.6	23.8	20.3	17.4	17.1
Cu	75	67	17	46	111	23	95	98	57	15
Zn	67	71	71	95	65	41	64	64	69	36
Co	12	17	13	17	29	<1	8	16	21	<1
Ba	627	578	981	704	452	844	696	568	443	2256
La	25	23	13	21	21	20	21	20	19	28
Ce	38	37	26	31	42	27	27	34	40	32
U	0.5	<0.5	<0.5	<0.5	<0.5	<0.5	0.5	0.5	0.7	1.1
Th	3.1	1.7	<0.5	<0.5	1.6	1.3	<0.5	0.9	0.5	2.8
Sc	11	111	12	20	17	<1	8	13	23	1
Pb	<1	<1	<1	25	<1	1	25	7	<1	30

***Note*: All major element data expressed as raw weight % oxides; all other concentrations in ppm. Fe_2O_3* is total Fe, N.D. = not determined. Dad = Dadina, Che = Chetaslina, Kot = Kotsina, Nad = Nadina, Kusk = Kuskulana.**

Sample	Cross 6	Cross 7	Kot 11 7/23	Kot 12 7/23	Kot 14 7/23	Kot 15 7/23	Kot 16 7/23	Kot 1A-1	Kot 1A-2	Kot 1B-1
Age (Ma)	87.65	26.6	0.66	0.02	0.85	0.11	215.07	0.43	0.64	152.31
± Ma	0.65	0.31	0.12	0.32	0.12	0.1	14.23	0.38	0.21	1.09
SiO_2	60.27	67.42	60.97	60.66	59.61	63.22	48.49	59.94	59.34	58.22
TiO_2	0.4	0.39	0.8	0.73	0.88	0.76	2.00	0.96	0.97	0.28
Al_2O_3	18.66	16.41	16.91	16.78	17.10	16.14	14.01	16.25	16.12	20.69
Fe_2O_3*	5.19	3.09	5.55	6.02	6.35	5.30	13.40	6.50	6.73	4.59
MnO	0.19	0.07	0.1	0.11	0.13	0.10	0.17	0.11	0.11	0.13
MgO	2.25	2.29	3.36	3.77	3.68	2.75	6.91	4.24	4.38	1.73
CaO	4.3	4.37	6.01	6.05	6.24	5.06	11.55	5.88	6.17	8.14
Na_2O	5.56	4.62	3.89	3.91	4.02	4.09	2.88	3.83	3.80	3.93
K_2O	2.51	1.18	1.83	1.54	1.70	2.10	0.05	1.91	1.83	1.96
P_2O_5	0.27	0.15	0.21	0.2	0.20	0.19	0.19	0.21	0.21	0.20
LOI	1.61	3.49	1.11	0.4	0.77	-0.13	3.79	0.86	0.88	0.89
Total	99.6	99.99	99.63	99.77	99.91	99.71	99.65	99.83	99.66	99.87
Rb	57.0	26.9	44.3	39.0	59.4	41.6	0.7	51.8	51.4	39.8
Sr	1950	665	710	580	528	534	38	576	571	1468
Y	15.1	10.5	18.5	17.5	19.9	20.4	35.0	20.6	20.1	13.1
Zr	139	115	183	157	192	188	124	216	209	82
V	110	64	143	140	133	137	391	160	165	110
Ni	7	46	47	69	52	50	91	84	84	5
Cr	12	54	40	75	58	52	204	131	132	13
Nb	13.8	5.6	5.4	4.7	6.8	4.2	10.5	4.8	5.3	2.0
Ga	22.6	19.6	20.7	19.5	19.9	19.7	18.5	19.4	19.3	20.9
Cu	50	28	80	29	79	74	69	100	97	13
Zn	74	48	63	68	61	65	70	64	64	45
Co	8	5	15	18	12	18	46	20	22	4
Ba	1482	719	617	527	617	558	13	569	565	626
La	35	18	22	21	21	22	12	24	24	19
Ce	64	23	36	37	42	34	16	43	46	23
U	3.6	<0.5	<0.5	3.4	1.2	0.8	<0.5	<0.5	0.5	<0.5
Th	0.5	0.6	<0.5	<0.5	4.6	0.5	0.6	5.6	5.6	<0.5
Sc	7	4	13	14	10	13	42	14	13	11
Pb	14	16	12	20	15	<1	<1	4	1	<1

***Note*: All major element data expressed as raw weight % oxides; all other concentrations in ppm. Fe_2O_3* is total Fe, N.D. = not determined. Dad = Dadina, Che = Chetaslina, Kot = Kotsina, Nad = Nadina, Kusk = Kuskulana.**

Sample	Kot 1B-2	Kot 1B-3	Kot 1B-4	Kot 1B-5	Kot 1B-6	Nad 1A-1	Nad 1A-2	Nad 1A-3	Nad 1A-4	Nad 1A-5
Age (Ma)	0.49	1.54	0.55	0.68	150.27	0.57	0.47	0.77	0.36	0.17
± Ma	0.18	0.45	0.17	0.16	0.39	0.17	0.1	0.33	0.16	0.13
SiO_2	61.48	59.96	64.55	59.93	67.96	60.67	65.22	62.95	60.50	64.71
TiO_2	0.79	1.01	0.73	0.95	0.26	0.65	0.50	0.54	0.79	0.43
Al_2O_3	16.36	16.14	16.01	16.36	17.35	17.58	17.01	17.48	17.42	16.98
Fe_2O_3*	5.78	6.67	4.79	6.45	2.56	5.84	4.21	4.91	6.14	4.15
MnO	0.10	0.12	0.08	0.12	0.05	0.11	0.09	0.10	0.12	0.08
MgO	3.56	3.88	2.15	3.94	1.13	3.54	1.98	2.93	3.27	2.73
CaO	5.59	5.97	4.46	6.19	3.09	6.24	4.58	5.52	6.31	4.98
Na_2O	4.01	3.81	4.13	3.81	5.48	4.09	4.43	4.23	4.14	4.16
K_2O	1.88	1.89	2.55	1.77	1.72	1.31	1.68	1.41	1.16	1.80
P_2O_5	0.21	0.24	0.19	0.23	0.13	0.23	0.16	0.17	0.19	0.14
LOI	1.11	0.88	0.31	0.76	2.31	0.00	1.04	0.75	0.92	1.05
Total	99.76	99.69	99.64	99.75	99.73	100.26	99.86	100.24	100.04	100.16
Rb	50.7	46.2	68.8	43.4	36.7	26.7	35.5	29.9	26.6	36.4
Sr	551	516	457	568	998	743	628	715	629	795
Y	20.7	23.0	23.6	22.1	2.8	14.0	12.7	12.2	16.2	10.5
Zr	188	203	251	199	84	137	145	118	131	125
V	143	153	111	171	67	141	80	100	154	97
Ni	65	58	31	54	6	47	35	45	32	53
Cr	73	85	54	87	17	68	27	54	37	67
Nb	6.5	6.3	6.8	6.2	<0.5	4.0	3.9	2.5	5.6	3.0
Ga	19.4	19.2	20.0	19.8	21.7	20.9	19.9	21.4	20.3	21.0
Cu	81	71	52	55	20	48	27	58	56	67
Zn	66	64	54	65	62	61	58	64	72	58
Co	15	19	8	18	1	14	4	11	15	10
Ba	605	520	684	545	832	533	639	556	486	648
La	22	28	28	16	10	20	24	15	20	17
Ce	35	40	45	31	10	33	35	24	25	32
U	0.9	0.9	0.7	0.5	<0.5	<0.5	0.6	1.3	1.0	1.3
Th	3.2	3.4	5.9	1.9	<0.5	<0.5	<0.5	<0.5	<0.5	<0.5
Sc	12	15	7	16	3	12	5	9	13	7
Pb	1	7	16	10	7	5	7	2	<1	25

***Note*: All major element data expressed as raw weight % oxides; all other concentrations in ppm. Fe_2O_3* is total Fe, N.D. = not determined. Dad = Dadina, Che = Chetaslina, Kot = Kotsina, Nad = Nadina, Kusk = Kuskulana.**

Sample	Nad 1A-6	Nad 1B-1	Nad 1B-2	Kusk-1A-1	Kusk-1B-1	Kusk-1B-2	Kusk-1B-3	Kusk-1B-4	Kusk-1B-5	Kusk-1B-6
Age (Ma)	0.29	0.39	0.88	3.08	3.04	3.16	2.79	2.89	3.77	3.45
± Ma	0.18	0.29	0.11	0.12	0.51	0.16	0.14	0.19	0.25	0.17
SiO_2	62.32	63.65	59.86	65.61	64.57	64.73	64.85	65.30	65.11	65.54
TiO_2	0.55	0.50	0.74	0.60	0.59	0.60	0.59	0.57	0.59	0.61
Al_2O_3	16.47	17.09	17.10	15.97	16.48	16.36	16.95	16.35	16.58	15.92
Fe_2O_3*	5.31	4.84	6.20	4.29	4.54	4.39	4.27	4.21	4.26	4.26
MnO	0.11	0.10	0.11	0.08	0.09	0.08	0.09	0.09	0.08	0.08
MgO	3.53	2.80	3.90	2.26	2.47	2.45	2.49	2.31	2.42	2.43
CaO	6.00	5.23	6.18	4.30	4.62	4.63	4.69	4.81	4.56	4.36
Na_2O	3.80	4.16	3.90	4.37	4.30	4.26	4.45	4.21	4.27	4.00
K_2O	1.36	1.52	1.53	2.19	2.02	2.03	1.50	1.91	2.08	2.26
P_2O_5	0.18	0.17	0.21	0.16	0.15	0.15	0.15	0.15	0.15	0.16
LOI	0.17	0.57	0.69	1.13	1.70	1.66	0.34	1.07	1.13	1.58
Total	99.63	100.06	99.73	99.83	99.83	99.68	100.03	99.91	100.10	99.62
Rb	29.4	34.7	29.8	51.1	45.2	45.2	29.4	35.6	47.7	49.1
Sr	560	712	753	552	595	574	585	590	574	561
Y	17.7	12.1	18.2	18.0	18.0	17.2	18.3	18.2	18.6	18.2
Zr	148	123	153	181	163	168	157	164	152	177
V	182	102	143	105	98	94	101	98	94	99
Ni	67	46	76	35	36	35	40	35	34	37
Cr	95	61	106	45	43	44	52	40	45	43
Nb	4.1	3.3	3.5	5.0	4.3	3.6	3.1	3.6	4.1	4.1
Ga	19.1	21.8	21.3	20.5	20.6	20.5	20.3	20.9	20.6	20.1
Cu	41	49	38	49	44	49	31	45	45	49
Zn	72	66	71	58	58	59	63	58	57	58
Co	15	11	17	8	8	8	10	8	8	8
Ba	645	564	582	696	693	692	614	708	687	711
La	24	20	19	22	20	20	20	23	25	21
Ce	34	26	30	33	35	35	30	35	35	38
U	0.9	0.5	0.5	<0.5	<0.5	0.5	2.5	<0.5	1.3	1.2
Th	<0.5	0.5	<0.5	5.2	0.7	3.1	0.5	2.3	1.9	3.3
Sc	11	8	11	8	8	8	8	8	8	7
Pb	8	9	6	7	<1	<1	6	11	15	9

***Note*: All major element data expressed as raw weight % oxides; all other concentrations in ppm. Fe_2O_3* is total Fe, N.D. = not determined. Dad = Dadina, Che = Chetaslina, Kot = Kotsina, Nad = Nadina, Kusk = Kuskulana.**

Sample	Kusk-1B-7	Kusk-1B-8	Kusk-1C-1	Kusk-1C-2	Kusk-1C-3	Kusk-1C-4	Kusk-1C-5	Kusk-1C-6	Kusk 1D	Root 1
Age (Ma)	3.31	3.12	3.72	4.47	4.55	4.06	4.03	3.61	3.31	N.D.
± Ma	0.27	0.18	0.31	0.41	0.23	0.4	0.15	0.47	0.18	N.D.
SiO_2	64.62	61.75	66.08	66.35	66.71	67.15	67.07	65.36	61.75	67.35
TiO_2	0.59	0.81	0.58	0.55	0.53	0.53	0.53	0.56	0.81	0.48
Al_2O_3	16.50	16.61	16.27	16.13	15.89	15.62	15.81	16.46	16.66	16.17
Fe_2O_3*	4.37	5.69	4.21	3.96	3.77	3.83	3.85	4.10	5.64	3.56
MnO	0.09	0.10	0.08	0.08	0.08	0.08	0.08	0.08	0.10	0.09
MgO	2.48	3.08	2.20	2.14	1.98	2.04	2.01	2.16	3.29	1.73
CaO	4.59	5.69	4.27	4.11	3.92	3.93	3.86	4.44	5.63	3.92
Na_2O	4.22	4.16	4.33	4.43	4.33	4.22	4.34	4.32	4.33	4.18
K_2O	1.99	1.81	2.19	2.31	2.33	2.27	2.31	2.16	1.73	2.33
P_2O_5	0.15	0.17	0.15	0.14	0.14	0.14	0.14	0.15	0.18	0.14
LOI	2.47	0.45	0.87	1.08	1.17	0.90	1.15	1.04	0.33	2.48
Total	99.60	99.87	100.36	100.20	99.68	99.81	100.00	99.79	100.12	99.95
Rb	44.1	41.8	56.2	61.0	58.3	58.9	56.5	51.5	39.3	58.2
Sr	589	541	571	514	527	503	526	544	554	516
Y	18.7	20.1	18.8	19.0	17.0	16.6	17.2	18.2	20.5	13.8
Zr	162	159	180	165	161	163	165	164	162	134
V	98	130	97	92	85	87	88	98	135	65
Ni	36	45	40	34	29	30	30	31	46	29
Cr	55	56	45	49	36	44	36	44	56	43
Nb	3.7	3.7	5.3	3.6	4.2	4.1	3.8	4.0	3.7	5.6
Ga	21.0	20.4	20.9	20.2	19.8	20.1	19.7	19.9	20.2	19.7
Cu	41	53	40	28	32	27	32	35	55	51
Zn	63	66	63	54	55	53	55	56	72	66
Co	10	15	7	7	5	6	6	6	16	6
Ba	677	585	626	725	747	769	707	727	586	768
La	20	22	22	22	21	22	22	20	20	25
Ce	37	33	35	41	36	39	36	38	29	32
U	0.8	0.8	0.5	1.6	1.6	1.0	2.1	1.9	2.0	3.1
Th	2.9	0.5	3.3	4.3	3.7	5.0	5.2	2.9	1.5	7.0
Sc	8	12	7	7	5	5	5	7	11	5
Pb	9	4	17	8	<1	6	12	17	1	9

***Note*: All major element data expressed as raw weight % oxides; all other concentrations in ppm. Fe_2O_3* is total Fe, N.D. = not determined. Dad = Dadina, Che = Chetaslina, Kot = Kotsina, Nad = Nadina, Kusk = Kuskulana.**

Sample	Root 3	Root 4	Root 6	Root 7	Root 8	Root 9	Root 10	Root 11	Root 12	Root 13
Age (Ma)	N.D.	N.D.	N.D.	N.D.	N.D.	N.D.	N.D.	N.D.	N.D.	N.D.
± Ma	N.D.	N.D.	N.D.	N.D.	N.D.	N.D.	N.D.	N.D.	N.D.	N.D.
SiO_2	61.03	66.34	58.03	67.25	48.83	65.51	66.63	51.66	56.45	67.01
TiO_2	1.02	0.44	1.23	0.36	2.05	0.53	0.41	2.18	0.98	0.37
Al_2O_3	17.19	16.79	16.50	16.58	14.56	16.06	16.68	14.41	18.00	16.59
Fe_2O_3*	5.50	3.96	7.30	3.43	14.56	3.92	3.17	14.76	7.10	3.59
MnO	0.11	0.08	0.14	0.08	0.20	0.09	0.06	0.17	0.13	0.08
MgO	2.44	1.80	4.43	1.54	6.19	1.95	1.90	7.23	3.98	1.61
CaO	5.01	4.30	6.60	3.88	10.66	4.99	4.17	4.36	8.27	4.08
Na_2O	4.80	4.84	4.29	4.64	2.63	4.25	5.01	5.11	4.31	4.57
K_2O	2.20	1.62	1.47	1.85	0.33	2.16	1.92	0.13	0.72	1.84
P_2O_5	0.26	0.13	0.23	0.13	0.19	0.14	0.14	0.21	0.21	0.13
LOI	0.96	1.27	1.01	1.98	1.95	1.95	1.54	4.27	1.21	1.13
Total	99.56	100.30	100.22	99.74	100.20	99.60	100.09	100.22	100.15	99.87
Rb	51.1	37.7	30.4	42.4	3.5	49.1	39.6	1.5	10.6	42.8
Sr	513	695	419	635	229	553	837	92	565	648
Y	28.9	12.2	34.4	12.3	34.9	14.7	10.6	40.4	24.3	10.4
Zr	467	122	122	119	130	135	127	126	157	118
V	126	83	149	69	399	63	77	390	179	67
Ni	25	13	68	26	89	30	27	75	39	16
Cr	39	34	145	47	113	42	43	135	32	40
Nb	8.7	2.7	6.6	2.9	9.0	5.3	0.8	11.7	5.4	2.5
Ga	21.5	22.4	19.6	20.7	19.3	19.7	19.9	15.4	19.6	21.2
Cu	44	47	49	40	112	54	87	157	31	41
Zn	49	58	77	58	99	63	42	112	73	60
Co	12	3	22	2	52	6	1	58	21	2
Ba	694	636	554	684	71	688	629	21	410	699
La	26	21	18	20	10	22	17	10	16	19
Ce	51	29	37	29	16	37	25	18	28	33
U	1.3	0.6	1.3	1.3	<0.5	3.2	0.6	<0.5	2.3	<0.5
Th	7.0	0.5	1.5	0.8	0.5	4.5	0.7	12.4	<0.5	0.6
Sc	12	6	17	4	41	8	6	33	16	4
Pb	<1	17	<1	2	6	12	<1	<1	<1	10

***Note*: All major element data expressed as raw weight % oxides; all other concentrations in ppm. Fe_2O_3* is total Fe, N.D. = not determined. Dad = Dadina, Che = Chetaslina, Kot = Kotsina, Nad = Nadina, Kusk = Kuskulana.**

Sample	Root 14	Root 15	Root 16	Boulder 1	Boulder 2	Boulder 4	Boulder 6	Boulder 7	Boulder 8	Boulder 9
Age (Ma)	N.D.	N.D.	N.D.	N.D.	N.D.	N.D.	N.D.	N.D.	N.D.	N.D.
± Ma	N.D.	N.D.	N.D.	N.D.	N.D.	N.D.	N.D.	N.D.	N.D.	N.D.
SiO_2	63.43	55.60	58.63	63.45	66.39	53.52	61.50	75.21	66.99	55.68
TiO_2	0.56	0.87	1.53	0.44	0.69	0.58	1.34	0.05	0.57	1.24
Al_2O_3	18.51	17.24	16.01	16.58	15.77	19.22	15.78	14.50	15.68	17.17
Fe_2O_3*	4.46	6.80	9.16	4.44	4.88	8.34	6.87	0.78	4.05	8.01
MnO	0.09	0.16	0.17	0.09	0.14	0.20	0.15	0.08	0.08	0.15
MgO	1.41	5.28	2.15	3.22	0.90	3.23	1.89	0.29	1.97	4.74
CaO	3.75	8.40	5.17	5.27	2.38	9.12	4.05	1.45	3.85	7.33
Na_2O	5.46	3.79	3.91	4.15	5.66	3.69	5.34	4.63	4.18	3.97
K_2O	2.15	1.31	2.84	1.89	3.31	1.64	2.51	2.87	2.38	1.33
P_2O_5	0.30	0.21	0.48	0.15	0.21	0.40	0.46	0.07	0.15	0.39
LOI	4.46	3.05	2.77	0.58	0.08	0.73	3.84	0.24	1.11	0.34
Total	100.12	99.66	100.05	99.68	100.33	99.94	99.89	99.93	99.90	100.01
Rb	45.2	33.6	54.6	38.8	89.1	28.7	53.2	77.6	48.5	30.1
Sr	664	494	390	859	275	1241	363	359	490	521
Y	19.3	24.7	46.7	9.6	60.6	29.7	49.0	7.2	18.6	30.5
Zr	207	139	321	133	635	94	428	78	175	232
V	51	163	161	96	33	208	117	8	88	203
Ni	4	54	2	70	4	8	4	4	35	83
Cr	22	143	20	87	24	19	32	32	62	112
Nb	4.5	3.9	13,1	2.3	19.1	3.4	17.2	5.9	5.4	7.4
Ga	22.6	18.3	21.0	20.9	24.3	18.8	22.2	18.8	19.6	19.4
Cu	31	83	24	68	22	41	41	9	53	119
Zn	76	97	82	58	87	82	93	46	54	91
Co	4	23	17	10	1	19	10	<1	7	26
Ba	577	277	926	683	1098	654	782	1011	749	503
La	30	15	25	23	46	27	31	31	21	20
Ce	54	26	57	30	90	38	59	51	39	37
U	2.9	<0.5	1.0	0.8	2.7	1.1	2.4	2.0	2.5	1.4
Th	7.1	<0.5	7.0	<0.5	12.0	<0.5	9.4	10.6	6.5	<0.5
Sc	4	21	18	8	7	20	13	<1	7	20
Pb	15	<1	5	19	20	7	15	6	10	<1

***Note*: All major element data expressed as raw weight % oxides; all other concentrations in ppm. Fe_2O_3* is total Fe, N.D. = not determined. Dad = Dadina, Che = Chetaslina, Kot = Kotsina, Nad = Nadina, Kusk = Kuskulana.**

Sample	Boulder 10	Boulder 11	Boulder 12	Boulder 13	Boulder 14	Boulder 15	Boulder 16	Boulder 17	Boulder 18	Boulder 20
Age (Ma)	N.D.	N.D.	N.D.	N.D.	N.D.	N.D.	N.D.	N.D.	N.D.	N.D.
± Ma	N.D.	N.D.	N.D.	N.D.	N.D.	N.D.	N.D.	N.D.	N.D.	N.D.
SiO_2	53.19	62.83	54.17	54.40	64.80	54.62	62.28	62.49	57.03	54.42
TiO_2	1.36	0.52	1.11	1.30	0.46	1.66	0.67	0.99	1.38	1.91
Al_2O_3	17.71	17.32	17.91	17.98	17.12	16.70	16.73	16.01	16.79	16.35
Fe_2O_3*	9.19	4.94	8.27	8.39	4.28	9.57	5.40	6.51	8.03	10.09
MnO	0.16	0.10	0.14	0.14	0.10	0.16	0.10	0.16	0.13	0.20
MgO	4.70	2.96	4.72	4.35	2.07	4.21	3.24	1.75	3.82	3.27
CaO	7.80	5.55	7.79	7.83	4.73	7.44	5.44	3.90	6.70	6.05
Na_2O	4.15	4.28	3.91	4.10	4.28	4.02	4.28	5.42	4.12	4.82
K_2O	1.21	1.40	1.50	1.18	1.99	1.35	1.54	2.31	1.86	1.87
P_2O_5	0.36	0.17	0.29	0.32	0.16	0.42	0.18	0.33	0.48	1.15
LOI	0.09	0.25	0.37	0.07	1.50	1.72	0.23	0.02	-0.04	1.65
Total	99.83	100.07	99.81	99.99	99.99	100.15	99.86	99.87	100.34	100.13
Rb	26.5	34.1	29.0	27.5	43.0	30.2	37.7	52.8	46.9	32.6
Sr	631	671	630	589	639	520	608	369	548	616
Y	28.9	11.2	22.6	27.4	12.5	35.1	13.7	44.1	34.8	47.9
Zr	206	126	184	205	135	248	145	378	306	381
V	222	85	225	207	83	242	106	106	200	122
Ni	51	48	59	66	20	58	57	3	72	2
Cr	67	72	72	68	35	75	95	10	110	18
Nb	11.0	3.7	6.7	6.0	3.5	8.6	3.3	13.6	10.7	19.6
Ga	20.2	20.6	20.5	19.6	20.8	19.7	19.5	22.7	20.2	21.2
Cu	98	51	128	112	52	160	65	50	146	28
Zn	91	63	84	82	62	90	66	91	80	107
Co	28	11	27	26	7	28	14	8	20	24
Ba	428	617	464	444	658	502	589	830	651	632
La	22	18	18	21	20	18	17	33	29	28
Ce	40	30	36	30	33	38	28	61	51	53
U	2.0	1.3	2.0	0.6	2.3	2.5	1.1	2.6	2.7	0.8
Th	<0.5	<0.5	0.7	<0.5	4.0	2.3	<0.5	9.5	2.3	6.1
Sc	23	9	22	19	8	22	11	13	16	18
Pb	<1	<1	10	1	15	1	7	11	21	9

***Note*: All major element data expressed as raw weight % oxides; all other concentrations in ppm. Fe_2O_3* is total Fe, N.D. = not determined. Dad = Dadina, Che = Chetaslina, Kot = Kotsina, Nad = Nadina, Kusk = Kuskulana.**

Sample	Boulder 21	Hawkins 1	Hawkins 2	Hawkins 3	Hawkins 4	Hawkins 5	Hawkins 6	Hawkins 7	Hawkins 8	Hawkins 9
Age (Ma)	N.D.	N.D.	N.D.	N.D.	N.D.	N.D.	N.D.	N.D.	N.D.	N.D.
± Ma	N.D.	N.D.	N.D.	N.D.	N.D.	N.D.	N.D.	N.D.	N.D.	N.D.
SiO_2	54.33	62.91	65.92	71.23	77.62	69.83	72.40	65.19	70.77	71.88
TiO_2	1.48	0.61	0.47	0.33	0.05	0.46	0.28	0.36	0.37	0.31
Al_2O_3	17.33	16.75	15.90	14.96	12.40	15.32	14.54	16.64	15.03	14.64
Fe_2O_3*	9.18	5.13	4.80	2.46	0.85	2.85	2.46	4.56	2.83	2.35
MnO	0.15	0.12	0.06	0.07	0.03	0.07	0.07	0.13	0.04	0.07
MgO	4.42	2.66	1.97	0.76	0.10	0.70	0.61	0.87	0.88	0.62
CaO	7.50	4.52	4.83	2.15	0.37	1.69	2.24	2.04	2.17	1.86
Na_2O	4.13	4.48	3.12	4.83	3.93	5.16	3.98	5.72	4.79	4.82
K_2O	1.30	2.22	2.94	3.06	4.65	3.99	3.49	4.14	3.20	3.21
P_2O_5	0.37	0.26	0.11	0.10	0.03	0.12	0.11	0.12	0.11	0.09
LOI	0.59	2.43	5.40	0.36	0.18	0.27	0.28	1.61	0.30	0.37
Total	100.19	99.66	100.12	99.95	100.03	100.19	100.18	99.77	100.19	99.85
Rb	29.7	45.9	44.2	91.6	145.4	102.9	102.5	133.8	92.3	102.5
Sr	546	619	110	225	16	177	261	264	233	183
Y	30.9	14.6	23.1	21.6	38.9	32.1	23.0	50.6	23.9	25.4
Zr	219	138	111	206	121	397	216	498	221	221
V	237	101	133	32	4	36	36	28	43	28
Ni	62	20	3	3	4	6	5	5	6	5
Cr	78	44	26	23	9	18	21	16	17	21
Nb	7.2	7.3	1.5	7.6	12.8	15.6	8.5	54.7	8.8	8.5
Ga	19.3	19.7	14.5	19.4	17.8	21.6	17.6	23.3	20.4	19.2
Cu	148	39	54	17	11	20	26	16	77	14
Zn	96	83	70	49	14	54	37	69	23	45
Co	29	8	4	<1	<1	<1	<1	<1	<1	<1
Ba	436	1086	752	888	227	1047	1450	648	926	942
La	19	19	18	27	37	37	29	51	27	29
Ce	33	46	27	52	56	62	57	104	39	51
U	1.3	0.5	2.1	3.4	6.4	2.8	2.8	12.1	2.7	2.5
Th	1.3	1.4	4.0	12.0	28.2	18.0	12.4	41.7	10.0	13.6
Sc	22	10	19	1	<1	2	3	1	1	<1
Pb	4	10	2	6	3	25	9	27	11	1

***Note*: All major element data expressed as raw weight % oxides; all other concentrations in ppm. Fe_2O_3* is total Fe, N.D. = not determined. Dad = Dadina, Che = Chetaslina, Kot = Kotsina, Nad = Nadina, Kusk = Kuskulana.**

Sample	Hawkins 10	Hawkins 11	Hawkins 12	Hawkins 13	Hawkins 14	Hawkins 15	Hawkins 17	Hawkins 18	Chitistone 1	Chitistone 2
Age (Ma)	N.D.	N.D.	N.D.	N.D.	N.D.	N.D.	N.D.	N.D.	N.D.	N.D.
± Ma	N.D.	N.D.	N.D.	N.D.	N.D.	N.D.	N.D.	N.D.	N.D.	N.D.
SiO_2	48.33	65.61	48.89	62.40	51.62	70.71	70.07	57.74	49.88	51.68
TiO_2	1.15	0.49	2.33	0.80	1.93	0.35	0.40	1.27	1.72	1.89
Al_2O_3	15.24	16.46	14.35	16.48	17.73	14.95	15.33	15.56	18.09	16.39
Fe_2O_3*	11.17	5.36	14.21	6.71	12.35	2.45	2.94	8.36	10.82	10.16
MnO	0.30	0.13	0.21	0.18	0.24	0.07	0.08	0.15	0.26	0.16
MgO	13.14	1.70	6.04	1.80	4.20	0.95	0.97	4.35	4.03	5.56
CaO	7.51	2.41	10.79	3.55	6.80	2.46	2.44	6.24	7.41	7.85
Na_2O	2.12	4.62	2.53	5.13	3.65	4.66	4.98	3.92	4.10	3.91
K_2O	0.89	2.90	0.41	2.56	1.04	2.90	2.72	1.86	2.66	1.49
P_2O_5	0.28	0.19	0.23	0.35	0.55	0.10	0.11	0.32	0.68	0.55
LOI	0.71	3.64	0.85	1.58	2.33	0.38	0.48	0.61	2.99	1.95
Total	100.13	99.87	99.99	99.96	100.11	99.60	100.04	99.77	99.65	99.64
Rb	28.1	59.8	7.4	69.1	22.7	86.6	90.0	45.9	45.0	22.8
Sr	127	240	227	206	511	265	253	441	691	607
Y	32.4	36.9	33.3	40.0	53.2	18.0	24.2	44.4	39.0	39.2
Zr	82	353	155	288	314	177	223	165	230	268
V	253	59	419	68	170	43	45	183	229	218
Ni	265	5	69	5	8	8	7	40	22	88
Cr	685	19	124	21	37	28	29	69	21	163
Nb	5.3	23.3	11.4	21.3	14.7	7.2	7.6	8.9	18.9	12.1
Ga	15.9	22.0	20.1	20.3	22.7	19.1	20.2	19.0	17.4	19.5
Cu	41	18	220	14	66	15	14	58	57	46
Zn	309	59	105	119	157	49	48	104	129	102
Co	66	6	48	8	37	<1	<1	24	30	33
Ba	114	706	113	997	443	869	908	530	1197	515
La	15	47	12	27	21	25	26	20	29	22
Ce	33	90	21	53	48	42	52	42	75	45
U	<0.5	5.6	<0.5	1.4	1.2	1.5	1.3	1.8	1.3	4.0
Th	5.5	23.6	<0.5	13.9	9.0	12.9	12.9	4.4	2.4	3.0
Sc	35	4	34	8	19	2	3	19	19	19
Pb	45	30	7	3	8	6	<1	<1	5	<1

***Note*: All major element data expressed as raw weight % oxides; all other concentrations in ppm. Fe_2O_3* is total Fe, N.D. = not determined. Dad = Dadina, Che = Chetaslina, Kot = Kotsina, Nad = Nadina, Kusk = Kuskulana.**

Sample	Chitistone 3	Chitistone 4	Chitistone 6	Chitistone 7	Chitistone 8	Chitistone 9	Chitistone 10	Chitistone 11	Chitistone 12	Chitistone 13
Age (Ma)	N.D.	N.D.	N.D.	N.D.	N.D.	N.D.	N.D.	N.D.	N.D.	N.D.
± Ma	N.D.	N.D.	N.D.	N.D.	N.D.	N.D.	N.D.	N.D.	N.D.	N.D.
SiO_2	49.60	65.81	54.04	68.30	74.51	57.76	48.80	52.27	75.34	70.52
TiO_2	1.95	0.54	0.83	0.59	0.20	1.44	2.83	1.88	0.07	0.37
Al_2O_3	15.43	16.50	20.88	14.79	14.05	16.70	15.07	17.01	14.68	14.91
Fe_2O_3*	12.58	4.21	8.93	3.50	1.94	7.95	15.23	9.90	0.98	3.65
MnO	0.18	0.09	0.13	0.07	0.02	0.13	0.24	0.15	0.05	0.08
MgO	6.37	2.15	3.95	1.58	1.37	3.08	4.40	3.88	0.38	1.18
CaO	8.93	4.55	3.77	2.79	1.63	5.70	9.71	8.25	1.86	1.79
Na_2O	4.27	3.95	5.72	4.17	3.89	4.64	3.14	4.28	4.24	5.07
K_2O	0.70	2.04	1.92	3.61	2.10	2.06	0.41	1.41	2.44	2.05
P_2O_5	0.18	0.17	0.16	0.15	0.06	0.37	0.22	0.46	0.07	0.10
LOI	3.08	6.50	5.53	1.85	3.88	0.09	0.39	3.93	2.05	2.24
Total	100.19	100.01	100.33	99.55	99.77	99.83	100.05	99.49	100.11	99.72
Rb	5.4	43.3	35.8	94.9	36.2	49.4	8.5	34.8	62.1	29.2
Sr	384	485	201	331	93	477	254	485	363	183
Y	32.4	15.6	21.5	26.1	19.8	31.0	32.5	36.9	9.2	34.2
Zr	119	159	67	315	153	259	147	285	109	149
V	349	90	293	74	27	161	417	188	9	45
Ni	91	15	11	25	4	25	28	33	2	4
Cr	189	46	31	60	19	47	52	71	7	16
Nb	8.1	3.3	0.6	7.1	4.3	9.3	15.1	13.8	8.3	3.1
Ga	18.1	19.1	19.3	18.8	14.2	21.7	21.8	19.9	18.3	17.5
Cu	128	28	181	39	11	54	438	52	14	11
Zn	92	65	92	76	39	86	104	90	14	36
Co	46	5	28	2	<1	21	37	25	<1	<1
Ba	157	660	465	843	557	716	117	502	813	1052
La	7	25	14	33	24	25	8	20	32	22
Ce	13	48	23	62	36	47	15	35	53	40
U	<0.5	1.8	<0.5	3.7	3.4	2.8	<0.5	2.7	1.9	1.8
Th	1.4	7.8	9.3	17.6	13.7	3.8	1.3	2.6	11.9	7.5
Sc	33	9	27	4	3	13	33	21	<1	6
Pb	<1	!	2	14	18	<1	<1	9	1	<1

***Note*: All major element data expressed as raw weight % oxides; all other concentrations in ppm. Fe_2O_3* is total Fe, N.D. = not determined. Dad = Dadina, Che = Chetaslina, Kot = Kotsina, Nad = Nadina, Kusk = Kuskulana.**

Sample	Chitistone 14	Chitistone 15	Chitistone 17	Chitistone 18	Chitistone 19	Chitistone 20	Chitistone 21	Chitistone 22	Chitistone 23	Chitistone 24
Age (Ma)	N.D.	N.D.	N.D.	N.D.	N.D.	N.D.	N.D.	N.D.	N.D.	N.D.
± Ma	N.D.	N.D.	N.D.	N.D.	N.D.	N.D.	N.D.	N.D.	N.D.	N.D.
SiO_2	50.41	69.27	49.05	59.86	51.97	57.55	57.48	63.06	83.05	52.05
TiO_2	1.93	0.55	1.47	0.99	1.54	1.39	0.58	0.96	0.13	1.79
Al_2O_3	14.01	14.65	16.34	16.67	18.25	17.64	18.47	16.56	9.40	16.91
Fe_2O_3*	13.44	3.03	11.95	6.51	9.00	7.51	6.89	5.54	1.55	9.86
MnO	0.23	0.06	0.17	0.12	0.13	0.15	0.19	0.16	0.02	0.16
MgO	6.48	1.40	7.47	3.40	4.38	2.65	2.53	1.88	0.44	5.60
CaO	10.16	2.55	9.43	5.57	9.27	6.13	7.43	3.78	0.71	8.15
Na_2O	2.65	4.13	3.75	4.47	4.05	4.66	3.98	5.17	3.75	3.93
K_2O	0.45	3.80	0.41	1.85	0.70	1.97	1.86	2.27	0.83	1.26
P_2O_5	0.18	0.14	0.14	0.26	0.31	0.32	0.23	0.38	0.05	0.52
LOI	0.24	1.97	2.75	0.92	2.57	1.51	1.00	2.52	1.31	1.85
Total	99.94	99.58	100.18	99.70	99.60	99.97	99.64	99.76	99.93	100.23
Rb	11.5	97.8	5.3	40.0	5.8	49.5	41.5	71.4	15.6	16.6
Sr	197	315	399	556	618	546	1050	564	159	637
Y	30.7	24.0	28.2	28.7	32.0	30.6	22.1	37.8	16.3	37.6
Zr	113	306	91	178	168	261	112	313	111	253
V	365	71	310	136	191	150	147	74	32	210
Ni	47	20	150	30	53	7	5	3	4	89
Cr	44	51	335	59	119	28	19	16	27	168
Nb	9.5	6.5	4.8	5.1	6.4	11.4	5.7	18.5	3.1	11.5
Ga	19.2	19.1	16.8	20.1	19.6	22.4	19.3	21.8	11.9	20.0
Cu	230	51	37	34	37	39	19	24	15	53
Zn	107	47	93	85	81	100	69	92	26	95
Co	48	1	52	17	31	16	10	3	<1	33
Ba	105	806	301	603	371	619	999	1255	483	501
La	8	32	10	25	15	25	21	42	20	21
Ce	19	58	10	49	27	44	46	84	23	41
U	<0.5	2.9	<0.5	2.3	1.2	3.8	<0.5	3.1	3.2	4.0
Th	<0.5	17.0	<0.5	1.3	<0.5	5.2	<0.5	9.7	11.4	0.6
Sc	36	4	33	13	21	11	13	9	1	19
Pb	<1	15	4	3	13	4	18	7	19	<1

***Note*: All major element data expressed as raw weight % oxides; all other concentrations in ppm. Fe_2O_3* is total Fe, N.D. = not determined. Dad = Dadina, Che = Chetaslina, Kot = Kotsina, Nad = Nadina, Kusk = Kuskulana.**

Sample	Nizina 1	Nizina 3	Nizina 4	Nizina 6	Nizina 7	Nizina 8	Nizina 9	Nizina 11	Nizina 12	Nizina 13
Age (Ma)	N.D.	N.D.	N.D.	N.D.	N.D.	N.D.	N.D.	N.D.	N.D.	N.D.
± Ma	N.D.	N.D.	N.D.	N.D.	N.D.	N.D.	N.D.	N.D.	N.D.	N.D.
SiO_2	71.60	59.78	67.40	64.99	71.19	72.25	71.62	57.58	72.58	71.32
TiO_2	0.19	0.87	0.58	0.91	0.49	0.34	0.16	1.29	0.36	0.38
Al_2O_3	16.32	17.08	16.17	15.12	14.58	14.14	15.98	17.93	14.47	14.73
Fe_2O_3*	1.88	5.84	3.21	6.01	2.81	2.46	1.87	7.20	1.88	2.26
MnO	0.09	0.12	0.12	0.14	0.07	0.07	0.09	0.15	0.08	0.09
MgO	0.27	3.76	0.90	1.34	0.62	0.79	0.23	3.38	0.36	0.60
CaO	2.63	6.79	2.34	3.01	1.72	1.68	2.14	6.36	0.96	1.54
Na_2O	5.24	3.82	5.90	5.05	6.20	4.87	5.37	4.23	5.81	5.38
K_2O	1.97	1.67	2.83	2.58	2.47	3.00	2.10	1.31	3.18	3.32
P_2O_5	0.12	0.22	0.16	0.34	0.11	0.10	0.11	0.30	0.06	0.10
LOI	1.35	2.54	0.58	1.31	1.62	1.26	2.10	4.84	0.57	0.22
Total	100.31	99.95	99.61	99.49	100.26	99.70	99.67	99.73	99.74	99.72
Rb	45.7	38.4	68.0	58.1	53.7	66.2	53.1	24.0	74.4	86.8
Sr	467	586	326	342	184	193	442	539	149	196
Y	12.9	23.2	36.5	51.6	36.8	25.0	13.1	31.8	43.1	34.0
Zr	172	194	391	397	382	228	178	207	437	312
V	18	151	48	63	36	41	16	151	19	31
Ni	4	53	5	5	4	8	4	28	4	5
Cr	9	95	14	19	6	10	5	50	9	5
Nb	3.5	4.6	15.5	10.8	12.2	10.9	3.6	5.9	13.8	16.5
Ga	20.1	18.9	22.2	22.6	18.6	18.7	19.5	21.0	21.7	21.0
Cu	12	67	15	31	20	21	12	43	16	18
Zn	53	68	86	79	50	50	60	87	60	53
Co	<1	17	<1	7	<1	<1	<1	18	<1	<1
Ba	761	555	1253	906	803	988	784	415	1116	1228
La	24	21	35	33	36	35	25	21	41	39
Ce	41	34	73	65	67	67	44	35	86	75
U	<0.5	0.8	2.6	2.5	2.5	0.9	1.1	0.6	3.1	4.2
Th	3.9	1.1	10.1	10.6	15.8	14.2	5.4	6.3	14.6	13.1
Sc	<1	15	2	9	3	1	<1	18	3	<1
Pb	9	7	12	8	10	11	<1	1	15	8

***Note*: All major element data expressed as raw weight % oxides; all other concentrations in ppm. Fe_2O_3* is total Fe, N.D. = not determined. Dad = Dadina, Che = Chetaslina, Kot = Kotsina, Nad = Nadina, Kusk = Kuskulana.**

Sample	Nizina 14	Nizina 15	Nizina 16	Nizina 17	Nizina 18	Nizina 19	Nizina 20	Nizina 24	Jasksina 1	Jasksina 2
Age (Ma)	N.D.	N.D.	N.D.	N.D.	N.D.	N.D.	N.D.	N.D.	N.D.	N.D.
± Ma	N.D.	N.D.	N.D.	N.D.	N.D.	N.D.	N.D.	N.D.	N.D.	N.D.
SiO_2	71.07	61.32	60.72	77.83	53.88	73.82	58.02	58.24	67.42	63.79
TiO_2	0.45	0.76	0.40	0.06	1.01	0.37	1.14	1.22	0.52	0.62
Al_2O_3	14.99	16.93	17.19	12.67	16.86	13.71	18.24	18.73	16.31	16.93
Fe_2O_3*	2.80	5.38	6.65	0.60	8.24	1.84	7.20	5.77	3.62	4.89
MnO	0.07	0.14	0.15	0.04	0.15	0.07	0.14	0.10	0.12	0.13
MgO	0.68	2.89	2.63	0.12	5.29	0.27	2.78	1.92	1.20	1.67
CaO	1.81	5.80	6.87	0.49	9.33	0.84	6.32	6.66	3.19	4.33
Na_2O	5.55	4.69	3.54	4.08	3.63	5.65	4.57	4.42	5.16	5.09
K_2O	2.89	1.49	1.55	4.20	0.92	2.88	1.51	2.16	2.20	1.84
P_2O_5	0.11	0.18	0.17	0.03	0.23	0.06	0.35	0.44	0.19	0.23
LOI	0.52	1.66	0.77	0.37	5.23	1.89	2.22	1.53	0.48	1.46
Total	100.42	99.58	99.87	100.12	99.54	99.51	100.27	99.66	99.93	99.52
Rb	63.2	44.4	33.8	117.4	15.5	65.8	28.6	45.1	46.6	37.1
Sr	189	548	735	82	552	152	618	769	430	497
Y	37.4	20.3	15.6	13.8	26.5	41.6	30.3	28.9	19.8	21.0
Zr	346	145	85	95	146	430	233	299	241	185
V	32	119	138	4	178	26	145	138	58	71
Ni	6	5	6	3	110	4	14	25	7	8
Cr	8	13	15	9	306	11	24	54	14	10
Nb	10.8	5.5	2.5	11.7	5.1	13.6	8.4	12.9	7.5	6.3
Ga	21.3	19.3	17.4	16.6	17.3	19.8	20.5	22.4	20.5	20.6
Cu	15	22	31	9	39	12	35	55	24	30
Zn	36	85	48	25	83	64	89	73	64	71
Co	<1	12	8	<1	32	<1	20	12	1	4
Ba	874	482	847	1235	380	1169	658	788	863	556
La	33	19	16	40	19	37	25	33	30	21
Ce	62	36	25	71	32	80	45	56	55	40
U	2.9	2.0	1.2	2.9	0.7	3.3	1.9	2.9	2.2	1.3
Th	10.9	2.1	<0.5	19.0	<0.5	15.5	2.4	3.3	2.2	0.5
Sc	2	13	16	<1	20	1	16	11	3	6
Pb	15	10	16	20	<1	12	<1	3	2	5

***Note*: All major element data expressed as raw weight % oxides; all other concentrations in ppm. Fe_2O_3* is total Fe, N.D. = not determined. Dad = Dadina, Che = Chetaslina, Kot = Kotsina, Nad = Nadina, Kusk = Kuskulana.**

Sample	Jasksina 3	Jasksina 4	Jasksina 5	Jasksina 6	Jasksina 7	Jasksina 8	Jasksina 9	Jasksina 10	Jasksina 11	Jasksina 12
Age (Ma)	N.D.	N.D.	N.D.	N.D.	N.D.	N.D.	N.D.	N.D.	N.D.	N.D.
± Ma	N.D.	N.D.	N.D.	N.D.	N.D.	N.D.	N.D.	N.D.	N.D.	N.D.
SiO_2	58.92	67.90	72.31	58.86	55.02	61.58	62.07	69.09	67.66	60.46
TiO_2	0.92	0.41	0.13	1.15	1.00	0.76	0.61	0.36	0.29	0.74
Al_2O_3	17.08	16.23	15.75	16.53	16.79	17.66	17.83	16.18	16.78	16.69
Fe_2O_3*	6.79	3.25	1.61	7.23	7.51	5.51	5.36	3.20	3.25	6.04
MnO	0.13	0.14	0.09	0.13	0.14	0.08	0.11	0.14	0.08	0.11
MgO	3.50	0.98	0.45	3.42	6.93	2.31	2.49	0.91	1.44	3.72
CaO	6.22	2.72	2.04	6.01	7.65	5.85	5.72	2.71	3.85	5.96
Na_2O	4.24	5.56	5.39	4.42	3.72	4.25	4.39	5.48	5.33	3.97
K_2O	1.47	2.24	1.95	1.85	1.18	1.74	1.38	1.98	1.26	1.74
P_2O_5	0.23	0.19	0.11	0.28	0.26	0.20	0.17	0.21	0.12	0.20
LOI	0.72	1.56	0.34	0.96	0.24	1.59	0.55	0.25	1.47	0.87
Total	99.50	99.62	99.83	99.88	100.20	99.94	100.13	100.26	100.06	99.63
Rb	31.3	46.2	46.8	42.4	18.5	41.5	31.8	41.0	24.4	44.5
Sr	540	463	347	460	592	500	601	408	655	548
Y	24.8	27.4	8.0	31.7	21.4	20.5	17.4	22.5	10.0	21.8
Zr	177	269	132	252	147	165	137	242	98	203
V	148	23	17	162	175	139	114	25	63	131
Ni	25	3	3	26	156	22	14	5	13	59
Cr	45	5	4	54	287	43	30	19	34	107
Nb	5.9	11.3	7.9	8.3	9.1	4.7	3.8	13.1	0.8	7.1
Ga	19.8	21.6	20.2	19.6	18.7	20.3	20.8	20.4	20.6	19.2
Cu	54	16	15	55	78	40	40	18	23	87
Zn	84	78	51	75	71	65	62	72	53	73
Co	16	<1	<1	19	29	12	9	<1	2	16
Ba	557	912	831	588	329	707	576	763	476	592
La	22	38	26	21	17	20	20	33	17	22
Ce	33	69	52	38	30	39	33	58	24	41
U	0.5	1.8	0.8	1.5	0.6	2.1	<0.5	1.0	<0.5	0.7
Th	<0.5	7.7	4.1	5.3	<0.5	3.8	<0.5	5.3	<0.5	2.6
Sc	16	1	<1	15	17	12	9	1	4	11
Pb	<1	7	1	5	1	15	19	18	19	7

***Note*: All major element data expressed as raw weight % oxides; all other concentrations in ppm. Fe_2O_3* is total Fe, N.D. = not determined. Dad = Dadina, Che = Chetaslina, Kot = Kotsina, Nad = Nadina, Kusk = Kuskulana.**

Sample	Jasksina 13	Jasksina 14	Jasksina 15	Jasksina 16	Copper 2	Copper 3	Copper 4	Copper 5	Copper 6	Copper 8
Age (Ma)	N.D.	N.D.	N.D.	N.D.	N.D.	N.D.	N.D.	N.D.	N.D.	N.D.
± Ma	N.D.	N.D.	N.D.	N.D.	N.D.	N.D.	N.D.	N.D.	N.D.	N.D.
SiO_2	66.97	58.52	56.31	66.79	58.92	55.86	64.60	62.79	70.33	56.59
TiO_2	0.33	0.84	1.01	0.55	0.94	1.88	0.46	0.82	0.32	1.09
Al_2O_3	16.65	17.21	17.06	16.14	16.01	15.85	17.16	16.05	16.50	16.94
Fe_2O_3*	3.45	6.83	7.73	4.59	6.78	9.79	4.40	5.75	2.44	7.24
MnO	0.07	0.12	0.13	0.12	0.12	0.15	0.09	0.10	0.05	0.12
MgO	1.45	4.62	4.87	0.79	4.77	3.53	1.88	3.18	0.34	4.87
CaO	4.18	6.55	7.07	2.28	6.47	6.58	4.73	5.23	2.88	7.68
Na_2O	4.61	3.80	3.85	5.96	3.75	3.98	4.52	4.04	4.87	3.43
K_2O	1.61	1.64	1.36	2.87	1.71	1.97	1.61	2.17	2.08	1.85
P_2O_5	0.12	0.19	0.26	0.18	0.22	0.62	0.19	0.19	0.12	0.25
LOI	1.03	0.57	0.22	0.19	0.07	0.34	1.79	0.05	1.68	-0.06
Total	99.44	100.32	99.65	100.27	99.69	100.21	99.64	100.32	99.93	100.06
Rb	32.1	43.0	28.9	53.6	45.9	45.8	33.4	63.8	44.1	46.8
Sr	598	524	546	275	617	496	578	585	487	685
Y	9.9	22.8	25.7	45.3	21.5	39.1	14.2	21.9	8.0	21.8
Zr	100	176	187	412	199	353	138	232	164	236
V	61	156	168	23	161	276	85	132	36	194
Ni	6	80	83	4	81	45	15	53	6	57
Cr	21	140	135	13	152	83	35	92	18	136
Nb	2.6	4.9	6.5	17.3	6.1	13.6	5.8	6.5	6.7	6.5
Ga	20.4	18.5	18.7	23.7	19.1	19.6	19.8	19.1	19.1	19.4
Cu	36	83	97	13	89	209	36	90	16	123
Zn	54	71	77	89	74	110	64	64	48	66
Co	3	32	27	<1	20	27	5	12	<1	21
Ba	655	512	429	992	538	621	582	643	749	608
La	17	20	20	45	22	26	24	22	26	26
Ce	25	37	28	89	39	42	40	40	42	45
U	0.8	0.8	0.7	2.2	1.8	1.8	1.4	1.0	2.0	2.6
Th	<0.5	1.9	0.8	11.1	3.6	6.8	2.6	5.6	5.0	1.9
Sc	5	16	18	8	16	20	6	9	1	19
Pb	6	<1	5	5	13	<1	1	<1	7	5

***Note*: All major element data expressed as raw weight % oxides; all other concentrations in ppm. Fe_2O_3* is total Fe, N.D. = not determined. Dad = Dadina, Che = Chetaslina, Kot = Kotsina, Nad = Nadina, Kusk = Kuskulana.**

Sample	Copper 10	Copper 11	Copper 12	Copper 13	Copper 14	Copper 15	Copper 16
Age (Ma)	N.D.	N.D.	N.D.	N.D.	N.D.	N.D.	N.D.
± Ma	N.D.	N.D.	N.D.	N.D.	N.D.	N.D.	N.D.
SiO_2	54.42	62.26	56.49	59.81	69.35	64.53	65.06
TiO_2	1.14	1.12	0.87	1.05	0.32	0.46	0.70
Al_2O_3	17.55	15.76	18.61	16.32	15.81	17.28	16.22
Fe_2O_3*	7.96	6.34	7.81	6.71	3.10	4.53	4.89
MnO	0.14	0.19	0.14	0.12	0.10	0.12	0.12
MgO	5.18	1.69	3.62	3.85	1.01	2.13	1.35
CaO	8.44	3.78	6.62	5.94	3.11	4.81	3.39
Na_2O	3.82	5.53	4.26	3.81	4.79	4.58	5.46
K_2O	0.88	2.62	1.22	2.27	2.06	1.51	2.39
P_2O_5	0.23	0.45	0.21	0.29	0.15	0.20	0.24
LOI	0.38	0.88	0.61	1.73	0.66	0.86	0.39
Total	99.76	99.74	99.85	100.17	99.80	100.15	99.82
Rb	21.5	60.4	25.8	68.8	44.5	33.4	51.5
Sr	530	368	639	421	460	600	363
Y	23.9	61.0	19.6	28.1	12.6	13.5	34.7
Zr	145	503	145	277	152	139	280
V	176	64	168	152	31	83	70
Ni	69	3	34	66	6	13	5
Cr	144	10	53	123	14	32	17
Nb	2.4	20.1	3.6	7.9	6.7	5.9	10.0
Ga	18.8	24.4	20.6	19.3	18.6	19.7	22.4
Cu	103	20	66	103	23	28	31
Zn	76	115	81	74	55	67	76
Co	26	3	24a	17	<1	5	3
Ba	361	879	395	611	703	593	830
La	14	36	19	21	26	25	30
Ce	24	79	23	50	40	35	54
U	0.5	1.9	<0.5	1.3	1.5	0.9	0.6
Th	<0.5	10.1	0.5	3.6	5.5	1.4	6.2
Sc	23	15	16	13	3	5	6
Pb	5	14	<1	1	<1	8	7

***Note*: All major element data expressed as raw weight % oxides; all other concentrations in ppm. Fe_2O_3* is total Fe, N.D. = not determined. Dad = Dadina, Che = Chetaslina, Kot = Kotsina, Nad = Nadina, Kusk = Kuskulana.**